UNIVERSITY OF SOUTHAMPTON

FACULTY OF ENGINEERING, SCIENCE & MATHEMATICS

SCHOOL OF ENGINEERING SCIENCES

SURFACE ENGINEERING AND TRIBOLOGY RESEARCH GROUP

THE FEASIBILITY OF USING ELECTROSTATIC CHARGE CONDITION MONITORING FOR LUBRICANT ADDITIVE SCREENING

BY

James Edward Booth BEng, AMIMechE

THESIS SUBMITTED FOR THE DEGREE OF

DOCTOR OF PHILOSOPHY

March 2008

UNIVERSITY OF SOUTHAMPTON

ABSTRACT

FACULTY OF ENGINEERING, SCIENCE & MATHEMATICS
SCHOOL OF ENGINEERING SCIENCES
SURFACE ENGINEERING AND TRIBOLOGY RESEARCH GROUP

Doctor of Philosophy

THE FEASIBILITY OF USING ELECTROSTATIC CHARGE CONDITION MONITORING FOR ADDITIVE SCREENING

By James Edward Booth

International standards require lubricant formulators to develop additive packages that increase fuel economy, reduce environmental impact and minimise wear over ever increasing service intervals. However, additive behaviour and interactions between additives is not well understood. An absence of real-time technology has hindered understanding of additive behaviour and interaction between additives in tribo-contacts. The work presented in this thesis assessed whether electrostatic charge monitoring, which is sensitive to changes in surface chemistry, can offer insight into additive-surface behaviour and how this affects tribological performance.

Electrostatic sensors were deployed on tribological test apparatus used to simulate: engine valve-train, manual transmission synchroniser and automatic transmission clutch tribo-contacts. Additive performance in these simulated contacts was assessed by electrostatic surface charge measurements and cross-correlated with friction, wear and off-line surface chemistry analysis.

The first study involved electrostatic monitoring of valve-train contacts, which was a continuation of previous electrostatic monitoring work carried out to relate wear and electrostatic charge. During a simulated TU3 cam-follower wear test, charge signals underwent a sign inversion; this was due to a transition between tribocharging of the lubricant under running-in and mild wear, and contact potential difference generated at the onset and progression of adhesive wear. It was found that charge signals differed between different oils, which could not be explained by the wear performance alone; this indicated that lubricant chemistry significantly affected charge generation.

Dynamic charge peaks produced by simulated valve-train contacts lubricated with zinc dialkyldithiophosphate (ZnDTP) additive were related to the stripping of the tribofilm. The source of this charge peak was an increase in negative charge, which correlated with a dominance of phosphate and sulphate (anions) compared to zinc (cations), as the film was worn away. When friction modifier (FM) and dispersant additives were combined to lubricate a simulated wet clutch contact, x-ray photo-electron spectroscopy (XPS) analysis and friction data indicated that the dispersant dominated the tribofilm composition; evidenced by nitrogen levels and friction levels similar to the dispersant alone. Electrostatic charge data showed that competition for surface sites is an extremely dynamic process; as indicated by charge levels which alternated between the levels of the FM and dispersant alone. When a potassium borate additive was added to a polysulphide additive containing oil during testing (seeding), the charge data showed a transition from being predominantly positive to predominantly negative. This correlated with the formation of a borate rich (anions) layer on top of the sulphur film.

Further novel tribological discoveries were found through investigation into these additive-surface charge behaviours. An underdeveloped ZnDTP tribofilm, which predominantly contained sulphur, was formed at room temperature; the sulphur promoted tribochemical wear and resulted in a pro-wear affect for primary ZnDTP. The combination of FM and dispersant showed a clear antagonism resulting in increased wear compared to the individual additives.

XPS of brass and steel simulated synchroniser contacts lubricated with potassium borate and polysulphide identified the affect of surface chemistry on film formation. For the potassium borate additive: potassium (cation) preferentially adsorbed to brass, and borate (anion) preferentially adsorbed to steel. Seeding the borate additive into the oil, and therefore the contact, produced the same film composition and structure as the combination from the start. This inferred that the polysulphide additive drove initial film formation. Seeding is an extremely powerful technique, but its use is almost absent in the literature.

It has been shown that lubricant chemistry dominates charge levels even in a wearing contact. Electrostatic monitoring is sensitive to the type of additive-surface adsorption and interaction between additive and additive or contaminant. Also, cross-correlation of surface charge and tribofilm chemical composition demonstrated that electrostatic sensors have the ability to detect tribofilm kinematics. This is a significant finding; no current real-time technique used to monitor tribofilm kinematics derives its measurements from the tribofilm composition. Although interpretation of electrostatic charge data is currently an intensive process, in the long term, lubricant development could see a move towards charge informed formulation.

CONTENTS

LIST OF FIGURES

LIST OF TABLES

NOMENCLATURE

Term	Meaning	Unit
W	Normal Load on a surface	N
W'	Normal Load per unit length	N m^{-1}
L	Length of contact	m
b	Half the contact width for a line contact	m
a	Radius of circular contact area for a point contact	m
R^*	Reduced radius of curvature	m
R_1	Radius of cylinder or sphere 1	m
R_2	Radius of cylinder or sphere 2	m
E^*	Contact modulus	Pa
E_1	Elastic modulus of cylinder or sphere 1	Pa
E_2	Elastic modulus of cylinder or sphere 2	Pa
υ_1	Poisson's ratio of cylinder or sphere 1	-
υ_2	Poisson's ratio of cylinder or sphere 2	-
x,y,z	Cartesian coordinates	-
P	Contact Pressure	Pa or N m^{-2}
P_0	Maximum contact pressure	Pa or N m^{-2}
P_m	Mean contact pressure	Pa or Nm^{-2}
Y	Yield stress in tension	Pa or N m^{-2}
$\sigma_1, \sigma_2, \sigma_3$	Principle stresses	Pa or N m^{-2}
k	Yield stress in pure shear	Pa or N m^{-2}
$\tau_{\max}$	Maximum shear stress	Pa or N m^{-2}
W_Y	Load for first yield (point contact)	N
W_Y'	Load per unit length of the contact (line) for first yield	N m^{-1}
$(P_0)_Y$	Peak contact pressure at first yield	Pa or N m^{-2}
H	Hardness	H_v
μ *or COF*	Coefficient of friction	-
F_F	Frictional force	N
F_N	Normal force	N
Q	Tangentially applied force	N
μ_S	Static friction	-
μ_D	Dynamic friction	-
B	Length of wedge	m
h_{inlet}	Film thickness at inlet of wedge	m
h_{outlet}	Film thickness at outlet of wedge	m
W^*	Estimated non-dimensional load	-
U_1	Velocity of body 1	m s^{-1}
U_2	Velocity of body 2	m s^{-1}

$\overline{U}$	Horizontal entrainment velocity, $\overline{U} = \frac{1}{2}(U_1 + U_2)$	m s^{-1}
h	Film thickness	m
$\overline{h}$	Film thickness at which maximum pressure occurs	m
h_c	Central film thickness	m
η	Dynamic viscosity	kg m^{-1} s^{-1}, or N s m^{-2} or cP
$h_{\min}$	Minimum film thickness	m
α	Pressure viscosity index/coefficient	Pa^{-1}
η_0	Low shear rate viscosity	N s m^{-2} (cP)
λ	Ratio of minimum film thickness to combined roughness	-
R_{q1}	rms surface roughness of body 1	m
R_{q2}	rms surface roughness of body 1	m
p_n	Nominal bearing pressure	Pa or Nm^{-2}
ω	Rotational speed	Rad s^{-1}
k_w	Dimensionless wear coefficient	-
κ or *SWR*	Specific wear rate	m^3 N^{-1} m^{-1} or m^2 N^{-1}
SD	Sliding Distance	m
VL	Volume Loss	m^3
E	Elastic Modulus	Pa or Nm^{-2}
A	Area	m^{-2}
F	Force	N
τ	Shear stress	Pa or N/m^2
$\dot{\gamma}$	Stain rate	s^{-1}
V	Velocity	ms^{-1}
ρ	Density	kg m^{-3}
ν	Kinematic viscosity	m^2/s or cSt
T	Oil temperature	^oC
k_{temp}	Lubricant constant	Pa s
θ_1 & θ_2	Lubricant constants	^oC
a_{temp}	Lubricant constants (around 0.6)	-
c_{temp}	Lubricant constants	-
η_{atm}	The base viscosity at atmospheric pressure	N s m^{-2} (cP)
p_0^*	Universal constant, $p_0^* \approx 2 \times 10^8$	Pa
Z	Modifies the increase in viscosity at high pressures	-
η_{LSR}	The low shear rate viscosity at a particular temperature	N s m^{-2} (cP)
η_∞	The limiting shear viscosity	N s m^{-2} (cP)
γ	Shear rate	S^{-1}
γ_c	Shear rate at which the viscosity is midway between η_0 and η_∞	S^{-1}
$\dot{h}_{effect}$	Growth rate of the effective film thickness	m s^{-1}
$\dot{h}_{physisorbed}$	Physisorbed growth rate	m s^{-1}
$\dot{h}_{chemisorbed}$	The chemisorbed film growth rate	m s^{-1}

$\dot{h}_{react}$	Chemically reacting film growth rate	m s^{-1}
$\dot{h}_{scrape}$	Tribofilm removal rate	m s^{-1}
$E^{\bullet}$	Indentation modulus	Pa or Nm^{-2}
Q	Isolated point charge	C
E_f	Electric field strength	N C^{-1} or V m^{-1}
S	Surface area	m^2
ε	Permittivity	F m^{-1}
r	Radius of the sphere or the distance between the particle and the surface	m
Q_A	Charge induced on the surface	C
C	Capacitance	F
V	Potential difference	V
eV_{CPD}	Contact potential difference	V
t	Time	s
ϕ	Work function	eV
ESA	Electrokinetic Sonic amplitude	A_{ESA} E^{-1}

ABBREVIATIONS

Abbreviation	*Definition*
A/D	Analogue to digital
AISI	The American Iron and Steel Institute
ANOVA	Analysis of Variance
API	American Petroleum Institute
ASTM	American Society for Testing and Materials
AT	Automatic Transmission
ATF	Automatic Transmission Fluids
CPD	Contact Potential Difference
DAT	Digital Analogue Tape Or Direct Acting Tappet
ECR	Electrical contact resistance
EDX	Energy Dispersive X-ray spectroscopy
EHL	Elasto-hydrodynamic lubrication
EP	Extreme Pressure
ESA	Electrokinetic Sonic Amplitude
FM	Friction modifiers
GMO	Glycerol Mono-Oleate
HPLC	High performance liquid chromatorgrahpy
IC	Internal Combustion
ICP-AES	Coupled Plasma-Atomic Emission Spectroscopy
IDMS	Ingested Debris Monitoring System
MoDTC	Molybdenum-DiThioCarbamate
MTF	Manual transmission fluids
MTM	Mini-Traction-Machine
OCP	Olefin Copolymers
ODR	Oil Droplet Rig
OEM	Original Equipment Manufacturer
OHC	Over-Head-Cams
OHV	Over-Head-Valve
OLS	Oil Line Sensor
PAO	Poly-Alpha-Olefin
PC	Personal Computer
PIBS	Polyisobutylene
PMA	Poly Methacrylates
PoD	Pin-on-Disc
RMS	Root Mean Squared
SDC	Spinning Disc Charger
SEM	Scanning Electron Microscopy
TBN	Total Base Number
VI	Viscosity Index
VII	Viscosity Index Improvers
WSS	Wear Site Sensor
XPS	X-ray Photoelectron Spectroscopy
ZnDTP	Zinc-Dialkyldithiophosphate

DECLARATION OF AUTHORSHIP

I, James Edward Booth declare that this thesis titled 'the use of electrostatic monitoring for additive and lubricant evaluation' is an account of the work carried out as part of the Surface Engineering and Tribology Group, Engineering Materials, School of Engineering Sciences, University of Southampton, UK, under the supervision of Prof. Robert JK Wood. The work presented in this thesis is my own, and has been generated by me as the result of my own original research.

No part of this thesis has been previously submitted for a degree at this university or any institution. Where works of others have been drawn upon appropriate referencing has been included in the text. Parts of the work presented in this thesis have been published prior to submission and a list of Journal and conference publications are given on the subsequent page.

Signed:

Date:

PUBLICATIONS

Many of the Chapters, particularly the experimental Chapters, have been presented at conferences, submitted for publication and published. Listed below are the publications and conference presentations which relate to work presented in specific Chapters.

Section 2.4
Booth JE, Harvey TJ, Wood RJK, Powrie HEG. Advances in Electrostatic Health Monitoring of Tribo-contacts. Conference proceedings of 50th IMechE tribology group anniversary conference: Surface Engineering and tribology for future Engines and Drivelines, 12-13 July, London, 2006.

Chapter 4
Booth JE, Harvey TJ, Wood RJK, Powrie HEG. Scuffing detection of TU3 cam-follower contacts by electrostatic charge condition monitoring. Presented at the 34th Leeds-Lyon Symposium on Tribology 2007 and accepted to Tribology International on condition of minor revisions.

Booth JE, Harvey TJ, Wood RJK. Monitoring Of Cam and Follower Wear. IMechE Mission of Tribology, 6th December, London, 2006.

Booth JE, Harvey TJ, Wood RJK, Powrie HEG. Monitoring of cam and follower wear by electrostatic charge detection. Poster presentation, RSC Additives: Applications for future transport 17-19 April, Hotel Russell, London, 2007.

Chapter 5
Booth JE, Nelson KD, Harvey TJ, Wang L, Wood RJK, Martinez JM, Powrie HEG. The feasibility of using electrostatic monitoring to identify diesel lubricant additives and soot contamination interactions by factorial analysis. Presented at the 32nd Leeds-Lyon Symposium on Tribology 2005 and Tribology International 2006;39:1564-1575.

Chapter 6
Booth JE, Nelson KD, Harvey TJ, Wood RJK, Martinez JG, Powrie HEG. Mini-traction-machine tests to assess the effect of base oil and additive interactions on surface charge and friction. Proceedings of the STLE/ASME International Joint Tribology Conference, October 22-24, 2007, San Diego, USA. IJTC2007-44317.

Chapter 7
Booth JE, Harvey TJ, Wood RJK, Nelson KD & Powrie HEG. Evaluation of the tribological properties of dispersant and friction modifiers within a simulated automatic transmission tribo-couple. Presented at the 34th Leeds-Lyon Symposium on Tribology 2007 and to be submitted to Tribology International.

Chapter 8
Booth JE, Nelson KD, Harvey TJ, Wood RJK, Powrie HEG. Evaluation of gear oil additives in a simulated manual transmission contact. Presented at the 34th Leeds-Lyon Symposium on Tribology 2007 and Submitted to Tribology International December 2007.

ACKNOWLEDGEMENTS

When first embarking on a PhD I was somewhat eluded into thinking that, as compared to a '*real job'*, I would have more time to concentrate on my career as a drummer. So I will start by apologising to my drum kit for 3 years of neglect. Secondly, I must acknowledge the driving force behind this thesis - without the stimulant of coffee and the relaxant of great red wine, this thesis would never have materialised. Thanks go to the coffee growers of Africa, South America and Hawaii and thank you fair-trade for making my coffee consumption ethical. I think over 10% of my annual income has been spent on red wine and for this I thank Dana Robbers and Martin Browne for their wonderful encouragement and teachings. If, three years ago, I knew what I know now, a PhD in viniculture and oenology would have probably been more suitable.

Although a PhD is designed to be the soul contributions of one individual, there are many people who have been of great help to me over the last three years and, as is customary, I would like to acknowledge them.

Supervision
The most instrumental people involved with the details of this thesis are the official and unofficial supervisors of Robert Wood, Terry Harvey and Ken Nelson. Robert's greatest trait is his encouragement (although sometimes under duress) of those interested in research and the fact that he values enthusiasm as much as intellect. Without this attitude I think it unlikely that I would be in this position today. For want of a better analogy, Terry is the *glue* that holds this department together. His knowledge in so many aspects of tribological laboratory work is second to none (although pipe fittings are not his strong point) and he has been an invaluable soundboard for ideas and concepts. I am grateful to the inspirational, sharp and quick working mind of Ken which is in stark contrast to my slow *'work-horse-like*' approach to research. Although on the face of it this difference in approach – along with the barrier that multiple languages provide, whether UK/US or Engineer/Chemist – may not have had the promise for success, I am extremely pleased with the way things turned out. I am sincerely grateful for Ken's advice and patience.

Industrial support
I am extremely grateful for Steve Stults' and Ken Nelson's belief in work I proposed as an inexperienced researcher at the beginning of the PhD programme. I am really impressed that they were willing to invest in what was a high risk project with a long term focus; they showed great vision and had more confidence than I did.

Internship
Without my two internships at Chevron Oronite I would never have been able to achieve a fraction of the work bound in this thesis. Indeed, the fact that three of five Chapters are based on work I conducted during my internships is a testament to this. The input and willingness of Chevron staff to help me to develop my own skills during my stay has significantly impacted on my personal development as a researcher. Steve and Ken were at the forefront of resolving many issues regarding my internship and, despite this, never complained or made me feel like a burden. They allowed me to get on with my research agenda, complications aside, and for this I am truly grateful.

I would like to thank Paula Rogers for blending oils, running analytic studies, shipping equipment and samples – the fact that she did this for a *'young-up-start'* at the drop of a hat and without quibble is very endearing. Although statistics was the source of many headaches, it has given great strength to my research. I am indebted to Jo Martinez for her role in this and for not getting annoyed at the constant request to re-analyse numerous permutations of results. Thanks also go to Sheila Yeh for her invaluable help with XPS analysis and for not getting irritated by the constant badgering for results. Thank you Vivek Palekar and his tribology group for making me feel welcome and for allowing me to use your equipment, and to Elaine Yamaguchi for allowing me to use her Tribometer. Without Vivek and Elaine's co-operation, no testing would have been possible. I would also like to thank Jim Robbers for his help at

work, for being a useful source of information as-well-as being willing to help and offer advice whenever necessary.

Other members of the Chevron team who had a great impact on my work include: Walter Andaluz, Tom Balk, Angelo Bufalini, Juan Buitrago, Nancy Egan, Jim Harrison, Erin Kerrigan, Trevor Miller, Frank Plavac, Casey Stokes, Patrick Williams and James Wilson. This is but a fraction of people who made my stay and working environment a pleasurable one.

Without Honor Powrie from GE Activation, who supplied sensors and software, the work may never have had the capacity to be so novel. Thanks Honor for your technical support and monthly lunch!

University of Southampton
There are many other members of staff at the University of Southampton who have played an important role in my PhD. In particular: Dawn Attree, Robert Barnes, Alistair Clark (who help me to obtain great SEM micrographs) Sonya Davie and Steven Pilcher. I am also so very appreciative of my fellow graduate students: Adam Briscoe, Jonathan Jeffers, Suk Kinch, Lucy Knight, Polly Sinnett-Jones, Mandar Thakare. I would also like to specifically mention Lilly Chambers, who was a great companion to go through the process of an engineering PhD programme with and together we created a form of *'academic bitch club'*, which was cleansing for the soul.

Friends
There are many people without whom I would have been unable to achieve a fraction of the things I have during the last three years and I have tried to mention them specifically. Four years ago, a PhD never even featured on my radar and I must acknowledge those people whose influence equipped me with the skills and frame of mind to tackle the steep learning curve that was to follow. Thank you to Cliff Wilson (Scouts & Reltek Engineering), Bruce McFarlane (Jessamine Motor Co), Mick McFarlane (Jessamine Motor Co), David Warner (St. Helen's School), Robert Hawks (Verulam School) and Colin Parfree (Maths and Physics Tutor).

I apologise to all the friends that I have neglected over the past 3 years. I hope to mend bridges very soon. A special thanks to Ollie Bevington and Martin Browne, who have been a great support and who have never grumbled during my self-centred conversations/monologues. Thank you also to Anne Roques for keeping my feet on the ground with the continual reminder that whatever I have achieved in this PhD, an IMechE prize is not on the list.

Thanks to Dana, Jim, Pat, Cooper, Sydney and Smokey for being so generous and hospitable to the strange British chap that I am. They made my personal life in California immensely enjoyable. Thank you also to Roseanna, who kept me highly amused and Richard who so kindly took me on a 24hour trip to Hawaii. Thank you Dana for being my social secretary and Jim for letting me play with your cool toys (I mean essential items). Also Pat, thanks for being such a great house mate and for having me to stay… so many times! Without the support of these five people, the level of my achievements would have undoubtedly suffered. I can not believe how lucky I am to have met you young *'old farts'*!

Family
I would like to extend my deepest gratitude to my family: Brian, Carolyn, Timothy, Anthony and Topper. Your willingness to give me support and freedom to develop independently has helped me to be the ambitious person that I am. Thanks Dad, for trying to keep me grounded and for promoting rational thinking and for teaching me the importance of perspective. Mum, I am really grateful to you for uniquely balancing subtle presence with unwavering support. You have been invaluable – as too have the care packages. Although something of a cliché, thanks dear Topper for being the only one to ever really understood me.

Jessica, it was extremely hard to write your acknowledgement section and it is because you impact on my PhD was not the result of just one thing; it is a case that the sum of all the parts is greater than the individual components. Don't get me wrong I appreciate, you: bring breakfast in bed, making my lunch, supplying doughnuts, washing everything, chauffeuring, being a constant source of amusement, for listening to my ranting, reading my work, offering a distraction and for letting me squat with you for ~~a~~

~~couple of months~~ over half a year (oooops). I think my mental health would be in a far worse state if it were not for your fantastic support. Thank you for everything, and then some. I look forward to being able to provide some *'TV psychology'* to help your thesis writing.

1 INTRODUCTION

1.1 MOTIVATION

The 20th century saw the greatest advances in technology since civilisation began and oil was the great enabler for this rapid progress. The century was nearly half over when the nuclear age began, and more than half over when the computer revolution swept the world [1]. The development of both technologies may have never developed or may have taken much longer to develop if oil was not available to provide fuels for: heating, lighting, power and transportation, and lubricants for almost any moving mechanical component. But as oil has created the greatest growth in technology it has also meant that the world has become dependent on it. As oil stocks dwindle and more is known about the harmful effect that burning oil based products have on the environment, so countries and industries involved in the supply and consumption of oil are under greater political and economic pressure. The automotive sector is under continued media and public scrutiny for its major role in consuming oil and fuel and the effect this has on the environment. Additive chemists and lubricant formulators, for their part, are facing challenges of producing lubricants which increase fuel economy, reduce environmental impact and allow service intervals to be lengthened, while keeping wear to a minimum. Lubricants must conform to national and/or international standards, such as the Peugeot TU3M valve-train wear test [2], to assess the antiwear performance of a lubricant. This approval process is extremely expensive; the rate at which classifications are superseded is increasing (particularly driven by environmental targets), and as a consequence, lubricant development costs are escalating [3]. This thesis assesses whether electrostatic charge monitoring can be used to aid additive chemists and lubricant formulators in the lubricant development process.

1.2 CONDITION MONITORING AND THE ORIGINS OF ELECTROSTATIC MONITORING

The development of condition monitoring techniques was originally driven by the need to carry unscheduled maintenance to prevent failure of machine components. More recently, condition monitoring techniques have been used as a research tool to understand contact degradation, more specifically wear mechanisms. Electrostatic sensing was originally developed for detection of electrostatic charge associated with wear debris in the gas path of jet engines and gas turbines [4-6] which was correlated with a specific component problem such as turbine blade rub. The early success, of electrostatic charge detection as a condition monitoring technique, led to the deployment of electrostatic sensors on a wide range of lubricated contacts. Experiments over the last 10 years at the University of Southampton have covered fundamental, bench and industrial levels, with the aim of de-coupling specific aspects relating to

charge generation within tribo-contacts to investigate if surface charge can be linked to wear/friction processes.

During lubricated wear studies it was noted that charge signals, generated by simple pin-on-disc contacts, differed between a base oil and a fully formulated lubricant [7], could not be explained by the level of wear alone. In addition oxidational wear was successfully monitored by electrostatic sensors and revealed the oxidation-delamination-reoxidation mechanisms [8], due to the varying work functions on the surface that result at different stages of the wear mechanism. Differences in work function drives contact potential difference (CPD) and thus charge separation and variation in surface charge density on worn surfaces. Work over the last 3 years has been based on the hypothesis that if electrostatic monitoring can detect the growth and removal of a chemical film such as an oxide, then there is the potential to monitor the growth and/or breakdown of a physically or chemically adsorbed additive tribofilm.

1.3 AIM

The aim of the work carried out during this PhD was to assess whether electrostatic monitoring could be an insightful technique to aid additive screening/development to optimise tribological contact performance.

Objectives

To achieve this, a number of objectives were set, namely to:

- Successfully install a electrostatic charge sensor to monitor the;
  - Cam surface charge in engine valve-train contacts.
  - Disc surface charge in pin-on-disc tribometers.
- Assess the sensitivity of electrostatic monitoring to wear and lubricant chemistry.
- Relate electrostatic charge signals to additive-surface interactions.
- Relate electrostatic surface charge to additive-contaminant and additive-additive interactions.
- Relate electrostatic surface charge to additive tribofilm chemical composition.
- Seek electrostatic surface charge signatures associated with additive tribofilm kinematics (film formation, removal and replenishment).

1.4 THESIS STRUCTURE

The work presented in this thesis is multi-disciplinary, drawing on understanding from three scientific research areas: automotive tribology, lubricant chemistry and electrostatic condition monitoring. The *Literature review* Chapter starts with *Surfaces and tribology*, which introduces the tribological concepts pertinent to the experimental work presented in this thesis. The *Automotive tribology* Section draws on the concepts identified in the *Surfaces and tribology* Section and applies them to automotive contacts. The drivers affecting automotive power-train design and how these affect the tribological performance

(lubrication, friction and wear) are discussed for: the engine valve-train, manual transmission synchroniser contacts, and automatic transmission frictional clutch plates. Environmental legislation and consumer requirements are influencing automotive engine and power-train design, and as such are putting greater demands on the lubricant. The *Lubricant chemistry & surface interaction* Section examines how lubricant chemists formulate oils, with additives, to minimise friction and wear in engines, while keeping the engine clean for extended drain intervals. The need for technology, such as electrostatic monitoring, to assist in the lubricant development process is identified. *Advances in the electrostatic health monitoring of tribo-contacts* are discussed, with specific reference to charge generation mechanisms within the tribo-contact and the factors affecting these charge mechanisms.

The experimental work presented in this thesis discusses the results from the first ever deployment of electrostatic sensors in a cylinder head (to monitor cam wear), and on a PCS Instruments Mini-Traction-Machine. Testing was carried out on a variety of contact materials, using a range of additives. The *Experimental Equipment and Procedures* Chapter (Chapter 3) discusses the rational behind the test: procedure employed, apparatus, conditions, material and additives used for the experimental studies.

The experimental studies discussed in this thesis are the first to use electrostatic sensors to help understand additive-surface behaviour. There were 5 discrete experimental programmes.

Chapter 4 presents work from experiments where electrostatic sensors were used to monitoring the cam/follower contact in a TU3 motorised engine. Mild wear tests, which used a fully formulated oil and a oil starvation test, were carried out to try to decouple the charging mechanism generated during a carbon black contaminated oil test and identify charge features associated with the transition from mild wear to scuffing.

Chapter 5 details the first investigation into the use of electrostatic monitoring to aid understanding of additive-additive and additive-contaminant interactions. An additive and contaminant matrix study was carried out, on a in-house pin-on-disc tribometer, to investigate the affect additives and contaminant have on electrostatic charge and wear.

Chapter 6 describes work designed to understand charge, friction and wear behaviour of six single additive types in three different base oils. A full factorial matrix was run, to minimise issues of de-coupling more than one variable. Correlations between particular additive-surface interaction, whether physical and chemical adsorption, and electrostatic surface charge are made. For the first time electrostatic charge features are correlated with tribofilm thickness and elemental composition (by x-ray photoelectron spectroscopy (XPS) analysis) and tribofilm kinematics.

The final two Chapters (7 & 8) explore the deployment of electrostatic sensors on non-ferrous surfaces and explore additive-additive interactions in great detail. These studies investigated whether electrostatic monitoring can inform the interaction of binary additive systems on the dissimilar tribo-couples of brass-steel to simulate manual transmission components, and cellulose based friction material-steel to simulate automatic transmission clutches. These are the only studies to have implemented electrostatic monitoring on brass-steel and paper-steel contacts. Both studies cross-correlated charge signals and tribofilm composition.

2 LITERATURE REVIEW

This literature review aims to cover Surfaces and tribology, lubricant chemistry and condition monitoring concepts, on which the experimental work in this thesis is based. This literature review details current understanding and highlight areas this thesis sought to advance.

2.1 SURFACES AND TRIBOLOGY

This part of the literature review aims to review specific tribological background relevant to subsequent literature and experimental Chapters. It is the foundation on which, the more industrially applied, *Automotive tribology* section (see Section 2.2) is based. This Section starts with the important concepts for tribo-contacts, such as contact pressure, which is the driver for friction and wear, the two most important parameters for tribological systems presented in this thesis.

2.1.1 CONTACT MECHANICS

2.1.1.1 Hertzian contact pressure

The contact of two curved bodies can be described initially as a single point or a line contact. Even under the slightest load, localised elastic deformation around and within the point or line of contact will occur. Making some assumptions (see reference [9] for details of assumptions), the method for determining the contact pressure was first described by Henrich Hertz (1881). Figure 1 presents schematics of a point and line contact, and the geometric parameters required to calculate the contact area and pressure. The contact geometry and pressure for these two types of contacts are given by eq (1)-(10) in Table 1.

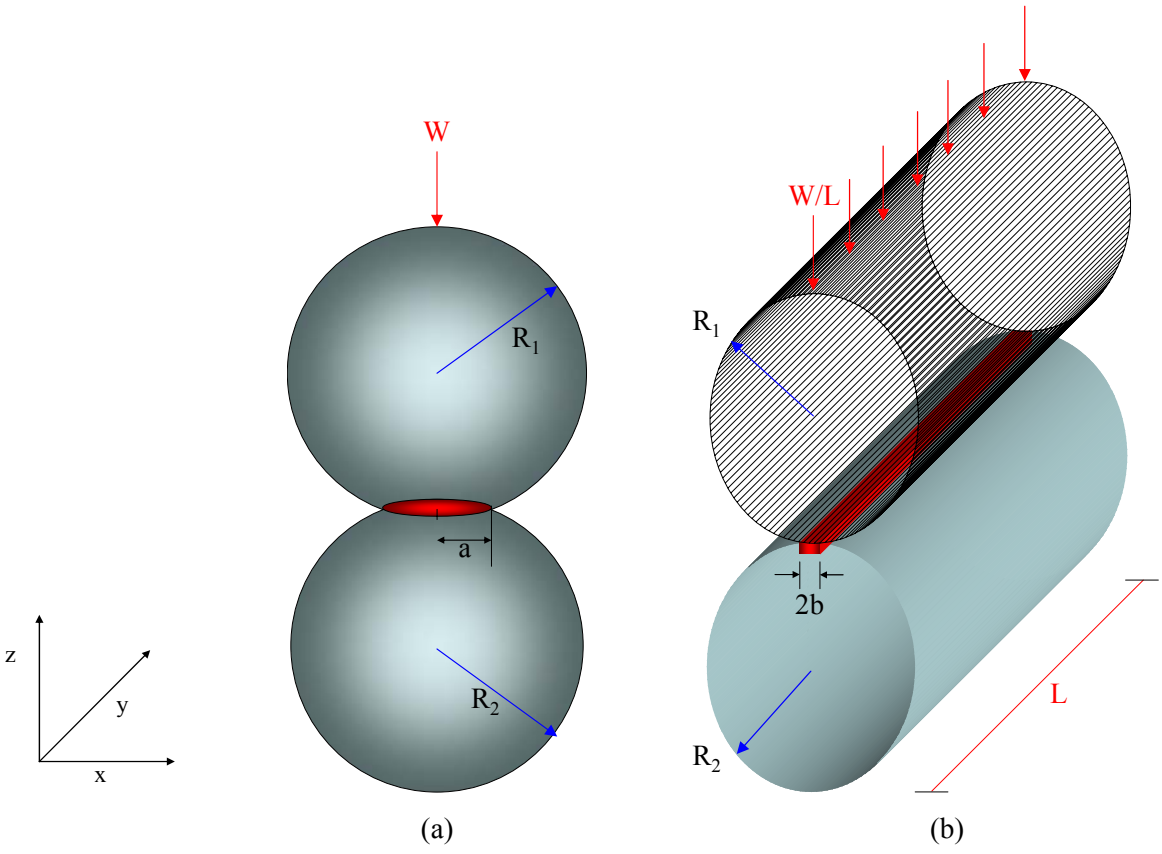

Figure 1. Schematic of a (a) point contact and (b) line contact.

	Line contact – Parallel Cylinders	Circular point contact – Spheres
Dimensions of the contact	$b = \sqrt{\frac{4WR^*}{L\pi E^*}}$ (1)	$a = \sqrt[3]{\frac{3WR^*}{4E^*}}$ (2)
Relative radius of curvature, R^*	$\frac{1}{R^*} = \frac{1}{R_1} + \frac{1}{R_2}$ (3)	
Reduced Modulus, E^*	$\frac{1}{E^*} = \frac{1-\upsilon_1^2}{E_1} + \frac{1-\upsilon_2^2}{E_2}$ (4)	
Contact pressure distribution, P	$P(x) = P_0\sqrt{1-\frac{x^2}{b^2}}$ (5)	$P(r) = P_0\sqrt{1-\frac{r^2}{a^2}}$ (7)
	Where $x = \pm b$ (6)	Where $r^2 = x^2 + y^2$ (8)
Mean contact pressure, P_m Max contact pressure, P_0	$P_m = \frac{\pi P_0}{4} = \frac{W}{2bL}$ (9)	$P_m = \frac{2P_0}{3} = \frac{W}{\pi a^2}$ (10)

Table 1. Contact geometry and contact pressure for line and point contacts.

Figure 2 shows the contact pressure distribution, applicable for point of line contacts. The pressure distribution is elliptical with a maximum value of *Po* at the axis of symmetry (*x=0* or *r=0*). The contact pressure falls to zero outside the area of contact.

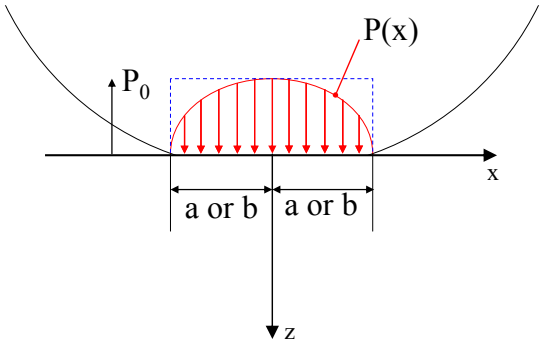

Figure 2. The pressure profile developed when two spheres or cylinders are pressed together.

The majority of automotive contacts, including the cam and follower, can be simplified to model line contacts. For research purposes these automotive components are often simulated, in terms of maximum contact pressure, by Pin-on-Disc (PoD) tribometers. The PoD Tribometer can be run with a point contact, where the radius of the flat disc is taken as $R_2 = \infty$.

2.1.1.2 Shear stresses & onset of yield

There is a value of W for which the material of the weaker object (cylinder or sphere) starts to deform plastically rather than elastically. To estimate this critical value, W_y' (load at which yield of ductile metals occurs) the *Tresca* maximum shear stress criterion or the *von Mises* strain energy criterion is typically

used. Tresca criterion describes that a material under a multi-axis state of stress will yield when the max shear stress reaches some critical value. The maximum shear stress for static Hertzian line and point contacts subjected to normal loading occurs on the axis of symmetry ($x = 0$); contacts are considered to produce a uniaxial tensile stress. At the moment yield occurs one principal stress will be equal to the yield stress ($\sigma_1 = Y$) and the other principal stresses will be zero ($\sigma_2 = \sigma_3 = 0$). This condition defines the critical value of the shear stress at which yield occurs (see eq (11)). It should be noted that this value is half the value of the tensile yield stress (see eq (12)).

$$\tau_{\max} = \frac{\sigma_1 - \sigma_3}{2} \qquad (11) \qquad\qquad \tau_{\max} = k = \frac{Y}{2} \qquad (12)$$

The maximum shear stress, the depth z that $\tau_{\max}$ occurs, the load required for yield, and contact pressure at first yield for steel point and line contacts are given in Table 2.

	Line Contact		Point Contact	
Maximum sheer stress	$\tau_{\max} \approx 0.30P_0$	(13)	$\tau_{\max} \approx 0.31P_0$	(14)
Depth of maximum shear stress	$z = 0.78b$	(15)	$z = 0.4a$	(16)
Load for first yield	$W_Y' = \frac{\pi R^* (1.67Y)^2}{E^*}$	(17)	$W_Y = \frac{\pi^3 R^{*2}}{6E^{*2}}(1.60Y)^3$	(18)
Peak contact pressure at first yield	$(P_0)_Y = 3.3k = 1.67Y$	(19)	$(P_0)_Y = 3.2k = 1.60Y$	(20)

Table 2. Yield parameters for line and point contacts[*].

When yield initially occurs beneath the surface, the plastic region is still totally surrounded by a region in which the stresses and strains are still elastic; changes in shape are therefore small. If the normal load is increased further, the plastic zone grows until eventually it breaks out at the free surface, known as the state of full plasticity. The hardness of a material is quantified by measuring the plastic indentation of a material. Therefore the hardness, *H*, may be related to the material yield stress by eq (21). Thus the point at which yield will occur can be approximated to eq (22):

$$H \approx 2.7Y \qquad (21)$$

$$P_m > 0.4H \qquad (22)$$

The hardness of TU3 cam and followers range between 600-800 H_v. This equates to a mean contact pressures at which yield occurs (P_m) of 230-380 MPa and a peak contact pressure at first yield of between 350-480 MPa. This is not insignificant when considering the reported maximum contact pressure for this contact is 680MPa.

[*] These equations have been derived by assuming contacts are steel and have a Poisson's ration of 0.3

2.1.2 FRICTION

Although the work remained unpublished for several centuries, Leonardo da Vinci carried out scientific studies around 1500 A.D. and was first to define the coefficient of friction (COF) as a ratio between the friction force and normal force. The laws of friction were rediscovered by Guillaume Amontons in 1699 and later Leonard Euler (1750) who derived an analytical definition of friction using the symbol μ [10].

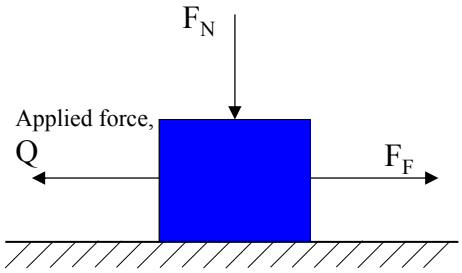

Figure 3. Schematic showing the forces involved in defining the coefficient of friction.

This is the basis of the COF, which is defined as the ratio of the frictional force between the two bodies and the normal force (pressing them together) (see Figure 3). In practice, the common causes of frictional force are adhesion, abrasion and deformation (see Section 2.1.4.2). COF is shown in Eq (23), and is a dimensionless scalar value.

$$\mu = \frac{F_F}{F_N} \qquad (23)$$

The definition of friction by Charles Augustin Coulomb (1785) is the most commonly used today. Coulomb confirmed the results of the previous investigations, but in addition found that friction is independent of sliding velocity. He also made a clear distinction between static and dynamic friction.

If a force (Q) is applied tangentially to one of the contacting bodies in addition to the Normal force (F_N) then the bodies will not move if:

$$Q < \mu F_N \qquad (24)$$

If Q increases such that:

$$Q > \mu F_N \qquad (25)$$

then sliding will occur. Static friction (μ_S) is the maximum friction force (F_F) that the surface can sustain without relative motion to the normal force (F_N). Dynamic friction (μ_D) is the resistance force encountered when the surfaces in contact move relative to each other. This is actually an over simplification; Dokos (1946) and Rabinowicz (1951) showed that the static COF is time dependant and that the dynamic COF is dependant on the sliding velocity [11]. In addition, the general relationship between normal force and frictional force is not exactly linear so the frictional force is not entirely

independent of the contact area of the surfaces. This relationship is a function of scale – a single asperity in contact is dependent on area. However, the strength of the approximation is its simplicity and versatility. In generally the Coulomb approximation is an adequate representation of friction for the analysis of many macro physical systems found in automotive engine and transmission.

The COF is a useful property of tribological systems as it represents the energy loss caused by friction. In the majority of cases where high efficiency is required, particularly when the source of energy is from fossil fuels (such as IC engines), friction needs to be kept to a minimum. In some applications, however, friction is necessary and instead of reducing friction a high and well defined level of friction is required; such applications are brakes, clutches and synchronisers (Table 3 shows the friction values of some of the material pairs used for these applications). The benefit of using a lubricant to reduce friction can be seen in Table 3. The friction of a fluid (e.g. lubricant) is termed traction coefficient; because the work presented in this thesis assesses lubricant performance, under conditions where there is a degree of contact between two solid surfaces, COF is the terminology used throughout. Additives are used to change the friction properties of the bulk materials through adsorption and formation of additive-surfaces layers within the contact (see Figure 8 (e)). These films are known as tribofilms. There are different mechanisms by which the tribofilms ensure low friction. These films can also offer wear protection.

Contacting Surface	Static Friction, μ_S	Dynamic Friction, μ_D
Steel on Steel (dry)	0.6	0.4
Steel on Steel (greasy)	0.1	0.05
Brass on Steel (dry)	0.5	0.4
Brake lining on cast iron	0.4	0.3

Table 3. Typical values of coefficient of friction (COF) for commonly found material pairs [12].

2.1.2.1 Stick-slip

Stick-slip is the alternation of two surfaces sticking to each other and sliding over each other, with a corresponding change in the friction force. Typically, the static COF between two surfaces is larger than the dynamic COF (see Table 3). If an applied force is large enough to overcome the static friction, then the reduction of the friction to the dynamic friction can cause a sudden jump in the sliding velocity (slip). Stick occurs when the applied force decreases to a point at which it becomes insufficient to overcome the dynamic friction. The source of the shudder phenomenon comes from a friction characteristic that is velocity dependent, therefore the shudder performance of a lubricant or wet-friction material is typically analysed using a friction vs. velocity (μ-V) graph.

2.1.3 LUBRICATION REGIMES

Successful separation of two surfaces requires a convergent geometry into which viscous fluid is entrained by the relative motion of the solids (see Figure 4). A pressure is generated which tends to push the faces of the wedge apart and it is the integrated effect of this pressure distribution within the fluid that balances the normal load on the bearing. Reynolds was the first to establish a relationship between the velocity of sliding, the geometry of the surface, the properties of the lubricant and the magnitude of the normal load the bearing can support. Despite several assumptions (e.g. fluid incompressibility, Newtonian viscosity (see Section 2.1.5.1)), constant viscosity, negligible inertia, rigid/solid surfaces, constant pressure through thickness of film and smooth solid surface) this one dimensional solution (see eq (26)) is applicable to a wide range of technologically important problems.

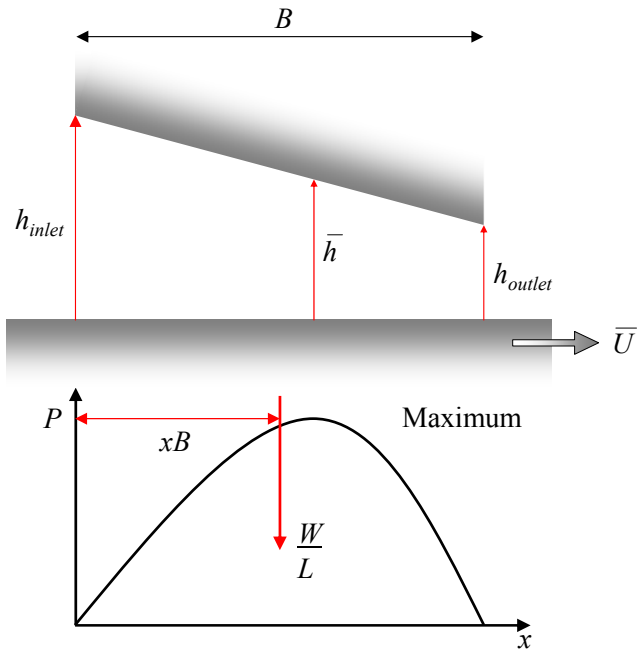

Figure 4. *The convergent geometry that viscous fluid is entrained into by the relative motion separates the two surfaces through the generation of pressure which balances the normal load.*

$$\frac{dp}{dx} = 12\eta\bar{U}\frac{h-\bar{h}}{h^3} \tag{26}$$

Reynolds did develop a solution of the problem in 2 dimensions to analyse short or narrow bearings. Reynolds 2-dimensional solution with the half Sommerfeld boundary conditions (pressure distribution through the contact) applied leads to an equation for the non-dimensionalised bearing load (W^*) (see eq (27)). Under sufficiently high contact loads, Reynolds equations suggest that unacceptable surface damage would result. However, in practice many mechanical components such as gears run quite satisfactorily. The reason for the difference is that Reynolds solution does not take into account the increase in oil film thickness which arises from the thickening of the oil within the contact due to the localised high pressures.

$$W^* = \frac{Wh_c}{\eta R^* L \overline{U}} = 4.89 \tag{27}$$

The one dimensional Reynolds equation based on continuity of volume flow (see eq (26)) can be combined with the Barus equation (see Section 2.1.5.3, eq (41)) which describes variation between lubricant viscosities with pressure. Solving these two equations results in the reduced Reynolds equation for piezoviscous (variable viscosity) fluids (see eq (28)). This is similar to the Reynolds equation for constant viscosity, but the pressure is replaced by a variable known as the pressure viscosity index (α).

$$h_{\min} = 1.66\left(\alpha \eta_0 \overline{U}\right)^{2/3} R^{*1/3} \tag{28}$$

Having accounted for local increases in lubricant viscosity under high contact loads, how machines operate under severe contact conditions with little damage is still not completely explained. The reason for the discrepancy is that Reynolds assumes that the surfaces are solid and ridged. This is not the case, even under light loads, surfaces will deform. The elastic deformation of surfaces plays an important role in providing beneficial contact geometries to generate of the all important hydrodynamic film.

There is no complete analytical solution to describe the contribution of surface elastic deformation to fluid film thickness, but Grubin [13] and many researchers thereafter, assumed in the presence of a fluid the elastic deformation of solids are exactly the same as the dry Hertzian contact geometry and pressure distribution. This simplification implies that the numerical film thickness will be governed by the shape of the convergent wedge at the entry of the contact. The linking of hydrodynamics and solid mechanics spawned the field of research known as elasto-hydrodynamic lubrication (EHL).

$$\frac{\overline{h}}{R^*} = 2.08\left(\frac{\eta_0 \alpha \overline{U}}{R^*}\right)^{8/11}\left(\frac{E^* R^* L}{W}\right)^{1/11} \tag{29}$$

With some calculus, algebra and substituting in the Hertzian contact geometry Ertel and Grubin arrived at a relationship with non-dimensional groupings (see (29)). This analysis assumed that the surfaces have the rectangular deformed shape of an unlubricated Hertzian contact, but set apart by distance, $\overline{h}$. However, eq (26) shows that the film profile is more complicated than the rectangle of constant film thickness, $\overline{h}$. If this was the case then the pressure gradient would have to be positive throughout; there would be a build-up to a high pressure at the inlet, remain high through the Hertzian region and then increase further in the outlet. Clearly this is not possible as the pressure at the exit must fall to ambient pressure. To re-establish ambient pressure at the exit of the contact there must be some local constriction of the film, where the film thickness falls below $\overline{h}$, this is known as the minimum film thickness $h_{\min}$. Numerical solutions have shown that, just prior to the point of constriction there exists a pressure spike, which has a maximum value considerably greater than the maximum Hertzian contact pressure [14] (see Figure 5 (a) & (b)). For point contacts the constriction of the oil film and associated pressure spike towards the exit of the contact also extends around the side of the contact forming a 'horse-shoe' shaped constraint [15,16] (see Figure 5 (c)).

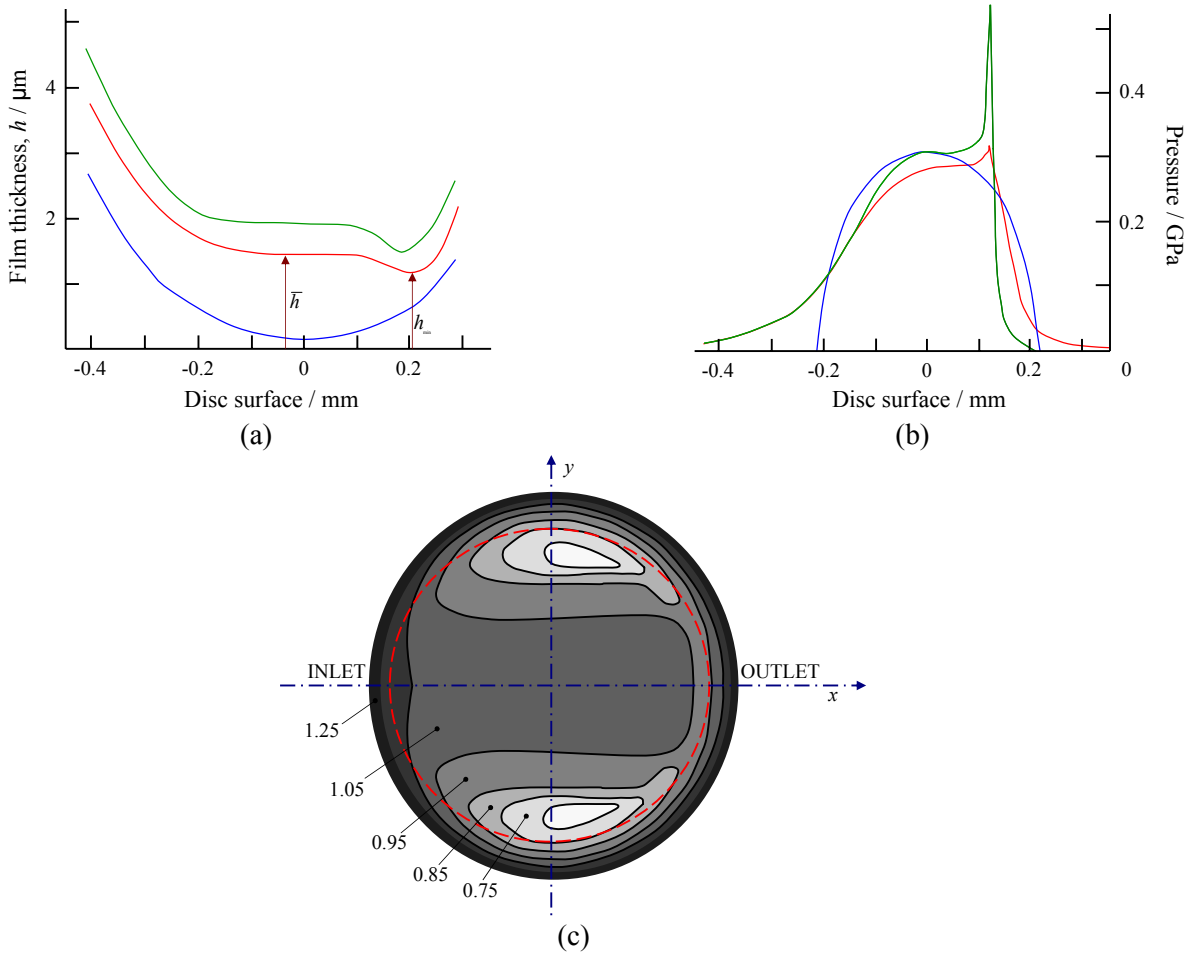

Figure 5. *Comparison between calculated (green) and measured (red) (a) film thickness and (b) pressure distributions in elasto-hydrodynamically lubricated contacts; Hertzian semi-ellipse is shown in Blue [14]. (c) elasto-hydrodynamically lubricated circular point contact film thickness contours in which the dotted line is the Hertzian dry contact area. Figures are fractions of the central value [17].*

The problem with the Ertel and Grubin eq (29) was that the localised film constriction was not taken into account and the non-dimensional groupings do not give any insight into the physical significance of the contact. Dowson and Higginson's pioneering work [18,19] developed an equation for the minimum film thickness with insightful dimensionless groupings. The equation is split into a load parameter, $W/(2E^*R^*L)$, a speed parameter , $\overline{U}\eta_0/(2E^*R^*)$, and a material (oil and surface) parameter, $2\alpha E^*$, all of which are equated to the minimum film thickness normalised by the reduced radius. A semi-empirical power law equation for point and line contacts was developed (see eq (30) & (31) respectively).

$$\text{Line contact: } \frac{h_{\min}}{R^*} = 2.65\left(2\alpha E^*\right)^{0.54}\left(\frac{\overline{U}\eta_0}{2E^*R^*}\right)^{0.7}\left(\frac{W}{2E^*R^*L}\right)^{-0.13} \qquad (30)$$

$$\text{Point contact: } \frac{h_{\min}}{R^*} = 1.79\left(2\alpha E^*\right)^{0.49}\left(\frac{\overline{U}\eta_0}{2E^*R^*}\right)^{0.68}\left(\frac{W}{2E^*R^{*2}}\right)^{-0.073} \qquad (31)$$

The theories of EHL, discussed thus far, have assumed that the surfaces are perfectly smooth and therefore, in theory, as the load increases so the film thickness reduces without any limits. However, in practice, surfaces under a certain load will begin to show signs of wear and failure may result. It is intuitive that wear is dependent on the ratio (designated lambda, λ) of minimum film thickness to combined surface roughness (see eq (32)) and Figure 6).

$$\lambda = \frac{h_{\min}}{\sqrt{R_{q1}^2 + R_{q2}^2}} \qquad (32)$$

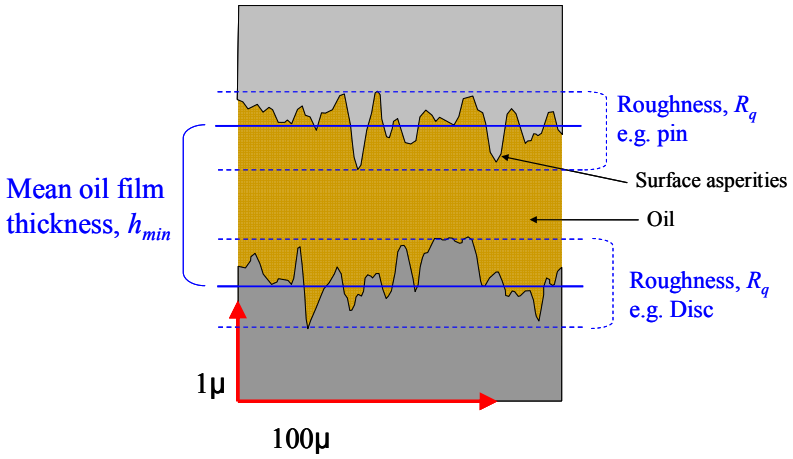

Figure 6. The film thickness between two rough surfaces.

Stribeck carried out a great number of experiments on bearings and plotted the results against two non-dimensional parameters; μ versus the group $\eta\omega / p_n$ (Sommerfeld number). Using dynamic similarity, Stribeck's data led to a single curve. This is a powerful tool for enabling extrapolation of performance for a given machine element (of any dimension), which is based on non-dimensional groupings. The lambda ratio (λ) over the years has replaced the Sommerfeld number because it is more insightful, in terms of the extent of surface interaction between the two bodies. The characteristics of the single curve lead to identification of regimes (see Figure 7). Further details can be found in [20].

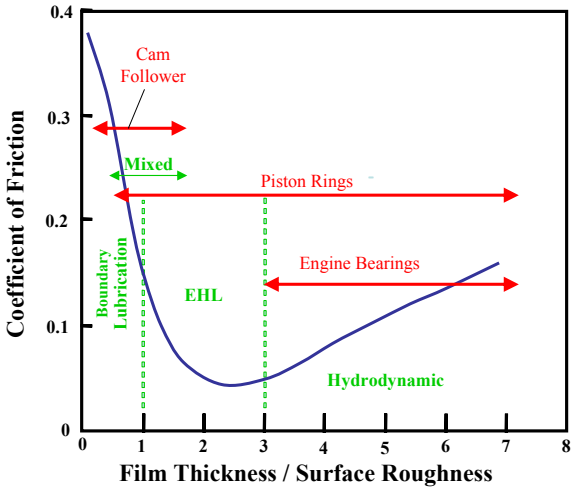

Figure 7. *Modified Stribeck diagram which describes the friction levels of contacts with different film thickness to surface roughness ratios (lubricant regimes); with the lubricant regimes of the major IC components: cam & follower, piston rings and engine bearings, superimposed.*

The contact conditions for each lubricant regime are described below;

- **Hydrodynamic lubrication** $\lambda>3$

  The two surfaces are completely separated by a fluid film. Generation of pressures in the film carries the load. The main characteristic of the fluid is the dynamic viscosity.

- **Elastohydrodynamic lubrication** $1<\lambda<3$

  In theory the surfaces are separate, but due to the thinner oil films the contact becomes far more concentrated, resulting in elastic distortion of the surfaces. The effect of pressure on dynamic viscosity is influential (pressure viscosity index).

- **Mixed or partial lubrication** $0.5<\lambda<1.5$

  As inferred by the name this region is a mixture of the characteristic of Elastohydrodynamic and Boundary in which a fluid contact has overall load bearing capacity and some degree of asperity contact between surfaces (assuming no tribofilm has formed).

- **Boundary** $\lambda<1$

  Under these conditions there is a great deal of asperity contact and the lubricant exhibits minimal load bearing capacity. Within this range of operation the bulk properties of the fluid, such as its density and viscosity, are of relatively little importance, while its chemical composition and action of thin surface tribofilms, as well as that of the underlying metals or substrates, will be important to the performance.

  Friction can increase substantially with the transition to boundary conditions, perhaps by as much as two orders of magnitude over the minimum value which occurs within the fully hydrodynamic regime.

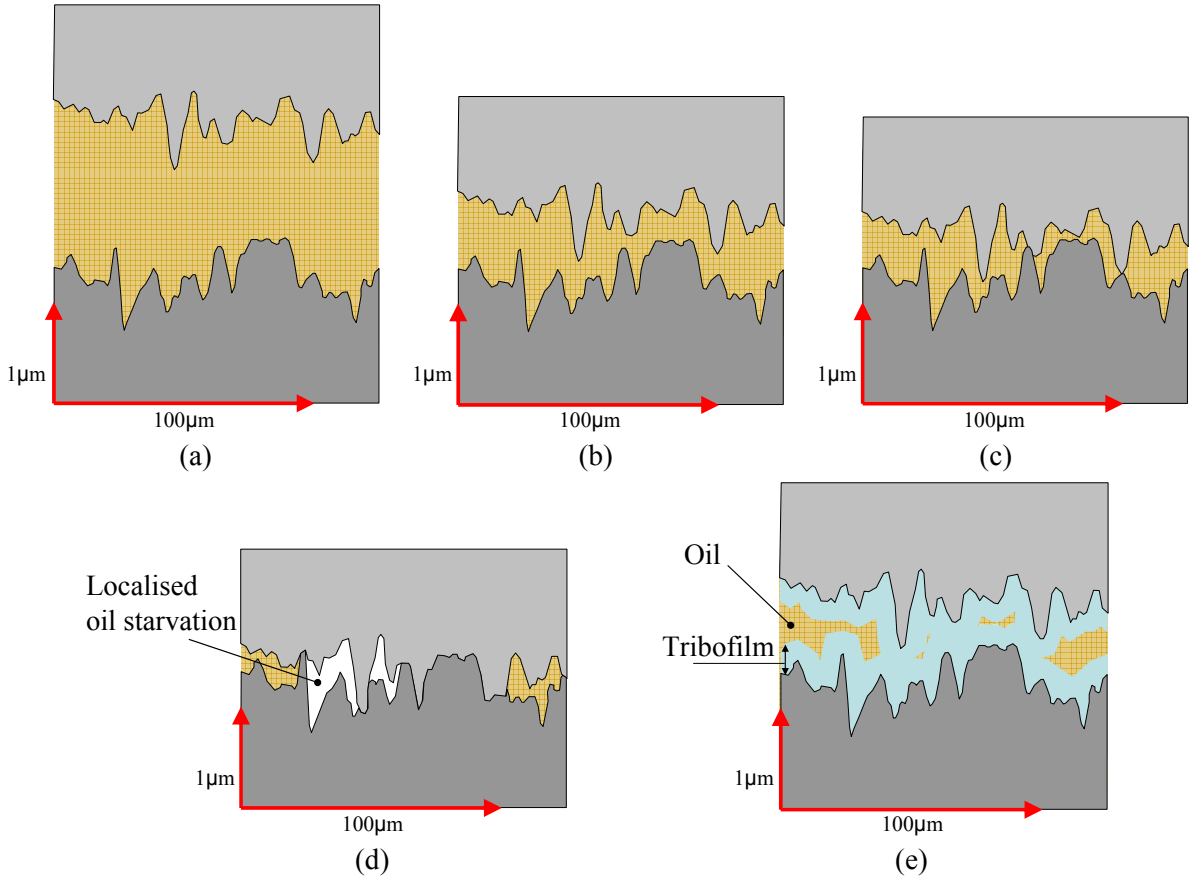

Figure 8. *Schematics of lubrication regimes: (a) hydrodynamic, (b) elastohydrodynamic, (c) mixed, (d) boundary and (e) boundary with tribofilm.*

The obvious conclusion from the Stribeck diagram is that in order to achieve minimal energy loss, components should operate under elastohydrodynamic lubrication, because this region produces the lowest friction. Indeed, the promotion of elastohydrodynamic lubrication in internal combustion (IC) engines, through design and surface modifications, has been reported in [21,22]. However, the slightest change in contact conditions (e.g. oil temperature, surface roughness), can result in lubrication conditions going from EHL to boundary.

2.1.4 WEAR

Wear is the progressive damage, involving material loss that occurs on the surface of a component as a result of its motion relative to the adjacent working parts. Although this definition does not strictly cover mechanisms such as corrosive wear and erosion, it is applicable for describing the general grouping of wear mechanisms which occur in the power-train. Wear is the almost inevitable companion of friction [9]; yet the relationship between friction and wear is not linearly dependent. Figure 9 shows the specific applications which demand certain levels of friction and wear. The automotive market is driven to increase fuel efficiency by reducing the friction caused by the lubricant and by increasing manufacturing precision. This has reduced component clearances. Both encourage smaller film thickness, but these will

have a tendency to increase wear. This problem is tackled by changes to engine design, material selection, surface finish and lubricant formulation.

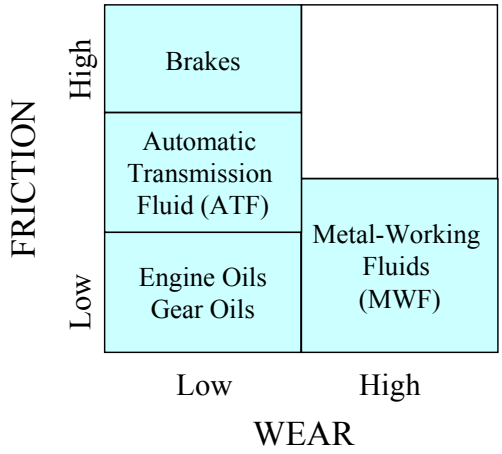

Figure 9. The friction and wear demands for different systems.

2.1.4.1 Component life

The wear during a component's life can be split into idealised regimes of running-in, mild wear and severe wear (see Figure 10). During running-in the wear rate is often initially quite high, but as prominent surface asperities are lost (or flattened) the surfaces become smoother (conformal matting of surfaces reduces effective load) and the wear rate drops off. During the running-in process both abrasion and adhesion occur simultaneously. Once running-in is complete, a period of low-wear-rate (mild wear regime) is maintained. Under mild wear conditions there is little metallic contact between the two lubricated surfaces, occasionally extremely small wear debris is produced (typically only 100nm diameter). The resulting surfaces are smoother than the original. For longer durations fatigue processes become important due to the cyclic loading nature of lubricated mechanical components. Fatigue can produce cracking, pitting and spallation which will roughen the surface and accelerate other wear processes such as abrasion and adhesion.

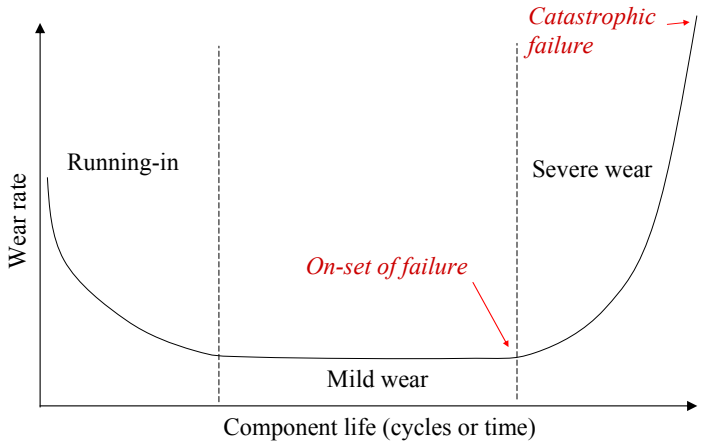

Figure 10. Idealised component bath tub type curve describing the wear rate.

2.1.4.2 Wear mechanisms

There are four basic wear mechanisms that are found in the automotive power-train: adhesive wear, abrasive wear, surface fatigue and tribochemical wear.

Adhesive wear is the localized welding of asperities of two solids moving relative to one another. The asperities of two surfaces in relative motion come into contact with each other and plastically deform. Due to the high localised pressure and temperature in the contact, some of the asperities weld together. Further motion causes plastic shearing of the junctions resulting in the tips of the softer asperities being plucked off. The broken asperity tip is either adhered to the harder surface or ejected out of the contact in the form of wear debris – which may cause abrasive wear if entrained into the contact. This type of wear is a particular problem when both surfaces are made of the same material, or when there is poor lubrication, or high sliding speeds and temperature. The term scuffing is used to describe adhesive wear between two lubricated surfaces. During scuffing localised areas are starved of oil, causing the adhesion process discussed above; the significance of the lubricant is that, if it gets back into the previously oil deficient area, it quenches the surface. Tearing of macroscopic 'chunks' of material from (often non-lubricated) surfaces at low sliding speeds is known as galling.

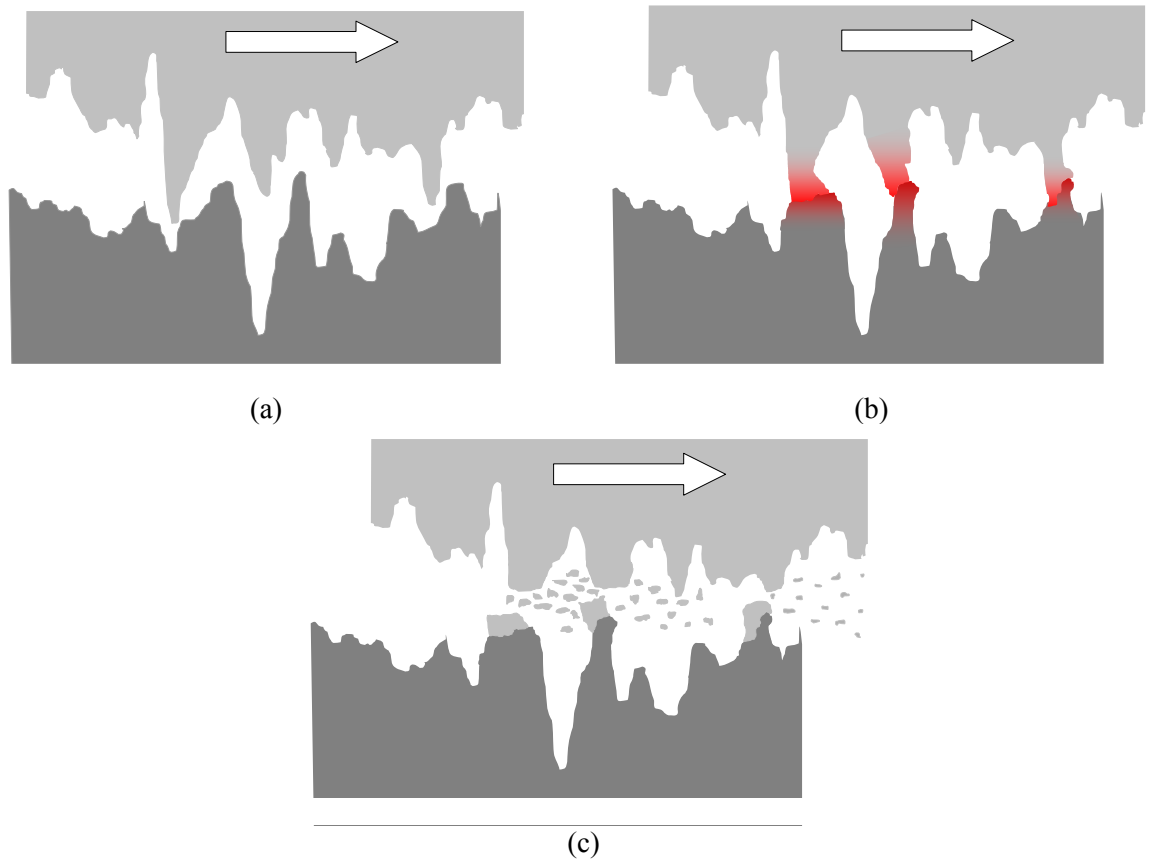

Figure 11. Schematic of adhesive wear, showing (a) asperities of two counter surfaces approaching, (b) contact between the asperities results in plastic deformation and welding of the asperities (c) asperity tips are broken off the softer material and remain adhered to the harder surface, wear debris is also generated.

Abrasive wear is damage to a component surface because of the relative motion of either harder asperities or hard particles to the softer component surface (see Figure 12). If abrasive wear is the result of a harder counter face then it is termed two-body-abrasion or grooving abrasion (see Figure 13 (a)). Grooving abrasion can also occur via a hard particle becoming imbedded (see Figure 13 (b)) in a softer surface which is in relative motion with another component. If abrasive wear is dependent on the presence of free rolling particles it is termed three-body-abrasion or rolling abrasion (this does not tend to occur in engine or transmission contacts).

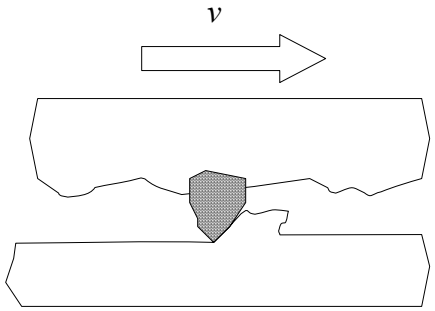

Figure 12. Schematic representation of two-body abrasion mechanism [23].

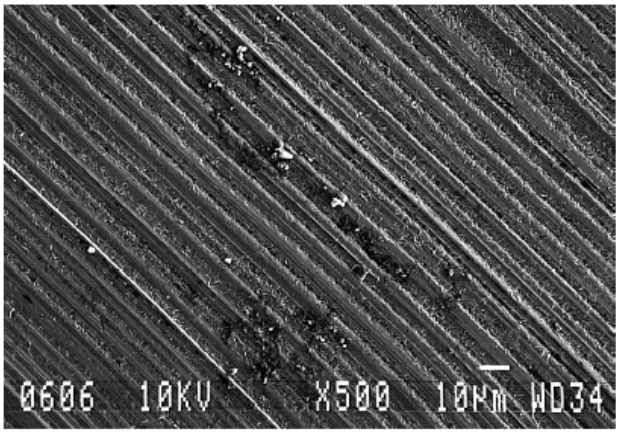

(a)

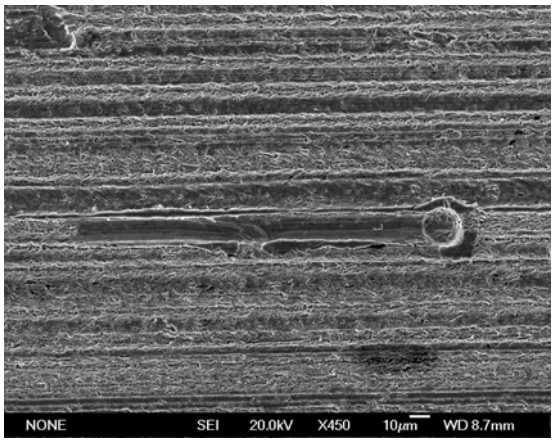

(b)

Figure 13. Micrograph of a typical wear scar due to (a) two-body abrasion [24], (b) seeded debris embedment onto the pin surface [25].

Hard particles may have arisen by chemical (oxidation) or mechanical processes or as a contaminant. There is a fundamental relationship between component wear, the size of contaminant particles, and the thickness of dynamic oil films separating opposing surfaces. Particles responsible for the greatest damage are in the size range of the dynamic lubricant films separating moving component surfaces [26]. Light abrasion is called *scratching* and severe abrasion is called gouging.

In **surface fatigue** wear, delamination occurs after a prolonged period of contact stress loading. Cyclic events (usually millions) eventually initiate and propagate cracks on the surface or sub-surface. Although renowned as the primary wear mechanism in rolling contacts, such as bearings, surface fatigue also occurs in sliding contacts. When two surfaces are loaded together, a stress field is generated; as discussed in Section 2.1.1.2 the magnitude and location of maximum shear stress is dependent on the normal load and the COF. For lubricated systems where the maximum shear stress and associated plastic flow lies beneath the surface, and the plastic strain accumulated by each sliding pass is small. Eventually this can lead to nucleation and growth of subsurface cracks, which eventually become large enough to cause discrete regions near the surface to be ejected / spalled away from one of the surfaces as debris. Particles from fatigue wear are typically much larger than the small fragments associated with abrasion or adhesion; the formation of lamellar wear particles (delamination wear) through fatigue is common. Wear debris or contaminant particles, although primarily thought to influence abrasion, can also initiate fatigue. Particles making simultaneous contact with opposing surfaces focus the load onto a small area, which can result in the generation of sub-surface cracks, leading to fatigue (see Figure 14). This type of wear is characterised by pitted surfaces.

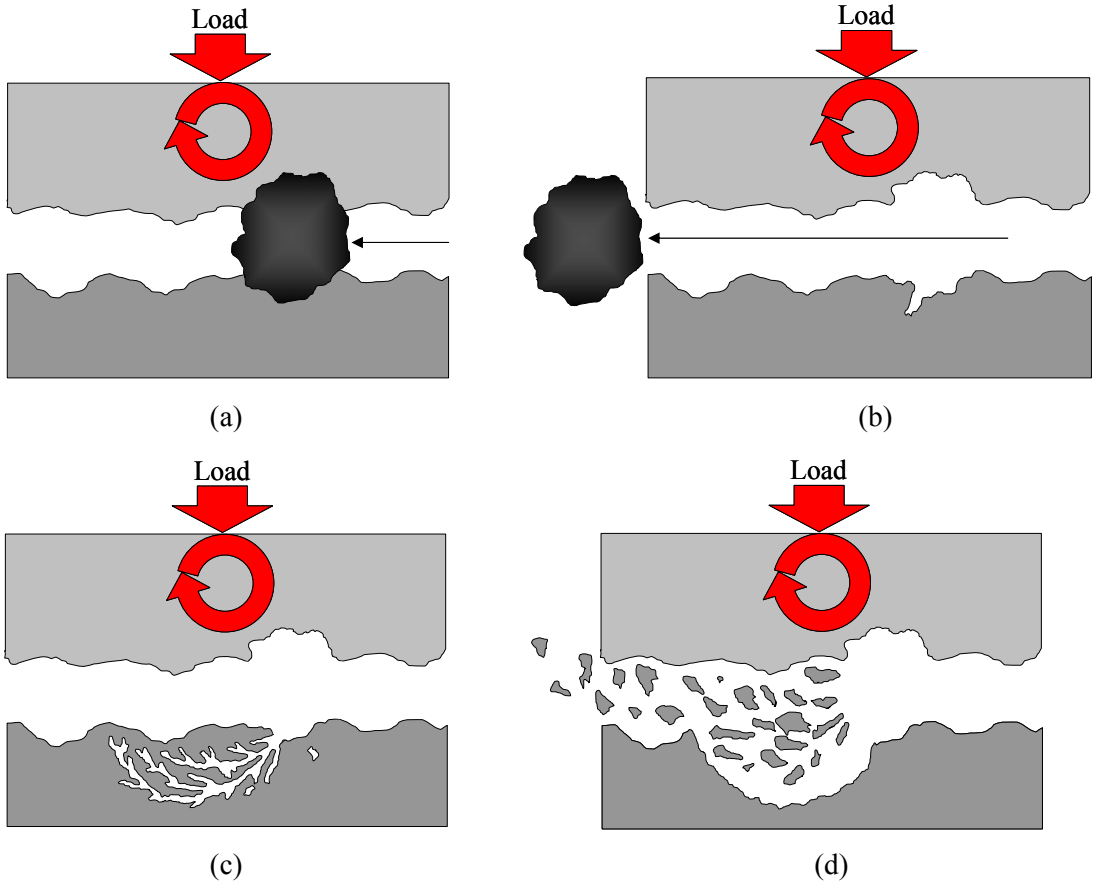

Figure 14. Schematic of surface fatigue as a result of particle entrained into contact; (a) particle making simultaneous contact with both surfaces; (b) focused load leads plastic deformation and sub-surface stresses; (c) subsequent cycles lead to sub-surface cracking, and (d) subsurface cracks progress to the surface and ejection of debris (spalling).

Tribochemical wear involves a coupling between mechanical and thermo-chemical processes that occur at the interface and with the environment (in lubricated contacts, this is chemical species contained within the oil). Chemical reactions between the environment and a surface produce a mechanically mixed layered surface film that can be worn away (see Figure 15). If this film is more readily worn away than the bulk material, this leads to greater wear than would be expected by the bulk material. Alone, the chemical reaction at the surface or shearing at the surface (e.g. abrasion) may not be that detrimental; it is the combination of a chemical reaction and tribological action together which exacerbates wear. The chemical reactivity effects wear; in general the higher the reactivity the greater the tribochemical wear. Not only does tribological action remove the material, it also enhances chemical reaction; high temperatures and pressures found in the tribo-contact accelerate chemical reaction.

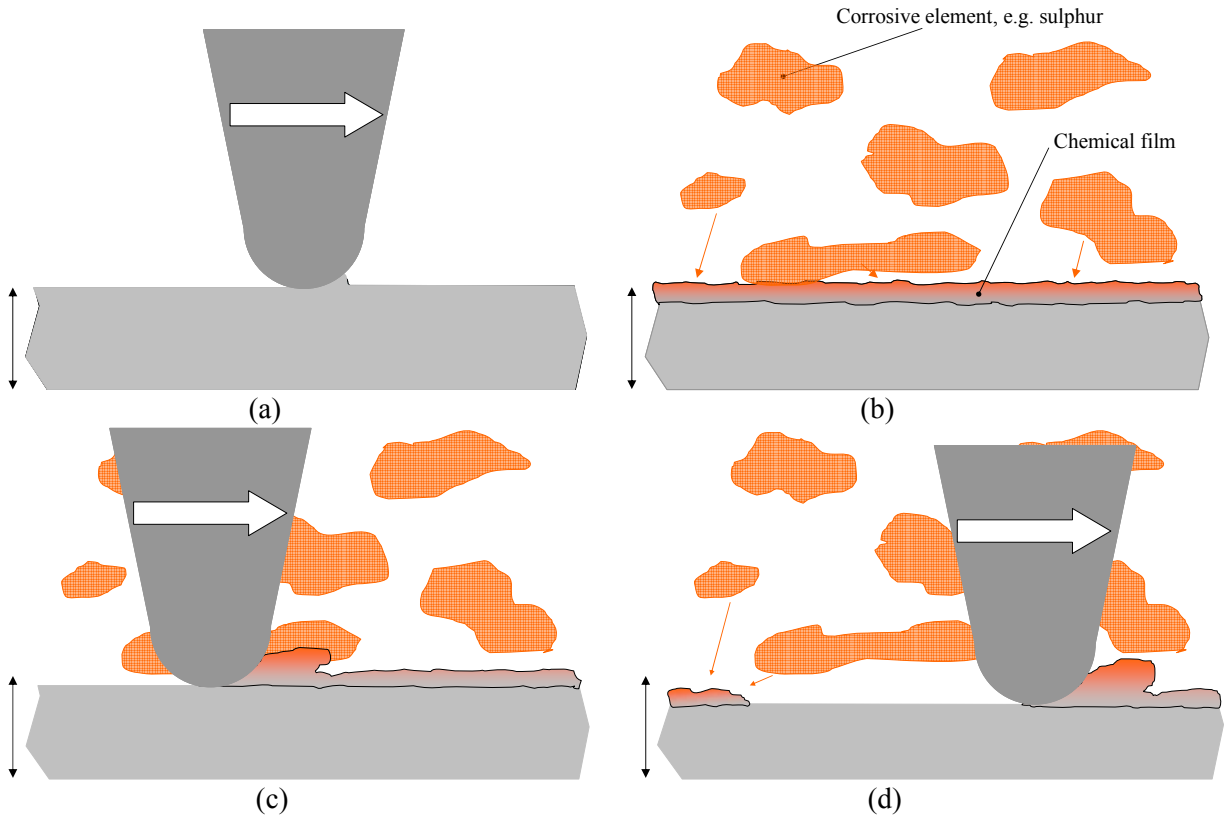

Figure 15. Schematic of tribochemical wear.

2.1.4.3 Wear model

The most well known wear model is the well known Archard wear law (see eq (33)) [27] which suggests that, for a system with constant, the wear rate is directly proportional to the load on the contact, but inversely proportional to the surface hardness (H) of the wearing material.

$$SWR = \kappa = \frac{(VL)}{W(SD)} = \frac{k_w}{H_c} \qquad (33)$$

Where κ is the dimensional specific wear rate (mm^3/Nm or m^2/N), (VL) is the volume loss, (W) the applied load, (SD) is the sliding distance (k_w) is the dimensionless wear coefficient and (H) is the material surface hardness.

Archard's wear law was derived from adhesion, but Preston [28] derived the same equation by considering the interactions between asperities as grooving abrasion. The Archard's theoretical prediction of modelling wear has been proved experimentally. However, the relationship between sliding distance and wear falls down during short tests with a non-linear running-in period. Also, proportionality between wear rate and normal load is not often found; abrupt transitions from low to high wear rates (and sometimes back again) are often found with increasing load. Another issue for contention is that the equation is used broadly in the research community, even for wear mechanism other than those used in its derivation. Nonetheless, the Archard wear law is the basis for more sophisticated wear models. Figure 16 shows typical specific wear rate ranges as a function of lambda ratio for different severities of wear.

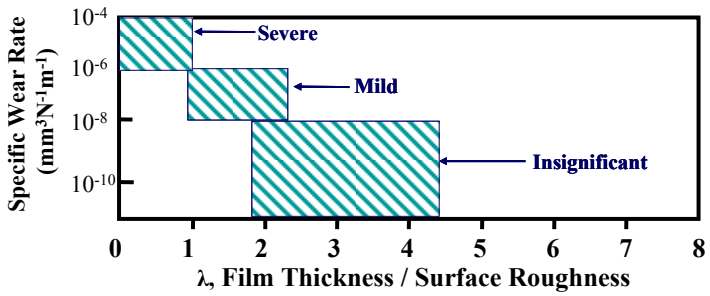

Figure 16. Schematic showing a range of specific wear rates as a function of lambda ratio (film thickness/composite roughness).

2.1.5 LUBRICANT RHEOLOGY

The viscosity of a fluid depends on temperature, pressure, shear rate and strain rate. Many empirical functions relate viscosity and pressure (in some cases temperature) [29] including those by Briant et al. [30], Gohar [15], and Jacobson [16].

2.1.5.1 Viscosity

Dynamic viscosity is defined as the tangential force per unit area required to move one horizontal plane with respect to the other at unit velocity, when maintained a unit distance apart by the fluid (see Figure 17 and eq (34), (35), (36)).

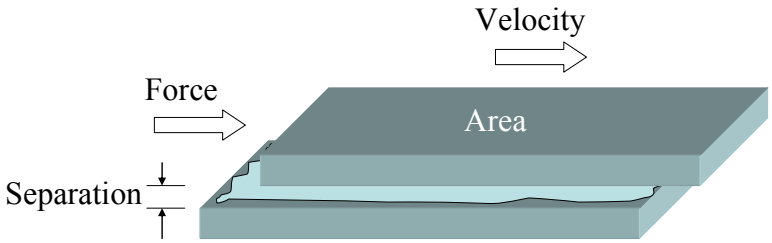

Figure 17. Schematic depicting the parameters involved in dynamic viscosity calculation.

$$\text{Shear Stress} = \frac{\text{Force}}{\text{Area}} = \frac{F}{A} = \tau \qquad (34)$$

$$\text{Strain Rate} = \frac{\text{Velocity}}{\text{Separation}} = \frac{V}{h} = \dot{\gamma} \qquad (35)$$

$$\text{Viscosity} = \frac{\text{Shear Stress}}{\text{Strain Rate}} = \frac{\left(\frac{\text{Force}}{\text{Area}}\right)}{\left(\frac{\text{Velocity}}{\text{Separation}}\right)} = \frac{Fh}{AV} = \frac{\tau}{\dot{\gamma}} = \eta \qquad (36)$$

Kinematic viscosity describes how the lubricant flows due to its own weight under gravity, with no external force involved (see eq (37)).

$$v = \frac{\eta}{\rho} \qquad (37)$$

2.1.5.2 Temperature

Viscosity is approximately exponentially dependent on temperature. This dependency is a result of the van de Walls and electrostatic forces of attraction reducing with increasing temperature. Vogel's eq (38) described the variation of viscosity with temperature. Where T is the oil temperature, and k_{temp}, θ_1 *and* θ_2 are constants for a lubricant.

$$\eta_0 = k_{temp} . \exp\left(\frac{\theta_1}{\theta_2 + T}\right) \qquad (38)$$

For a range of typical temperatures encountered in most situations involving mineral oils an empirical equation has been developed (see eq (39)).

$$\log\log\left(\eta/\rho + a_{temp}\right) = \text{constant} - c_{temp} \log T \qquad (39)$$

Experience has shown that if the kinematic viscosity is measured in centistokes then the constant a_{temp} has the value of 0.6. This is the basis of the ASTM chart on which the value of the term on the left hand side of eq (40) is plotted against the log of temperature to give a linear trend to oil properties (see Figure 18).

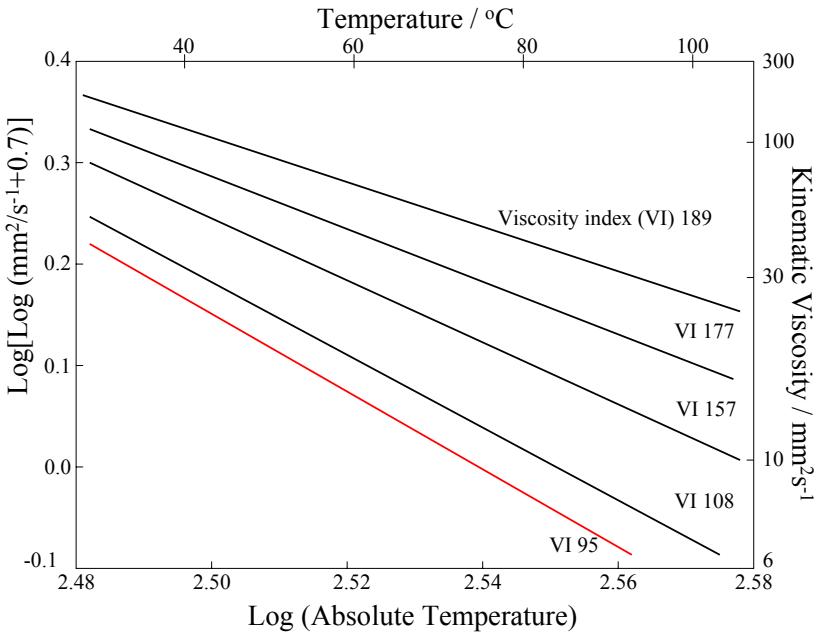

Figure 18. ASTM chart†, which describes how the viscosity of an oil changes with temperature, this is characterised by the viscosity index.

Lubricants are often designed to provide a viscosity that is low enough for good cold weather starting and high enough to provide adequate film thickness and lubricity in hot, high-severity service. Therefore, when hot and cold performance is required, a small response to changes in temperature is desired. The lubricants industry expresses this response as the viscosity index (VI). A higher VI indicates a smaller, more favourable response to temperature [31].

2.1.5.3 Pressure

The effect of local high pressures on viscosity can be described by the Barus relationship (see eq (41)) [9].

$$\eta = \eta_{atm} \exp(\alpha P) \qquad (41)$$

The Barus relationship can adequately model the viscosity dependency on pressure for many mineral oils and other fluids. In the case of fully formulated oils (those containing additives), the most successful expression is the Roeland equation (see eq (42)).

$$\eta(p) = \eta_{atm} . \exp\left\{ \frac{\alpha p_0^*}{Z} \left[\left(1 + \frac{p}{p_0^*} \right)^Z - 1 \right] \right\} \qquad (42) \quad [32]$$

Where $0.5 < Z < 0.7$ and $p_0^* \approx 2 \times 10^8$ Pa. All of these parameters can be found experimentally. These equations describe a local increase in viscosity under load. Therefore it might be possible to successfully lubricate heavily loaded sliding contacts under conditions of greater severity than would be predicted by

† Additives 2005: Optimising Automotive Power Trains - Training Day. The Burling Hotel, Dublin 4th April 2005.

the constant viscosity, hydrodynamic analysis. Oils become glassy like in most contacts (i.e. semi-solid (see Section 2.1.3)).

2.2 AUTOMOTIVE TRIBOLOGY

The work presented in this thesis investigates lubricant performance in simulated valve-train and transmission contacts. This part of the *Literature review* aims to examine these specific tribological contacts and set the context of lubricant testing. Unfortunately published literature on transmission tribology, on the whole, has not been discussed at the same scientific level as other sections in this *Literature review*. This area of research has received industrial treatment with minimal tribological analysis. This Section discusses the drivers in automotive design and the tribological performance of cam-follower, frictional clutch and synchroniser contacts. The experimental work presented in Chapters 4-8 are based on the fundamental and applied tribological conditions identified in this Section.

The automotive sector is the 6th largest economic sector worldwide, with a value of € 2 trillion; it also encompasses interrelationships with more than 300 different fields [33]. Thus, even small changes in the automotive sector could have huge global benefit.

The oil crisis of the 1970's generated public awareness of the dwindling supply of fossil fuels. More recently, the need for change in all aspects of automotive design has been highlighted by; high fuel prices (due to high demand from a dwindling supply and political instability); greater understanding about the impact of harmful emissions on global warming, and the ever increasing number of vehicles in the world (particularly in China and India). Ever since the invention of the internal combustion engine there has been a desire to improve the design. This originally took the form of producing greater power, but has recently focused on satisfying conflicting demands of increased durability and reduced environmental impact (though engine cleanliness and smaller engines providing better fuel efficiency), while maintaining the same power that automobile customers expect.

Improvement in vehicle efficiently alone has a direct impact on fossil fuel consumption; because less fuel is required to travel the unit distance, and because less fuel is being burnt, there are fewer harmful gases being produced over that unit distance. The total power from fuel is 32kW, of which 4.9 kW is lost in the engine and power-train compared to 3.8kW from rolling and air resistance and acceleration [34] (see Figure 19). A 10% reduction in mechanical losses would lead to a 1.5% reduction in fuel consumption; this is significant when noting that only 12% of the available energy in the fuel finds its way to the driving wheels [35].

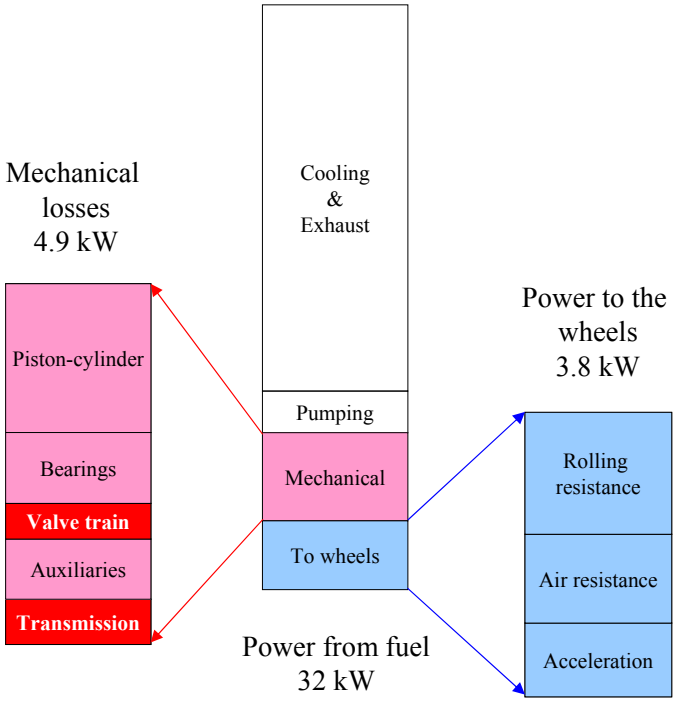

Figure 19. Power distribution in an automobile during city driving [35].

The evolution of the internal combustion engine has resulted in higher specific outputs, higher surface speeds, higher temperatures and smaller components for the major frictional components in the engine, and transmission, namely: piston assembly, valve-train, journal bearings and gears. Reducing frictional losses requires lower viscosity engine oils, resulting in a decreasing oil film thickness between the interacting surfaces (see eq(31)), which has obvious durability implications for engine components. During the 20th century the thickness of lubricating films in machine elements has reduced by several orders of magnitude [36]. Of particular concern are those contacts which operate with a film thickness of a fraction of a micron, as often these contacts have surface roughness's of a similar order of magnitude ($\lambda \leq 1$). Under these conditions (boundary lubrication, see Section 2.1.3) surface interaction is inevitable; additives are required to minimise the affect contact between component surfaces have on wear and friction.

Improvements in fuel efficiency must not be at the detriment to durability; durability and fuel efficiency improvements need to be advanced together. Many studies have been carried out on the greatest sources of automotive failure. Heyes [37] has shown that the most failed parts are from the engine and its components (41%) followed by the drive-train (which includes transmission) failures (26%). Although these aspects of automotive tribology are not the greatest in terms of energy loss they are important areas of research because they operate under some of the most severe contact conditions (see Table 4).

Some Power-train component	Oil film thickness (μm)
Piston ring-to-cylinder	3.0 – 7
Connecting-rod bearings	0.5 – 20
Main shaft bearings	0.8 – 50
Turbocharger bearings	0.5 – 20
Piston pin bushing	0.5 – 15
Valve-train	0 – 1.0
Gears	0 – 1.5

Table 4. The operating film thickness of major contacts in a IC engine and transmission [26].

2.2.1 VALVE-TRAIN TRIBOLOGY

It is generally accepted that out of the three major frictional components in the internal combustion engine (the piston assembly, engine bearings and valve-train), the valve-train is the least energy absorbing (see Figure 20). However, the valve-train experiences the greatest contact pressures of these three major frictional components and thus operates under the lowest oil film thickness. Satisfactory lubrication of the cam and follower contact in internal combustion (IC) engines has proven to be the most difficult of all the tribological components [38,39]. Wear of valve-train components is one of the most critical factors limiting the life and performance of automotive engines [40] as cam and follower wear will affect valve timing and therefore combustion and performance.

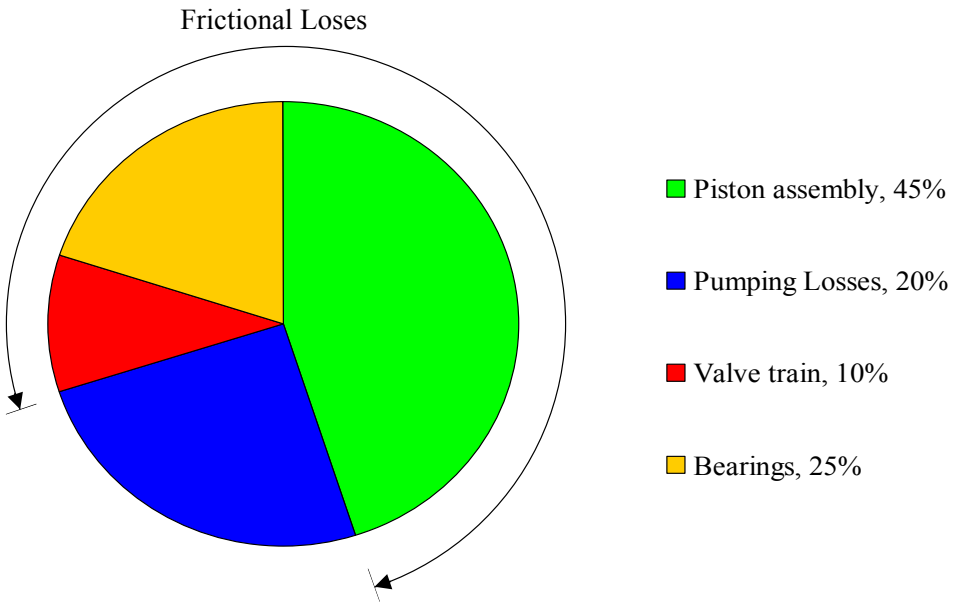

Figure 20. Mechanical losses distribution in an internal combustion engine [35].

The valve-train incorporates a wide spectrum of interesting contacts to tribologists: the cam/follower, camshaft bearings, valve guides, lash adjusters, bucket guides, pivots and belt drives. This thesis focuses

on the cam/follower contact. This Section on valve-train tribology discusses the drivers behind valve-train design and how this affects tribological performance, with particular reference to cam and follower adhesive (scuffing) wear. The cam and follower materials are also discussed as part of the general background to valve-train design.

2.2.1.1 Kinematics

The primary aim at the engine design stage is to improve combustion, and therefore maximising efficiency. The valve lift profile is highly influential to the performance/efficiency of the IC engine. The kinematic cam profile/lift profile (see Figure 21) is heavily dependent on the valve-train stiffness and mass. Thus material and configuration are important considerations for valve-train design. The effect of valve-train stiffness and mass is exasperated at significantly high engine speeds. More information on how kinematics influence valve-train design can be found in [41].

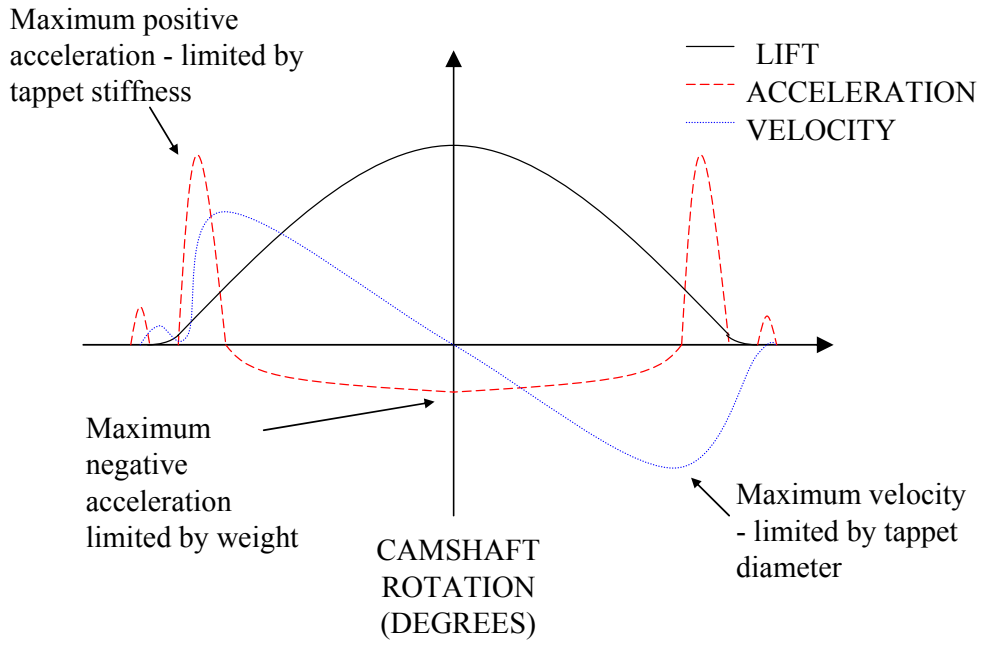

Figure 21. Kinematic cam profile characteristics [34].

2.2.1.2 Valve-train design

Over 20 years ago the move to OHC configurations, such as the PAS TU3, was driven by manufacturing and kinematics (see 2.2.1.1). The OHC allowed improved production arrangements because the cylinder head could be assembled separately from the engine block and was less expensive to manufacture [42]. High valve-train reciprocating mass and low stiffness became increasingly undesirable as engine speeds increased; OHC valve-trains were inherently lighter and stiffer than over-head valve 'push-rod' designs [43] and operated better at higher speeds [42] (see Section 2.2.1.1). The advantages and disadvantages of

a range of valve-train architectures are discussed in Appendix A. The development of the valve-train to improve fuel economy is a complex process in its own right, and one that unfortunately does not seem to have been linked directly to the tribological operating environment [35]. The following sections discuss the tribological performance, and surface engineering involved in TU3 cam-follower contacts.

2.2.1.3 Valve-train materials

Camshafts are generally produced by casting or forging. For sliding contact valve-train systems (like rocker-followers/direct acting tappet (DAT)), the cam lobe and followers, tend to be made from chilled grey cast iron, nodular cast iron and malleable cast iron [33].

The TU3 camshaft is made from nodular cast iron. Nodular cast iron has good fluidity and is easily cast and machined. Nodular graphite cast iron has a number of properties similar to those of steel, such as high strength, toughness, ductility, hot workability, and hardenability as well as good wear resistance. The carbon content of unalloyed ductile iron ranges from 3.0% to 4.0% C and the silicon content from 1.8% to 2.8% [33]. The spherical nodules in ductile cast iron are formed during the solidification of the molten iron; these spherical nodules are responsible for high fracture toughness. Impurities, such as sulphur and phosphorous, must be kept to a minimum because they interfere with the formation of graphite nodules. Magnesium is introduced to the metal just before it is cast to react with sulphur and oxygen so that these elements do not interfere with the formation of spherical nodules [44].

The TU3 followers are made from stainless steel. The presence of chromium creates a passive layer (when exposed to air), which makes the follower more corrosion resistant. This is important for followers in cylinder-heads where incomplete combustion gases may collect. For roller followers both the cam and followers are made out of steel rather than cast iron because of the high contact stresses inherent in roller followers.

Fuel economy depends on the reduction of friction losses and weight reduction of engine components [45]. These can be achieved by the development of two key areas: materials technology and lubrication technology. Alternative non-ferrous materials have been investigated and improved kinematic performance (see Section 2.2.1.1) has been shown when lighter materials are used.

2.2.1.4 Surface treatments/finishing

The wear resistance of cast or forged valve-train components can be improved through surface hardening. By infusing elements into the ferrous surface, a thin harder alloy is formed. Surface hardening techniques include: fame hardening, carburizing, nitriding, carbonitriding and Nitrosulphurising. Sliding followers tend to be harder than the cam [46] because the area in contact for one cycle is smaller than that of the

cam, thus followers require greater wear resistance. The TU3 cam has a hardness of approximately $600H_{v30}$ compared to the follower hardness of around 800 H_{v30}.

The surface topography is a valve-train design consideration that has not seen much development and there are still conflicting views regarding its effect on lubricated contacts. Limited research has investigated the effect of surface finish of cam and follower components on wear.

The surface finish of automotive metallic cams and followers is widely published at around 0.2 μm R_a. The traditional view has been that the smoother the finish the better, as this will promote EHL lubrication rather than boundary (see Section 2.1.3). However, in reality it is not that simple. Contacts with rough surfaces could encourage lubricant retention in valleys. There is evidence that smoother surfaces may not encourage lubricant retention, because of the lack of valleys in the contacting surfaces, and therefore wear may result [35].

2.2.1.5 Wear

The first part of this Section discusses general valve-train wear mechanism, the conditions which exacerbate wear and the consequence this has on engine operation. The second part uses some of the tribological concepts introduced in Section 2.1.4.3 to aid understanding about the tribological conditions in cam and follower contacts, which enabled models for cam and follower wear to be developed.

General valve-train wear

The change in valve-train design from crankcase location to OHC gives inherently poorer tribological performance [35] resulting in high friction and wear, especially for the finger and rocker-follower design. Between 1980 and 2000, almost all the major automobile manufacturers have experienced cam and follower failures [38]. In general, the failure mechanisms observed in valve-trains are: abrasion/polishing, pitting, and scuffing [35], all of which are influenced by valve-train design, materials, lubricant and operating conditions.

Under boundary lubrication, the asperities of the cam and follower surfaces interact causing grooving and breaking of asperity tips (debris ejection). Although initially this can have a polishing affect, reducing surface roughness, over a period of time, at some point contact between the surfaces will cause grooving and new valleys to be formed. Usually there are contaminants such as wear debris or soot in the case of diesel engines; these extremely small particles circulating in the lubricant can transmit load between the surfaces and produce abrasive wear. This results in the gradual removal of material, which at the very least will have an affect on component tolerances. More importantly, abrasion may initiate scuffing (see Section 2.1.4.2); deep valleys and narrow asperities reduce the surface area increasing the chances for plastic deformation and localised welding.

Scuffing is thought to occur under transient conditions such as start-up, shutdown, and high torque conditions (e.g. driving up steep gradients) [26,47]. These driving conditions lead to low speed and high load between the cam and follower. This produces the most severe boundary lubrication, increasing the amount of asperity contact between the surfaces (wear). In addition, scuffing is likely during running-in periods, because the two surfaces are not conformed (small contact area), leading to high contact pressures between asperities.

The immediate affect of wear is furrowed and roughened surfaces, which increases friction and therefore reduces fuel efficiency (see Section 2.1.2). In addition it opens up clearances between cam, follower and valve components, causing the timing of the engine port openings and closings to vary, leading to incomplete combustion and the possibility of combustion in the exhaust manifold (backfiring). This will lead to a much greater loss of engine performance. Ultimately progression of severe adhesive wear can lead to engine seizure.

A survey in 1986 concluded that scuffing was one of the most critical lubricant related valve-train wear mechanisms [48]. The Lubricant group of the Co-ordination European Council, CEC IGL-17 looked into valve-train wear and recommended the standardisation of a scuffing test method using an overhead camshaft and pivoted rockers/finger-followers engine unit [49]. The PSA TU3 engine[‡] was used as the basis for developing the test method [2]. Other standard industry engine tests have joined the PSA TU3 engine to assess for cam and follower wear, such as the Sequence VE [50], and the Toyota 3A tests (both single over-head camshaft (SOHC) valve-train systems with pivoted followers). Although most modern engines now use the Direct Acting Tappet (DAT) design (which significantly reduces wear (see Table 5)), finger follower engines continue to be the industry standard test engines for assessing valve-train wear. Wear in these test engines occurs principally by abrasive and adhesive processes [38] and in some cases there is a significant corrosive element under low-temperature conditions [51,52], as acidic combustion products retained in the cam-casing do not evaporate at low temperatures. At an advanced stage of wear, a transition to severe adhesive wear (scuffing) is frequently observed [52].

Valve-train wear Models

The combination of EHL theory (see Section 2.1.3) and Archard's law (see Section 2.1.4.3) have been incorporated to predict valve-train wear. EHL theory enabled prediction of the minimum film thickness (see eq(31)) and therefore the ratio of film thickness to composite roughness (see eq(32)). Archard's wear law is combined with EHL theory to give a wear model that incorporates a specific wear rate (κ), which is a function of the oil film thickness (h), based upon EHL lubrication theory.

[‡] The engine is a 1360cc displacement, 4 cylinder OHC petrol engine having a compression ratio of 9.3:1 and an output of 47kW. Typically, these engines are used in Citroen Ax, Bx, Peugeot 205, 405. the follower unit is also used in the Renault 21 and the Volvo V6 engine.

Cam-follower contact pressure and entrainment velocity, as a function of cam angle, can be found through computation. (The kinematics of finger follower systems are rather complex and lead to wide changes in loading and sliding speed [53,54]; consequently, many researchers have simplified the configuration to a cam-tappet arrangement (e.g. ref [55]). There are very few papers predicting cam and finger follower wear.) Using Dowson's (see eq (31)) equation for line contact the film thickness can be calculated, as a function of cam angle and follower sliding distance, for one rotation of the cam. The oil viscosity, for a given temperature, used in the EHL equation, can, to a first approximation, be derived from the base oil viscosity [56]; at the high shear stresses and shear rates in the EHL contact the viscosity of multigrade oils is similar to the base oil.

	Rocker follower	Equivalent tappet follower
Maximum load (kN/m)	63.94	32.84
Maximum contact pressure (MPa)	684.5	358.9
Entrainment velocity (m/s)	0-3.059	0-6.253
Maximum film thickness	0.76	2.38
Minimum film thickness	0.07	0.14
Load at minimum film thickness (kN/m)	41.0	32.8

Table 5. TU3 cam and follower contact parameters at 40^{o}C and 750rpm [52].

The lubrication regime of the cam-follower varies around the cam cycle, due to varying load, entrainment velocity and contact geometries as a function of cam angle. Thus the minimum film thickness does not necessarily occur at the point where minimum sliding speed and maximum contact pressure co-inside. (Although it is not usually that far away from the minimum sliding speed and maximum contact pressure). Table 5 shows that the minimum film thickness occurred at a load below the maximum; entrainment velocity and maximum contact pressure for the TU3 valve-train are also given. It is generally accepted that the lubrication regime from the base circle, flank and nose is EHL-mixed [38]. Boundary lubrication occurs at various points around the cam nose. Typically the minimum oil film thickness is found either side of the cam nose (see Figure 22).

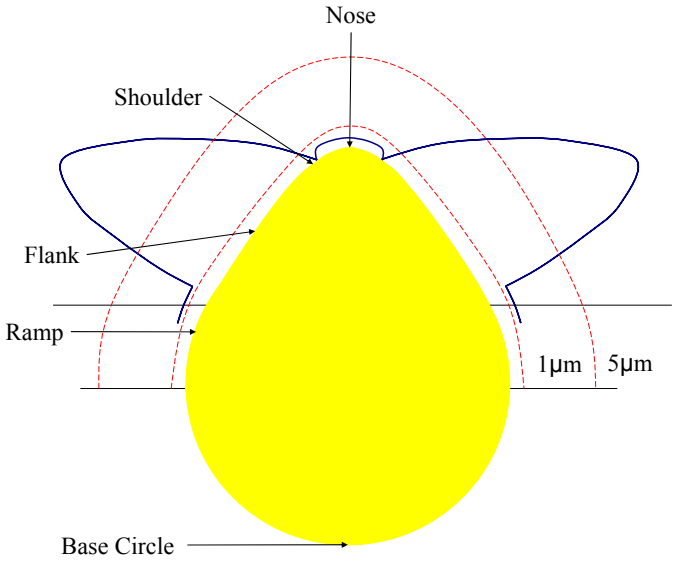

Figure 22. Butterfly diagram showing typical film thickness variation around cam [57].

In most case cams and followers undergo steady, but non-catastrophic, wear. Based on the assumptions of steady state wear, a mathematical model was developed [53,58] based on a simple Archard's wear law [27], in the form proposed by Lancaster [59]. The specific wear rate is a function of the film thickness and therefore is also a function of the interacting materials, their surface topography, the lubricant and the operating conditions. The variation in specific wear rate thus follows the different lubrication regimes due to change in oil film thickness (see Figure 23). The variation of the wear coefficient is obtained from subsidiary well controlled experiments. Fired engine tests have shown that the overall specific wear rate for the cam/follower contact was 1-3 x 10^{-18}m^3/Nm [60,61]; a transition to scuffing (see below) results in a specific wear rate of 50 x 10^{-18}m^3/Nm [61].

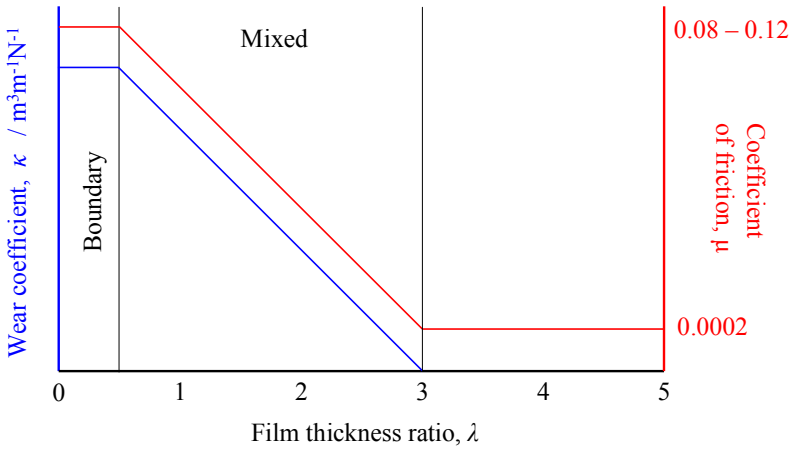

Figure 23. Transition models for specific wear coefficient and coefficient of friction [40].

The friction in valve-trains can be predicted using a similar model to the wear model. The hydrodynamic COF is approximately 0.0002. Under boundary lubrication the coefficient of friction (COF) is assumed to be around 0.08 for friction modified oil to 0.12 for conventional formulations. These values enable the power loss between the cam and follower contact to be predicted.

Models versus real wear

The wear model described above is capable of predicting the wear profiles of both cams and followers (see Figure 24). Bell [52] used the model to predict the wear for a pivoted finger follower and DAT valve-trains. The effectiveness of the model can be assessed by comparing the predicted follower wear profile to those of an exhaust follower obtained in a standard engine test. The predicted follower wear profile is fairly similar to that of the retrieved follower (see Figure 24 (a)). Particularly worthy of note is the tendency for wear to increase towards the end contact path closest to the pivot of the follower on both the predicted wear and on the worn follower. This is because it is the position of maximum contact duration in the main loaded part of the cycle. In practice it has been found at this particular point there is relatively poor antiwear film formation [62].

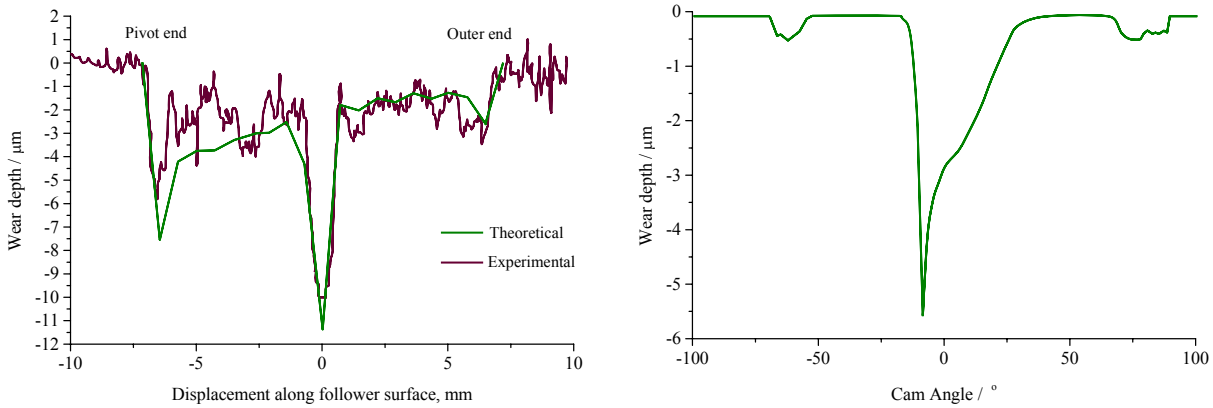

Figure 24. Wear profiles (a) theoretical and predicted follower and (b) predicted cam [52].

The maximum cam wear is predicted approximately 10° from the cam peak (see Figure 24 (b)); it occurs close to the point of minimum sliding speed. Unfortunately there is not any worn cam profile data in the literature which enables direct comparison; this is likely to be because of the difficulty in profiling a curved surface with a small radius. However there are reports which that noted little change in roughness of the cam flanks [63,64], which corresponds with the low wear rate predicted for the flanks.

Problems with models

Experimental measurements in a pivoted follower valve-train system [56,65] have shown that the theoretical predictions may significantly overestimate oil film thickness in places and underestimates oil film thickness in others (see Figure 25(a)). The agreement between predicted and actual wear is not exact

for two reasons, changing contact conditions and squeeze film effects. The initial roughness is used to calculate the film thickness ratio; in reality the roughness will change rapidly from the initial value. This may lead to reduced contact area and increased Hertzian contact pressure. Or the surface may become correlated after running-in, which promotes full film lubrication [54,66].

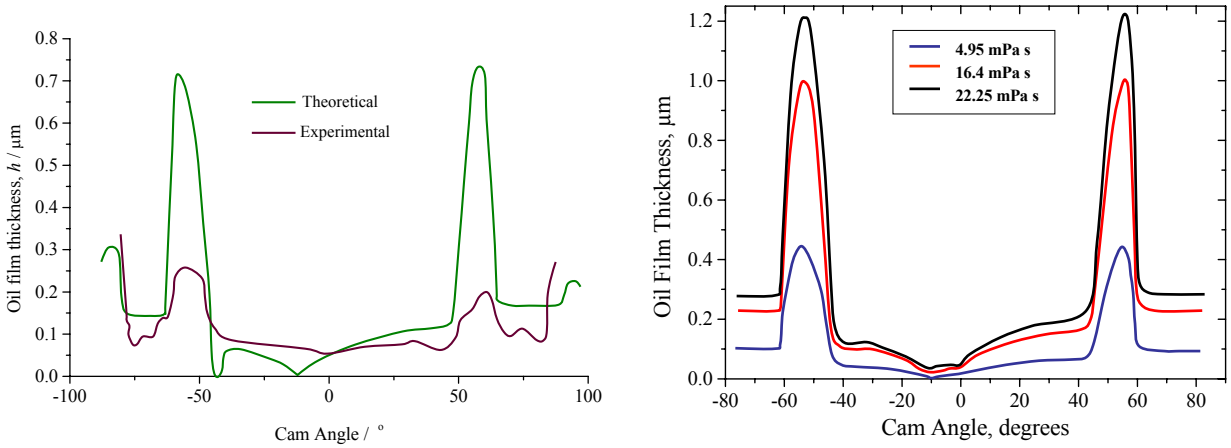

Figure 25. Oil film thickness between TU3 cam and follower (a) experimental and EHL theoretical prediction, and (b) dynamic EHL theoretical prediction (taking into account squeeze film effects) [40].

Experimental measurements highlight the major discrepancies with static EHL theory predicting zero oil film thickness (see Figure 25) around zero entrainment velocity [56]. EHL theory neglects squeeze film effects, which are important at small oil film thicknesses. The measured wear at zero entrainment velocity is not as severe as the predicted model suggests. It therefore signifies that transient effects need to be accounted for.

Dynamic EHL models

To get more quantitative results, non-linear, time dependent wear models involving wear transitions [67] combined with dynamic EHL models have been developed. Figure 25 (b) shows the oil film thickness calculated using dynamic EHL models, which correlates far better to the experimental oil film thickness shown in Figure 25(b) than the non dynamic EHL models.

Midlife scuffing

The previous wear model predicted the level of wear around the cam and along the follower, assuming steady state wear. The problem with this model is that is not sophisticated enough to take into account wear transitions, such as mild wear to sever adhesive failure. Bell and Willemse [61] investigated the processes leading up to scuffing, without any increase in the severity of the externally applied condition, termed mid-life scuffing. They recorded cam and follower surface roughness and wear at regular intervals

during a series of valve-train wear tests in a fired engine. The *shakedown* conditions in cam and follower contacts in these tests were modelled using both a statistical description of the surfaces, in the form proposed by Kapoor et al. [68], and also a numerical technique similar to that of Webster and Sayles [69] which employs actual measured surface profiles. This work enabled the following observations to be made regarding the transition to scuffing; a) surface roughening in the mild wear regime, which progressively increased maximum asperity contact pressure until b) the elastic *shakedown* limit was exceeded, causing plastic deformation wear, accelerated roughening and enlargement of valleys, leading eventually to c) a transition to high rates of wear, probably resulting from hydrodynamic pressure loss and oil-film collapse.

2.2.2 TRANSMISSIONS

Transmission of power from the IC engine to the vehicles wheels requires a geared system because the range of operating rotational speeds of the engine and wheels are different (700-7000rpm and 0-1900rpm respectively). In addition, moving a vehicle from rest, or when travelling slowly, requires a gearing that transmits high torque at low speeds. The key difference between a manual and an automatic transmission is that the manual transmission locks and unlocks different sets of gears to the output shaft to achieve the various gear ratios, while in an automatic transmission, the same set of gears (planetary gearset) produces all of the different gear ratios.

The following sections focus on two transmission contacts; the synchroniser used in manual transmission and the frictional clutch used in automatic transmission. In the majority of automotive lubricated contacts it is desirable for friction to be kept to a minimum (e.g. the valve-train), but where power transmission is required, such as the synchromesh and frictional clutch, a certain amount of friction is needed to enable quick and smooth operation. The literature discussing these two contacts is extremely limited and has not seen the same academic insight as valve-train tribology.

2.2.3 MANUAL TRANSMISSION SYNCHRONISERS

Synchronisers are used to equalise the rotational speeds of the output shaft and the desired active gear (the gear to be selected), preventing the need for double clutching. The synchroniser rotates at the same rotational speeds as the shaft, whereas the gear(s) along the shaft(s) run on bearings, synchronisers lock the active gears to the shaft(s). The synchroniser consists of a taper, which fits over a corresponding cone section of the desired active gear and makes frictional contact to equalise peripheral speeds before dog teeth make contact (see Figure 26(b)). A lockout mechanism prevents positive gear engagement prior to completion of the synchronisation process (see Figure 26(a)). Once equalisation of active gear and synchroniser rotational speeds have occurred, the synchroniser sleeve slides to engage the collar dog teeth with the corresponding teeth on the gear (see Figure 26(c)).

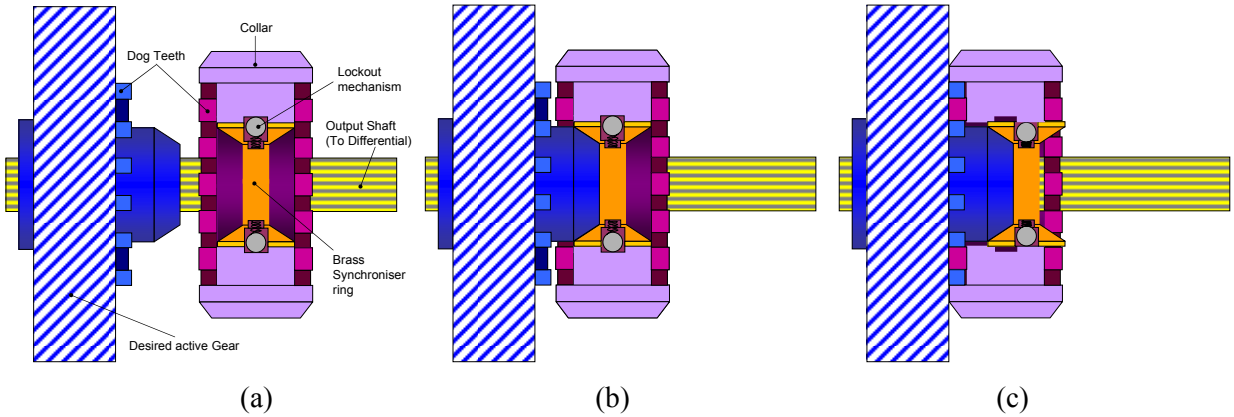

Figure 26. *Synchronising process; (a) collar and output shaft are rotating at a different speed to the desired active gear; (b) friction between the cone and collar synchronises the collar and gear rotational speed and (c) the collar then slides to engage the collar dog teeth with the corresponding teeth of the desired active gear.*

2.2.3.1 Tribological considerations for manual transmission synchronisers

Synchronisers must equalise rotational speeds of the output shaft and the desired active gear. Whether the synchroniser needs to increase or decrease the rotational speed of the active gear to match the output shaft, the equalisation is achieved through frictional forces between the synchroniser ring and active gear. When the rotational speeds between the active gear and output shafts are vastly different, friction between the two contacts occurs through viscous effects. As the difference between rotational speeds of the two surfaces decreases, frictional forces are generated through solid-solid contact up until there is no relative movement between the two surfaces. Transition between gears needs to occur as quickly (few tenths of a second) and as smoothly as possible, from the stand point of power transmission and efficiency, as well as driveability. To achieve this, high friction between the contacts is required, but not to the detriment of wear, which will inhibit equalisation and result in the clashing of dog gears and eventually lead to the inability to select the gear.

Almost all car manufactures use Borg-Warner synchronizers [70], which are conical in shape. The rings are made of forged brass and the gear is typically made from cast steel; other materials are used, in particular Molybdenum coatings, but brass synchronisers remain the major synchroniser ring material. Hard and soft material couplings have been used for a very long time due to their good friction and wear characteristics; cast steel and brass have a hardness of 700 and 100 Hv respectively [71]. The brass-steel pairing is used because of excellent friction characteristics (see Section 2.1.2); the ability to endure high temperatures generated during high friction contact, and good thermal conductivity [72]. In addition, brass is able to withstand high stresses.

Groves are machined onto the friction surface [70]. The surface topography fulfils a complex, and conflicting, range of functions; the groves provide some cooling as well as promote lubricant retention (see Section 2.2.1.4), the pattern of these groves is designed to give best braking performance (high friction). Generally, synchroniser performance deteriorates because the grooves diminish as a result of wear [70]. Due to the difference in surface hardness between brass and steel, wear of synchroniser rings is abrasive and adhesive (see Section 2.1.4.2); the main type of failure observed in the field is severe adhesion which results in seizure of the gear and synchroniser ring [73].

2.2.4 AUTOMATIC TRANSMISSION CONTACTS

A basic automatic transmission (AT) contains two complete planetary gearsets folded together into one component, called a compound planetary gearset. In this configuration there are four wet-plate clutches to lock parts of the gearset to create the desired input/output gear ratio. Each clutch is actuated by pressurised hydraulic fluid that enters a piston inside the clutch. The clutch consists of a plate of friction material and a steel plate (see Figure 27). The friction material is splined on the inside to lock onto one of the gears. The steel plate is splined on the outside to lock onto the clutch housing.

Wet friction materials must transmit and cut-off power repeatedly based on frictional force. Environmental pressures have driven the need for improved fuel economy, through among other things, more efficient automatic transmissions. Current design development is set to achieve this with smaller size units with lower lock-up speeds, which means that wet friction materials and automatic transmission fluids (ATFs) must provide greater durability.

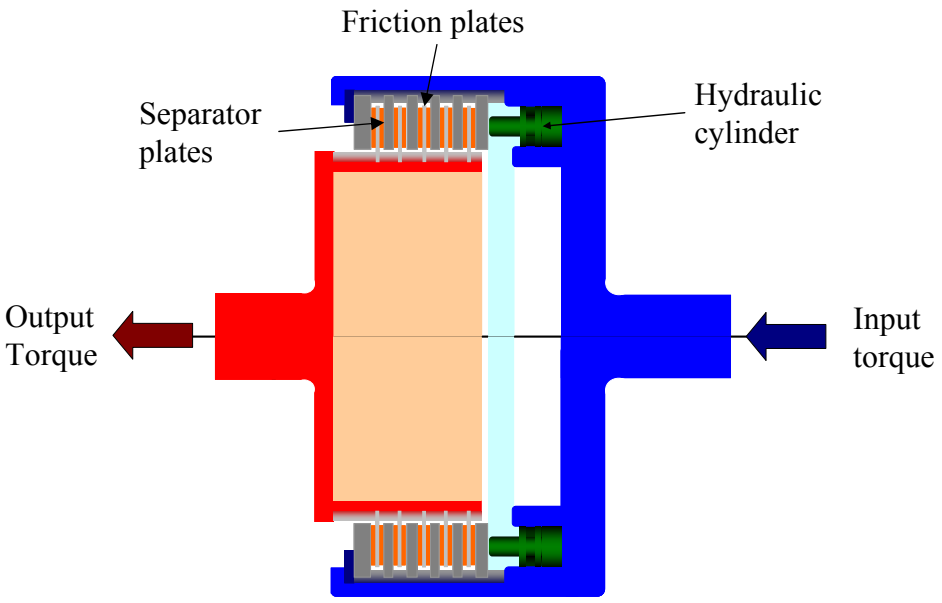

Figure 27. A multiple disc wet clutch showing the friction material and steel plates.

2.2.4.1 Tribological operation of wet-plate clutches

There is very little theoretical work on wet friction material; this is principally because Hertzian and EHL calculations are not valid for wet friction material due to inhomogeneity and porosity (between 25 and 60% porosity). Even though an elastic modulus can be experimentally obtained to describe the friction material, at the microscopic level the elastic modulus will vary. Most of the literature therefore employs a qualitative experimental approach to understanding wet frictional clutches tribology.

Wet-plate clutches require a certain amount of friction to enable quick and smooth operation. The lubrication of a wet friction clutch can be split into four stages; (1) disengaged rotating clutch operates under full film lubrication, where viscous shearing fluid produces a small torque; (2) initial engagement of the clutch squeezes the film out of the contact creating a hydrodynamic pressure, which supports the load and prevents asperity contact; (3) the onset of asperity contact, deforms the porous friction material pushing out fluid [74], and in the final stage (4) the two plates are locked together, torque is transmitted by asperities and boundary film. In the earlier stages the rheological properties of the base oil play a significant role in friction performance; in the latter stages additives and friction material mechanical properties dominate friction response [75,76].

Wet friction material must produce specific friction characteristics (see Section 2.2.4.2) over long durations; they must also provide sufficient heat adsorption and be compatible with oils and additives [77,78]. Porosity may be desirable for certain wet friction clutch applications, because it promotes fluid retention in the contact and improves heat transfer from friction material to fluid. Higher porosity increases COF [79] and inhibits shudder (see Section 2.2.4.2) [80]; however porosity also promotes cavitation [79].

The most commonly used friction materials are paper, sintered bronze, steel, carbon fibre, cork, asbestos and aramid fibres. From the viewpoint of stable friction coefficient and price, the paper type friction material [81] has been the favoured friction material for AT wet clutches. In general paper-based wet friction materials are porous composites consisting of phenol resin-impregnated cellulose fibres [82] (see Figure 28). In addition, diatomaceous earth, carbon fibres, graphite, cashew dust, aramid fibres and asbestos fibres can be found in cellulose / phenolic resin based wet friction material [83,84]. Fibres are included for their frictional properties, their heat resistance, and their thermal conductivity [85]. Diatomaceous earth and graphite are included as fillers [86], graphite and cashew dust are used as friction modifiers, and aramid fibre and carbon fibre are occasionally used to toughen and strengthen the binder (phenolic resin), which is quite brittle in its pure form [83]. Fibres coated with phenolic resin are bound to each other at their intersections leaving spaces between the fibres (pores). Since fibres are laid perpendicular to the direction of thickness, their strength shows an anisotropic characteristic [87].

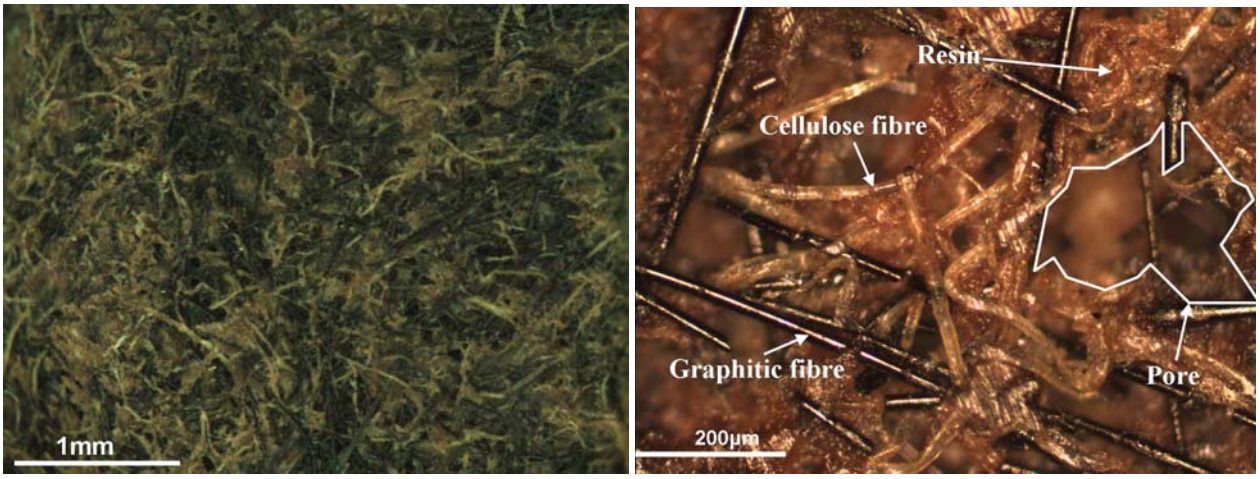

(a) (b)

Figure 28. Disc wet friction material (a) macro image and (b) micrograph.

2.2.4.2 Challenges for wet plate clutches

There are three interconnected problems with the wet clutch in AT: efficient transmission of power (torque capacity), smooth transmission of power (minimise shudder) and wear.

It has been reported that AT are the least energy efficient component in a vehicle drive-train [88]. Conventional ATs are 5-10% less efficient in fuel consumption than a manual gearbox *'on the open road'*, yet demand for ATs remains high because of their *'driver friendly operation'* [89,90]. This is significant considering 89% of cars in Japan (in 1999) [87,91] and 90% in US (in 2000) are equipped with ATs [89,92]. Thus, in the current political climate, there is a need to improve AT efficiency, to improve fuel economy.

Slip-stick behaviour (see Section 2.1.2.1) of the clutch, which creates shudder (friction-induced vibration) and hinders smooth transition of power, is a major problem. To eliminate shudder a low static COF (μ_s) and a dynamic COF (μ_d) that increases with increasing sliding velocity is required [93]. This is described by a positive $d\mu/dV$ curve for *oil A* in Figure 29 [94]. In reality, a low static COF will limit the torque capacity (the amount of torque that can be transmitted before slipping occurs, which directly affects transmission efficiency), thus there is a trade off between good anti-shudder properties and high torque capacity [95]. *Oil B* may be susceptible to vibrations since it exhibits a negative slope. Increasing the system damping can reduce or completely eliminate friction-induced vibration. This can be achieved by modifying the friction-velocity characteristic of the fluid and interface materials [74].

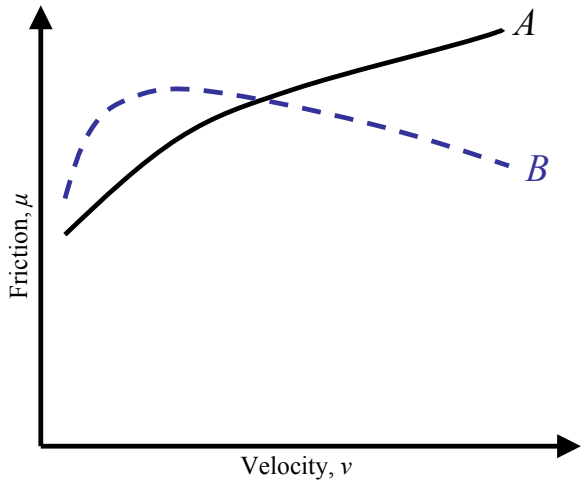

Figure 29. Friction vs. velocity graph, used to assess friction induced vibration. Oil A does not exhibit shudder, oil B is likely to cause shudder due to the reduction in friction with velocity.

The strength of wet friction materials decreases under repeated compression loading as pores grow in the direction parallel to the surface of the friction material. Pore growth occurs through cleavage of cellulose fibre from the matrix (failure). The fatigue life of friction material is dependent on the Automatic Transmission Fluid (ATF). It has been observed by Chiba et al. [87] that the fatigue life of wet clutch friction materials differed depending on the fluid used, but the strain level at the time of failure was equal for various types of fluid. Wear of wet friction material leads to a reduced torque capacity (low efficiency) and increased likelihood of shudder. Wear on the steel friction plate tends only to be mild abrasion.

2.3 LUBRICANT CHEMISTRY & SURFACE INTERACTION

This Section outlines the background to lubricants[§] so that, in assessing whether electrostatic charge monitoring can be used to aid additive chemists, cross-correlation between additive performance and electrostatic charge can be made.

2.3.1 BACKGROUND: LUBRICANT FORMULATING AND TESTING

Alone, Basestock oil properties are insufficient to meet the current demands of engine efficiency (low friction), durability, longer drain times and emissions regulations. Additives are therefore blended with base oils to perform two basic functions, to minimize destructive processes and to confer beneficial properties. Almost all lubricants contain additives, to enhance their performance, in amounts ranging between 5–25% wt. [96,97]. Additive components are generally classified by primary function, but can have other properties which can be beneficial to achieve the desired lubricant performance.

Function	Component	Concentration, %wt.
Base oil (mineral and/or synthetic		75-95
Friction and wear	Viscosity index improver	0-6
	Antiwear additive	0.5-2
	Friction reducer	0-2
	Rust/corrosion inhibitors	0-1
Contamination and cleanliness	Antioxidant	0-1
	Dispersant	1-10
	Detergent	2-8
Maintain fluid properties	Pour point depressant	0-0.5
	Anti-foam additive	0.001

Table 6. Type and concentration of additives typically found in engine lubricants [97].

Formulating a lubricant does not involve blending all the best additives together as this can lead to undesirable interactions between additives. Additives interact in a variety of ways, both in the bulk oil (forming complexes) and on surfaces (competition with other additives for surface sites), resulting in synergies or antagonisms which greatly complicate the task of oil formulation [98]. The most prevalent issue is that additives which perform functions unrelated to friction and wear may affect the performance of friction and wear additives. The interaction between formulation components is not fully understood and therefore a matrix approach is usually adopted to screen lubricant performance; there are several iterative process to optimise the lubricant formulation. The screening tests used during this initial process are typically small scale laboratory (e.g. Pin-on-disc) or engine tests that are cheap to run and can be carried out at a high rate either by being short in duration or by being easy to complete in large numbers. It is important that the screening tests mimic as closely as possible the phenomena that occur in the

[§] The term 'lubricant' and 'oil' are interchangeable and are different from the terms 'base oil', 'basestock' and 'base fluid'. Lubricant and oil imply base oil, basestock or base fluid plus additives.

contacts of interest so that improvements in screening test performance can be relied upon to represent improvements in performance in the engine.

It is necessary for the lubricant formulator to prove (for classification) a lubricant's performance through a wide range of bench and engine tests as specified by the OEMs and industry bodies. Once a formulation has passed the small-scale tests the next stage is full-scale testing, which is very expensive (a typical European passenger vehicle test costing between $15,000 and $20,000). The cost largely depends on the number of rated parameters. Some engine tests required by VW Mercedes Benz and Porsche cost up to $100,000. For US heavy duty diesel engines the average cost is between $80,000 and $100,000; however tests with a greater number of rated parameters range from $250,000 - $500,000. By the time a new range of engine lubricants has been developed, proven and launched, the overall investment was approaching £5 million in 1992 [99]. As newer classifications are introduced the number of engine test and the parameters which are assessed have increased. It is therefore easy to see how the cost of lubricant development is ever increasing. Clearly there is a need to maximise the information gained from each test at both the small and large scale. A real-time measurement which is able to produce information about additive behaviour throughout testing could be of great benefit to the lubricant industry.

2.3.2 BASE OIL

Originally the function of base oils was to provide a fluid layer which separates moving surfaces and wear particles, removes heat, while keeping friction to a minimum. As greater demands were put on lubricants, additives were heavily relied upon, with little change to base oil chemistry. Between 1940s and the late 1980s the lubricants industry relied heavily on additive technology to improve the performance of finished oils. This was the only strategy until a significant improvement in base oil technology was available. The type of basestock, like the additive package, needs to be tailored for specific application/performance requirements. Background information on base oils, including discussions about refinement processes can be found in [31].

2.3.2.1 Important base oil characteristics

In order to determine how well base oils perform, as a component of an automotive lubricant, the following properties must be considered: VI (see Section 2.1.5.2), pressure viscosity index (see Section 2.1.5.3), pour point, cold crank, NOACK volatility and oxidation stability (see Table 7). The type and concentration of *'impurities'* within base oils affects these properties. One of the main *'impurities'* is aromatics. These are good solvents for additives, but they make poor quality base oils because they are among the most reactive components in the natural lube boiling range. Oxidation of aromatics can start a chain reaction that can dramatically shorten the useful life of a base oil. Also the viscosity of aromatic components in a base oil respond relatively poorly to changes in temperature (low VI).

	Test Method	Automotive significance
Viscosity Index	The kinematic viscosity of the oil is measured at 40°C and 100°C using a calibrated glass capillary viscometer (test method ASTM D 445). Test method ASTM D2270-04 assigns a number (see eq(39)) which describes how viscosity varies between these two temperatures.	A high viscosity index indicates that an oil's viscosity is not as dramatically affected as an oil with a low viscosity index. It is a useful parameter to predict whether sufficient lubrication is maintained over a range of service conditions (temperatures).
Pressure viscosity index		Describes how an oil's viscosity changes under load. This is particularly useful for predicting lubricant performance of highly loaded components (e.g. valve-train).
Pour Point	The lowest temperature at which oil will pour or flow	The lowest temperature at which oil is readily able to be pumped in an engine
Cold Crank Simulator	Apparent viscosity of engine oils by cold cranking at temperatures between -5 & -35°C, at shear stresses of 50-100 kPa and shear rates of 10^5 to 10^4 s^{-1}. ASTM Method D 5293	Viscosity in engine journal bearings during cold temperature start-up – the lowest temperature at which an engine will start.
NOACK Volatility	The oil is heated to 150°C for 1 hr. The lighter oil fractions vaporize oil. The test reports results as % weight loss. ASTM D 5800	oil consumption thickening of oil and therefore reduced performance
Oxidation Stability	Assessing resistance to oxidation by Dornte-type oxygen absorption apparatus [100]. Conditions are one atmosphere of pure oxygen at 340 F., reporting the hours to absorption of 1000 ml of O_2 by 100 g of oil. A soluble metal catalyst is used to simulate the average metal content of a used crankcase oil.	Chemical reactions result in the formation of acids (can cause corrosion), sludge and varnish (see Appendix B). This increases viscosity, causes sluggish operation, plugs oil lines and increases wear . Better base oil oxidation stability – better additive stability and longer life.

Table 7. Important properties to assess base oil quality.

Once the oil is refined the additive chemist then adds an appropriate blend of additives to fulfil specific requirements. Therefore the base oil must be able to solubilise the additives under all normal working conditions.

2.3.2.2 API base oil classification

When base oils made by hydrocracking and wax isomerisation showed differentiated performance, the API in 1993 categorize base oils by composition (see Table 8).

Group	Sulphur, wt.%		Saturates, wt.%	Viscosity index (VI)
I	>0.03	*and/or*	<90	80-119
II	≤0.03	*and*	≥90	80-119
III	≤0.03	*and*	≥90	≥120
IV	All polyalphaolefins (PAOs)			
V	All stocks not included in Groups I-IV (e.g. Pale Oils)			

Table 8. API base oil categories [101].

Group I

Group I base oils are manufactured through solvent refinement, but contain a high level of impurities.

Group II

Group II base oils are differentiated from Group I because they contain significantly lower levels of impurities; this is achieved through hydroprocessing. This means the oil is more inert and forms less oxidation by-products that increase base oil viscosity and react with additives. However the VI range for Group I and Group II is the same.

Group III[**]

The difference between Group II and III base oils is increased temperature or time in the hydrocracker, producing higher VI.

Group IV[**]

In recent years the market for poly-alpha-olefin (PAO) has significantly increased. This is attributed to the stricter lubricant specifications in Europe that created a niche market for synthetics and semi-synthetic products. One of the main advantages is that it has a high oxidative stability, which enables it to operate more effectively than other base oils at higher temperatures. However, there are also some disadvantages with synthetic basestocks such as the absence of some naturally occurring components, which can act as anti-oxidants and form a weak tribofilm [26]. Also, synthetic lubricants can be very expensive.

2.3.3 GENERIC ADDITIVE-SURFACE INTERACTION

2.3.3.1 Additive-surface interaction: physical and chemical adsorption

In addition to classifying additives into their primary function they can also be classified into chemically inert and chemically active types. Chemically inert additives improve the lubricant physical properties (e.g. emulsifiers, demulsifiers, pour point depressants, foam inhibitors, viscosity modifiers etc.). All the additives tested in this thesis are chemically active. Chemically active additives interact with metals to form protective films to reduce wear, and contaminants to prevent viscosity increases, as well as wear. Chemically active additives include dispersants, detergents, anti-wear, extreme pressure (EP) agents, oxidation inhibitors, friction modifiers (FM), and rust and corrosion inhibitors. The temperature at which an additive reacts with the metal or metal oxide surface significantly affects its activity. Each additive type has a range of temperatures over which it is active [102].

[**] Traditionally, synthetic is the name given to oils which do not contain any of the molecules which are present in crude oil; however Group III base oils are sometimes referred to as synthetic. The use of the word synthetic in the lubricants industry has historically been synonymous with poly-alpha olefins (PAOs) and is made by polymerizing (poly) ethylene.

The term 'chemically active additives' is a misnomer, because these active additives may not chemically react to the surface, but rather physically adsorb. Physical adsorption is achieved through van der Waals forces, hydrogen bonding, ionic bonding etc. Fundamentally, physical adsorption is reversible; usually by temperature. Physical adsorption takes place at the lower end of the temperature range over which the additive is active and can occur at ambient and higher temperatures depending on the polarity of the additive and the impact the additive has on surface energy. Additives that are only weakly bound to the surface may desorb as the temperature rises. The greater the reduction in surface energy, the more strongly absorbed the surface film will be and the greater the likelihood that the additive will remain in place [103]. The latter point is particularly important for those additives which initially physically adsorb and then go on to chemically react with the surface, which is known as chemical adsorption and is irreversible. As the temperature increases so does the surface reactivity, hence chemically adsorbed films tend to occur at high temperatures. A reaction film is similar to chemical adsorption, but where as chemical adsorption only requires temperature, a reaction film involves tribochemical action.

2.3.3.2 The effect of surface composition on additive film formation

The reactivity of a surface affects how additives interact with it. Surfaces generated under rubbing conditions are more reactive towards additives, because the fresh nascent metal surface has a higher reactivity than its oxidised predecessor. Engineers tend to use harder and harder metallurgies to combat abrasive wear. These surfaces are less and less reactive to anti-wear agents and consequently the risk of adhesive wear increases [104].

Most additives are developed and extensively tested on ferrous components. Additives optimised for ferrous components may perform differently on non-ferrous surfaces. How additives perform on non-ferrous surfaces, which have different surface reactivity and adsorption site density, has received increasing interest in recent years, particularly for coatings [45,105-107], but less so for bulk materials. Work investigating additive compatibility with coatings has led to a new generation of additives which are derivatives of those used for ferrous contacts and where a synergistic approach to both coating development and additive development is undertaken [108]. However the behaviour of additives specifically developed for use with non-ferrous contacts is not well understood; this is especially the case for tribofilm formation on non-ferrous/ferrous contacts. The reactivity of the surfaces of a tribo-couple consisting of dissimilar materials is likely to be different. It is therefore predictable that different additives will preferentially adsorb or react onto one surface. Thus the nature of an additive film which forms on each surface is likely to be different.

2.3.3.3 Kinematics of film formation

Although the chemical and physical principles of additive adsorption are relatively well known, the dynamic process of tribofilm formation is not. Tribofilm formation is a dynamic process which involves formation (whether chemical or physical adsorption), removal and replenishment [109]. Understanding the kinematics of surface active additives is of great importance to the lubricant formulator; how readily these additives form surface films and how easily they are removed (tenacity) will dictate their ability to reduce friction and wear.

The thickness of an additive tribofilm is determined by the balance between the rate of film formation/replenishment and the rate of film removal. Lin et al. [110] proposed a very simple model for ZnDTP tribofilm thickness, which is applicable to all surface active additives (see eq(12)). This model is based on the components that contribute to the growth rate of the effective film thickness ($\dot{h}_{effect}$); where ($\dot{h}_{physisorbed}$) is the physisorbed film growth rate, $\dot{h}_{chemisorbed}$ the chemisorbed film growth rate and $\dot{h}_{react}$ the chemically reacting film growth rate.

$$\dot{h}_{effect} = \dot{h}_{physisorbed} + \dot{h}_{chemisorbed} + \dot{h}_{react} \qquad (43)$$

Lin et al. [110] also suggested a generic relationship for good antiwear performance – although it is also valid for friction performance – the rate of tribofilm removal should always be lower or equal to the rate of the tribofilm formation (see eq (44)); where $\dot{h}_{scrape}$ defines the tribofilm removal rate.

$$\dot{h}_{effect} \geq \dot{h}_{scrape} \qquad (44)$$

There are several issues related to the dynamic process of tribofilm formation which are still not fully exploited because of the lack of technology to make truly *in situ* measurements which would enable a more detailed understanding [111]. As will be shown in the following discussions, understanding of additive film kinematics is based on many static observations '*stitched'* together to give an explanation of what happens in real-time.

2.3.4 ADDITIVES

In this subsection the additives used in experimental work are described in detail, such as the additive chemical and physical properties, how they function, what type of film they produce and how this affects friction and wear.

2.3.4.1 Dispersants

The function of deposit control agents is to keep combustion and oxidation products dispersed within the oil; they increase engine life and control oil consumption by maintaining clean, engine operation.

2.3.4.1.1 Chemical & physical composition

Dispersants typically consist of a polar-group, usually oxygen or nitrogen based, and a high molecular weight non-polar-group (between 950-2000 Mwt.) (see Figure 30 (a)). Dispersants will aggregate in oil, the polar-ends group together inwards and the non-polar-ends stick out (see Figure 30 (b)), forming a reverse micelle. It is thought that the driving force for the aggregation of dispersants is H-bounding between amino groups [112].

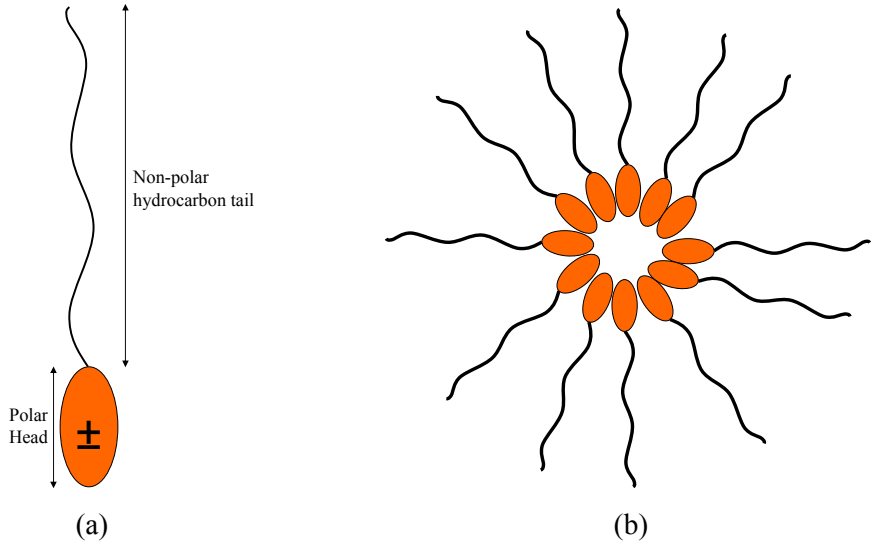

Figure 30. Simplified (a) dispersant molecule and (b) dispersant micelle.

The micelles size is affected by the size of the hydrocarbon tail. For this reason, commercial succinimide dispersants contain high molecular weight polyisobutylene (PIBS) groups, which can form smaller micelles and associated with more material than hydrocarbon tails of a lower molecular weight. Two of the most common dispersants are mono-succinimide and bis-succinimide (see Figure 31); aggregation numbers[††] for mono are more than twice those for bis due to steric effects of the hydrocarbon tail(s). Bis-succinimides are often used instead of mono-succinimides because they give better dispersancy per number of N atoms; in addition H-atoms of the amino groups are more masked and thus not so involved in undesirable reactions [98]. Polymeric succinimides are also used; they exhibit greater dispersancy still.

[††] Micelles form aggregates when their concentration exceeds a characteristic value known as the critical micelle concentration. The number of molecules per micelle is called the aggregation number

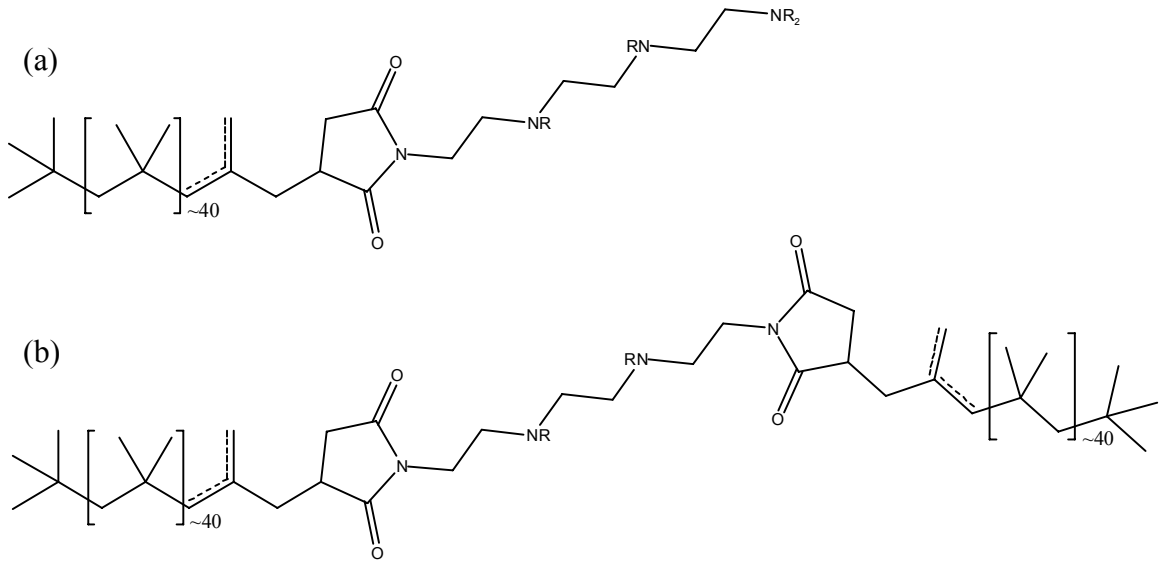

Figure 31. Chemical structure of (a) mono-succinimide and (b) bis-succinimide dispersants.

2.3.4.1.2 Dispersant behaviour in bulk lubricant

Before 1955 only detergents (See Section 2.3.4.2) were used to keep engines clean. This was effective provided that the engine was operated at relatively high temperatures. Low operating temperatures as a result of short-distance/stop-and-go type driving, do not allow engine oil temperature to rise sufficiently. Dispersants are better at suspending oil insolubles at low temperature than detergents [98]. In diesel engines the major contribution to insolubles comes from carbon/soot (see Section 2.3.8.2) and oxidation products of the fuel and oil. More recently, European OEMs have identified low temperature wear as an area of concern [99].

Dispersants control sludge and reduce formation of large soot particles. The mechanism whereby this occurs can be represented by a basic dispersant molecule attaching itself to an acidic site on the soot surface (see Figure 32 (a)). Proton transfer from the acid group to the succinimide group (dispersant) can lead to charge formation (see Figure 32 (b)). The non-polar-groups (hydrocarbon chains) keep soot suspended in the bulk lubricant and prevent soot particles from coming together. Coalescence is prevented through either steric or electrostatic factors [113]. The stability of the dispersion is influenced by the molecular weight of the non-polar-group and the level of reactive sites within the polar-region. Desorption of polar-head groups of dispersants can leave charge on the soot surface. These soot surface charges lead to mutual electrostatic repulsion of modified soot particles (see Figure 32 (d)) [114]. Dispersants can have secondary properties such as lowering the surface/interfacial energy of the polar species and reducing their adherence to metal surfaces and some act as VII (see Section Appendix D).

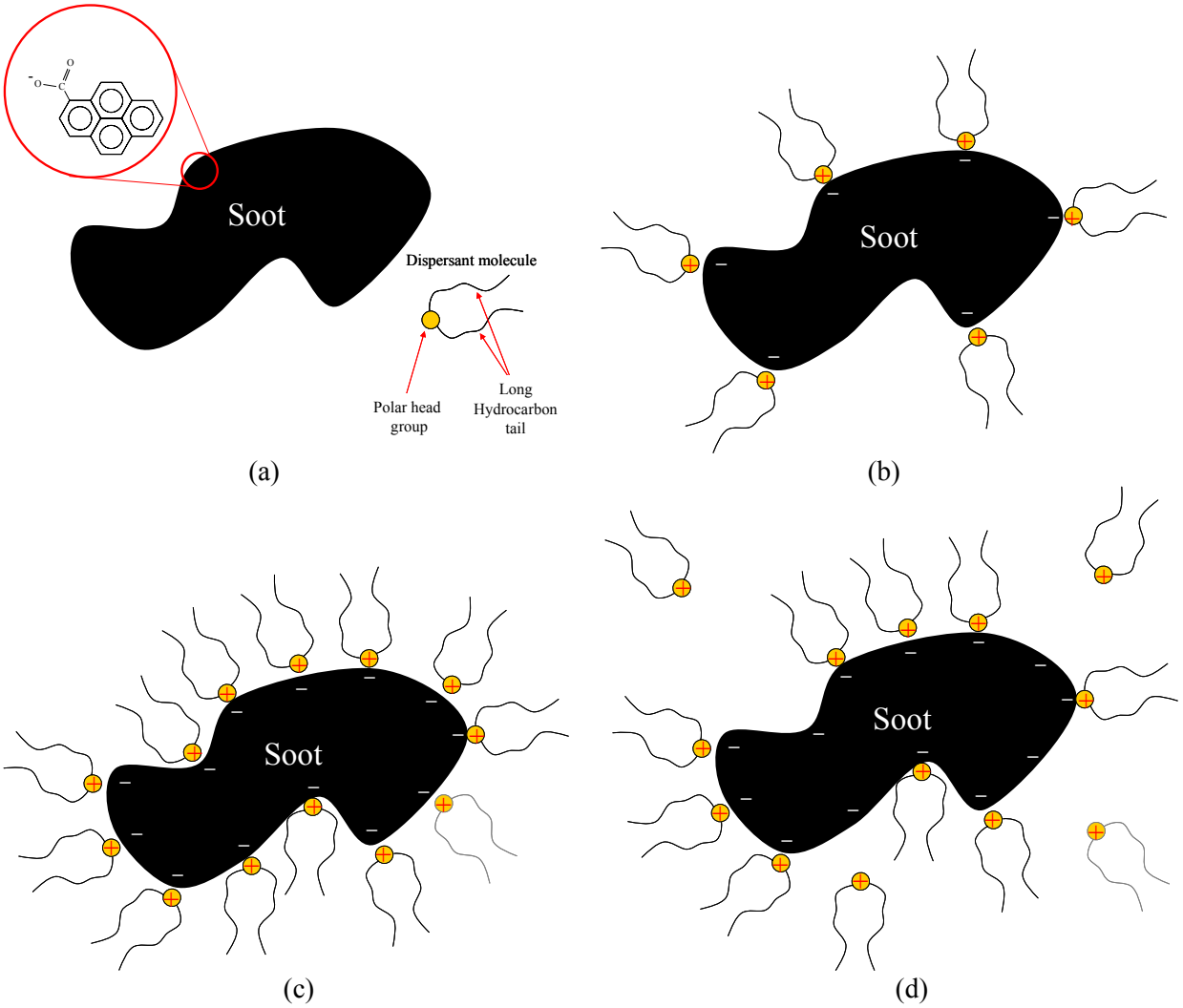

Figure 32. *Dispersant action on soot and charge formation; (a) Dispersant molecule can attach to an acidic site on the soot surface; (b) proton transfer from the acid group to the succinimide group leads to charge formation; (c) coalescence is prevented through either steric or electrostatic factors, and (d) if the dispersant molecule desorbs from the soot particle, a charge can be left on the soot surface, which leads to mutual electrostatic repulsion of modified soot particles.*

2.3.4.1.3 Surface films composition and kinematics

Dispersants can also physically adsorb onto an acidic site on a metal surface. The stability of the dispersant film is influenced by the molecular weight of the hydrocarbon tail and the number of functional groups contained within the polar-region of the dispersant.

2.3.4.1.4 Tribological properties

Apart from their use in wet frictional clutches (see Sections 2.2.4 & 2.3.7), the tribological properties of dispersants films has not been heavily studied. A dispersant film may yield some wear reducing

properties, but generally dispersants offer little or no benefit to wear performance. Similarly there is little information about the friction performance of dispersants, but it is intuitive that the high molecular weight of the hydrocarbon tail will increase the viscosity locally and thus increase friction. Dispersants may have a greater affect on tribological performance of additive packages as they may compete with antiwear and/or friction modifier additives for surface sites or interfere with their surface activity, thus reducing the coverage of the friction modifying and antiwear additives.

2.3.4.2 Detergents

Originally detergents were developed and used to control corrosion and minimise high temperature engine varnish and lacquer deposit (see Figure 161) build-up in engines. More recently it has been observed that detergents exhibit very good extreme pressure[‡‡] (EP) properties [115-117] and are therefore used in automatic transmission fluids and industrial oils [118].

2.3.4.2.1 Chemical structure and physical form

Many alkaline and earth-alkaline mineral salts (e.g. carbonate & borate (see Section 2.3.4.5.3)) possess potentially excellent tribological properties (e.g. low wear), but they are insoluble in organic solvent (oil) [116]. However, mineral salts can be incorporated into organic solvent in the form of a reverse micelle [119,120] (similar to dispersant, see Section 2.3.4.1.1). Surfactant surrounds the mineral salt to form a stable micelle within the oil [121,122]. Ottewill et al. [123] investigated the physical properties of overbased calcium carbonate (the most common metal salt used in detergents) detergent and proposed a concentric shell model consisting of a spherical core (1-10nm) of metal carbonate surrounded by a monolayer (shell) of surfactant (1-5nm) (see Figure 33). The surfactant polar-group is located near the polar mineral core while the hydrocarbon tail is unfolded to the organic solvent, thus keeping the metal salt in solution. This model has also been proposed by several other authors [124-126]. Detergents have aggregation numbers[††] from 5 to 20 [112].

[‡‡] The discussion of detergents could equally fit in the extreme pressure additive section, but due to the similarity to dispersant and the fact that it is primarily a deposit control agent it is discussed here, after the dispersant

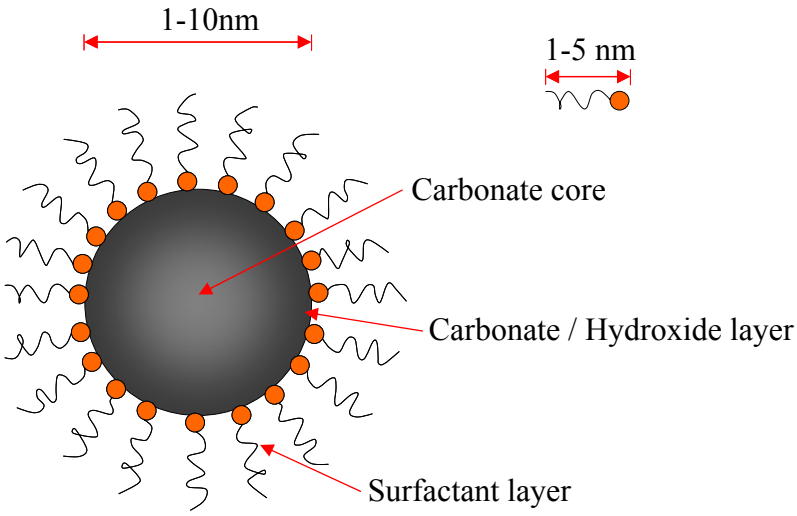

Figure 33. Schematic diagram of thee concentric shell model of overbased detergents. The model consists of a spherical core of metal carbonate surrounded by a monolayer of surfactant.

The most studied mineral salts are calcium, magnesium or sodium carbonates [123,127,128129] and calcium borate [130,131]. Usually detergents contain an excess base and are described as overbased; this is derived from the fact that the metal cation to surfactant ratio is greater than one. Detergent classification usually involves the total base number[§§] (TBN). The mineral core can be crystalline or amorphous; in general the mineral core in detergents is amorphous [132]. The literature suggests that a stable system requires a certain amount of residual calcium hydroxide, thus the inorganic core is amorphous [133]; if carbonation is driven to completion, the cores transform into crystalline calcite.

The surfactant polar-head that binds to the mineral salt is typically: carboxylic acid, glycol, alcohol, sulphonate, phenate, salicylate, phosphonate and naphthenate [129,134]. Phenate [135,136] stabilised systems have been found to have a similar structure to the sulphonate species. However, phenate surfactants are thought to produce micelles which are discus-shaped (oblate spheroidal / flatter structure) with an axial arrangement of the surfactant molecules around the equator [135,137,138]; sulphonate and slicylate [139] are more spherical by comparison [140]. For sulphurised calcium phenate, the sulphur bridge constrains the geometry of the molecule so that the two phenyl rings do not fall in the same plane but are out of plane by approximately 20 degrees [135]. Some of these polar-heads can give other desirable properties, for example, sulphonates have particularly good antirust properties and phenates provide oxidation inhibition properties. Connected to the polar-head are one or more alkyl chains (hydrocarbon tails) ranging in size from C_9 to C_{60} [129].

[§§] The base number is defined as the amount of potassium hydroxide that would be equivalent to a gram of the material, and therefore is expressed as mgKOH/g. (ASTM D-2896).

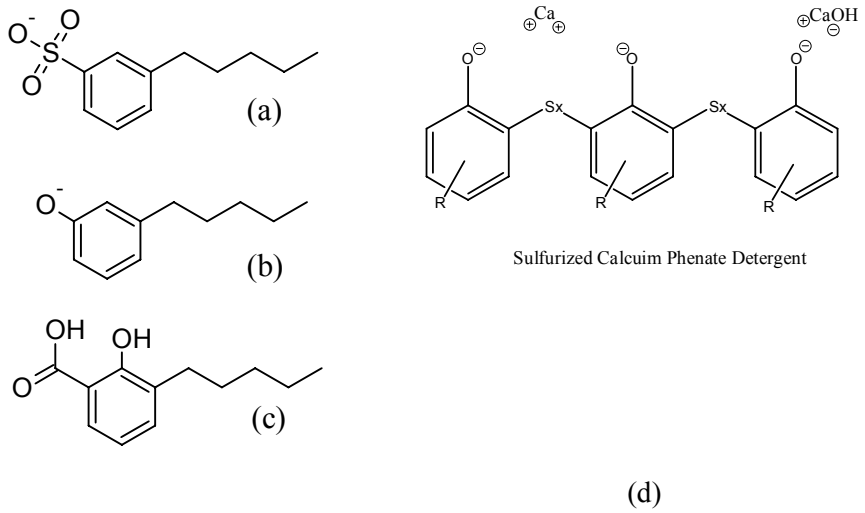

Figure 34. Chemical drawings of (a) sulphonate, (b) phenate (c) salicylate and (d) sulphurised calcium phenate detergent, surfactants used to stabilise excess base, usually in the form of calcium carbonate.

Electrophoretic studies of these systems have given evidence that overbased detergents can carry an appreciable electrostatic charge [135]. Miller [141] suggested that this arises from a dynamic equilibrium between the surfactant adsorbed to the base and the solvent strength. However, it has been argued, principally through molecular modelling, that strong Coulombic forces (originating from the inorganic core material) binding the surfactant to the carbonate core [140] and that once nanoparticles of $CaCO_3$ are formed, the stabilising surfactant molecules are essentially *'locked'* in place on the surface.

2.3.4.2.2 Neutralisation

Detergents neutralise acidic combustion (see Section 2.3.8.1) and oxidation products, thereby minimising corrosion, rust and deposit formation on surfaces in engine. The mechanism of acid neutralisation involves base transfer from detergent to the acid-containing droplet (see Figure 35) [142,143]. The organic proportion of the detergent enables solubilisation of the salts formed by neutralisation and keeps them suspended in the bulk lubricant. Although the TBN is a good guide to the neutralisation capacity of a detergent it does not give any indication of the neutralisation efficiency of the additive. Detergents containing an excess base not only neutralise corrosive products but also form surface films that isolate metal surfaces from corrosive agents [113,144].

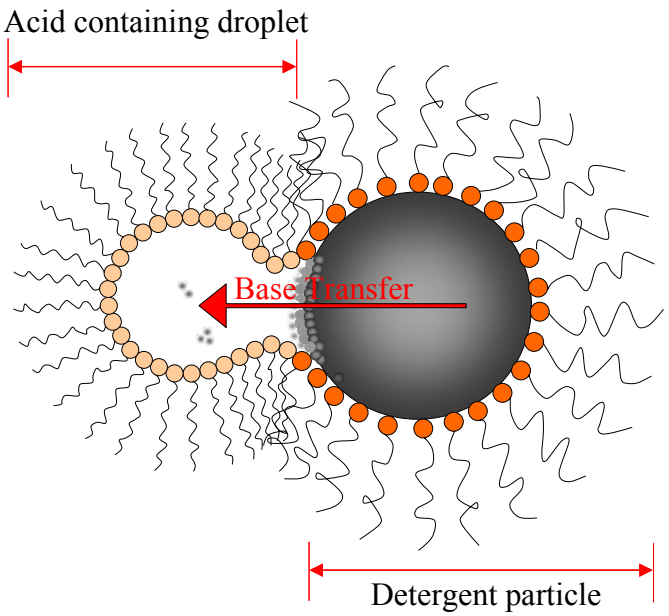

Figure 35. Schematic diagram of the transfer of base from a detergent particle to an acid-containing droplet (without micro-emulsion), during an effective collision [132]. This is a key step in the mechanism of the neutralisation proposed by Hone et. al [143] for their measurement system.

2.3.4.2.3 Detergent surface film composition & kinematics

In addition to engine oils, overbased metallic detergents are also used in gear oils, automatic transmission fluids and other industrial oils. In these applications, the additive does not act primarily as a detergent, but rather as a rust inhibitor and antiwear/extreme pressure agent or for stabilizing friction characteristics [116,145- 150].

2.3.4.2.3.1 Surface film composition

In the literature there is a great deal of variation in the description of detergent surface films. Early work led to the belief that the surface film was just physically adsorbed detergent; this was based on the observation that proportions of sulphur and calcium (from calcium sulphonate detergent) were identical at the surface and in the oil [151]. More recently, Costello et al. [152] reported that both crystalline and amorphous calcium sulphonate formed thin layers of $CaCO_3$ on top of a thicker layer of iron sulphide. However, there are papers which suggest that both amorphous and crystalline overbased calcium sulphonate form a thicker layer of CaO (from $CaCO_3$ decomposition, see Section 2.3.4.2.3.2) on the ferrous surface [153-155]. On the uppermost surface sulphonate and $CaCO_3$ are present and are derived from adsorbed overbased calcium sulphonate. The reported thickness of these films varies from 100 nm [156] to 250 nm [155], however thin films (<10 nm) [153] that do not react strongly with the substrate have been reported. There are no discussions in the literature on the relative proportions of CaO layer and

adsorbed calcium sulphonate, although the CaO layer has been reported to be thicker than the adsorbed $CaCO_3$ and sulphonate layer [154].

2.3.4.2.3.2 Kinematics of film formation

The stoichiometry of the calcium carbonate detergent tribofilm as identified by XPS has been found to be different to the theoretical stoichiometry of calcium carbonate [156]. In addition, it has been found that the thickness of CaO on the wear track was 15 times higher than off the wear track [155]. Both the excess calcium and the greater tribofilm thicknesses are indicative of a tribochemical process on the wear track. Overbased detergents have been reported to form films on rolling contacts, which indicated that elevated pressure and elevated temperature are more important than abrasion (revealing of nascent surface) in promoting the formation of a detergent tribofilm [151].

The current view of the processes involved with detergent tribofilm formation is that micelles are first adsorbed on rubbing surfaces – detergent particles adsorb on metal surfaces even without rubbing [98] – then undergo tribochemical reactions (see Figure 36). Although the mechanism is still unclear, it has been conjectured that part of the $CaCO_3$ decomposes to CaO and CO_2 after deposition on the surface [156]. The conversion of $CaCO_3$ into CaO with loss of CO_2 is thought to be as a result of pyrolysis, rubbing and pressure [155]. Under these conditions CaO crystallises in the tribofilm [145,156].

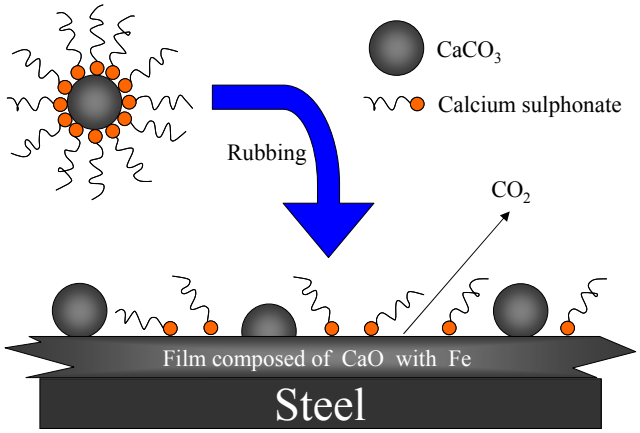

Figure 36. Model structure of boundary films produced by overbased calcium sulphonate [155].

The existence of adsorbed surfactant outside of the wear track has been observed [155]; on the wear track there was a significantly lower amount of surfactant chains. It is thought that because the surfactant is only physically adsorbed (rather than chemically bound) to the carbonate particle, it is expelled from the contact [98]. Cizaire et al. [156] investigated the presence of the surfactant in the tribofilm, under different contact conditions and concluded that;

(1) For lower pressure and shearing, long hydrocarbon surfactant chains are split into smaller units.

(2) At higher contact pressure or for longer sliding distances, the ionic bonds between sulphur and calcium are broken. The Sulphur element is mechanically expelled out of the tribofilm.

2.3.4.2.4 Tribological performance

Overbased calcium sulphonates, in particular, exhibit good wear protection of metallic surfaces [117,146] through the formation of a surface boundary film [145,157]. Over the past few decades the antiwear properties of overbased sulphonates have been explored: Morizur et al. [149], Shirahama et al. [158], Sugimoto [159], Giasson et al. [160] and Willermet et al. [161]. It has been suggested that the surfactants are responsible for the antiwear effect [146]. However, other experiments have shown that surfactant alone does not provide any antiwear properties [126]; the antiwear properties were attributed to the $CaCO_3$ colloidal particles [126,148]. More specifically, it is thought that the antiwear performance is related to the pseudo-graphitic CaO boundary film [149,150,158-162]. Sacrificial shearing of this film is responsible for EP performance [163].

The antiwear properties of detergents depend on their colloidal structure [164] and on their overbased character [165]. Delfort et al. [126] linked the antiwear performance of colloidal calcium carbonates to the size of the mineral $CaCO_3$ particles. Particles of 42.2Å diameter produced a weak antiwear effect, whereas greater antiwear performance was observed for colloidal species having larger (64.3Å) colloidal sizes. Overbased metal detergents have been found to reduce pin and disc wear to a greater extent than neutral metal detergents [155]. It has been observed that the crystalline overbased sulphonates are superior to amorphous overbased sulphonates in EP/AW testing [154,166]. Costello et al [154] presented XPS tribofilm (on steel) depth profiles showing a higher amount of $CaCO_3$ for crystalline overbased sulphonates than amorphous overbased sulphonates. However, in this study the authors had not normalised for particle size (Particle size: amorphous 10-30 nm, crystalline 40-80 nm). Analyses of wear particles by energy-filtered transmission electron microscopy (EFTEM) show the presence of crystallized calcite grains separated by a homogenous pseudo-graphitic layer [146]. Shearing of carbon in these grains prevents cracking, plastic deformation and abrasion [163]. Detergents containing a crystallised core already contain the optimal structure to minimise wear [167], whereas amorphous detergent cores need to be converted into a crystalline structure to provide good EP properties; for this reason crystallised detergents are thought to be better EP additives than amorphous detergents.

The literature is inconclusive about the friction behaviour of detergent tribofilms. Detergents have been shown to increase friction compared to base oil [156] (although given sufficient time it dropped to a level close to the base oil). Other researchers have reported outstanding friction reduction and low fluctuation even at prolonged test [155]. This inconsistency is probably due to the wide variety of detergent surfactant structures.

Many investigations have tried to relate aspects of the tribofilm to friction performance, including: film topography, CaO grain structure, adsorbed surfactant and the source of base. Costello et al. [154] observed that many of the tribofilms studied contained calcium-rich regions which were rough or contained particles >100 nm; a rough film may increase friction (see Section 2.1.3). Minami et al. [162] suggested that CaO deposited on rubbing surface plays an important role on reduction of friction (and wear); shearing of the pseudo-graphitic layer; could have a friction reducing affect. Also, the hydrocarbon tails of the surfactant could produce a friction reducing affect, provided they are able to remain adsorbed to the surface and not shear off; their hydrocarbon tails are not dissimilar to organic friction modifier tails (see Section 2.3.4.3.1). The source of base has also been found to affect friction. Costello et al. [166] found that the friction performance of the amorphous overbased calcium sulphonate, was slightly lower than a magnesium sulphonate detergent. The authors sited the difference in hardness as a possible explanation; the softer calcium carbonate providing more lubricity than the harder magnesium carbonate (3 versus 4 Mohs hardness).

2.3.4.3 Friction modifiers

Friction modifiers (FMs) were originally developed to minimise shudder (see Section 2.1.2) in automatic transmissions. However, since fuel economy became an international issue, FMs have been used in crankcase lubricants (see Section 2.3.5.1) to improve fuel efficiency. FMs are surfactants that significantly reduce COF at low concentrations (see Table 9). Friction modified lubricant films consist of closely packed multi-molecular layers which are loosely adhering to each other. The outer layers of the film can be easily sheared off, allowing for a low coefficient of friction (COF). Unfortunately, due to the requirement of surface active sites deterioration in anti-wear, performance can become an issue.

Lubrication mode	Coefficient of friction
Non lubricated surface	0.5 – 7
Antiwear / EP films	0.12 – 0.18
Friction modified films	0.06 – 0.08
Elasto-hydrodynamic lubrication	0.001 – 0.01

Table 9. Lubrication modes versus coefficient of friction [113].

Broadly, there are three main categories of FM organic, metallo-organic and mechanical, all with differing modes of action. This thesis presents work involving organic FMs which physically adsorb to the surface and metallo-organic FMs, which chemically react to the surface.

2.3.4.3.1 Organic friction modifiers

Organic friction modifiers generally have long, straight hydrocarbon chains consisting of at least 10 carbon atoms and a polar-group at one end (similar to dispersant and detergent surfactant (see Sections

2.3.4.1.1 & 2.3.4.2.1 respectively)). There are a large number of organic modifiers, which have differing modes of action and result in varied friction reduction. Table 10 shows FMs classified by mode of action.

Mode of action	Examples
Formation of adsorbed layers	Long-chain carboxylic acids, esters, ethers, amines, amides, imides
Formation of reacted layers	Saturated fatty acids, sulphur-containing fatty acids
Formation of polymers	Unsaturated fatty acids, methacrylates, sulphurised olefins
Mechanical types	Organic polymers

Table 10. Friction modifier mode of action and examples.

The formation of absorbed layers occurs by attachment of the polar-head to metal surfaces by hydrogen bonding. The polar-head is anchored to the metal surface, while the hydrocarbon tail is left solubilised in the oil, perpendicular to the metal surface. The polar-heads of other friction modifiers are attracted to each other by hydrogen bonding and Debye orientation forces (see Figure 37). Van der Walls forces cause the molecules to align themselves such that they form multi-molecular clusters that are parallel to each other. The orienting field of the absorbed layer induces further clusters to position themselves with their methyl groups stacking onto the methyl groups of the tails of the adsorbed monolayer [168]. As a result, all molecules line up straight, perpendicular to the metal surface, leading to a multilayer matrix of friction modifier molecules (see Figure 38 (a)). The FM layers are easy to shear at the hydrocarbon tail interfaces (see Figure 38 (b)). Sheared-off layers are easily rebuilt to their original state, due to the strong orienting forces mentioned above. A conventional organic friction modifier will reduce the boundary COF from about 0.13 to 0.11, an improvement that will result in a modest but nevertheless useful gain in fuel efficiency performance.

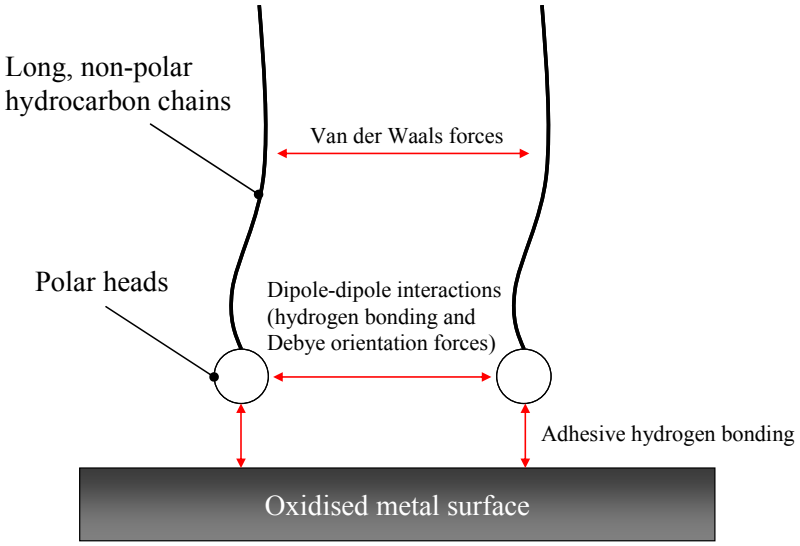

Figure 37. Formation of organic friction modifier adsorbed layers.

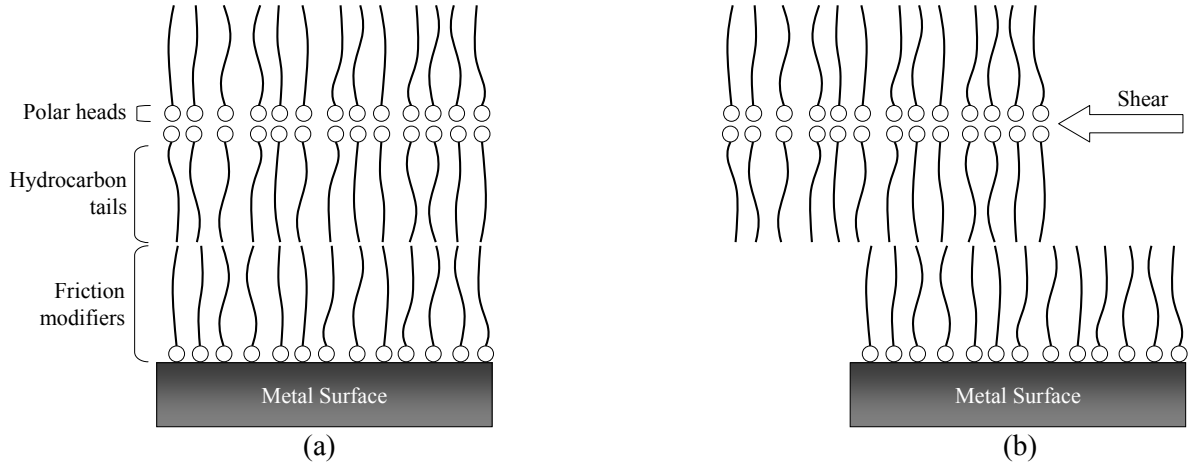

Figure 38. (a) Multilayer matrix of friction modifier molecules and (b) stripping of multilayer.

The thickness and effectiveness of the adsorbed friction modifier depend on: polar-group, hydrocarbon chain length, molecule configuration and temperature. The degree of hydrogen-bonding capability of the polar-head affects the adsorption. One of the most frequently used organic FMs, glycerol mono-oleate (GMO) is strongly polar due to the presence of hydroxyl groups [169] (see Figure 39)). Longer hydrocarbon chains increase the thickness of the adsorbed film as well as increasing Van der Walls interactions between the hydrocarbon chains [170]. Thin molecules increase packing efficiency (denser additive coverage) which also increases van der Walls interactions between adjacent chains and leads to more tenacious films. Temperature affects the FM film tenacity and thickness (see Section 2.3.3.1); adsorption of FMs to the surface occurs at relatively low temperatures, high temperatures might provide enough energy to desorb the FM molecules.

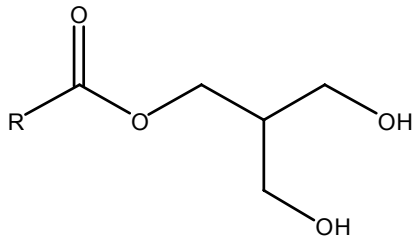

Figure 39. Structure of glycerol mono-oleate (GMO).

2.3.4.3.2 Reacted layers

Some FMs chemically react with the surface to form friction reducing films. Unlike other chemical film forming additives (e.g. antiwear and EPs), the reaction of FMs with the surface has to occur under the relatively mild conditions (temperature, load) in the mixed lubrication regime. A fairly high level of chemical activity is therefore required for FMs; hence, the presence of phosphorus and sulphur in chemical film forming FM additives.

The most popular FM, which reacts chemically to the surface, is Molybdenum-dithiocarbamate (MoDTC), a metallo-organic FM (see Figure 40). The typical friction response for a MoDTC-containing lubricant shows two distinct regions, an initial high friction region, called the induction phase, followed by a reduced friction phase [111]. Morina et al. [171] reported that the initial film contained N and S; no Mo-containing tribofilm is formed [172]. MoDTC breaks down to form a carbon-based tribofilm containing a few per cent of highly dispersed Molybdenum disulfide (MoS2) in the form of individual sheets less than 10 nm [173] in length. It is MoS_2 that is responsible for reducing friction [172-175]; the layer-lattice structure of the MoS_2 facilitates low friction between the tribo-couple [172]. The MoS_2 molecule contains strong covalent bonds between atomic species, but weak van der Waals attraction between lattice layers (see Figure 41). The low friction properties result from weak van der Waals forces enabling the lattice layers to be easily sheared.

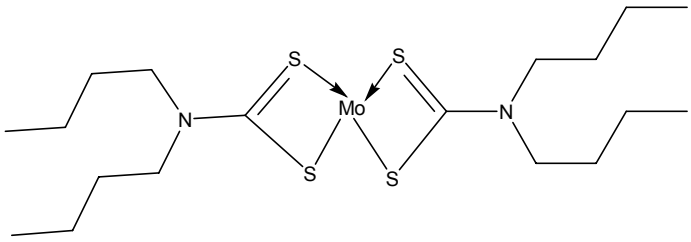

Figure 40. Structure of molybdenum dithiocarbamate (MoDTC).

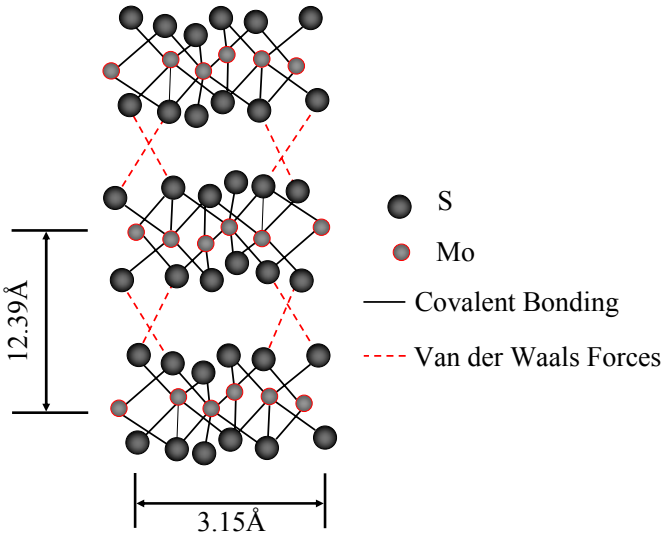

Figure 41. MoS_2 solid state structure [111].

2.3.4.4 Antiwear additive – ZnDTP

Antiwear additives are types of compounds that provide good wear resisting properties in mixed to boundary lubrication. Such materials have the capacity to build strong layers under severe load conditions and protect metallic surfaces moving relative to each other from damage.

Antiwear performance in the automotive industry has largely been met by the use of zinc-dialkyldithiophosphate (ZnDTP) additives. Although introduced in the 1940s as antioxidants, their role as antiwear additives was only realized in the 1950s. Recently there have been increased restrictions[***] on the amount of phosphorus allowable in lubricants (see Table 11), ZnDTP film formation remains heavily researched. This is for two main reasons; to actively make a reduced amount of ZnDTP more efficient at antiwear performance, and to understand the mechanisms behind ZnDTP film formation, which may enable a replacement for ZnDTP in the long term. This Section discusses chemical and physical properties of ZnDTP films, current proposed mechanisms for film formation and the tribological performance of the film. More extensive recent reviews can be found in [176-178].

Year	Standard	P & S restriction
1989	SG	No P, S limits
1994	SH, GF-1	$\leq$ 0.12% wt. P
1997	SJ, GF-2	$\leq$ 0.10% wt. P
2000	SL, GF-3	$\leq$ 0.10% wt. P
2004	GF-4	0.06% wt. $\leq$ P $\leq$ 0.08% wt.
2007/8	GF-5	-

Table 11. Phosphorous and sulphur limits in engine oil specifications modified from [176].

2.3.4.4.1 Chemical structure

The type of ZnDTP is defined by the organic alcohol used to synthesise it: alkylphenols for aryl ZnDTP, primary alcohols for primary ZnDTP ($CH_3CH_2CH_2CH_2O$–), and secondary alcohols for secondary ZnDTP ($CH_3CH_2CH(CH_3)O$–) (see Figure 42). A primary ZnDTP is more thermally stable than a secondary ZnDTP; aryl ZnDTP is more thermally stable than both primary and secondary ZnDTPs [179]. There is

[***] In the 1970s, due to the concern vehicle emissions have on photochemical smog – and is now accompanied by global warming concerns – legal requirements on limiting exhaust products was brought in. One of the major design changes to the automobile was the use of a catalytic converter, positioned between the exhaust outlet and rear silencer. The most common is a three-way catalyst, the nitrogen oxide content in exhaust gas acts as the oxidizing agent to promote combustion of carbon monoxide and hydrocarbons to carbon dioxide and water, while the nitrogen oxides, being stripped of their oxygen, are reduced to nitrogen. Cheaper catalytic converters using base metals, instead of precious metals, have been developed but these are poisoned by small quantities of elements such as sulphur and phosphorus which are the active agents in ZnDTP additives. This has major implications for the use of ZnDTP additives in oil, as any oil that is combusted will reduce the efficiency of the catalytic converters, preventing the required conversion of exhaust products. Lubricant regulatory bodies are therefore continually reducing the amount of phosphorous allowable.

an inverse relationship between temperature of thermal decomposition and the potency of antiwear protection. The ZnDTP which is the most efficient for antiwear film formation is likely to be the one which suffers depletion due to thermal effects. Secondary ZnDTP gives superior wear protection at lower temperatures than primary ZnDTP but is destroyed more quickly at high temperatures. For this reason, the primary ZnDTPs are generally preferred for use in diesel engines while the secondary ZnDTPs are preferred for use in gasoline engines [180] (gasoline engines operate at a lower temperature than diesel engines).

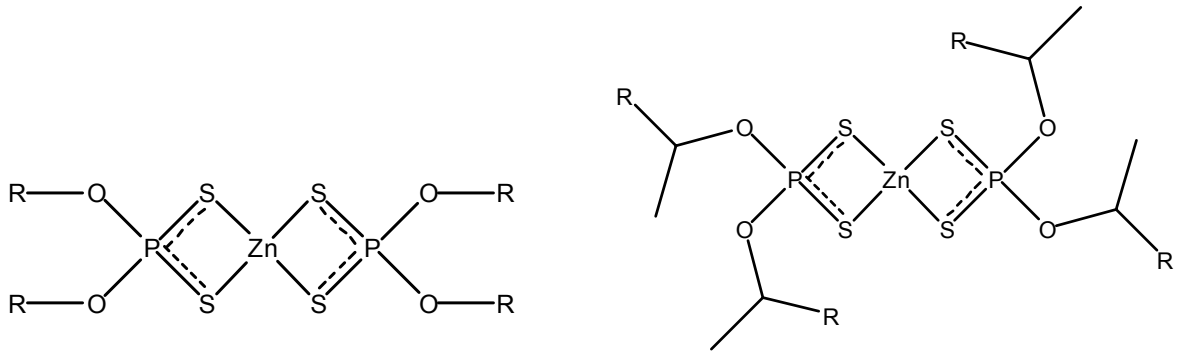

Figure 42. General chemical structure for (a) primary and (b) secondary alcohol zinc dialkyldithiophosphate (ZnDTP).

2.3.4.4.2 Oxidation inhibition

ZnDTPs are highly effective oxidation inhibitors because they decompose hydroperoxides[†††] [181] and peroxy-radicals [182,183]. This combined action makes them very effective as an antioxidant. In addition, the reaction products that ZnDTP generates when it reacts with hydroperoxides and peroxy radicals are also effective oxidation inhibitors [184], making ZnDTP a highly efficient inhibitor. Empirical determination of the relative antioxidant capability of the three main classes of ZnDTP shows secondary > primary > aryl [96]. There is agreement that when ZnDTPs act in their peroxide-decomposing role, the species that they form are no longer able to produce effective zinc phosphate antiwear films [185].

2.3.4.4.3 ZnDTP tribofilm

2.3.4.4.3.1 Structure of ZnDTP antiwear film

The chemical structure of a ZnDTP tribofilm is complex, consisting of three layers: an inner chemically reacted film, a chemisorbed layer and a physisorbed gel-like layer [110,186,187] (see Figure 43).

[†††] The oxidation of hydrocarbon chains is caused by the peroxide oxidation cycle.

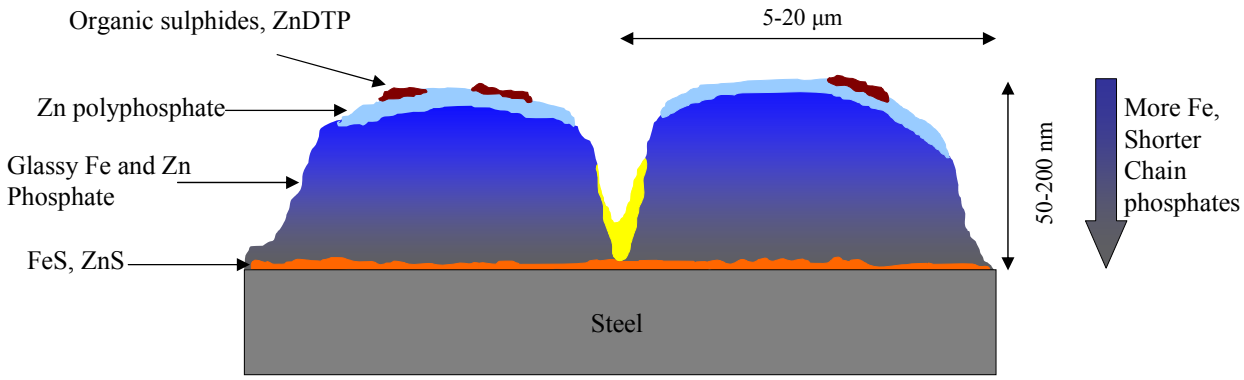

Figure 43. Schematic diagram of pad structure and composition [176].

Chemically reacted layer (FeS)

On the metal surface there is generally thought to be a chemically reacted sulphur-rich layer of zinc or iron sulphide [187-189].

Chemically adsorbed layer (Phosphate)

Above the zinc and/or iron sulphide layer there exists a relatively thick layer consisting mainly of glassy iron and zinc phosphate. Zinc and iron cations act to stabilise the glass structure. The phosphate chains are shorter towards the steel surface than at the top of the tribofilm. (Basic ZnDTPs form very similar tribofilms to neutral salts but with shorter polyphosphate chains in the tribofilm [190]). In addition there is more iron phosphate towards the steel surface [191] and mainly zinc phosphate away from the steel surface. Pyro- or orthophosphate also exists in this layer [191,192], there is negligible thiophosphate (O atoms replaced by S) [179,193]. On top of the glassy iron and zinc phosphate layer there is a thin (less than 10 nm thick) outer layer of zinc polyphosphate.

Gel-like Layer (Organic sulphides, ZnDTP)

Atomic force microscopy (AFM) has enabled the discovery of a gel-like layer covering the solid ZnDTP; this layer had gone un-noticed for a long time due to solvent washing and the use of apparatus which requires a vacuum. This uppermost viscous layer consists of alky phosphate precipitates [187].

ZnDTP tribofilms initially form as separate patches on steel surfaces and these gradually develop to form almost continuous, but still pad-like structures separated by deep valleys (see Figure 43), which are 5-20 µm in diameter. They tend to grow to a thickness of about 50–150 nm on steel surfaces and then stabilise at this level [194-196]. However, the thickness of the full ZnDTP tribofilm, including the viscous over-layer of alkyl phosphate precipitates, is suggested to be up to 1000 nm thick [189,187]. These pads are solid-like up to 150^{o}C.

2.3.4.4.3.2 Kinematics of film formation

A very important area of ZnDTP behaviour, about which far too little is known, concerns the kinetics of formation, removal and replenishment. A lot of research work has tried to decouple different aspects of ZnDTP antiwear film formation; this subsection discusses the chemical processes involved in film formation and poses questions that still remain unanswered.

The thickness and composition of this anti-wear film is directly related to the temperature and the extent of surface rubbing [197]. The rate of film formation increases with increasing temperature [196]. Formation of the ZnDTP film is seen to be increased in more severe rubbing conditions, thicker films are observed when the sliding frequency is decreased and the contact pressure is increased [198].

Adsorption

Studies have shown that ZnDTP molecules physically adsorb on iron via the sulphur atoms [199]. As the temperature is raised above about 60^{o}C, a very striking loss of Zn ions occurs from the tribofilm and adsorption becomes irreversible [200]. Precisely what chemical processes are involved in the formation of ZnDTP antiwear films is not fully understood.

Thermal film formation

Understanding of the nature and formation of ZnDTP has largely been based on studying ZnDTP thermal film formation. This is because thermal films are easily controlled and analysis can be performed during formation – current technology cannot identify chemical intermediates during tribofilm formation. ZnDTPs react in solution at high temperatures (130-230 ^{o}C); this leads to a zinc phosphate solid deposit, alkyl sulphides, mercaptans, hydrogen sulphide and olefins. The mechanism of thermal degradation was proved in to be a result of oxygen and sulphur exchange [201]. The alkyl groups, which are initially bonded to oxygen atoms in ZnDTP are transferred to the sulphur atoms [202,203].

Film	Thermal films	Tribofilms
Found on	entire surface	rubbing tracks [197,204]
Composition	contain long chain polyphosphate on top of shorter chain poly- or orthophosphate glass material [179,192,205 206]	
	little evidence of iron [207]	contains iron within the film [207]
Thickness	similar magnitude up to 200 nm [205]	
Formation (bulk oil) temperature	130-230 ^{o}C	50^{o}C [204], and even at 20^{o}C [106,208]
Indentation modulus	$E^{\bullet} = 35$ GPa [209]	$E^{\bullet} = 35$ 90 GPa [176]
Hardness	$H = 1.5$ GPa [209]	$H = 1.5$ 3.5 GPa [176]
Antiwear performance	good [206]	excellent

Table 12. Similarities and differences between ZnDTP thermal films and ZnDTP tribofilms.

There is some justification in studying ZnDTP thermal films to further understanding in tribofilms; thermal films have similar physical and chemical properties to tribofilms (see Table 12). However there are some significant differences between ZnDTP thermal films and tribofilms. The differences between thermal ZnDTP thermal films and tribofilms infer that thermal decomposition is not the sole mechanism behind ZnDTP tribofilm formation. Thermal degradation products were found to be less effective as antiwear agents than ZnDTP [185,210]. One of the principal degradation products was found to be the disulphide, which on subsequent synthesis and wear testing was shown to be inferior to the ZnDTP. In addition, Fujita et al. [197] concluded, based on tests conducted at different sliding speeds, that thermal action alone cannot explain the kinetics of ZnDTP tribofilm formation and that the existence of some form of surface catalysis that arises during rubbing must be invoked to explain the observed behaviour. The problem is that there is a near absence of equipment which can monitor tribofilm growth and removal and a complete absence of equipment that can identify chemical intermediates formed at the surface of a ZnDTP lubricated contact. This would then help identify whether ZnDTP tribofilm formation is driven by a rubbing, thermal, pressure or a combination of all three to varying degrees.

2.3.4.4.4 Wear

Many researchers have reported ZnDTP tribofilm formation after a short period of rubbing [171,196, 211], and have concluded that ZnDTP works as an antiwear additive from the first stroke. There are currently a few differing views about how ZnDTP provides antiwear behaviour. The most generally accepted view is that the reaction film acts simply as a mechanically protective barrier [212], or that it preferentially wears, rather than the metallic surface. Other mechanisms proposed include; reaction with peroxides preventing corrosion of the metal surface [213,214]; digestion of oxide particles, that would cause abrasive wear, to form relatively soft iron phosphate, [215,216]. There is merit to these suggestions, but it is likely that the mechanical resistance of the film is the predominant factor for reducing wear.

Once formed, ZnDTP tribofilms are generally perceived to be very stable and durable. Their stability has been studied by many researchers; mainly by running a wear test with a ZnDTP containing oil for a period of time and then exchanging the oil to a non-additized oil. Chemical and physical analysis of the tribofilm were carried out at various intervals; it has been found that the ZnDTP tribofilms were worn off only very slowly [195,196,206,217,218]. However, the literature appears to over-look the problem of carrying out chemical and physical analysis *ex-situ*. Any short transient affects are unlikely to be captured by stopping the test at various intervals. Electrical contact resistance (ECR) has been heavily relied upon for information about the tenacity of the ZnDTP tribofilm. This real-time technique gives a good indication of tribofilm presence or absence, but its sensitivity to more subtle changes in film formation is questionable.

There is a relatively small amount of work which questions the view that ZnDTP forms a highly tenacious film. It has been demonstrated that phosphate film antiwear activity is a dynamic process of simultaneous formation and destruction, with films increasing at some points while disappearing at others [219]. A study by Minfray et al. [220] has shown that a ZnDTP tribofilm that was etched into narrow transverse strips, was quite rapidly worn off. Increased sliding distances have shown a reduction of the ZnDTP tribofilm thickness; it was suggested that species which contribute to the film formation can also act as abrasives in the contact region, stimulating the film removal [195,196].

2.3.4.4.5 Friction behaviour

When engine fuel economy became an important issue in the 1980s, lubricant formulators soon noted that some ZnDTPs had a deleterious effect on engine friction and thus fuel economy [221]. However the literature suggests that the friction-ZnDTP film relationship is not that clear. There are conflicting reports on the effect of ZnDTP on friction with some reports of neutral effects [222], some reports of ZnDTP increasing friction [223,224] (consistently over three temperatures [111]) and reports of ZnDTP decreasing friction [225]. The simplified view is that ZnDTP forms films which are semi-plastic deposits that are difficult to shear off. So, under shearing conditions their COF is usually moderate to high. The more widely held view is that ZnDTP reaction films are rough (see pad-like structure in Figure 43) and higher speeds are needed to generate a full separating fluid film than in the absence of a ZnDTP film [204,226] (see Sections 2.1.2 & 2.1.3).

However it has recently been shown that even smooth ZnDTP films give increased friction in mixed lubrication [227,228]. One possible explanation given by Spikes [176] in a review of ZnDTP drew reference to work which suggested the liquid lubricant may slip (inhibits fluid film entrainment, compared to bare metal) against the ZnDTP pad surfaces, which are extremely smooth [229] and coated with a polyphosphate chain material, and thus not be entrained into the rubbing contact. However discussions in [229] included no such statement. The notion that something slippery increases friction seems counter intuitive.

2.3.4.5 Extreme pressure additives

The use of the words antiwear and extreme pressure (EP) to describe the performance of an additive is somewhat subjective. In general, EP is the protection from shock loading, and intermittent applied heavy or sliding loads, whereas antiwear is the prevention of damage caused by moderate and continually loading. EP more commonly refers to highly reactive molecules; these tend to be more active and more corrosive than ZnDTP.

2.3.4.5.1 Organo-sulphides

Function

Sulphur lubricant additives are used [230], to help prolong gear fatigue life by minimising micropitting surface damage [231]. Organic sulphides, although possessing some wear-reducing capability are generally regarded as EP additives [232].

Chemical composition

Alkyl polysulphides have the general formula $R\text{-}(S)_n\text{-}R$ (see Figure 44). The sulphur molecules expected to be the least active are alkyl mono- and di- sulphides ($n=1, 2$); these are not aggressive towards yellow metals (brass). Higher polysulphides, $n>2$, are the most active towards tribofilm formation but are the most corrosive [230]. Long-chain sulphur bridges in polysulphides are thermally less stable than short sulphur bridges. For this reason, the reaction with the metal surfaces is possible at relatively low temperatures [103].

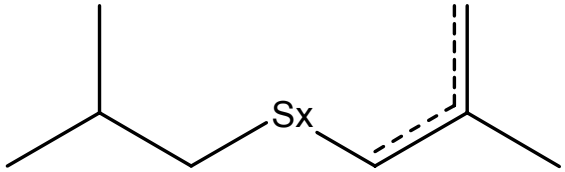

Figure 44. Simplified chemical structures of hydrocarbyl polysulphide gear oil additives.

Film Chemical composition and formation

Polysulphides chemically react with the surface; in the case of a ferrous surface, the reaction product is usually iron sulphide. Iron sulphide has a low shear resistance, which means that the film can easily be removed, but this is off-set by the speed that the film can re-form; the low molecular weight of the additives makes them highly mobile.

Tribological performance

The Polysulphide additive does not provide a mechanical barrier resistant to wear, but rather a film which is preferentially worn away instead of the component surface. The additive must have a sufficient reactivity to form a film quickly – to fulfil the replenishment requirements – yet the additive must not so reactivity that it causes tribo-corrosive wear (see Section 2.1.4). A balance must therefore be found between excellent load-carrying capacity and corrosion; the success of these additives comes from the range of molecular weight. Many reports have demonstrated that organo-polysulphides have excellent load-carrying capacity and low corrosion [233,234]. The low shear nature of an iron sulphide film means that polysulphide exhibits a friction reducing effect.

2.3.4.5.2 Boron containing additives

In the automotive tribology field, non-corrosive anti-wear additives are of particular interest. Potassium borate dispersions, as reported by Adams [235] for gear oils, were found to provide oxidation, wear, and load carrying benefits. This provoked an increasing interest in additives containing boron, as they could replace the more toxic and polluting sulphur and phosphorus compounds [236]. Stanulov et al. [237] reported that nearly half of the phosphorus, in the case of ZnDTP equivalent amounts of Zn and sulphur, can be beneficially replaced by approximately 10 times smaller amounts of boron.

2.3.4.5.3 Inorganic borates and nanoparticle dispersions

Extreme-pressure properties of some inorganic additives have been found to be superior to some organic additives [236,238]. Inorganic borate has been used in gear oil and metal working oil [239] for 40 years, because it possesses excellent load-carrying capacity, good anti-wear properties, friction reducing ability, high thermal stability, and good rust and corrosion characteristics [235].

Chemical and physical structure

Additives based on solids in suspension, such as potassium tri-borate, display anti-wear and extreme pressure properties in spite of high thermal stability [151]. These additives are similar to detergents in their physical structure (see Section 2.3.4.2.1), both contain surfactants which suspend a metal salt, that otherwise would be insoluble (see Figure 45). The main difference between detergents and dispersed potassium borate is the metal salt and the size; detergents are typically 20 nm in diameter whereas dispersed potassium borate is around 200 nm.

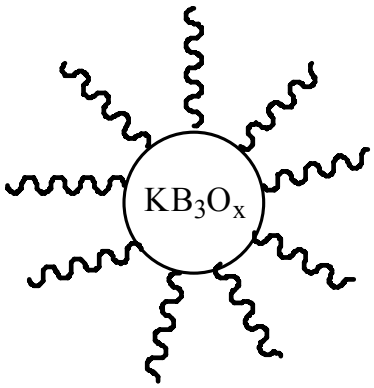

Figure 45. Simplified structures of dispersed potassium borate additive.

Potassium borates have been found to be excellent anti-wear additives [240-242] and perform very well in the FZG SSP180 (synchroniser) rig synchroniser durability test. Adams [243] discussed a potassium borate additive with a boron:potassium mole ratio of 2.5-4.5:1 that has good extreme pressure properties, good hydrolytic stability, improved seal and anti-wear properties, and improved compatibility with other lubricating oil additives, especially ZnDTP [244-246]. Despite claims that insolubility and difficulty of dispersion restrain the application of the inorganic material in lubricating oil [247], potassium borate is

commercially available and has received great interest in the research community. Improvements to the original art described by Adams [243] have shown excellent extreme pressure properties and excellent hydrolytic stability [248-250]. Recent changes have included dispersion of hexagonal boron nitride with dispersed hydrated potassium borate which exhibited excellent anti-wear performance [251].

The majority of publicly available information on the tribological properties of dispersed potassium borate comes from patents. These tend to state the wear performance relative to other additives, or performance during standardised tests. There is little discussion on the nature of the film which forms, how this performs the antiwear function and what friction characteristics it produces.

2.3.5 FORMULATION CONSIDERATIONS

The formulating process starts by understanding the specification set by the industry bodies. Although oils will be blended to try to maximise the number of applications that the oil can be used in, oils are generally formulated for a particular application (see Sections 2.3.5.1, 2.3.6 & 2.3.7). With a few exceptions the engine lubricant and drive-train lubricant are significantly different in terms of their additive content.

2.3.5.1 Crankcase lubricants / engine oils

Automotive engine oils must be able to function over a wide temperature range, lubricating effectively a wide range of contacts and minimise the disastrous affects contaminants can have on wear and friction. Engine oils must exhibit good lubricity at start-up temperatures, which can be sub-Zero ^{o}C, and have sufficient oxidative stability at high temperatures, which can be as high as 270^{o}C around the piston ring/cylinder interface.

Figure 7 shows the regimes in which critical IC engine components operate in, the tribological components rely upon different lubrication mechanisms. This highlights the complex task of formulating a single lubricant to operate effectively within all areas of the engine, thus the formulation will be a compromise in terms of durability, energy efficiency and emission requirements [39]. The engine lubricant, more than any other lubricant, is susceptible to contamination, the sources of which include coolant, fuel and air-borne particulates. Additives within engine oils must neutralise and suspend incomplete combustion products, to prevent them forming deposits on the surface, increasing viscosity and forming large abrasive particle; all of which will affect wear and friction performance. For this reason the drain interval for engine oils is significantly shorter than that for transmission lubricant; there is however increasing pressure to extend the drain interval.

2.3.6 MANUAL TRANSMISSION FLUIDS (MTFS) AND ADDITIVES

Manual transmission fluids (MTFs) must (1) protect against wear, (2) provide friction characteristics for smooth gear shifting, and (3) control oxidation. The synchroniser contact is one of the most complex automotive tribological components, which requires additives to achieve a balance between minimising wear and ensuring the right level of friction to enable smooth gear changes (see Section 2.2.3.1). The synchroniser poses an additional challenge, that of providing sufficient surfaces films on dissimilar tribo-contacts materials (see Section 2.3.3.2). To improve fuel efficiency, small transmissions and low viscosity base fluid are used; this increases demands on the additive system.

Typical MTFs contain highly surface active and reactive compounds such as organo-phosphorus, organo-sulphur [252] (see Section 2.3.4.5.1). Their extreme pressure effectiveness is related to the high reactivity of these decomposition products in the friction zone, and hence to the low thermal stability of the additives [151]. This property is not always compatible with the increasing thermal stability requirements of gearbox lubricants [253] as some transmissions will operate at high temperatures, especially if the exhaust system is in close proximity. The high reactivity is of a particular concern for yellow metals (e.g. brass) used in synchroniser contacts, because they are susceptible to corrosion; for this reason inorganic boron compounds (see Section 2.3.4.5.3) maybe used in MTFs because of their high thermal stability [244,245].

2.3.7 AUTOMATIC TRANSMISSION FLUIDS (ATFS)

ATFs must remove frictional heat, prevent corrosion, minimise wear and act as a hydraulic medium for the transmission of mechanical power quickly and smoothly. The selection of surface active molecules for ATFs is dependent on the friction materials used for the clutch pack [254]. ATFs must satisfy conflicting demands of maximising friction to improve power transmission efficiency (or torque capacity), whilst ensuring smooth gear changes (see 2.2.4.1). Typically dispersants (see Section 2.3.4.1) are used to improve torque capacity (the amount of torque that can be transmitted before slipping occurs), and FMs (see Section 2.3.4.3.1) ensure smooth gear changes and minimise shudder [255]. Matsuoka et al. [256] found that dispersants were effective at retaining the strength of the cellulose fibre, whereas antiwear agents such as ZnDTP and organic phosphates seriously deteriorated fibre strength.

Three functional groups, contained within dispersant and/or FM molecules: amine, amides/imides and acids may all adsorb via H bond to –OH of cellulose and phenolic resin (see Figure 28 & 46). Amines can also form a stronger ionic bond with -OH of phenolic resin [257]. It is expected that amines will form a stronger bond to paper/resin friction materials than amides and acids. Although amides and acids are generally equal in surface activity, the ionic bond created by amines is twice that created by the H-bond of acids and amides. On the other hand, acids can form a chemisorbed film on the steel plate; comparatively, adsorption of amide and amino groups onto steel is likely to be weak. As both dispersants and FMs, used

in work presented in this thesis (succinimides), contain amino groups, similar modes of bonding apply, but the stability of the adsorbed surfactant/surface complex will vary according to the molecular weight, structure, and degree of functionality (number of amine groups associated with the polyamine). FMs have been found to be more effective in reducing COF, when their bond strength to phenol resin is greater [257]; polar-groups are thought to directly effect COF [83]. Adsorption of succinimides to graphitic fibres is expected to be minimal [84], as there are no functional groups to react with.

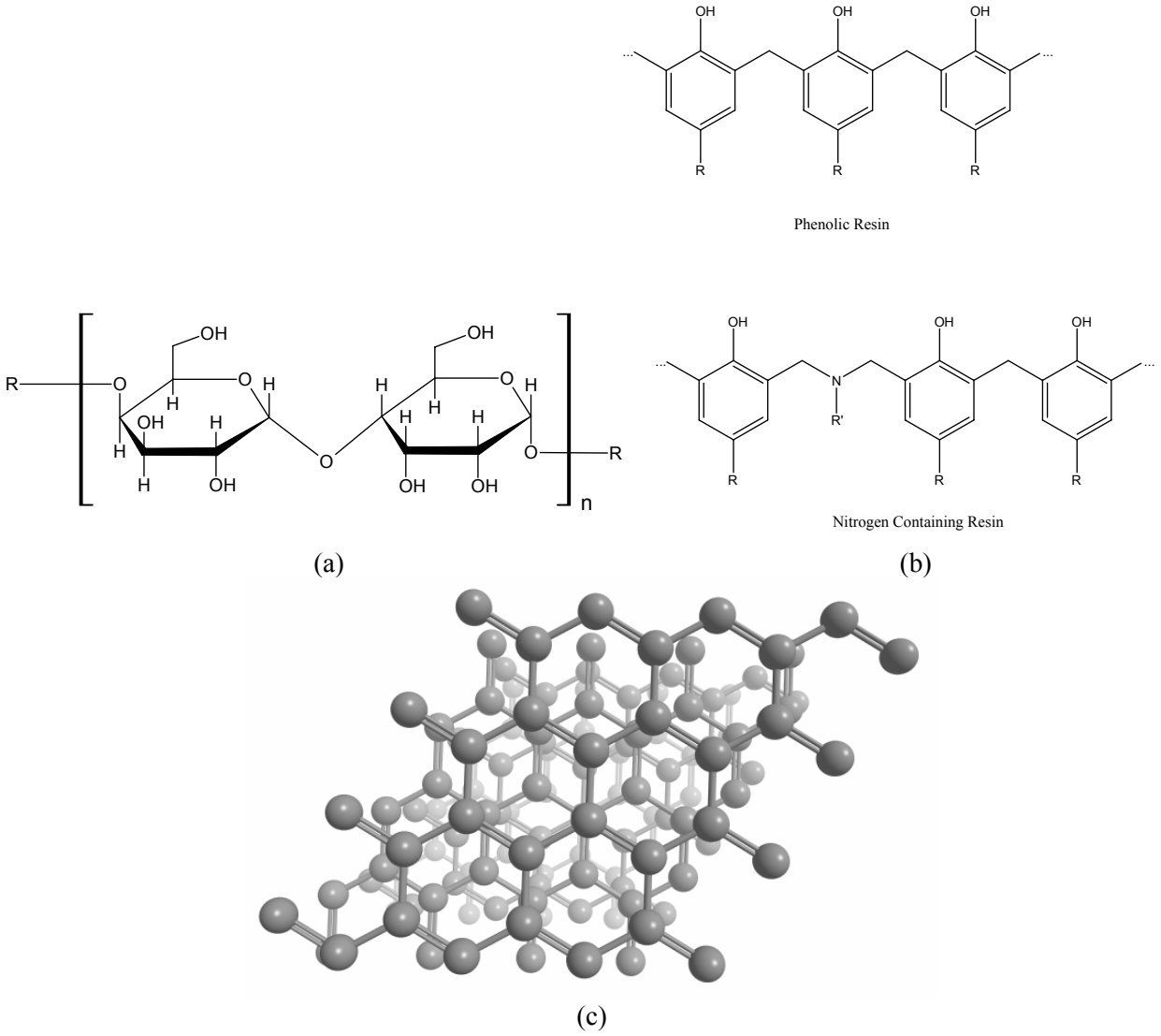

Figure 46. Typical chemical structures for materials found in wet friction material a) cellulose, b) phenolic resin and (c) graphite.

2.3.8 LUBRICANT DEGRADATION PROCESSES

The effect of contact conditions on wear and friction performance has been covered in the previous two sections (2.1 & 2.2). However, degradation of the lubricant itself can lead to undesirable friction and wear performance.

There are many ways to categorise the lubricant degradation processes, by: ingress (e.g. built in contamination, external ingression, internal generation or through maintenance), source (e.g. incomplete combustion, shear, temperature etc), contaminants (e.g. soot, acid, wear debris etc.), affect (e.g. adhesion, abrasion, thickening, corrosion). It is the effect of lubricant degradation on wear that reduces component life that is the ultimate concern. Wear and lubricant thickening that result in a loss in engine performance (primarily from an increase in friction, but changes in component tolerances will also have an effect) will reduce fuel efficiency. Therefore, at the very least, lubricant degradation can shorten useful oil service life, reduce efficiency, but at worst initiate component failure.

To gain an understanding of lubricant degradation processes a considerable amount of research has concentrated on the contaminants that are produced. Contaminants can be sub-categorised into: solids, liquids and gases. Solid particles, such as soot and wear debris, damage mechanical components and catalyse lubricant breakdown. The surfaces of fresh metallic wear particles provide convenient reaction sites for oil oxidation. The reaction products result in varnishes, sludges and increased oil acidity. Liquid contaminants, which include fuel, water and coolant, corrode metal surfaces and hinder function of lubricants. They react with additives; the products are often unable to fulfil functions of minimising wear and friction. Gaseous contaminants, including acidic combustion products, corrode component surfaces and degrade the oil. Needelman et al. [26] presented a table which shows the type of contaminants, the source or how it was generated and the problems associated with that particular type of contaminant (see Table 13).

Type	Primary sources	Major problems
Metallic particles	Component wear	Abrasion Surface roughening leading to adhesion Catalysis of lubricant breakdown
Metal oxides	Component wear Oxidation of metallic particles	Abrasion Surface roughening leading to adhesion
Minerals (i.e. silica sand)	Induction Air	Abrasion Surface roughening leading to adhesion
Exhaust gases	Combustion blowby	Acids promoting lubricant breakdown
Soot	Combustion blowby	Interfere with additives Abrasive wear Heavy deposits Oil thickening/gellation
Water	Combustion blowby Coolant leaks	Metal corrosion Promotes lubricant breakdown
Glycol	Coolant leaks	Lubricant breakdown
Fuel	Blowby-rich mixture	Lubricant breakdown
Acids	Combustion blowby Lubricant breakdown	Metal corrosion Autocatalysis of lubricant breakdown

Table 13. Lubricant contaminant type, source of contaminant and the problems the contaminant causes which hinders lubricant performance [26].

This thesis concentrates on the affect of soot (a contaminant produced through incomplete combustion) on additive performance and component wear. There are however, other lubricant degradation processes such as oxidation, corrosion and shear which also have an affect on additive performance and component wear (see Appendix B & C).

2.3.8.1 Incomplete combustion

Incomplete combustion is the main source of a range of contaminants found in internal combustion engines. The combustion gases in the cylinder are not completely exhausted into the environment; some of these gases pass between the piston rings and cylinder into the sump. These *'blow by gases'* contain incomplete combustion products of the air/fuel mixture such as carbon monoxide, unburned hydrocarbons (soot), water and reactive radicals (eq (45)) and these can become mixed within the lubricant.

$$\text{Fuel} + \text{Air} \Rightarrow CO_2 + H_2O + NO_x + SO_x + CO + C_aH_b(soot) + \text{Radicals} \qquad (45)$$

2.3.8.2 Soot

The work in this thesis focuses on one contaminant, soot. The following Section will therefore concentrate on the production, nature and antagonistic effect soot has on wear. Firstly, it should be noted, that 'soot', as it is frequently referred to actually incorporates exhaust and lubricant soot. **Exhaust soot** is formed through incomplete combustion of the fuel and contaminates the lubricating oil by travelling past the piston rings [258]. **Lubricant soot** is produced through oxidation in the crank-case or in-between the piston ring/liner face, where temperatures are extremely high (around 270^{o}C). Both exhaust and lubricant soot production is mainly a concern in diesel engines; incomplete combustion leads to a large amount of soot being generated and the higher operation temperatures in diesel engines increase the amount of lubricant soot. However soot can occur in direct injection gasoline engines, but the nature and concentration is different to that of diesel engines.

It is difficult to characterise soot in terms of chemical composition because engine, fuel, lubricant and operating conditions will all affect the type produced. It is also extremely difficult to distinguish between fuel and lubricant derived soot. In very general terms soot is made of hydrocarbon fragments, which form aromatic molecular networks [259]. Elemental analysis by inductively coupled plasma-atomic emission spectroscopy (ICP-AES) carried out by Rausa et al. [260] showed that 'typical' soot recovered from used diesel engine oils contain, in addition to carbon, significant levels of H, N, O and S with lower levels of lubricant additive derived species such as Ca (from detergents), Zn and P (from ZnDTP). In an attempt to understand the chemical composition of fuel derived soot Bérubé et al. [261] carried out analysis of diesel exhaust particles by electron probe microanalysis and ICP-AES. This work showed the presence of a wide range of elements including C, O, Na, Mg, K, Al, Si, P, S, Cl, Ca, Ti, Mn, Fe, Zn, Cr, Mo, Ba and Sr.

Clearly, many of these are metallic wear particles from the engine while others are fuel and/or lubricant derived. This is similar to other work, which also identified oil additive-related elements such as phosphorous, zinc and calcium in exhaust soot [262]. This highlights the difficulty in separating fuel and lubricant derived soot, as some of the lubricant manages to get into the combustion chamber and is burnt and exhausted. However it has been speculated that there may be some structural differences between soot from the used lubricant and exhaust soot, with the exhaust soot possibly showing a higher degree of crystallinity [263]. Lowenthal et al. [264] identified what was deemed to be the six most significant compounds and their average percent composition of diesel Particulate Matter/exhaust soot are nitrate (0.09%), sulphate (9.2%), silicate (0.008%), ammonium (0.31%), organic carbon (29.6%) and elemental carbon (53.4%).

Transmission electron microscopy (TEM) analysis has shown that primary soot particles are of the order of 20-30 nm in diameter [263, 265], whether they are collected from the exhaust [261] or extracted from the used lubricant [266]. Figure 47 (a) shows soot particles with a primary size of 28nm. Unless there are electrical and steric barriers to keep them apart (see Section 2.3.4.1.2), soot particles will agglomerate as they approach one another (see Figure 47 (b)). This agglomeration is caused by both van der Waals forces and electrostatic attraction of the charges present on the soot surface [114]. Primary soot particles have a tendency to agglomerate into a larger macrostructure, up to 1 μm in size [263,267], which can lead to a significant rise in oil viscosity, with fuel economy consequences. When aggregates occur on surfaces, such as those of the combustion chamber, soft and flaky soot deposits result.

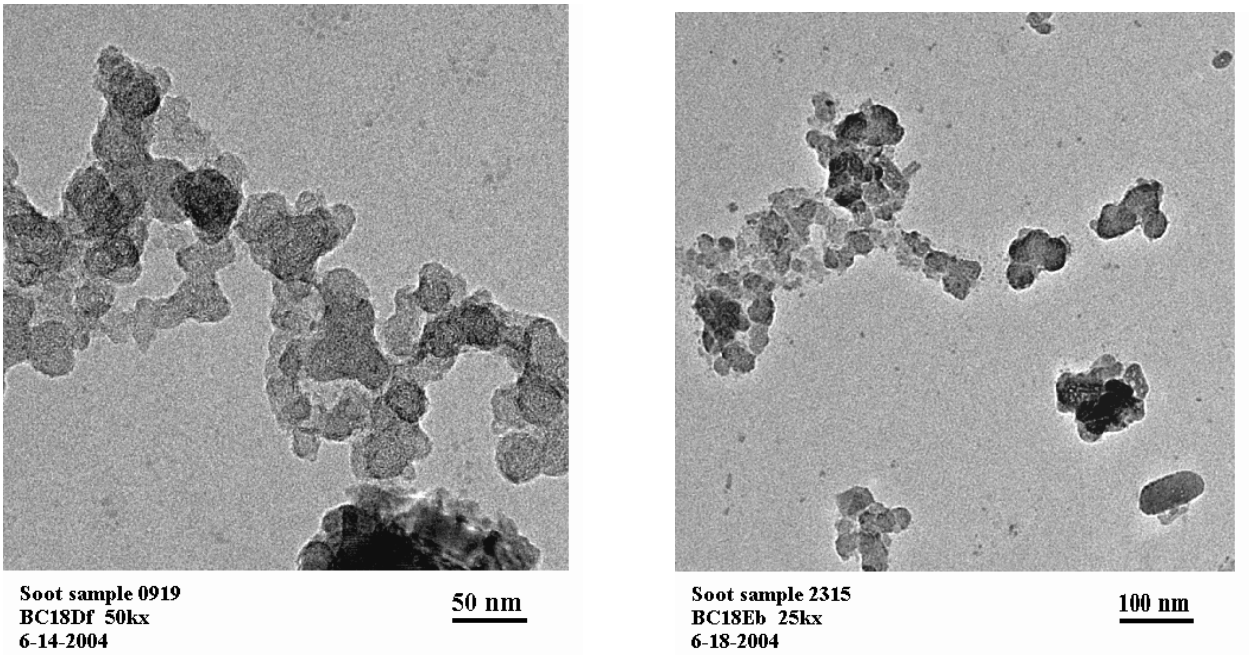

(a) (b)

Figure 47. TEM image[‡‡‡] of (a) primary soot particles and (b) agglomerated soot particles.

[‡‡‡] Courtesy of Chevron Oronite LLC ©

There is great difficulty in obtaining sufficient volumes of well characterised soot for research purposes and even if a sufficient quantity can be obtained, the soot generated will be specific to the engine, fuel, lubricant and operating conditions used. Several attempts have been made to synthesise suitable model soot [260,268]. Most popular have been thermal treatments and/or oxidation of carbon black/oil mixtures to mimic the effects that occur during engine operation. However, the processes used to generate industrial quantities of carbon blacks result in materials whose surface structure and chemistry are generally not well characterised, although their physical properties in terms of particle size, surface area and volatile content, for example, are accurately known [97]. A surrogate such as carbon black is frequently used in bench tests for lubricant screening to artificially stress the lubricant, when time, costs, control over the precise soot content are important and that there is sufficient quantity of soot surrogate available for the large number of tests usually involved in lubricant screening. In general, carbon black is found to be predominantly aromatic, with a high surface coverage of oxygen which may be in the form of hydroxyl, ether, carbonyl, ester or surface acid groups [269,270]. Rausa et al. [260] carried out XPS analysis on carbon black and soot and showed that the soot had a significantly greater degree of surface oxidation, and a lower graphitic content than comparative carbon black specimens. There are many commercially available carbon blacks used as a soot surrogate, but the relative proportions of the various surface groups and physical properties differ greatly. Consequently, model soot may be found to mimic certain aspects of the behaviour of real engine soot but may poorly reproduce other performance factors [97].

2.3.8.2.1 Industry demands

The increase in start-stop driving and the increase in diesel vehicles used in city and urban environments mean that these engines are generally being run on rich fuel mixtures (to compensate for the low operating temperatures); these operating conditions result in excessive soot generation [265,271]. In addition, tighter emission regulations, specifically for diesel engines, have lead to the use of exhaust gas re-circulation systems to reduce NO_x emission. Also, the deliberate ignition retardation, to reduce peak cylinder combustion temperature and therefore reduce NO_x production, increases the amount of incomplete combustion products, such as soot. Both of these systems increase the amount of soot finding its way into the lubricating oil. The consumer demand for longer service intervals and the increased cost for oil disposal have lead to lengthening of engine oil drain times. Soot levels as high as 5%, in certain types of duty cycles, have been noted [103]. The ‘soot’ concentration in gasoline engines is significantly lower than that produced by diesel engines, but with extended oil drain intervals gasoline ‘soot’ could become a problem for gasoline engines, as well.

2.3.8.2.2 The effect of soot on wear

The contamination of lubricating oil by diesel soot is a key factor relating to increased engine wear [96]. In general wear of engine components by soot particles is thought to be caused by chemical reactions between soot and the engine surface (corrosion) or abrasive action on surfaces. This is an oversimplification and ultimately the soot induced wear mechanism is still not fully understood and a more fundamental knowledge is needed in this area [96]. More sophisticated understanding of the mechanisms which can result in soot induced wear have been proposed since the 1970s [272-274]. The subsequent paragraph discusses five wear mechanisms which involve interactions between soot and additives, soot and metal, or among soot particles.

Many studies have shown that abrasive action by soot is the major wear mechanism [47,96,266,271,275,276]. Whether this is a result of soot as acting as an abrasive particle, or whether the presence of soot increases the metal-metal contact or a combination of both is a cause of division in the research community. Early work by Rounds [262] concluded that antiwear additives adsorb onto the soot, rather than the component surface. This was based on the hardness of soot compared to other known abrasive particles such as alumina. Rounds thought that soot was too soft to act as an abrasive, so concluded that the increase in wear was a result of antiwear additive adsorption onto the soot rather than the component surface, lessening the antiwear film formation on metal surfaces, causing direct metal-metal contact between the two surfaces. However, this conclusion was never directly tested; it is thought that the adsorption of antiwear additives onto soot is low and insufficient to affect antiwear film formation. Also the hardness measurements were carried out off-line and never took into account the change in hardness of soot in the contact. Soot is thought to become very hard under high-pressure conditions [277]. More widely accepted is that soot acts as an abrasive, weakening and removing antiwear films [47,273,277]. Needelman [26] suggested that, a special relationship is present between the size of the contaminant particles and the thickness of dynamic oil films. Soot particles that were larger than the oil film, but small enough to be entrained into the contact, caused the greatest wear of engine components, by making simultaneous contact with both the surfaces. Competition for metal surface sites between soot and antiwear additives is thought to reduce surface coverage [278]. Increased concentration and agglomeration of soot increases oil viscosity and eventually causing gelling of the oil [26]. This gives rise to pumpability problems; insufficient lubricant is able to get to the contact, thus partially or completely starving the contact. Oil drain analysis and exhaust soot analysis has showed that viscosity increases depended on the percentage of soot in the oil and the particle size of the soot [279]. More recently it has been suggested that soot may build-up at the inlet of two surfaces moving relative to one another and hinder/prevent the lubricant being entrained into the contact, which results in surface-surface contact.

2.4 ADVANCES IN THE ELECTROSTATIC HEALTH MONITORING OF TRIBO-CONTACTS

This Section discusses; initial use of electrostatic sensing as a condition monitoring technique, the benefits of a charge based condition monitoring system, the basic electrostatic theory, principle operation for electrostatic charge detection and types of sensors are outlined. The remainder of this Section discusses charge mechanisms generated by tribo-contacts and how charge has been related to wear and lubricant chemistry.

2.4.1 CONDITION MONITORING

Condition monitoring is defined as the assessment on a continuous or periodic basis of mechanical and electrical condition of machinery, equipment and systems from the observations and/or recordings of selected measurement parameters [280]. The ability to monitor the transition from mild to severe wear of *'high risk machines'* and oil quality could enable intervention before component failure and prevent any catastrophic secondary damage. Also, unnecessary component change often takes place simply because the machine operator has no information on the remaining life span of the components. A condition monitoring system which allows a less conservative approach to be taken for safe operating limits and allows preventative maintenance will lower operational costs. Condition monitoring is becoming more frequently used by the research community to try and understand the real-time tribophysics and tribochemistry of contact degradation that generates wear and ultimately failure; thus developing a better understanding of wear mechanisms.

2.4.2 ELECTROSTATIC MONITORING

Around 600BC a Greek mathematician, astronomer and philosopher, Thales of Miletus, noted that when amber was rubbed with silk it produced sparks and attracted particles of fluff and straw [281]. The intensity of rubbing has been found to affect the charge magnitude. Unger [282] compiled the triboelectric series (see Section 2.4.3.3, Table 15) to predict the polarity of charge produced on each member of a pair of solids that have been rubbed together.

Electrostatics has often been thought of as an undesirable phenomena, however, relatively recently, electrostatics has been developed to aid the understanding of component deterioration. Electrostatic monitoring was originally developed for detection of debris in the gas path of jet engines and gas turbines [5,283]. An Engine Distress Monitoring System (EDMS) [4] was installed in the outlet of the jet engine to monitor debris exiting the engine. Electrostatic sensors are also installed in the intake (Ingested Debris Monitoring System (IDMS)) of the engine in order to discriminate foreign objects entering the engine to wear debris leaving the engine [6].

Electrostatic monitoring has many benefits over other condition monitoring techniques, charge mechanisms are a primary result of changes in surface chemistry and it can be deployed on non-ferrous contacts. In highly stressed contacts many on-line condition monitoring techniques rely on significant increases in noise, temperature and vibration or the generation of significant quantities of larger wear debris to warn of imminent failure, but rely on some significant event to trigger this warning. Electrostatic monitoring has been able to detect the initial onset of failure and in advance of clear indication from vibration data [284].

2.4.2.1 Principle of electrostatics

If an isolated point charge of (Q) coulombs is considered, if the charge is enclosed in the centre of a spherical Gaussian surface, Gauss' law states that the outward flux of (E_f) over any closed surface (S) is equal to the algebraic sum of the charges enclosed divided by ε , or

$$\sum Q = \varepsilon \oint_S E_f .dS \tag{46}$$

The flux of electric field strength (E_f) from the surface may be deduced by Equation (47):

$$\frac{Q}{\varepsilon} = 4\pi r^2 E_f \tag{47}$$

Where ε is the permittivity and r is the radius of the sphere or the distance between the particle and the surface. If this Gaussian surface were placed just inside a Faraday cup, then all the charge (Q) would be induced on the cup surface and hence measurement of the total charge (Q) could be made. Consider now a small surface of area (A) within the Gaussian surface. The flux terminating on this surface may be approximated by Equation (48):

$$\frac{Q_A}{\varepsilon} \sim AE \tag{48}$$

Where Q_A is the charge induced on the surface. Q_A will be a fraction of Q, and can be deduced by dividing Equation (48) by equation (47):

$$\frac{Q_A}{Q} \sim \frac{A}{r^2} \tag{49}$$

The area (A) is taken as the surface of the electrostatic sensor and hence its sensitivity to the total charge (Q) maybe deduced by re-arranging Equation (49):

$$Q_A \sim \frac{QA}{r^2} \tag{50}$$

In practice, other factors, such as the presence / proximity of other earthed metal surfaces, will also influence the charge measured at the sensor face, so equation (50), at best, serves as an approximation to

the sensor's response. For a distributed surface charge, the sensor behaves more like a capacitor. The capacitance (C) can be related to charge by Equation (51).

$$C = \frac{Q}{V} = \varepsilon \frac{A}{r} \tag{51}$$

This can be rearrange to give charge

$$Q = \frac{\varepsilon V A}{r} \tag{52}$$

The potential difference (V) between the sensor and the surface will be proportional to the charge on that surface and thus can be approximated by Equation (53).

$$Q_A \sim \frac{QA}{r} \tag{53}$$

2.4.2.2 Principles of electrostatic sensing

If a charge source (debris particle, surface, etc.) passes in front (or passes the field-of-view) of the sensor, electric field lines will terminate on the sensing face. This will induce free electrons to be drawn to or away from the surface of the sensor (depending on the polarity of the charge source) due to electrostatic attraction/repulsion, see Figure 48(b). Holes will move in the opposite direction. This phenomenon is known as polarisation or induction.

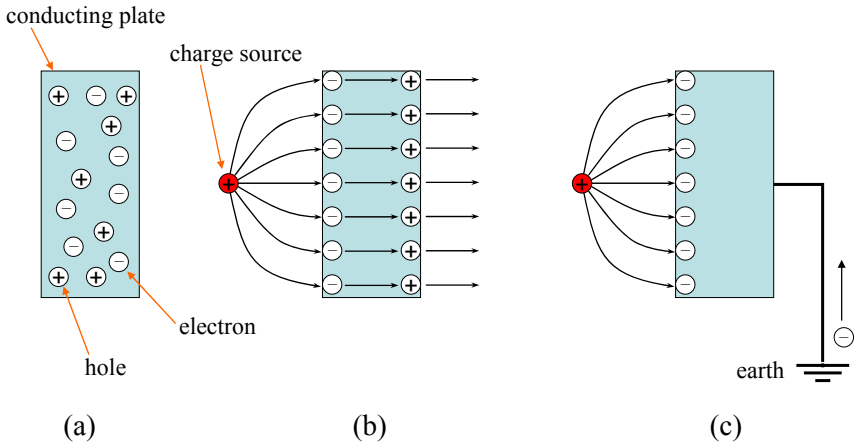

Figure 48. Principles of polarization in electrostatic sensor: (a) shows an isolated plate, (b) shows an isolated plate in the presence of charge source and (c) shows the same plate connected to earth.

If the sensor is connected to earth, electrons will flow to or from earth (depending on the polarity of the charge source) to counteract this polarisation as shown in Figure 48 (c). In an electrostatic system, the sensor (see Section 2.4.2.3) is connected to a signal-conditioning unit (a charge amplifier). This signal

conditioner will measure the flow of electrons and produce a measurable output. Figure 49 shows a schematic diagram showing the process of charge detection in an electrostatic sensor as moving charge passes the sensor face.

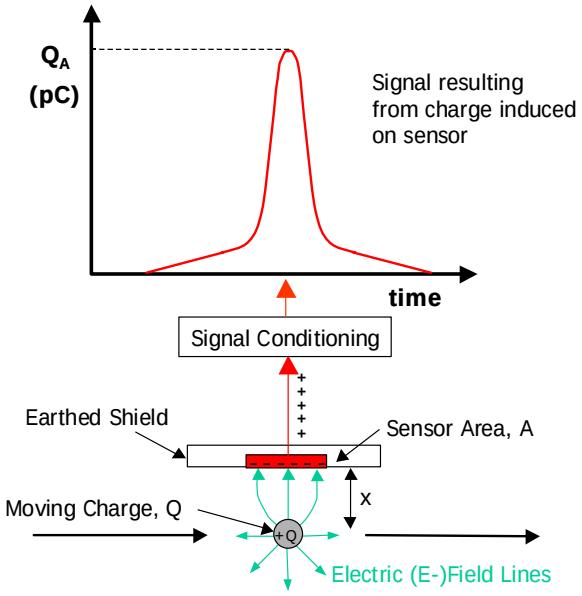

Figure 49. Schematic illustration of the electrostatic charge sensing system.

2.4.2.3 Electrostatic sensors

Electrostatic sensors are passive inductive sensors that can take several geometrical forms, for example planar button [285] or cylindrical ring (see Figure 50). Button type sensors are generally used to monitoring charge on surfaces (e.g. wear sites). Ring sensors are employed in pipe flow to detect charge on particles driven by fluid motion to act as a flow meter [286-288] or to detect the presence of wear debris in a lubrication oil line [284]. The advantage of the ring sensors is that the presence of any charged particle in the flow will be detected and is non-intrusive to flow.

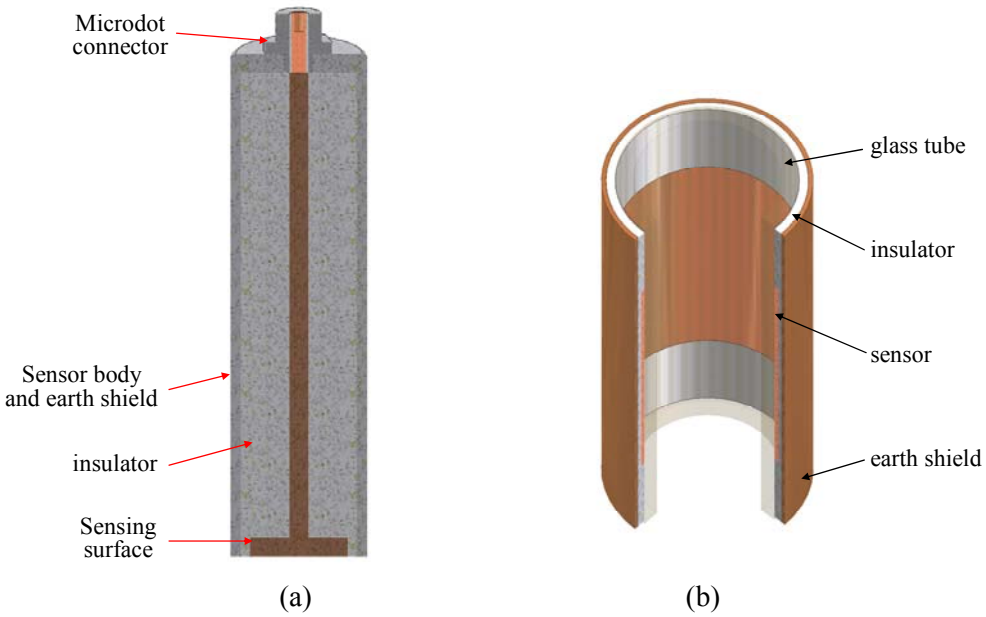

Figure 50. Schematic diagram of electrostatic (a) button and (c) ring sensor.

2.4.3 CHARGE MECHANISMS

This Section discusses the theory behind charge mechanisms thought to be dominant in lubricated tribo-contacts. Theses are tribocharging and contact potential difference (CPD), but other mechanisms such as contact charging, and debris generation are also thought to be important.

2.4.3.1 Tribocharging

It has been known since the early 1600's that an electric field could exert a force on a dielectric fluid and since the middle of the 18th century that electrostatic charging can occur in flowing dielectric fluids [289]. Tribocharging is a term used to describe the charging of a low-conductivity fluid by its relative motion over a surface. An electrical double layer forms naturally at any solid-liquid interface. A charged metal surface attracts opposite charges and repels like charges. Several theories relating to double layer structure and formation have been proposed and have been reviewed recently by Parsons [290]. There are two tribocharging theories *Double Layer Stripping theory* and *Differential Rate theory*. The first theory is based on the relative motion at the fluid-solid interface being sufficient to strip a portion of the charge double layer and entrain it into the main body of the lubricant (see Figure 51). The second theory suggests that charge is created by a differential rate of either diffusion of charge species to and from the interface or a differential rate of adsorption/desorption of these charged species.

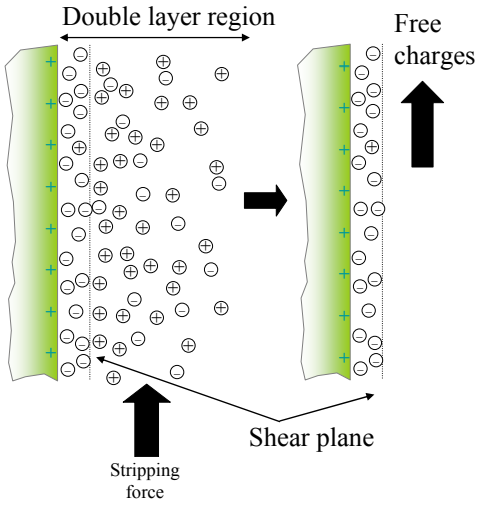

Figure 51. Schematic diagram of an electrical double layer, the dotted line indicates the shear line [291].

The chargeability of a lubricant is also dependent on its rheological properties, particularly the temperature viscosity relationship. Harvey et al. [291] reported that the electrostatic charging current increases with increasing temperature up to a point and then decreases with further increases of temperature (see Figure 52 (a)). This indicates that there are two competing mechanisms each with dominance over a particular temperature range. The two mechanisms are thought to be tribocharging at lower temperatures and charge relaxation at higher temperatures. At lower temperatures an increase in temperature will decrease the oil's viscosity (see Section 2.1.5.2), increase hydrodynamic flow, increase ionic mobility and therefore charge transportation, resulting in an increase in charging current. At higher temperatures the greater ionic mobility increases the rate of mixing, promoting the recombination of charges (charge relaxation). The conductivity of the fluid also affects the tribocharging, but not in a direct way. Indeed, an increase in concentration of charge species (higher conductivity), will lead to greater tribocharging. However there is an opposing factor; as conductivity increases the double layer thickness decreases [292], which will reduce the amount of charge species stripped as a greater proportion are more tightly bound in the double layer. Experiments have also shown that tribocharging increases with increasing surface roughness due to (see Figure 52 (b)) the increased surface area that can be stripped; also increasing roughness causes greater microturbulance which facilitates greater charge removal from the double layer.

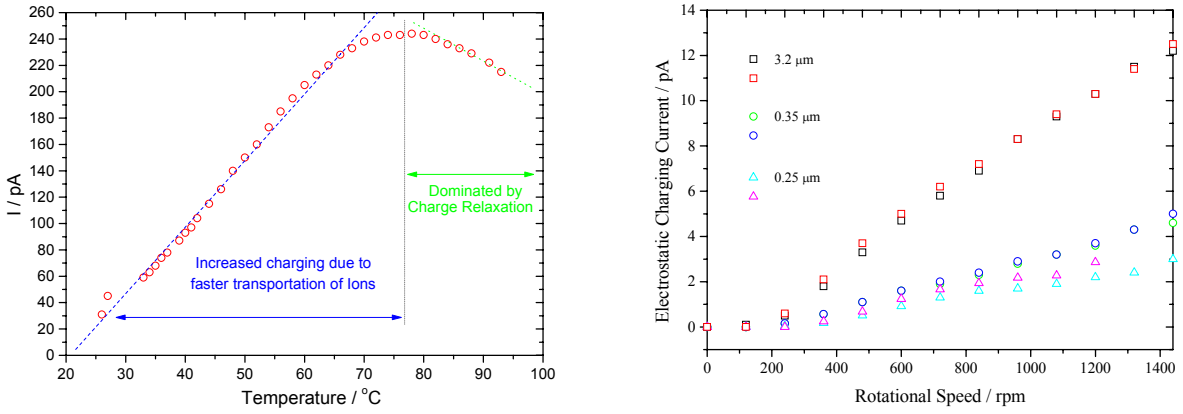

(a) (b)

Figure 52. The affect of (a) temperature and (b) surface roughness on charging current [291].

2.4.3.2 Contact potential difference

Contact potential difference is the surface charge generation mechanism which occurs when materials of different work functions[§§§] are brought together. Classically, this phenomena is described by the bringing together of two metals of different work functions, M_a and M_b. The difference in their work functions (ϕ_{Ma} and ϕ_{Ma}) drives a contact potential difference and thus charge separation. (see Figure 53) [293]. The contact potential difference, V_{CPD}, between the two surfaces is related to the difference in work function as shown in Equation (54).

$$eV_{PCD} = \phi_{Ma} - \phi_{Mb} \tag{54}$$

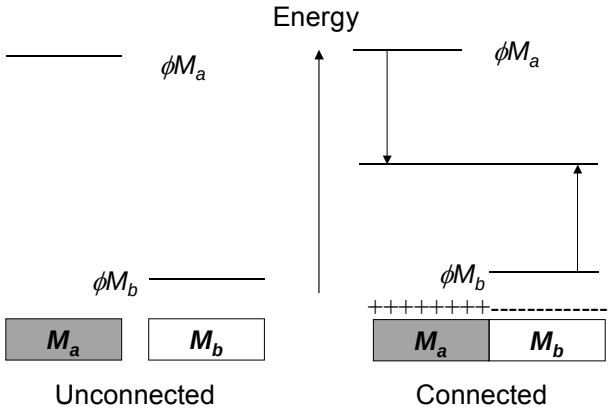

Figure 53. Schematic diagram of contact potential difference theory [8].

[§§§] The work of a material is the energy required to remove a surface-state electron from the surface, to infinity

Morris et al. [285] investigated the detection of contact potential difference using electrostatic sensing technology. Non-contact tests were carried out to investigate the sensitivity of the electrostatic sensor to variation in surface contact potential difference by inserting copper, aluminium, En31 and carbon steel inserts in a bearing steel disc (see Figure 54 (a)). The experiments produced positive peaks corresponding to the position of the aluminium insert indicating that it charges positively with respect to the steel (see Figure 54 (b)); the copper charged negatively with respect to steel (see Figure 54 (c)) [294]. The localised surface charge characteristics may be predicted from the work functions of the two metals (see Table 14), which indicate that the electrostatic sensor is detecting the CPD phenomenon. Of particular significance is the carbon steel test, which shows that electrostatic sensor is sensitive to small changes in surface composition (see Figure 54 (d)).

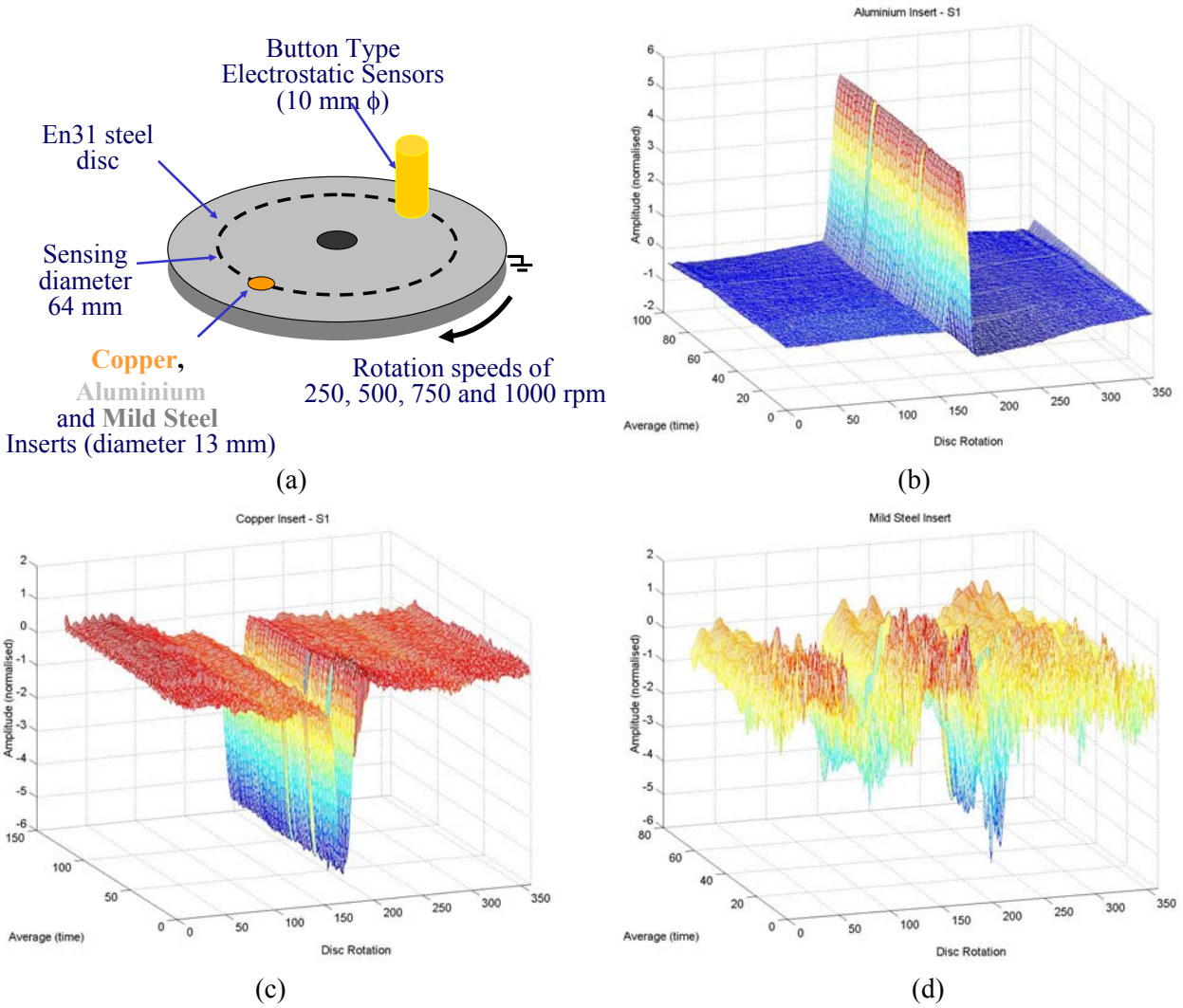

Figure 54. Schematic showing bimetallic disc (a) and charge results from (b) aluminium, (c) copper and (d) mild steel inserts [294].

Metal	ϕ_M (eV) (Photoelectric)
Zinc	3.63
Silver	4.26
Aluminium	4.28
Tin	4.28
Chromium	4.44
Tungsten	4.55
Iron	4.40
Copper	4.65
Gold	5.10
Nickel	5.15

Table 14. Work function of a range of metals [295].

2.4.3.3 Contact charging

Contact charging, also known as triboelectrification [296], occurs when two solid materials are touching or rubbing together. When two materials (similar or dissimilar) are placed in contact and then separated, electrons are transferred from the surface of one material to the surface of the other. Which material becomes negative and which becomes positive depend on the relative tendencies of the materials involved to gain or loose electrons. The drive for both contact charging and CPD mechanisms is the ability to give electrons. The difference is that under contact charging, when the materials are separated, there is a back flow of electrons which depends on the materials. For insulators this process is very slow hence high charge remains, for metals it is faster and only a portion of the charge remains.

Virtually all materials can be triboelectrically charged; the magnitude of charge transferred/generated is dependent on interfacial properties (e.g. chemical composition and surface roughness) and the nature of the contact. Generally, the total charge transferred during friction is greater than during static contact [297] due to the increase of actual contact area during friction [296].

The charge transfer between two metals is proportional to their work functions. A considerable amount of charge can be generated on the surface of an insulator, such as clutch friction material, because an insulating material does not readily allow the flow of electrons, which also means both positive and negative charges can reside (at different locations) on insulating surface at the same time. Electron transfer is thought to be the predominant charge mechanisms [298] although Diaz [299] suggested that the charge ordering of polymers infers that the charge develops from the transfer of protons (hydrogen ions). Compared to metal-metal contacts, steel-wet friction material and steel-silicon nitride contacts contact charging is thought to be more significant. Insulator-insulator contact charge densities are in the same range as for metal-insulator contacts.

Material	Charge
Air [302]	+++
Asbestos [302]	
Lead [302]	
Aluminium [302]	
Cellulose [300]	
Steel [302]	
Wood [302]	
Amber [302]	
Nickel [302]	
Copper [302]	
Silver [302]	
Brass [302]	
Sulphur [301]	
Silicon [302]	
Teflon [302]	---

Table 15. Tribo-electric series.

When two materials come into contact and separate, the charge polarity is indicated by their relative position in the triboelectric series (see Table 15), which ranks various materials according to their tendency to gain or lose electrons. A triboelectric series containing the main elements of interest in recent electrostatic monitoring of dissimilar tribo-couples was complied using results by: Coehn [300], Henniker [301] and Adams [302].

2.4.3.4 Debris generation

Debris generation involves the breaking of numerous bonds which produces charge on the debris particle upon detachment. The charged debris can be detected by an electrostatic sensor at the tribo-contact and at remote locations [25], provided that the debris is suspended in the insulating fluid or not discharged by contact with earth. If suspended in the lubricant, wear debris can be further charged by tribocharging and contact charging. The interplay between these three charge mechanisms on debris charge generation is currently not fully understood. However, Morris [23] proposed debris charging models for different scenarios that depend on surface work functions, oil chemistry, conductivity, wear rate and sliding velocity.

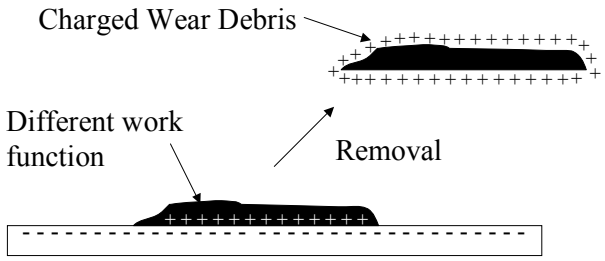

Figure 55. The removal of an area of different work function leads to the formation of charged debris [23].

2.4.4 CHARGE GENERATION FROM TRIBO-CONTACTS

The charge mechanisms generated by a lubricated tribo-contact are complex and affected by chemical and physical properties of the lubricant and contacting materials, as well as any tribochemical changes occurring between the contacting materials. Experiments at the University of Southampton, over the last 10 years, have been designed with the aim of de-coupling specific aspects relating to charge generation. Fundamental studies have investigated the chargeability of lubricants and wear tribometers have investigated the charge generation of predominant wear mechanisms in simple contact pairs. Electrostatic monitoring has also been implemented in industrial applications to assess progress in understanding the electrostatic charge response and to drive future charge de-coupling studies.

The following sections discuss the advances in understanding the affect of wear mechanism and lubricant chemistry on electrostatic charge. The ability of electrostatic sensors to detect the onset of wear and subtleties in lubricant chemistry has immediate potential for the lubricant industry, as well as how electrostatic monitoring could be used in the lubricant industry.

2.4.4.1 Charge generation related to wear processes

The electrostatic charge generated from wear is a result of CPD, through tribologically generated phase transformed regions or oxide stripping [303]. Kelvin probe[****] work with a modified atomic force microscope (AFM) by DeVecchio and Bhushan [304] has detected chemical and structural changes to specimen surfaces caused by nanoscale wear. Zharin and Rigney [305] have studied wear events with a vibrating Kelvin probe and reported that the probe was sensitive to CPD changes associated with wear.

Electrostatic sensing was originally developed for detection of electrostatic charge associated with wear debris in the gas path of jet engines and gas turbines [4-6] and was correlated with a specific component problems, such as turbine blade rub. This work has lead to the deployment of electrostatic sensors on a wide range of lubricated contacts. A significant proportion of work at the University of Southampton has sought to identify the charge mechanisms which relate to wear mechanisms/processes including: running-in [8,306], mild oxidative [8], adhesive [284,285,294,307,], abrasive [25,309], fatigue [310,311] and tribochemical [312-313] (see Table 16). The majority of this work has focused on identifying the onset of wear, so that a system can be developed to allow intervention before catastrophic failure [4,5,310,311,314].

[****] The Kelvin probe is based on a vibrating capacitor and measures the work function difference, or for non-metals the surface potential, between a conducting specimen and a vibrating tip.

Wear process	Description	Tribological activity resulting in charge generation
Running-in	1. removal of asperities 2. rougher surfaces will result in higher initial wear rates (greater removal of asperities)	1. reveals discrete areas of nascent metal surfaces 2. localised areas of nascent metal are being exposed at a greater rate
Mild Oxidational Wear	1. growth of oxides on the contact surface 2. full oxide film 3. delaminated oxide debris will expose clean metal surfaces	1. $\Phi_{oxide} > \Phi_{bulk\ metal}$ – increase in ES charge 2. no CPD (uniform oxide film) charge levels fall 3. $\Phi_{nascent\ metal} < \Phi_{oxide}$ – increase in surface ES charge and charged debris generated.
Abrasive Wear	1. carbon black resulted in minor to major increases in wear rate 2. seeding debris into tribo-contact	1. greater number of transient charge signals 2. transient charge signals associated with charged debris and increased wear rate (CPD)
Adhesive Wear	1. formation of phased transformed (white layer) regions (1^{st} Transition scuffing) 2. progression to second transition scuffing – increasing number of phase transformed regions	1. difference in work function between white layers and bulk steel 2. electrostatic charge increases until failure
Tribochemical polishing of hybrid contacts	1. Si_3N_4 - SiO_2 – ejection of debris which acts as a polishing paste 2. spallation (steel disc) wear 3. ceramic ball volume loss	1. this action has been monitored by a small increase in charge when debris has agglomerated 2. revealing nascent metal surface increase ES charge (CPD) 3. correlated with ES charge

Table 16. Predominant wear mechanisms and the corresponding charge response.

One of the most significant findings came from a series of electrostatic wear monitoring studies on adhesive failure of steel. The onset (first transition scuffing) has been detected by electrostatic sensors prior to adhesive failure (second transition scuffing) for PoD and reciprocating (TE-77) test rigs [307, 294]. This is particularly useful because little material loss is observed during first transition scuffing. Investigations found that the pre-cursor electrostatic charge signal was the result of CPD generated between the localised phase transformation (white layers) and the bulk steel. These *white layers* are produced during initial asperity-asperity contacts, friction or cold pressure welding and the resulting high, localised contact temperature transforms the region affected (see Section 2.1.4.2). A white layer may be identified, essentially, in two interrelated ways. White layers are more resistant to etchants used to prepare specimens for optical microscopy [315]. In addition, there is a substantial increase in local micro-hardness in white layers [316]. Multi-precursor events per-revolution were found which correspond to multiple 1st transition scuffing wear sites [7]. The test conditions used for these studies are accelerated wear test, thus under normal operating conditions pre-cursor signals could occur further in advance of component failure allowing more time for maintenance planning.

2.4.4.2 Charge generation related to lubricant chemistry

For lubricated sliding contacts, the lubricant has a major influence on charge generation. The lubricant quality/chemistry will influence wear and therefore CPD and debris generation. Also, the lubricant's chemical (type of charge species) and rheological (mobility of charge species) properties affect tribocharging and CPD irrespective of wear.

The majority of electrostatic monitoring work has been carried out to relate wear mechanisms and electrostatic charge, with the lubricant chemistry kept constant. Although the significance of lubricant chemistry was initially neglected, during a number of lubricated wear studies it was noted that charge signals differed between a base oil and a fully formulated lubricant [7], which could not be explained by the wear performance alone. This led to a series of fundamental studies investigating the bulk chargeability of different lubricants [291,293,319]. This Section discusses what was known at the beginning of the present work.

2.4.4.2.1 Pure hydrocarbons and base oils

Considering liquid hydrocarbon (base oils) as an inert matrix, conduction is generally governed by the concentration of impurities. These impurities are either molecular in scale or large particles [317] and can be ionic. Pure hydrocarbon liquids (e.g. decane, hexadecane and squalane) have very low conductivities, consistent with low impurity levels, which manifests as very low charge levels making detection difficult [318]. Harvey et al. [319] observed that both squalane and hexadecane have a stronger bias to positive

charge; thus it is concluded that the positively charged species (impurities) are more mobile than the negative ones for these liquids. For decane, the bias is slightly toward negative charging.

Bustin and Dukek [320] observed that hydrocarbons do not normally ionize appreciably, however it only takes one singly ionised impurity in $2x10^{12}$ molecules to produce a large electrostatic charge in a moving dielectric fluid. The ions involved in hydrocarbon liquids are likely to be polynuclear aromatics and organo-sulphur compounds (see Section 2.3.2), which are covalent in nature and are present, even in highly refined liquids. Such impurities are electroactive and are able to undergo charge transfer reactions at an electrode [318].

2.4.4.2.2 Formulated oils

Fundamental experiments using the oil droplet rig (ODR) and spinning disc charger (SDC), [7, 291], revealed that there is a greater affinity for pure hydrocarbons and base oils to give a positive charge, but fully formulated aviation oils gave a negative charge of a greater magnitude [319,291] (see Figure 56). This corresponds to the pre-cursor signals in scuffing experiments carried out on a PoD tribometer, which were positive for base oil and negative for fully formulated oil [8]. This was investigated further by performing a PoD test with a fully formulated oil until negative precursor signals were observed. The test was suspended and the wear track was cleaned with a solvent to remove the oil film. It was observed that several of the precursor charge signals underwent charge sign inversion [7]. There are two possibilities that could lead to charge sign inversion between formulated and mineral oils. The first possibility relates to studies carried out by Walmsley and Woodford [321, 322] who observed for low conductivity dielectric liquids that the polarity of the streaming current in pipeflow was related to the algebraic sum of charges and the sign was determined by the dominant species. The second possibility is that the adsorption of high concentrations of additives in formulated oils on the disc surface causes the sign of the space charge in the fluid to reverse [317,323].

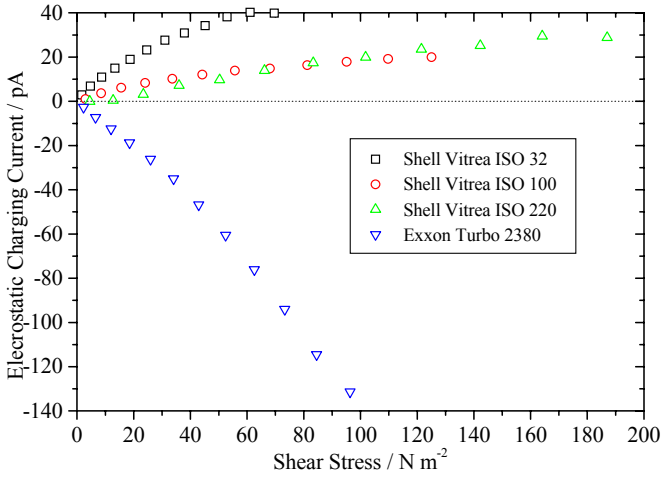

Figure 56. Electrostatic charging current for three base oils and a formulated aviation oil.

Harvey et al [319] showed that it was possible to relate the charging of two different oils; which were part of a gear micropitting programme, directly to their additive package. One of the oils was a low-grade (minimal package) oil and the other a high-grade (fully formulated) oil, with high and low micropit index respectively. The high grade oil had a high charging ability while the low-grade oil had behaviour similar to a base oil (i.e. low ionic mobility). The distinction is not as straightforward as relating a higher charge to an increased amount of additives, but demonstrates how additive packages affect charge.

2.4.4.2.3 Lubricant contamination & degradation

The effect of lubricant condition/aging on conductivity and chargeability has been investigated by Harvey et al. [291]. It was observed that an oil which had been distressed in a spinning disc charger for 5 hrs nearly doubled the conductivity. The relative motion between solid surface and liquid oil will involve high shear stresses that may be sufficient to shear the double layer and specifically shear molecules within the double layer, resulting in charged fragments. Other handling factors that affected charging tendencies included level of stagnation, exposure to the atmosphere and heat treatment [324].

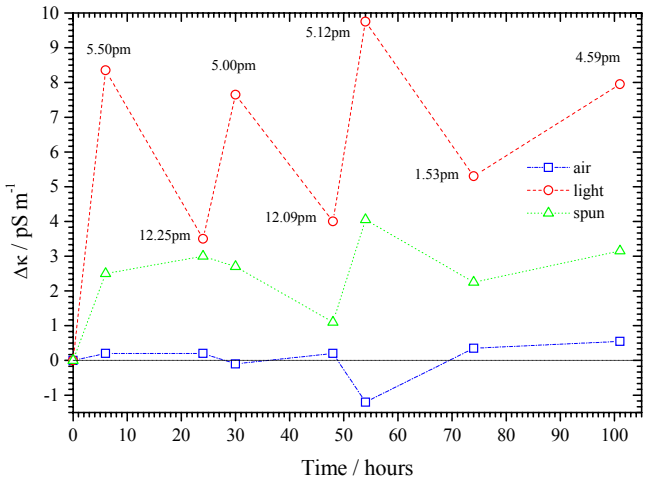

Figure 57. The change in conductivity of oils aged by air, light and mechanical shearing [291].

Wang et al. [313] investigated the electrostatic charge generated by aviation oils which had been aged, but analysis was focused on relating the severity of wear, due to lubricant age rather than relating the charge signal to the decomposition products in the aged oil and then how these affect wear. The effect of soot (a contaminant, see Section 2.3.8.2) on electrostatic charge depended on the base oil, additive type and the soot type. Wood et al. [309] found the conductivity in the presence of 2% carbon black (a soot surrogate) appeared to be lower in most cases than in its absence. This was thought to be due to the ability of carbon black to adsorb polar compounds. Studies by Ramkumar et al. [325] involving a basic additive package of VII, dispersant, Zinc dithiophophate and a detergent (see Section 2.3.5) showed that conductivity decreased with increasing moisture content. The effect of other contaminants and degradation processes, such as acid, oxidation soot, and soot have been investigated [309,325,326]. The discussions in these studies mainly focuses on the affect lubricant chemistry has on wear and the affect wear has on charge generation. Increasing oxidation levels resulted in decreasing charge. Increasing the sulphuric acid level produced an increase in charge; the combination of oxidation and sulphuric acid reduced charge [377]. No explanation was given for these three observations.

2.4.4.3 The potential use of electrostatic monitoring for additive/lubricant screening

Electrostatic monitoring of oxidational wear (induced by dry sliding) has revealed the oxidation-delamination-reoxidation mechanisms, resulting from varying work functions present at different stages of the wear mechanism [8,306] (see Table 16). Therefore, if electrostatic monitoring can detect the growth and removal of a chemical film, such as an oxide, then there is the potential to monitor the growth and/or breakdown of an adsorbed additive based tribofilm. Adsorption of charge species (such as impurities and additives) is known to alter the work function [327,328] (see eq (55) and Figure 58).

Tribocharging is thought to be a significant charge source in lubricated tribo-contacts due to the high shear nature of the contact. Additives and contaminants found in lubricating oils are generally charged or chargeable and therefore interact/adsorb to the surface. Thus they will form a large proportion of the charged species present in the charge double layer (see Figure 58 (a)). Part of the current focus of work is to assess whether electrostatic charge monitoring can detect the integrity of the tribofilm and if it is sensitive to film composition.

$$\Delta\Phi = \Phi_{Tribofilm} - \Phi_{Nascent-steel} \qquad (55)$$

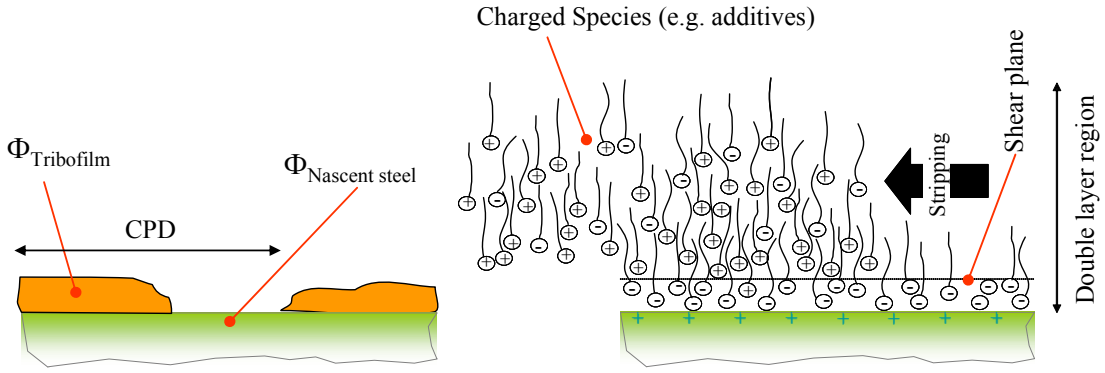

Figure 58. *Schematic showing: (a) how the difference in work function between the bulk metal and tribofilm may generate surface charge through contact potential difference, and (b) Tribocharging of additives.*

2.5 SUMMARY

Power-train design is continually evolving to meet environmental demands of lower emissions and increased fuel economy. These design improvements are often to the detriment of tribological performance. Tolerances between components are reduced to increase performance (e.g. improve combustion) and fuel economy; but these changes increase friction and the likelihood of wear. Friction is an important parameter because it is directly related to energy loss and therefore fuel economy. Component wear almost invariably results in an increase in friction, through roughening of the surface. Wear can also reduce performance by increasing clearances; valve-train wear can lead to incomplete combustion. Although the automotive manufacturer can mitigate some wear and friction issues through material selection or surface treatments it is usually requires the formulation of a new lubricant to minimise wear and friction.

There are similar environmental constraints on lubricants; they must increase fuel economy and reduce environmental impact for longer service intervals, while keeping wear to a minimum. Lubricants contain additives which minimise detrimental processes (e.g. acid and soot production, oxidation and wear) and confer beneficial properties (e.g. lubricity (low friction)). Some additives are required to function in the bulk of the lubricant; additives concerned with the reduction of friction and wear are surface active. These surface active additives adsorb either physically and/or chemically onto a surface; physically adsorbed additives can desorb or be mechanically removed, whereas chemically adsorbed additives can only be removed mechanically. In general, low friction is achieved by the formation of a film which easily shears; antiwear performance can also be achieved through the formation of a film which preferentially shears or by providing a mechanical barrier.

Lubricants must conform to national and/or international standards, such as the Peugeot TU3M valve-train wear test. Formulating new oils is not simply a matter of blending the best and latest additives, as this often results in undesirable interactions between additives. Unfortunately these interactions are not well known and change under different contact conditions. Thus lubricant testing usually involves an iterative matrix approach and is carried out at: fundamental, bench and fired engine or drive-train test levels. The cost of lubricant development and approval is escalating because the increasing rate at which classifications are superseded and the number of standard tests required for approval are increasing. It is therefore important that the lubricant formulator can extract the maximum amount of information from each test to make subsequent formulations better informed; instrumentation which can monitor wear and/or additive behaviour in real-time could be extremely useful.

Electrostatic charge sensing has been developed to monitor wear of a range of components. The main charge generation mechanisms in lubricated contacts are CPD and tribocharging. CPD arises from the difference in work function between discrete regions on the component surface and tribocharging occurs

through the stripping of the charged double layer formed, on a surface, in the presence of a low conductivity fluid (oil). Oxidational wear was successfully monitored by electrostatic sensors and revealed the oxidation-delamination-reoxidation mechanisms, due to the varying work functions on the surface that result at different stages of the wear mechanism. Therefore if electrostatic monitoring can detect the growth and removal of a chemical film such as an oxide, then there is the potential to monitor the growth and/or breakdown of a physically or chemically adsorbed additive tribofilm; adsorption of additives is known to alter the work function of a surface. Additives are charged or can be chargeable through interaction with surfaces or contaminants; it is therefore thought that electrostatic charge detection could be a new way of trying to understand additive behaviour. Initial fundamental lubricant charging tests have shown sensitivity to lubricant chemistry, but very little work has tried to relate surface charge generation to additive-surface interaction in a tribo-contact.

The literature review has identified some of the better understood additives; this understanding will enable greater comparison of charge data to additive behaviour. However, there is still a great deal that is not known or fully understood about additive film formation; and it is hoped that electrostatic monitoring could offer insight into the fundamentals of film formation ands stability. ZnDTP is the most heavily researched additive and a great deal is known about aspects of film formation through (predominantly) post-test analysis, but ZnDTP tribofilm kinematics is not particularly well understood due to the lack of technology to monitor film formation and removal in real-time. There are also additives such as dispersed potassium borate, for which comparatively little is known about film formation mechanism, friction characteristics and how it achieves its wear performance.

One of the biggest concerns for the lubricant formulator is the interactions between additive and base oil and interactions between additives, that leads to undesirable friction and wear performance. At the heart of managing antagonistic interactions is the ability to understand which additive(s) drive initial film formation and how this affects film composition of a multiple additive system. In most cases this interaction arises from conflicting performance requirements. For example, ATFs must provide high torque capacity in wet friction clutches and minimise shudder. For this purpose, dispersants are used to maximise torque capacity, but they also increase the likelihood of shudder and FMs reduces shudder, but also reduce torque capacity. Similarly, MTF must provide relatively high (stable) friction in the synchroniser contact to ensure quick and smooth transition of power, while at the same time maintaining low wear. The dissimilar materials of these two tribo-contacts pose additional problems to the lubricant formulator; additives may preferentially adsorb onto one of the surfaces which may have undesirable effect on friction and wear. These two contacts are therefore ideal for studying additive interactions and additive preferential adsorption.

3 EXPERIMENTAL EQUIPMENT AND PROCEDURES

This Chapter discusses the methodology employed to fulfil the aim and objectives identified in Section 1.3. The methodology involved an integrated approach; where specific additives were chosen because of their surface interaction behaviour; testing was designed to simulate automotive contacts, where these additives are used, and post-test analysis techniques were chosen to give maximum insight into the tribological processes and to identify the charge generation mechanisms (see Figure 59 & Table 17).

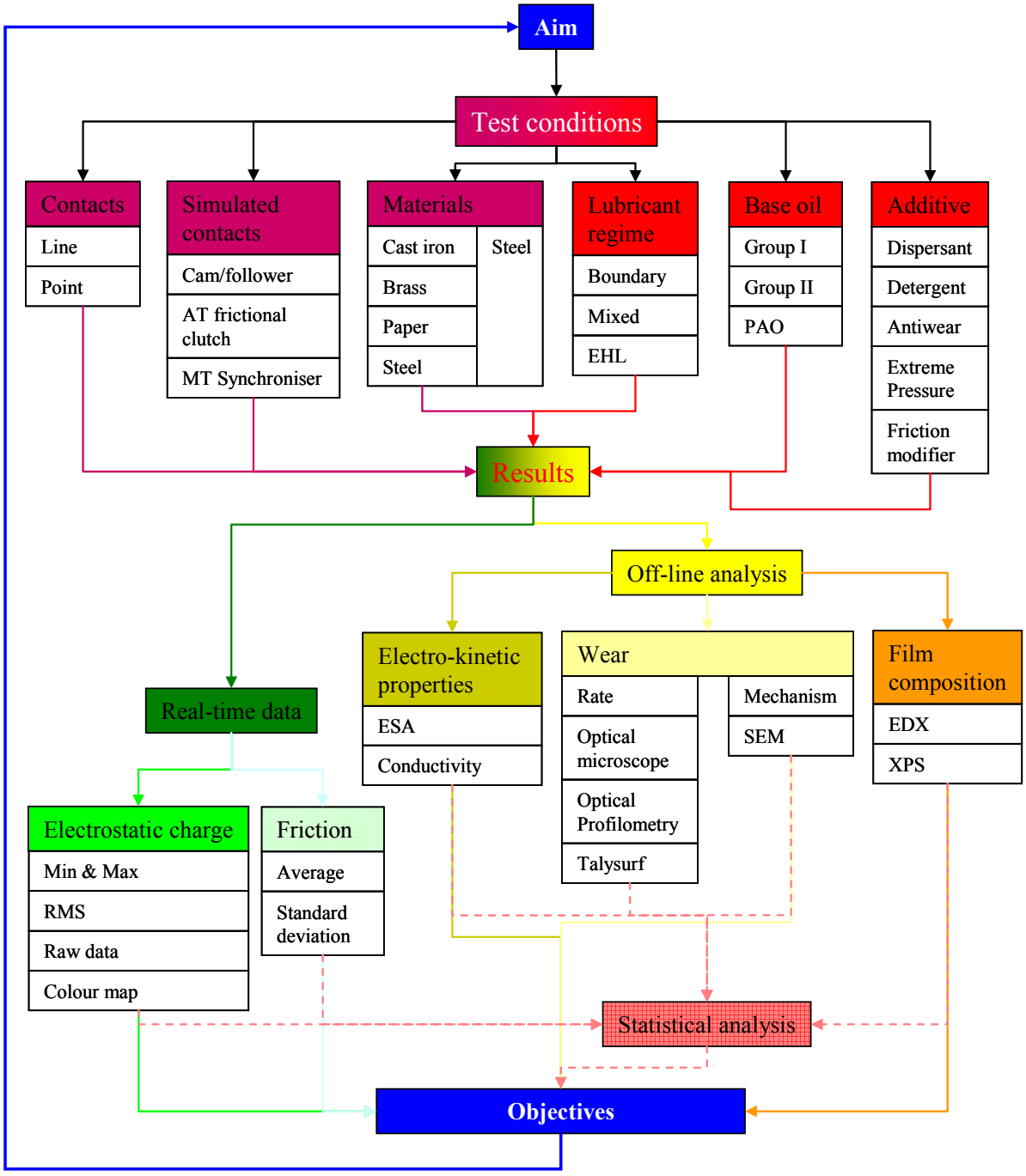

Figure 59. Schematic showing the flow of experimental aspects, which make up the overall test methodology.

				Thesis Chapter				
				4	5	6	7	8
Contact	Line							
	Point							
Simulated contact	Cam/follower							
	Automatic transmission frictional clutch							
	Manual transmission Synchroniser							
Material	Cast iron / steel							
	Steel / Steel							
	Wet friction material / Steel							
	Brass / Steel							
Lubricant regime	Boundary							
	Mixed							
	EHL							
Base Oils	Group I							
	Group II							
	PAO							
Additive	Dispersant							
	Detergent							
	Antiwear							
	Extreme pressure							
	Friction modifier							
	Antioxidants							
Contaminant	Soot							
Real-time data	Electrostatic charge		RMS					
			Negative & Positive					
			Raw data					
			Colour map					
	Friction		Average					
			Standard deviation					
Post-test analysis	Fluid electro-kinetic properties		Conductivity					
			ESA					
	Wear	Rate	Optical microscope					
			Optical Profilometry					
			Talysurf					
		Mechanism	SEM					
	Film Composition		EDX					
			XPS					
Statistical analysis								
Objectives	Assess the sensitivity of electrostatic monitoring to wear and lubricant chemistry.							
	Relate electrostatic charge signals to additive-surface interactions.							
	Relate electrostatic surface charge to additive-contaminant and additive-additive interactions.							
	Relate electrostatic surface charge to additive tribofilm chemical composition.							
	Seek electrostatic surface charge signatures associated with additive tribofilm kinematics							

Table 17. Shows similar and different experimental aspects between experimental studies (Chapters).

Lubricant chemistry

The aim of the work presented in this thesis was to assess whether electrostatic monitoring could be an insightful technique to aid additive screening/development. One of the main objectives was to relate surface charge signals to additive-surface interaction in a tribo-contact; to assess this, surface active additives were tested. To offset the lack of additive-charge related papers in the literature, additives with relatively well defined surface interaction(s) were used (e.g. friction modifiers and antiwear additives), so that surface charge signals could be related to known additive-surface behaviour. Both physically and chemically adsorbing additives were tested to investigate the surface charge generation by these two absorption mechanisms. In addition, different base oils and a contaminant were used in a few studies to alter additives/surface interaction, in order to assess whether electrostatic charge sensors can detect subtle changes in additive behaviour. The later experimental studies investigated the interaction between two additives for which little is known about their interaction, to assess whether electrostatic monitoring can offer understanding of the interaction between two additives. This was a significant shift from known additive chemistry training interpretation of charge signals, to charge signals being used to identify unknown additive interactions. Particular lubricant chemistry variables were carefully selected to suit the aims of each experimental study.

Test apparatus

A range of test apparatus and test conditions were devised to simulate the contact conditions that the additives selected would normally experience as a component in automotive lubricants. A motorised TU3 engine rig was purpose built to test lubricant performance using actual component geometry, material and contact conditions. The TU3 valve-train was selected as it is the European industry standard for assessing valve-train scuffing. Other studies involved tribometers with a pin-on-disc configuration; these allowed greater control over the tribological parameters (e.g. oil temperature, contact pressure, entraining velocity, surface roughness and contact materials). Appropriate test conditions and materials were used to simulate valve-train, synchroniser and wet frictional clutch contact conditions using the PoD configuration. Additive-surface interaction is dependent on the chemical properties of the surface; therefore materials similar to those found in real tribological contacts, relevant to specific additive performance, were used.

Real-time data

Additives are charged or are chargeable; there interaction with a surface will generate surface charge. Thus electrostatic charge monitoring has the possibility of detecting additive/surface interaction, by the surface charge it generates or neutralises. The work presented in this thesis is the first to use a charge based measurement technique to explore additive behaviour in tribo-contacts. The charge data was processed in different ways, so that charge parameters, which give the most insight into additive behaviour, could be identified.

Friction data was recorded during the PoD tests to give insight into the contact conditions within the tribo-contact. In corroboration with other data, usually post-test inspections, the growth/presence of an additive film, either by reducing or increasing the friction level relative to base oil can be detected. Wear will also affect the friction response. Thus it was a useful measurement to aid interpretation of electrostatic data.

Off-line test analysis

As identified in the *Literature review* Chapter, there are very few references related to additive-surface charge behaviour. Therefore suitable off-line analysis was chosen to differentiate the charge related to wear and lubricant chemistry. Thus, in the absence of relevant literature, off-line analysis could enable supposition of the charge generation mechanism. Surface chemistry analysis (e.g. energy dispersive x-ray spectroscopy (EDX) & x-ray photoelectron spectroscopy (XPS)) was one of the most powerful analysis tools; it produces information to confirm the presence of / and if so the chemical composition of the additive film. This provided critical information to which charge signals could be compared. Surface chemical analysis was used in all 5 experimental Chapters, but due to the expense of such analysis, in some cases it was used to investigate only the most interesting charge results.

Lubricant conductivity and electrokinetic sonic amplitude (ESA) measurements were taken to provide understanding of the level of charge species present in the bulk of the oils. Electrostatic signals generated by the tribo-contact were compared to the electrokinetic properties of the lubricant; disparity between the two infers that the charge generated within the tribo-contact is an important factor and justifies further investigation of additive-surface interaction and how this drives these charge characteristics.

Statistical analysis

To investigate whether surface charge measurements directly relate to additive-surface behaviour, large test matrices where run, in order to test a range of components (additives, base oils and contaminants). Statistical analysis was employed in two studies for two reasons. Firstly, to efficiently handle the large amount of real-time and post-tests data, and secondly to try to objectively identify the significance of additive effects and additive interactions on surface charge.

The remainder of this Chapter, discuses the common elements involved with the experimental programme (testing procedures and post-test analysis) in this thesis. Experiential methodology and analysis specific to each set of experiments are discussed at the beginning of the relevant Chapter.

3.1 TEST APPARATUS

3.1.1 PCS INSTRUMENTS MINI-TRACTION-MACHINE (MTM)

The majority of the work presented in this thesis was carried out on a PCS Instruments Mini-Traction-Machine (MTM), made available by Chevron Oronite Co LLC, and was employed in Pin-on-Disc mode (pure sliding). The MTM is widely used in the lubricant industry for additive screening tests, because it regulates lubricant temperature and automates load and speed, which improves repeatability. Modifications were made to the oil baffle and oil reservoir lid to allow the electrostatic sensor to be positioned over the wear track, while ensuring that the contact is fully flooded with lubricant. A purpose built sensor holder was mounted on the MTM calibration points (see Figure 60). The holder allowed two degrees of freedom for positioning the sensor; dial indicators were used to accurately (± 12.7μm) position the sensor above the wear track. The electrostatic probe monitored surface charge on the disc and was positioned 100° away from the pin/disc contact and 0.5 mm above the wear track (see Figure 61). A laser tachometer measured the disc rotating speed for data processing purposes (see Section 3.5) and to enable synchronisation of the electrostatic charge data and the MTM friction data.

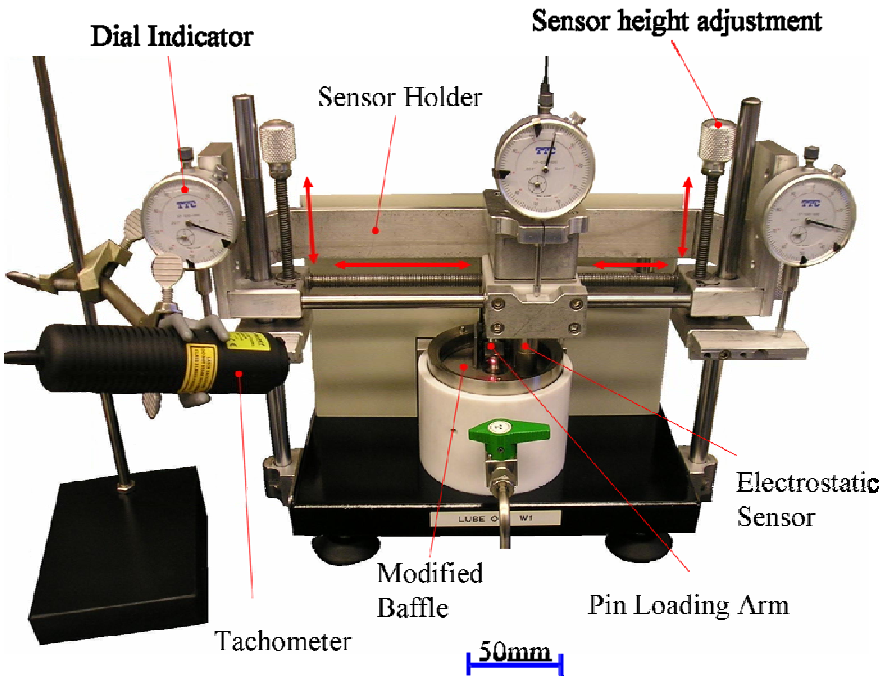

Figure 60. MTM with additional instrumentation: electrostatic sensor & holder and tachometer.

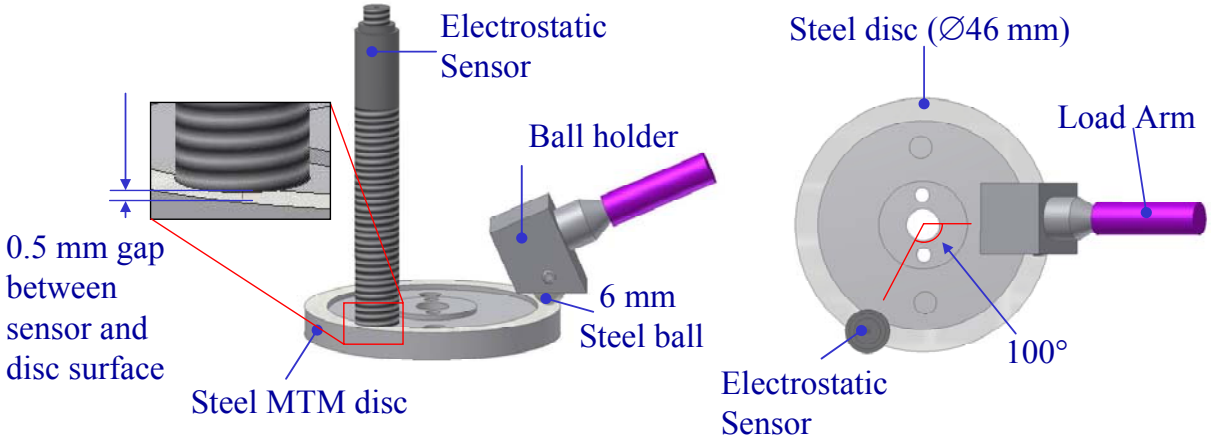

Figure 61. Schematic showing the position of the senor relative to the steel ball and steel disc.

3.2 MATERIALS

The work in this thesis involved a range of materials including cast iron, bearing steels, brass and a cellulose composite; these materials were used to replicate materials found in cam/follower, synchroniser and wet frictional clutch contacts. Chemical and physical properties of these materials are shown in Table 18 & 19 respectively.

In the PoD experiments, presented in Chapters 5-8, bearing steel instead of cast iron and/or steel was used for the pin, and sometimes for the disc. The chemical and physical properties of the bearing steel (pin and disc) are given in Table 18 and Table 19; these are similar properties to the ferrous components of interest. Bearing steel, rather than cast iron specimens, have been used by other researchers looking at the fundamentals of lubricant interactions with an iron based surface [47,329,330]. Homogeneous bearing steels are used to enhance the reproducibility and repeatability of experiments; both of which are integral to validate statistical analysis (see Section 3.7). For work presented in Chapters 5-8 a 6 mm diameter steel ball bearing was pressed into a brass cup (see Figure 62), which was then secured in a modified pin holder connected to the load arm (see Figure 60). This set-up enabled the ball bearing to be easily positioned in the correct place for post-test analysis on the wear scar. In addition, the ball bearing pressed into the cup prevents ball rotation.

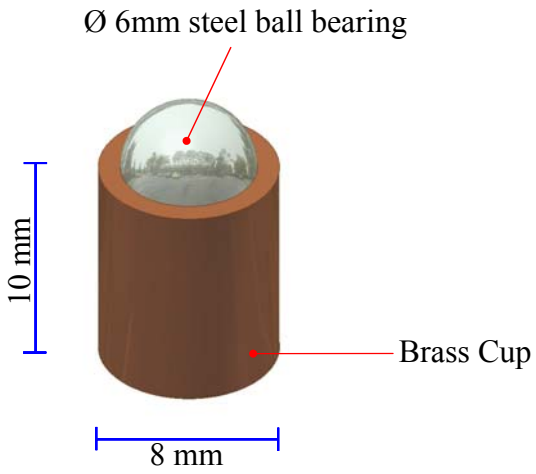

Figure 62. 6 mm ball bearing pressed into a brass cup.

		C	Si	Mn	P	S	Al	Co	Cr	Cu	Mo	Ni	V	W	Fe	Mg	Pb	Zn
Chapter 4	Follower	2.02	0.47	0.28	0.023	0.021	0.04	0.04	11.7	0.13	0.26	0.1	0.25	0.18	Bal.			
	Cam	3.60	1.88	0.68	0.15	0.046	0.01	<0.01	0.02	0.4	<0.01	0.03	<0.01	<0.05	Bal.			
Chapter 5	BS534A99 (En 31)	0.95-1.10	0.10-0.35	0.40-0.70					1.60						Bal			
Chapter 6, 7, 8	AISI 52100	0.98-1.10	0.15-0.3	0.25-0.4	0.025	0.025			1.30-1.60						Bal			
Chapter 8	Brass		<0.01				<0.01			Bal					0.16	<0.01	2.80	37.1

Table 18. Chemical composition of wear specimens used in experimental work presented in this thesis.

	Chapter 4		Chapter 5		Chapter 6		Chapter 7		Chapter 8	
	Cam	Follower	Pin	Disc	Pin	Disc	Pin	Disc	Pin	Disc
Material			BS534A99 (En 31)		AISI52100		AISI52100	Paper	AISI52100	Brass
Elastic Modulus [GPa]	-	201	210	210	201	201	201	0.780 [331]	201	102
Yield Strength [MPa]	-	502	-	-	2003	2003	2003	-	2003	-
Poisson's ratio	-	-	0.28		0.28	0.28	0.28	N/A	0.28	0.35
Hardness (Hv_{30})	570	780	640	220	650-870		650-870	N/A	650-870	130-150
Density, ρ [kg/m^3]	-	-	7800		7830		7830	N/A	7830	8450
Dimensions [mm]	Ø(14.3 – 19.5) x 19 Circum.100	15 x 20	Ø6	Ø100 × 10	Ø6	Ø46 x 4.5	Ø6	Substrate Ø46 x 4.5 Coating Ø46 x 0.38	Ø6	Ø46 x 4.5
Roughness, Ra [μm]	0.5-0.9	0.3-0.6	0.09	0.02	0.015	0.01	0.015	9.2	0.01	0.15

Table 19. Physical properties of wear specimens used in experimental work presented in this thesis.

3.3 LUBRICANT CHEMISTRY

3.3.1 BASE OIL

A range of base oils were used to replicate the base oil used for different contacts under simulation and to investigate how additives behave in different base oils. A list of their rheological and chemical properties is given in Table 20.

	Base Oil 1		Group I	Group II	PAO
Used in chapter	4, 5		6	6, 7, 8	6
Temperature, T [^{o}C]	20	100	100	100	100
Kinematic Viscosity, ν [cSt]	103.10	6.30	4.05	4.05	3.87
Viscosity Index	105		95	103	121
Density, ρ [kg/m^3]	871.56		864.07	862.39	816.98
Absolute Viscosity, η [cP]	103.1	5.49	3.50	3.49	3.16
Pressure viscosity index, α [1/GPa]	20		13.5	11.7	10.7
Sulphur [ppm]	3,830		4,120	6.6	<6
Nitrogen [ppm]	21.4		20.3	1.04	0.004
Aromatics [wt%]	23.5		23.2	0.219	<0.1

Table 20. Rheological and impurity levels of base oils used in work presented in this thesis.

3.3.2 ADDITIVES

For early studies, additives selected (see Table 21) had to be; surface active, commonly found in crankcase oils and therefore could be tested under conditions simulating the cam/follower contact, and finally their behaviour needed to be relatively well characterised in the literature. The mode of additive adsorption, as a group of additives, had to be split roughly equally into chemically and physically adsorbing. The latter two studies saw a change in investigative approach; additives were chosen because of their interaction with one another, and preferential adsorption to one material over another. For these additives comparatively little was known about their behaviour. The purpose of this was to assess whether electrostatic monitoring could give insight into additive behaviour.

The majority of lubricant testing involved single additives. It is acknowledge that in practice tribofilm formation, stability and removal processes will be affected by other additives in fully formulated oils. However understanding these processes in model tribofilms will facilitate the understanding of the more complex processes related with the tribofilm formed from fully formulated lubricants, a point noted by other researchers [111]. Combined, additives tend to behave differently to their singular use; the latter two studies addressed this to a degree, through systematic characterisation of the performance of binary additive systems, with different elements, alone and in combination. This is fairly common practice in the lubricant industry, to promote additive selection [237].

Unless stated, additives were blended into the base oils at 1% wt., to minimise any rheological changes, thus allowing additive chemistry effects to be easily assessed, rather than the more difficult task of decoupling lubricant mechanical properties from additive chemistry, where the concentrations are not controlled. Additives were dispensed into base oil and mechanically stirred for 10 minutes, on a magnetic hot plate stirrer, followed by 60 minutes in an ultrasonic bath at 30°C. All blends were ultrasonically shaken for 30 minutes prior to testing.

Generic description	Abbreviation	Description	Used in chapter
Dispersant	Dispersant 1	A commercially available post-treated conventional bis-succinimide made from polyisobutene having a number average molecular weight of 2300 Daltons. It is characterised by 1.0% nitrogen. It consists of one polar-head connected to two hydrocarbon tails and has a theoretical molar mass of about 5600 Daltons [332,333]. See Figure 31(b).	4, 5
	Dispersant 2	A polymeric succinimide dispersant. It is made from an alpha olefin/maleic anhydride copolymer, a polyisobutenyl succinic anhydride having a number average molecular weight of about 2300, and an ethylene polyamine. It is characterised by 1.2% nitrogen. It is a mixture, theoretically of one mole of polymeric succinimide, $M_n \approx 35000$, and four moles of bis-succinimide, $M_n \approx 5600$. The polymeric succinimide has about 10 polar-heads per molecule [332-334].	5
	Dispersant 3	A conventional mono- Mono-polyamine succinimide dispersant, made from polyisobutene having an average molecular weight of 1200. It contains one polar-head per hydrocarbon tail and according to molecular modelling[††††] is 70Å in length (tail-head). The polar-head contains 3 amine functional groups. See Figure 31(a).	6, 7
Detergent	Detergent	An overbased sulphurised calcium phenate, containing excess base in the form of calcium carbonate. It is characterised by a total base number of 250 mgKOH/g, and 9.25% Calcium. The surfactant hydrocarbon tail is branched C20-28, 450 Mwt See Figure 34(d).	5, 6,
Friction modifier	GMO	Glycerol mono-oleate. See Figure 39.	6
	MGMO	Modified Glycerol mono-oleate.	6
	MoDTC	Molybdenum dithiocarbamate. See Figure 40.	6
	FM 1	A FM used in Automatic transmissions, not IC engines. like Disp1 It is a bis succinimide, 2 hydrocarbon tails to one polar-head, but with a much smaller hydrocarbon tail; dimensions of 28Å tail-head[††††] and 41Å tail-tail[††††]. The polar-head contains one amine functional group. See Figure 31(b).	7
Antiwear	ZnDTP 1	Primary zinc dialkyldithiophosphate. Figure 42(a).	5
	ZnDTP 2	Secondary Alcohol zinc dialkyldithiophosphate. Figure 42(b).	6
Extreme Pressure	Borate	Dispersed potassium borate. The mean particle size of the colloid was 163nm[‡‡‡‡] in diameter. The surfactant length was approximately 7 nm, therefore the potassium borate particle was 149nm in diameter. More details of a similar potassium borate additive can be found in [243]. See Figure 45.	8
	Polysulphide	The hydrocarbyl polysulphide additive varies in molecular weight from 144 to 390, and has an average molecular size of about 9 Å. See Figure 44.	8

Table 21. Chemical and physical properties of additives used in work presented in this thesis.

(Further details regarding the structures of the chemicals can be found in [335].)

[††††] Minimum energy conformations, and molecular dimensions, for additives were determined using Cambridgesoft Company CSChem3d Pro software version 7.0.0. Conformations were minimised to an RMS gradient of 0.05.

[‡‡‡‡] characterised using a Horiba Instruments LA920 – Laser Particle Size Analyser

3.3.3 CARBON BLACK

Carbon black was used as a contaminant in two experimental studies; this follows other research work where carbon black was used as a model soot compound [278]. The carbon black used as a surrogate for diesel engine soot was Raven 1040, supplied by Columbian Chemicals Company, Marietta, GA, USA. Raven 1040 has the following properties [336]:

- Primary particle Size: 28nm
- Average agglomerated particle size: ~ 300nm
- Nitrogen Surface Area: $95 m^2/g$
- Cetyltrimethylammonium Bromide Surface Area: $100 m^2/g$
- Dibutylphthalate Oil Absorption: 100cc/100g
- Density: $192 kg/m^3$
- pH: 2.8
- Percent Volatile: 3.0

The contaminated oils contained carbon black blended at 2% wt. The carbon black-laden oil was mixed using a rotor stator type high shear mixer model T25 Basic Dispenser w/S25N-18G manufactured by IKA Laboratory Analytical and Processing Equipment. Oil and carbon black were mixed for one minute, and then the oil was degassed in a vacuum oven for 15 minutes at about 55°C. Like the non-contaminated oils, contaminant oil blends were ultrasonically shaken for 30 minutes prior to testing on the either the PoD or MTM tribometer

3.4 TEST CONDITIONS AND PROCEDURE

Sample preparation

All wear specimens were cleaned prior to testing. For both the MTM and PoD the pins and discs (as well as all removable components) were ultrasonically cleaned in HPLC-grade heptane for 30 minutes at 40^oC. The reservoir and non-removable parts were cleaned with HPLC-grade toluene followed by HPLC-grade heptane. The cam and follower, which were too large to be ultrasonically cleaned, were cleaned using hexane and a lint free cloth.

The test conditions and procedures are somewhat different across the 5 experimental studies (see Table 22), principally because different contacts were simulated and different test apparatus was used; details of these differences are discussed within each experimental Chapter. However there are some similarities, firstly all tribological studies presented in this thesis were carried out under pure sliding conditions. Secondly all experiments were designed around using contact pressure, sliding speed and lubricant temperature to simulate automotive contacts and conditions of interest. The contact pressure, oil film

thickness and lambda ratio equations discussed in Sections 2.1.1.1 & 2.1.3 respectively, were used to ensure the contacts were operating in the appropriate lubricant regime.

For all PoD work (whether on the 'in-house' PoD Tribometer or MTM) the test was split into two stages. The first involving a continually changing test condition (sliding speed or load) and for the second stage all test conditions were kept constant. As the MTM was used in 3 out of 5 experimental studies, the core experimental procedures are discussed below.

For all experiments involving the MTM, the reservoir was heated until the oil reached the test temperature of 100°C, which typically required 15 minutes. During this period the disc was rotated at 0.8 m/s without the pin in contact. Once thermal equilibrium was achieved the test was started. All tests were split into two stages; during the first stage the sliding speed decreased incrementally over 2.5 minutes and the second stage was run at constant speed, which was always the minimum sliding speed between the pin and disc. For all MTM tests the contact pressure remained constant throughout stage one and stage two.

	Chapter 4	Chapter 5		Chapter 6		Chapter 7		Chapter 8	
Contact simulated	Cam-follower	Cam-follower		Cam-follower		Automatic transmission frictional clutch		Manual transmission synchronizer	
Test apparatus	Motorized TU3 engine	In house Pin on Disc		MTM		MTM		MTM	
Stage		1	2	1	2	1	2	1	2
Duration [mins]	45-345	12.5	60.0	2.5	25.0	2.2	33.3	2.2	33.0
Sliding speed [m/s]	0 – 3.0 400-1000rpm	5.0		5.0 – 1.0	0.8	4.5 – 0.6	0.2	4.5-0.6	0.2
Load [N]		0-30	30	7		3		7	
Max Contact Pressure [MPa]	683 [52]	0-2050	2050	1219		400-425		964	
Mean contact pressure [MPa]	N/A	0-1365	1365	810		N/A		643	
Maximum Shear Stress [MPa]	N/A	0-635	635	381		N/A		299	
Max Tensile Stress [MPa]	N/A	0-317	317	183		N/A		149	
Depth of Max Shear [μm]	N/A	0-34	34	25		N/A		34	
Contact diameter [μm]	N/A	0-167	167	105		N/A		117	
Minimum Film thickness [μm]	0.76 – 0.07[§§§§]		0.47	0.04-0.01	0.01 – 0.01	N/A		0.04 - 0.01	0.01
Oil Temperature [^{o}C]	19.5-60	15-23		100		100		100	
Lambda ratio	1.3 - 0.06		3.12	3.07-0.85	0.88 - 0.73	Boundary		0.26-0.07	0.03

Table 22. Details of test conditions used for experiments presented in this thesis.

[§§§§] Calculated for an SAE 10W30 grade oil

3.5 REAL-TIME DATA

3.5.1 INSTRUMENTATION

A button-type inductive electrostatic sensor was used in all experiments (see Section 2.4.2.3 & 2.4.2.2, for construction and principle operation, respectively). Two sensors with differing sensing areas were used; one with a sensing area of 7.85 x 10^{-5} m^2 (10 mm diameter sensing face), and the second with a sensing area of 5.03 x 10^{-5} m^2 (8 mm diameter sensing face). The sensors, in all applications, were positioned (approximately) 0.5 mm above the component surface, through the use of feeler gauges or dial indicators.

The button-type electrostatic sensor was connected to a signal-conditioning unit (Endevco charge amplifier), which converted the charge into an amplified voltage signal (see Figure 63). This conditioning unit also gave a selectable gain range from 1 mV pC^{-1} to 1000 mV pC^{-1}. The conditioning unit also had switchable high pass and low pass filters, set at 1 Hz and 10 kHz respectively. The incorporation of a high pass was designed so that only dynamic charge events are monitored and is insensitive to static/constant charges. The unit also processed the signal to provide an inverted output to reproduce the same polarity as the charge monitored.

The component rotation speed was measured using an optical tachometer, purchased from Compact Instruments Limited, for data processing purposes. The tachometer was bench model BT10000 with optional pulse output (BT1000) giving a voltage output of 0-10 V and was connected to a VLS5/D Laser sensor (see Figure 63). A reflective strip was affixed to the PoD/MTM motor shaft, or the camshaft pulley, and the optical sensor was position adjacent to the shaft.

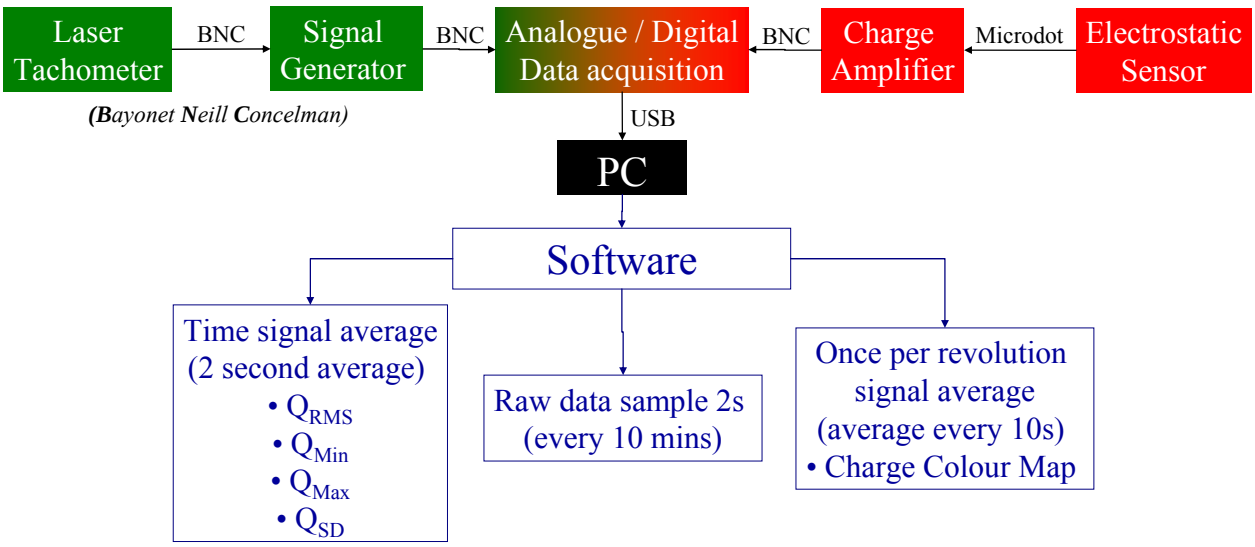

Figure 63. Instrumentation and software output parameters for electrostatic sensing systems.

3.5.2 ELECTROSTATIC CHARGE DATA ACQUISITION AND SIGNAL PROCESSING

Recording of on-line measurements was performed with a PC data acquisition system, using a Data Translation DT321 16-bit 8-channel A/D card, at a sample rate of 4096Hz. Figure 64 (a) & (f) show the electrostatic charge raw data over 10 second and 600 second periods respectively. Raw electrostatic charge data is noisy and the bi-polar nature tends to make observations, such as whether the charge level is increasing or becoming more dynamic, more difficult. Therefore signals produced by the charge amplifiers and tacho-generator were processed, analysed, displayed, and stored in real-time using a software analysis suite developed by GE Aviation (Smith Aerospace Information Systems). The software analysed the data in two ways, a time signal statistical algorithm and a once per revolution signal average (see Figure 63). In addition a raw data sample, 2 seconds in length was recorded every 10 minutes, so that processed data could be compared to raw data.

3.5.2.1 Time signal statistical algorithm

Time signal averages smoothes out the data enabling certain parameters to be isolated and trends to be identified over a period of time. Every 2 seconds of raw data is processed to give charge: rms average, minimum, maximum and standard deviation (designated as Q_{RMS}, $Q_{Min,}$ Q_{Max} and Q_{Sdev} respectively). An example of the processing of 10 seconds of raw data is plotted on top of the raw data graph to demonstrate how the data is sectioned (see Figure 64 (a)). Figure 64 (b)-(i) shows how, plotted individually, the analysed parameters vary over 10 second; many of these features would not be discernable by viewing the raw data. This is definitely the case when dealing with tests over a comparatively long duration (compare Figure 64(f) with (g)-(j)).

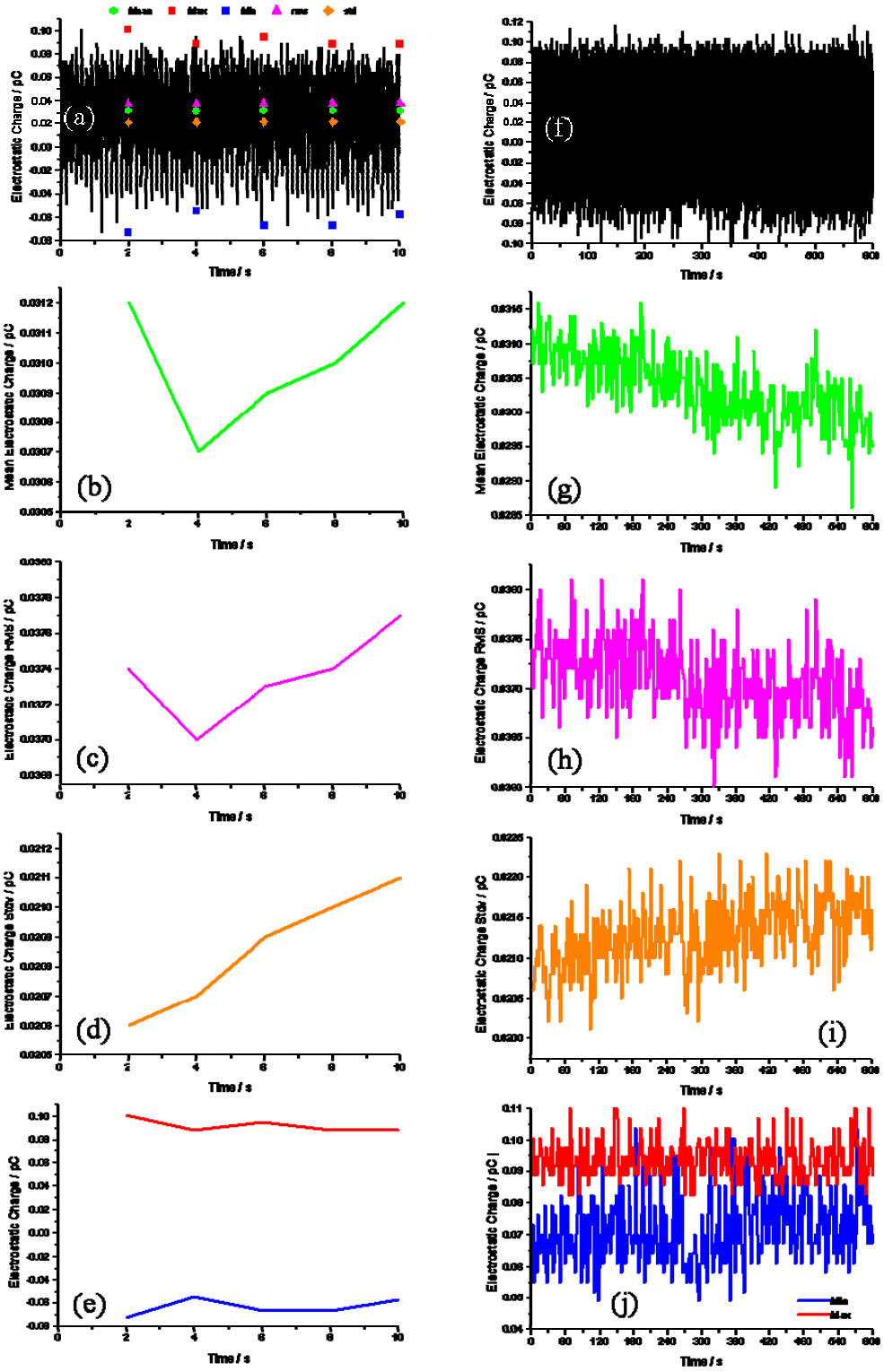

Figure 64. *10 seconds of electrostatic charge data: (a) raw (with time signal average parameters overlaid), (b) mean, (c) rms, (d) standard deviation, (e) minimum and maximum. And 600 seconds of electrostatic charge data: (f) raw, (g) mean, (h) rms, (i) standard deviation, (j) modulus of minimum and maximum.*

Mean & RMS

Due to the bi-polar nature of the charge signal (see Figure 64(a) & (f)), calculating the mean of the charge signal typically produces a value close to 0 pC. This parameter gives information about the positive charge relative to negative charge, rather than the charge magnitude (see Figure 64 (b)). A better parameter for charge magnitude is the root mean squared (rms) which enables the overall charge level (irrespective of sign) to be assessed (see Figure 64 (c)). RMS charge has been the main parameter used by other researchers using electrostatic monitoring. At the most basic level, rms charge is thought to give an indication of the severity of wear or the type of additive adsorption. More subtle changes in rms charge could correspond to changes in wear mechanisms or changes in additive film coverage; an increase in charge could result from a thickening of the additive film, or greater additive coverage.

Standard deviation

Charge standard deviation (see Figure 64 (d)) is a measure of data spread and is thought to be a parameter which indicates the transient nature of tribological processes, for example, the stability of the tribofilm.

Minimum Maximum

The minimum (Min) and maximum (Max) charge data is the lowest and highest charge magnitude respectively of the 2 second segment, but due to bi-polar nature of the electrostatic charge signal usually Max is positive and Min is negative (see Figure 64 (e)) The Min and Max charge data are useful to try and identify the charge generation mechanism. For example, if a particular additive is known to produce a negative surface charge through adsorption, then a high negative charge relative to background charge levels indicates adsorption of that particular additive. Although the way charge data is plotted in Figure 64 may infer that both positive and negative charges are coinciding at a single point in time and thus a single point on the component surface, this is not the case, merely that in a 2 second average both positive and negative charges have been detected. In fact taking a once per revolution average (see Section 3.5.2.2) of the 10 seconds raw data shows that the min data (see Figure 64 (e)) corresponds to a discrete region of negative charge at 120^{o}, while the max data relates to the remaining predominantly positively charged disc (see Figure 65). The presentation of the Min / Max data in Figure 64 (e) can make it difficult to observe the change in dominance of one charge sign over another; to clarify this the modulus is taken of the charge data (see Figure 64 (j)).

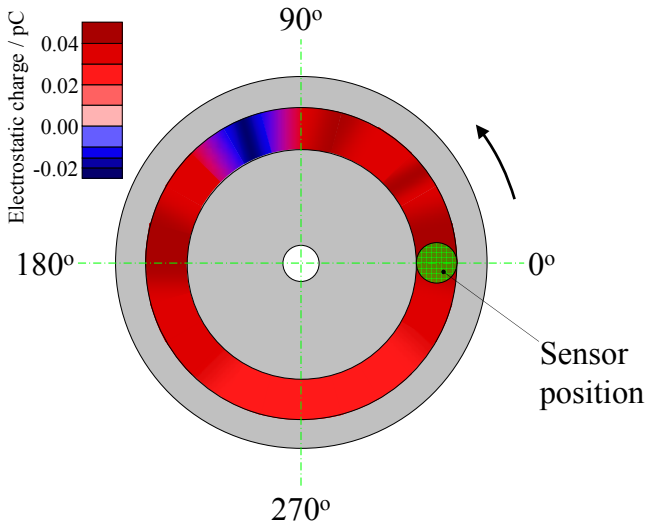

Figure 65. Positive and negative electrostatic charge distribution around the disc sensing area.

3.5.2.2 Once per revolution signal average

An alternative way of viewing charge data is to process the raw data into a once per revolution charge map. Raw data (see Figure 66 (a)) is split into 10 second segments (see Figure 66 (b)); using the tacho signal (see Figure 66 (c)) the data is further sliced into one revolution segments (see Figure 66 (d)). These segments are averaged across the angle of rotation (see Figure 66 (e)). A range of colours are assigned to represent a range of charge magnitudes (see Figure 66 (f)); the charge magnitude is plotted as a function of component rotational orientation and time. Over a 600 second period, 60 signal averages will be produced (see Figure 66 (h)). This technique enhances the cyclic content of the signals, suppresses random non-related effects, and can determine electrostatic charge features associated with a specific location on the component. Development of new features within the signal average as time progresses allows correlation of charge with areas of tribological interest; for example, additive film formation/removal or adhesive wear.

There maybe occasions where constant charge features mask other features of interest. By subtracting the first (or however many) signal averages away from subsequent data may reveal new features (background subtraction). For example the dominant negative charge at approximately 120° on the once per revolution colour map (see Figure 66 (h)), hides the charge feature just prior to 200 seconds, by subtracting the first 10 averages from the entire data set, the feature prior to 200 seconds is now obvious (see Figure 66 (g)); this technique is called normalisation. This does not necessarily work well when key features (always at the same angle) vary in magnitude across the test. In addition, using the first few once per revolution averages to subtract from the rest of the data, assumes that no transient processes are occurring at the beginning of the test; this is not always the case.

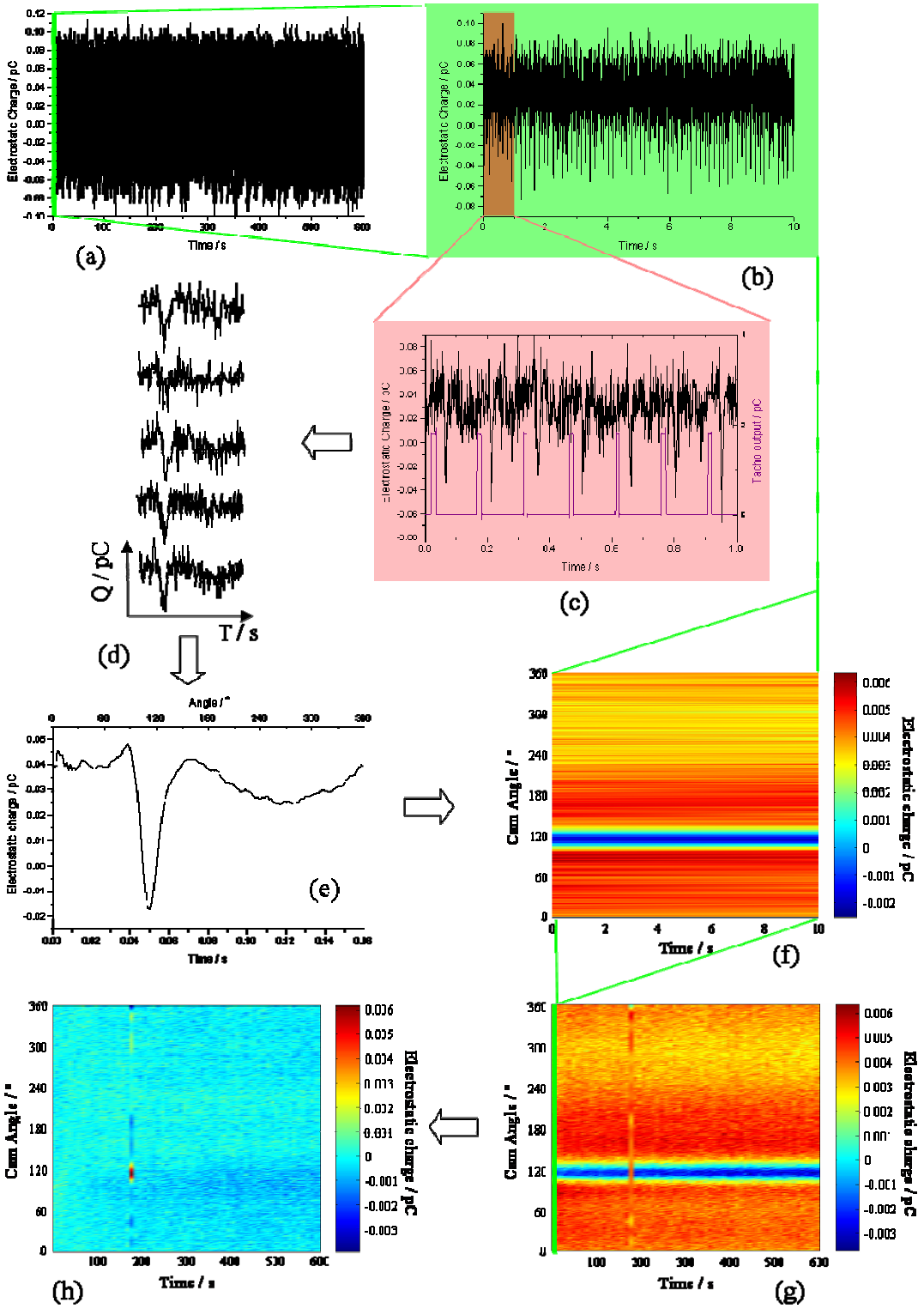

Figure 66. *Schematic showing how the once per revolution colour map is produced. (a) 600 seconds of raw charge data, (b) 10 seconds of raw data (c) raw charge and tacho data over 1 second, (d) raw data sliced into once per revolution segments, (e) an average of the raw data once per revolution segments, (f) a colour map representation of the average once per revolution charge profile, (g) a series of 60 successive 10 seconds averaged once per revolution profile, and (h) normalisation of (g).*

3.5.3 ADDITIONAL REAL-TIME MEASUREMENTS

All three pieces of test apparatus involved additional real-time measurements other than electrostatic surface charge. The oil sump temperature in the TU3 engine was monitored using a thermocouple and a stand-alone data acquisition system acquired at one data point every 10 seconds. The output from the force transducer on the 'in-house' PoD load arm was analysed through an auxiliary input in the GE software and was processed in a similar manner to the charge time signal statistical algorithm. This was converted to coefficient of friction (COF), using calibration plots. The MTM, using PCS software, produced averaged COF every two seconds, the auxiliary tacho was used to synchronise the MTM friction data and the electrostatic charge data.

3.6 OFF-LINE ANALYSIS

The literature review highlighted the limited number of papers that have related charge to wear and that very few papers relate additive behaviour to surface charge generation. For this reason, off-line analysis was relied upon to gain insight into the charge signals. Off-line analysis was carried out to identify lubricant electro-kinetic properties, and surface physical and chemical properties. Surface analysis involved; visual observations through optical and scanning electron microscopy; topographical analysis through contacting and laser profilometers, and chemical analysis through energy dispersive x-ray spectroscopy (EDX) and x-ray photoelectron spectroscopy (XPS).

3.6.1 CONDUCTIVITY

All conductivity measurements were performed prior to wear testing with a Wolfson Electrostatic liquid L30 conductivity meter (see Figure 67), made at the University of Southampton. The conductivity meter can measure in a range of 0.1 pS m^{-1} to 2.0×10^9 pS m^{-1}. Further details of this equipment can be found in [337,338].

Figure 67. Wolfson Electrostatic liquid L30 conductivity meter.

3.6.2 QUANTIFYING SPECIMEN WEAR

3.6.2.1 Non-contact optical surface profilometry

A XYRIS 4000WL TaiCaan Technologies 3-D profilometer was employed to examine pin and disc wear scars for both PoD and MTM tribometers. This system has an *x-y* table motion of 25 mm and a WL (white laser) sensor. The sensor has a 0.35 mm gauge range with 7 μm spot size.

For the worn ball samples the topographical measurements were compared to a 6mm diameter sphere (the dimensions of an unused ball) using *Bodies* (proprietary TaiCaan software); the difference between the two was deemed to be the volume loss. The disc wear track was analysed at 4 positions, 90^{o} from each other. The unworn area was used as a reference plane to calculate volume loss below the plane and volume gain above the plane; the difference between the two was used to calculate wear volume loss. The volume loss was calculated from an average scar area over the 4 positions and multiplied by a function of the circumference, to give the total disc volume loss. The wear volume loss for each tribo-couple was then inserted into equation (33) to calculate the specific wear rate (SWR).

3.6.2.2 Contact profilometry

Two dimensional topographical analyses of the cams, followers and discs were carried out using a Taylor Hobson Talysurf 120L profilometer. The analysis procedure for these components is described within

their appropriate experimental Section. The specifications of the Taylor Hobson 120L form profilometer are as follows:

Traverse Speed	10 mm s^{-1} maximum
Measuring Speed	1 mm and 0.5 mm s^{-1} ±5%
Return Speed	up to 5 mm s^{-1}
Gauge Type	6 mm Laser Stylus range
Measuring Range	10 mm
Resolution	12.8 nm @ 10mm range
Range to Resolution Ratio	780,000:1
Straightness Accuracy	0.5 µm over 120 mm traverse
	0.2 µm over 20 mm traverse
Data Resolution	0.25 µm
Dimensions (L x D x H)	396 x 127 x 195 mm

3.6.2.3 Optical microscopy

Surface wear mechanisms and wear scar geometry for dissimilar tribo-couples (Chapter 7 & 8) were more difficult to quantify than typical steel/steel contacts. The ball wear was analysed by measuring the wear scars using a digital optical microscope. Two optical microscopes, Olympus BH and Olympus BH-2, were employed; the Olympus BH has a black and white MOTIC 2000 digital camera attachment, while the Olympus BH-2 has Prosilica EC 1350 colour camera attachment using GigEViewer software. Due to the elliptical nature of some wear scars, they were characterised by two measurements; the first in the direction of sliding and the second perpendicular to the sliding direction.

3.6.3 SCANNING ELECTRON MICROSCOPY & ENERGY DISPERSIVE X-RAY

A Philips XL30ESEM environmental scanning electron microscope was employed to analyse the wear scar morphology to identify wear mechanism. The SEM was also equipped with an energy dispersive x-ray microanalysis spectrometer system, manufactured by EDAX Phoenix, which was used to reveal elemental composition. Operating voltages range from 0.5 to 30 kV and an ultimate resolution of 1.5 nm at 15kV. The SEM and EDX are controlled and analysed by proprietary software produced by Philips and EDAX respectively.

3.6.4 X-RAY PHOTO-ELECTRON MICROSCOPY

Post-test x -ray photoelectron spectroscopy (XPS) analysis was carried out, in collaboration with Dr Sheila Yeh[*****] at the Chevron Richmond Technology centre, on selected wear specimens in Chapters 5-8. XPS is a technique used to analyse the surface chemistry of a material (unlike EDX it can be conducting or non-conducting), without the need for time intensive preparation. XPS analysis was used to identify the composition of the additive tribofilm and how composition varies with depth, in order to try to relate charge and friction signals to additive-surface interactions. The XPS analysis carried out can be split into two techniques: on and off the wear scar surface chemistry analysis and elemental depth profiling. These were carried out on 3 XPS analysers.

3.6.4.1 Kratos AXIS-HS

The formation and chemical composition of additive tribofilms on steel, paper and brass (Chapter 6,7 & 8 respectively) on and off the wear scar/track were studied by XPS using a Kratos AXIS-HS analyser. The XPS analysis was performed by bombarding the surfaces with a beam of monochromatic Al K_α x-rays with energy of 1486.6 eV. The beam size used was 0.4 mm x 1.8 mm and the analysis averaged the elemental concentration over a 0-110 Å depth. The total acquisition time for each spot was 1.5 hrs and individual spectral regions were scanned at a high spectral resolution of 1.2 eV full width at half maximum. Tribofilm compositions were determined from the intensities of characteristic core-level electron peaks of the XPS spectra. The core-level electron peaks were fitted as Gaussian line shapes (by Kratos software). The atomic percentages of tribofilm constituents were determined from the calculated areas under the corresponding Gaussian profiles. Line positions were used to infer the various chemical states. Analysis of the discs was carried out in the centre of the wear track. For the brass and steel discs this was 1.0-1.2 mm either side of the wear track for the paper disc it was 1.2-1.4 mm.

3.6.4.2 PHI Quantum 2000 instrument

The surface chemistry of three balls were analysed in Chapter 5. These three balls had shown interesting topographical features (via laser Profilometry see Section 3.6.2); it was therefore desirable to relate these topographical features to surface chemistry. Due to the small scale of these topographical features XPS analysis was carried out on three worn pin samples by Evans Analytical Group (California, USA) using a PHI Quantum 2000 instrument. The x-ray source and the spectral resolution were similar to that of the Kratos system, but the x-ray beam had a spot size of 5μm across and 95% of the analysed signal originates from a depth of ~50-100 Å.

[*****] Chevron Energy Technology Company – Integrated Laboratory Technologies

3.6.4.3 Quantera SXM system

Elemental depth profiling of the additive tribofilm on steel (Chapter 6) and brass (Chapter 8) was carried out using a Quantera SXM system. The XPS analysis was performed by bombarding the surfaces with a beam of monochromatic Al K_α x-rays with energy of 1486.6 eV. The analysis beam spot size was 18μm diameter and was set at 45° to the surface. Surface etching was carried out to gain understanding about how the tribofilm elemental composition changes as a function of depth and to get an approximate value of the tribofilm thickness. The tribofilm was Argon etched at 2 keV, at a rate of 6.4 nm/min (relative to SiO_2); the tribofilm surface was analysed every 2-6nm.

3.7 THE USE OF STATISTICAL METHODS FOR MULTIPLE VARIABLES AND MEASURED PARAMETERS

The following statistical approach was devised in conjunction with Jo Martinez[†††††]. Statistical analysis of test data was carried out by Jo Martinez using SAS software.

Statistical analysis is an important tool employed in this thesis to relate additive behaviour to surface charge generation. Statistical analysis also makes interpreting interactions between multiple charged species in the oil more manageable. To evaluate the effect of two or more ***independent variables*** (e.g. additives) on a dependent ***variable*** (e.g. charge), a **factorial design** is employed and analysis of variance (ANOVA) is used to analyse the data. ANOVA determines the significance (***p-value***) of ***variable*** effects or ***variable interactions*** on ***measured parameter*** (see Table 23).

Independent variable		Dependent variable (Measured Parameters)	
Variable	Variable Interaction	Real-time data	Off-line analysis
Additive	Additive – Additive	Electrostatic charge	Disc wear
Base Oil	Additive – Contaminant	Coefficient of friction	Ball wear
Carbon black (contaminant)	Additive – Base oil		Conductivity or ESA

Table 23. ANOVA statistical terms and examples.

When experimental costs are high, or the risk (of success) is unknown, statistical methods can enable extraction of unbiased information, regarding the factors affecting a variable, from as few observations as possible. (This was the case for work presented in Chapter 5). **Fractionated factorial** matrices are used to reduce the number of tests required to evaluate varying order interactions, which is defined as the effect of one independent variable (e.g. additive A) as a result of the level (e.g. presence or absence) on another independent variable (e.g. additive B). Optimal design procedures are used for this purpose.

[†††††] Lead Research Statistician, Global Statistics/Global Partnership Services, Products and Technology, Chevron Oronite Company LLC

The aim of Optimal Design is to derive unbiased (or least biased) main effects and interactions with a minimum number of observations. The *D*- and *A*- optimal design procedures are methods used to select from a list of candidate points (combinations of factors), those points that will extract the maximum amount of information from the experimental region (the *n*-dimensional space where the model is applicable). *D*-optimal design maximises the determinant *D*- of a matrix, which indicates factor effects that are maximally independent of each other. *A*-optimal designs also seeks independence, but by maximising the diagonal elements of the matrix, while minimising the off-diagonal elements. Searching for the best design is not an exact method, but rather an algorithmic procedure that employs *D*- and *A*-optimal criteria along with the model (e.g. fractionated factorial) required to fit to the data and the number of tests desired to find the best design.

In Chapter 5 the effect of two dispersants, a detergent, an antiwear additive and carbon black on electrostatic charge, friction and wear, was tested. Standard analysis would require all 5 variables to be separated by running 32 tests. For the work presented in Chapter 5 a **fractionated** (half) **factorial** matrix $2^{(5-1)}$ (16 test oils) allowed the main effects and 2-factor interactions to be evaluated using **ANOVA**. The half factorial matrix described above has the disadvantage of insensitivity to three or more factor interactions. However it was decided that this number of interactions was not a key concern at this early stage of research. The original 16 blends were designed so that the factor effects are maximally independent of each other (*A*- and *D*- optimality), which are shown in Table 26.

In Chapter 6, six additive: detergent, dispersant, ZnDTP and three different friction modifiers, were blended into API Group I, Group II and poly alpha olefin (PAO) base oils. A full factorial matrix was constructed and each base oil test (non-additized) was repeated, giving 24 runs in total. A full factorial matrix was run in this study for two reasons: firstly the statistical approach was validated by the initial study (Chapter 5) and secondly, although the changing of multiple variables could be handled by the statistical approach, it meant that interpretation and comparison between real-time data was difficult.

The measured parameters (dependent variables) obtained from running the fractionated or full factorial matrix were disc wear, ball wear, conductivity and real-time data. The real-time data, including the COF and rms charge, were averaged for the duration of stage 2 of each test to assess correlation over the whole test period. The data in Chapter 5 were also averaged for every 5 minute interval (described as interval electrostatic charge hereafter) to try and assess correlations of dynamic real-time features.

ANOVA is used to analyse the measured parameters. ANOVA has the following assumption to make it valid:

1. Samples are randomly selected.
2. Sample distributions are normal.

3. Homogeneity of Variance - the variances of the different groups are equal.

Assumption 1 is achieved by randomising the test runs in the factorial matrix. If assumptions 2 and/or 3 are violated, the data can be **transformed** to make the data normally distributed and to stabilise the variance. The Box-Cox procedure was used to identify the appropriate transformation of the data. Typical transformations include: y^2, $\sqrt{y}$, $\log(y)$, $1/\sqrt{y}$ and $1/y$

With the above assumptions met, ANOVA is used to determine whether two or more means are different. This procedure tries to identify sources of variability from one or more factors and uses these variances to decide whether *'the means'* are significantly different. The **residual error** is required for estimating the probability of significance. The work in Chapter 6 achieved this through repeat base oil tests. The probability of errors (i.e. ***p-value***) is used to indicate the significance of the interactions on the variable and its associated response. For *p-values* less than 0.05, the interactions between the factors are considered **significant** because only 5% of the interaction could be explained by other factors. When, $0.10 > p\text{-}value > 0.05$ the variable or variable interaction is **marginally significant**.

Because of the fractionated nature of the matrix and because there were no randomised repeat tests in Chapter 5, there was no residual error for estimating the probability of errors (*p-value*). A model with only the most probable significant effects (as highlighted from the sum of squares plots) was introduced to overcome insufficient degrees of freedom for error estimating, required by a full model (i.e. randomised repeat tests). Essentially, this involves visually looking at the data to identify which factor(s) stands out from the rest of the data; the significance of the identified factor is calculated by using the rest of the data to simulate repeat tests, thus providing enough degrees of freedom. Extra degrees of freedom created by this model were used to estimate the error.

Further details of the statistical methods used can be found in references [339,340].

4 SCUFFING DETECTION OF TU3 CAM-FOLLOWER CONTACTS BY ELECTROSTATIC CHARGE CONDITION MONITORING

4.1 INTRODUCTION

The immediate affect of wear in an automotive engine is that it roughens component surfaces, which result in greater friction and therefore reduces fuel efficiency. One of the main contacts, that wear has a major impact on engine performance is the cam-follower. This Chapter presents work from experiments where electrostatic sensors were used to monitoring the cam-follower the contact. A series of experiments were carried out on a non-fired (motorised) TU3 engine to investigate the prominent charge mechanisms under no-wear conditions and adhesive wear. Carbon black contaminated oil test was carried out to simulate scuffing in a short duration. Mild wear tests, which used a fully formulated oil and oil starvation tests, were carried out to try to decouple the charging mechanism in the carbon black contaminated oil test and identify charge features associated with the transition to scuffing.

4.1.1 AIMS

The aims of this work are to:

- Instrument an industry standard automotive engine (TU3) with electrostatic sensors to monitor the surface charge of the cam.
- Characterise the background levels of the system and understand how it is affected by lubricant temperature and engine rotation speed.
- Assess the sensitivity of electrostatic sensors to detect the onset and progression of adhesive (scuffing) failure.
- Further understanding of soot initiated and oil starved adhesive failure.

4.2 EXPERIMENTAL PROCEDURE

4.2.1 MODIFICATIONS TO ENGINE

A 1.3L TU3 engine was used in a non-fired mode, driven through the crankshaft by a 5.5 kW motor. The camshaft was driven by a timing belt connected to the crankshaft. The pistons and part of the connecting rods were removed, to minimise the wear from other components in the engine which might influence the charge measurements. The crank shaft bearings were held by the remaining part of the connecting rod, to maintain the correct cylinder head oil pressure. All followers were removed except the one contact of interest (see Figure 68), again to minimise the effect other wearing components have on charge detection.

Spacers were used to replace the missing followers to ensure the designed oil pressure is maintained. An oil recirculation system was attached to the engine (where the oil filter is normally located). This enabled the oil temperature to be controlled by a heat exchanger. During the wear test, a cap was placed onto the oil filter adapter/spacer to replace the oil filter to avoid removal of the entrained carbon black.

Two WSSs were employed to monitor cam lobes 3 and 5 (from pulley end). These were located on the exhaust manifold side of the head, 6 mm below the cam centre line and 0.5 mm from the cam-nose (see Figure 68); previous tests indicated this positioning gave the best resolution. The sensing face of the WSS had a diameter of 10 mm; the cam and follower widths were 19 mm and 15 mm respectively.

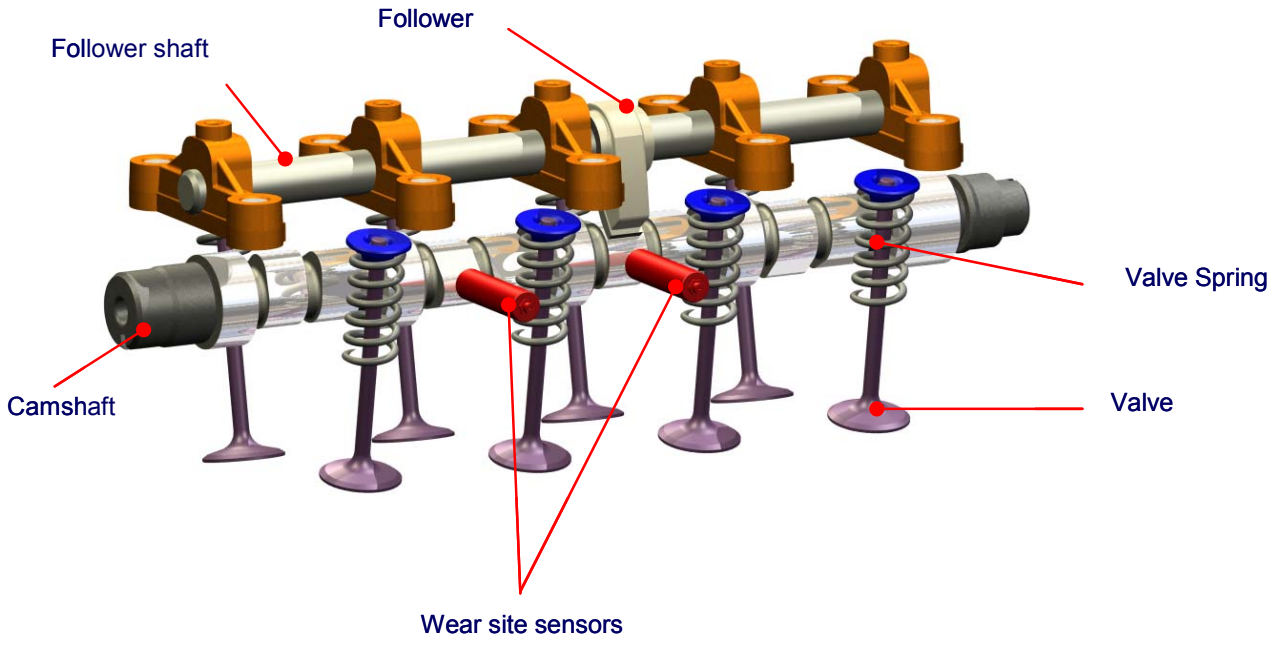

Figure 68. Schematic diagrams of the positioning of the two wear site sensors relative to the TU3 valve-train.

Details of the instrumentation, data acquisition and signal processing can be found in Section 3.5.1 & 3.5.2. The oil sump temperature was monitored using a thermocouple and a stand-alone data acquisition system.

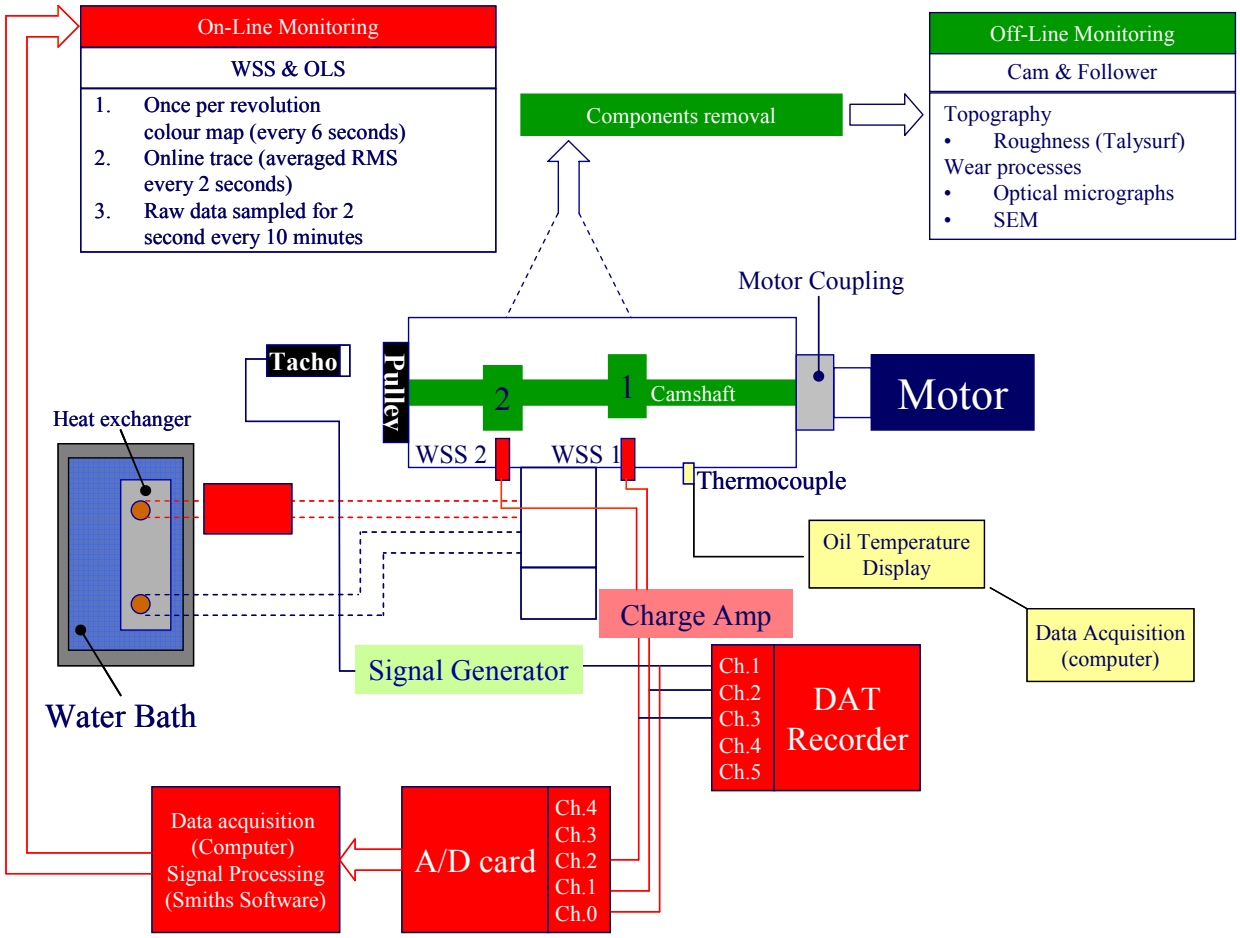

Figure 69. TU3 instrumentation and data acquisition systems.

4.2.2 TEST MATERIALS

The chemical composition of the followers and camshaft are shown in Table 18. The cams were made of chilled cast iron with a graphitic nodular structure (see Section 2.2.1.3) at the centre of the cam shaft, with reduced nodular content and increased graphite flakes towards the surface. The followers are high chromium cast steel (see Section 2.2.1.3). Table 19 shows the mechanical and physical properties of the camshaft and follower, which illustrates the difference in cam and follower hardness.

4.2.3 TEST METHODOLOGY

Experiments were divided into two categories: system characterisation and wear testing. The system characterisation tests, which were non wear tests, were conducted to understand the influence of operational parameters on charge levels. The information gained from these tests was then used to compare charge signals generated by the wear tests.

System characterisation tests investigated the effect of cam geometry, lubricant temperature and rotational speed on electrostatic charge. The first test kept the engine (camshaft) rotation speed and lubricant temperature constant. The second test investigated the influence of lubricant temperature by holding the rotation speed constant and increasing the temperature (from room temperature to 60°C). The third test investigated the influence of camshaft speed by holding the lubricant temperature constant and increasing engine speed. The test parameters are detailed in Table 24. To allow a direct comparison between the system characterisation and wear tests, the rotation speed was held constant at 400 rpm. To minimize wear for the system characterisation test a fully formulated oil was used. Surface profilometry of the follower and camshaft surfaces revealed that no measurable wear occurred during these tests.

Wear testing involved two tests, both employed a camshaft speed of 400 rpm to mimic increased wear [341] seen during start-up, shutdown, and high torque conditions (i.e. long hills), which can starve the contact zone of lubricant [26]. The first test employed 2% carbon-black laden oil with the primary aim of instigating wear in a reasonable time-frame. The oil temperature was allowed to increase naturally (under mechanical action), which resulted in a temperature similar to that used for the low temperature stage of the TU3 standard test. Previous studies of wear in the Peugeot TU3 test indicated that wear is more rapid at lower temperatures [51]. The second test was an oil starvation test (no lubricant was used), designed to remove lubricant-related charge generation mechanisms. Tests parameters are detailed in Table 24.

	System Characterisation			Wear testing	
Test Description	Cam profile (SCCP)	Variable lubricant temperature (SCVLT)	Variable cam rotational speed (SCVCS)	Carbon black contaminated oil (CBCO)	Oil starvation (OS)
Camshaft speed (rpm)	400	400	527, 760, 999, 1248	400	400
Lubricant temperature (°C)	40	19.5-60	40	2% carbon black + 4% Dispersant 1	No oil
Lubricant	Commercially available fully formulated oil			15-45	None

Table 24. Parameters for the system characterisation and wear tests.

4.2.4 LUBRICANT CHEMISTRY

An *'off the shelf'* fully formulated oil was used for the System Characterisation tests. For one of the wear tests the test oil contained a Group I base oil, 4% Dispersant 1 and 2% carbon black was blended to promote wear (see Section 3.3 for details of lubricant chemistry). For the other wear test (oil starvation), no lubricant was used.

4.2.5 POST-TEST ANALYSIS

The cam topography was measured, using a 2D Taylor Hobson Talysurf profilometer (see Section 3.6.2.2), at 7 positions perpendicular to the direction of sliding at the following cam angles:-30°, -15°, -5°, 0°, 5°, 15° and 30° (see Figure 70 (a)), because oil film thickness predictions discussed in Section 2.2.1.5 identified that this area of the cam experienced the greatest contact severity. The follower topography was measured at 5 equally spaced positions along the sliding direction and 5 equally spaced positions perpendicular to the sliding direction (see Figure 70 (b)). SEM and EDX analysis was carried out on the worn cam and follower samples to identify wear mechanisms and surface composition (see Section 3.6.3).

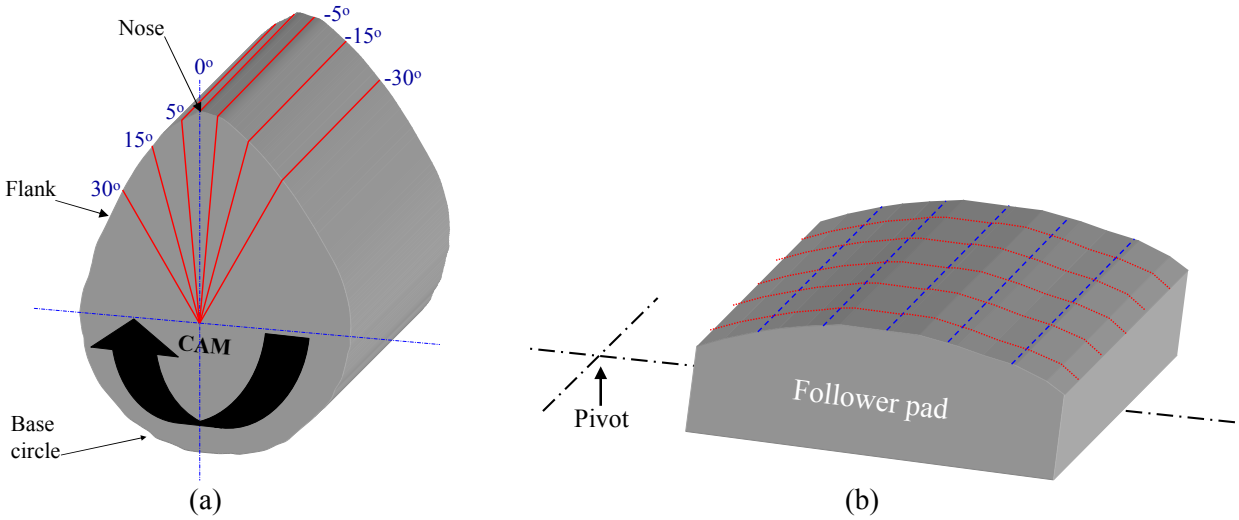

Figure 70. Position and direction of surface topography measurements on (a) cam and (b) follower.

4.3 CHARACTERISATION OF SYSTEM

4.3.1 THE EFFECT OF CAM PROFILE ON CHARGE

Figure 71 shows a once per revolution signal average of the cam surface charge as a function of cam angle. The peak cam surface charge occurs at 0° which corresponds to the position that the cam nose is closest to the sensor. In general, the further away a charge source is from the sensor, the fewer electric field lines terminate on the sensor surface (the lower the charge). The once per revolution charge profile is closer to a $1/x$ relationship than to a $1/x^2$ relationship (see Figure 71), because the charge on the cam surface is planar, rather than at a discrete point (see Section 2.4.2.1). However the correlation is not exact. This is for two reasons; firstly the cam surface is not flat, and thus not all the electric field lines terminate on the sensor surface; secondly, because contact pressure, and more importantly velocity, vary around the cam surface, the distance between the surface and double layer shear plane will vary, thus tribocharging is not constant around the cam surface.

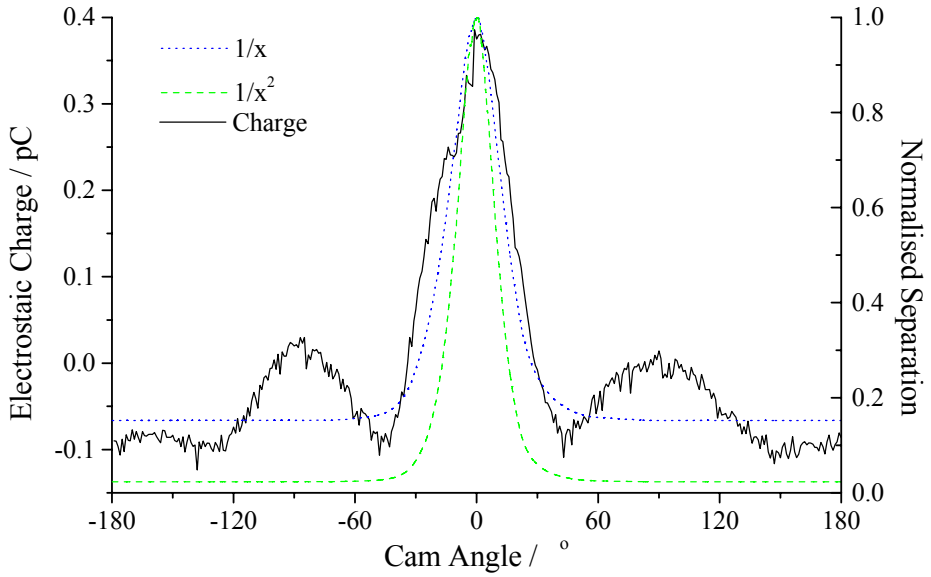

Figure 71. *Once per revolution charge trace (averaged over 10 seconds), depicting a once per revolution positive peak relating to the cam nose. Cam rotation 400 rpm, fully formulated lubricant temperature 40°C.*

4.3.2 EFFECT OF LUBRICANT TEMPERATURE ON CHARGE

The colour map (see Figure 72) shows a persistent positive charge associated with the cam nose at approximately 0°. However, as the test progresses and the lubricant temperature increases, the charge magnitude associated with this peak increases and broadens. The charge spread will increase with the increase in magnitude as there is higher charge to detect. The increase in charge with increasing temperature can be explained by tribocharging theory (see Section 2.4.3.1); as the temperature increases, so the oil viscosity decreases, which increases hydrodynamic entrainment and increases ionic mobility [291]. Figure 73 shows how the rms charge level varies with time and temperature; the charge does not increase linearly, but appears to have three temperature 'transients' or short periods of increased charge activity. Repeat tests have shown that these transients appear at approximately the same temperature despite different heating rates used. The fully formulated oil used contains additives, such as ZnDTP; at the temperatures observed these additives can start to decompose, the products of which then react with the surface to form a tribochemical film. There have been reports of film formation on steel, lubricated with oils containing ZnDTP, at 50°C even at 20°C (see Table 12); within the oil temperature range these charge transients occurred. In reality the contact temperature will be significantly higher than the bulk lubricant temperature, which will promote greater decomposition of the anti-wear additives.

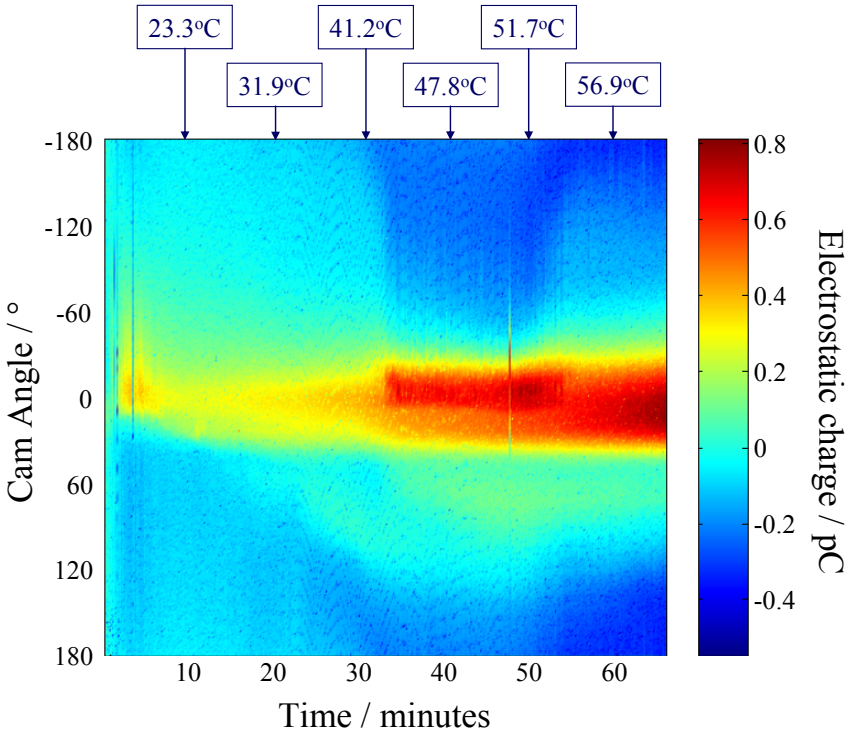

Figure 72. *Charge colour map for lubricant temperature test conducted at camshaft rotation speed of 400 rpm.*

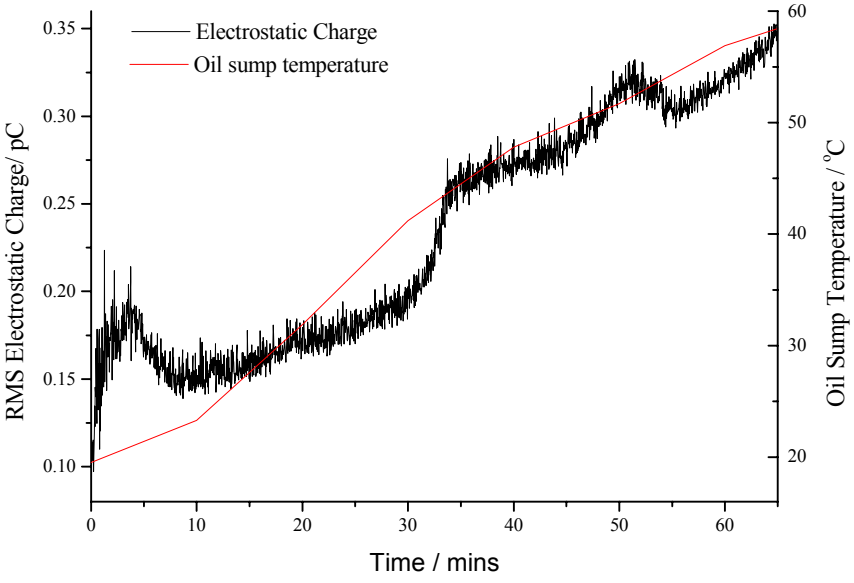

Figure 73. *Electrostatic charge (RMS) and oil sump temperature levels during lubricant temperature test conducted at camshaft rotation speed of 400 rpm.*

4.3.3 EFFECT OF CAM ROTATION SPEED ON CHARGE

Figure 74 illustrates charge as a function of rotation speed (stepped over 10 minute intervals) and clearly shows that charge intensity, as well as spread, increases with increasing rotational speed. Fluid velocity is an important factor in determining the charge magnitude produced by tribocharging [291]. As the cam rotational speed increases the shear stress at the surface/fluid interfaces increases. This can be explained by both the *differential rate theory* and the *double layer stripping theory* (see Section 2.4.3.1). For the *differential rate theory*, as rotational speed increases so there is a greater volume of charge species passing the surface, increasing the rate of transportation to/from the cam surface. For the *double layer stripping theory* the further away the double layer shear plane is from the surface the more diffused positive and negative charge species are. As the distance between the surface and double layer shear plane decreases so the charge species are less diffuse and one charge sign dominates. The increase in rotational speed decreases the distance between the double layer shear plane and the surface, thus increasing the dominance of one charge sign (see Figure 75). Many studies have shown that the charging increases with fluid velocity; with some showing a linear [342-345], log-log [346,347] and log-linear [324,344] relationships.

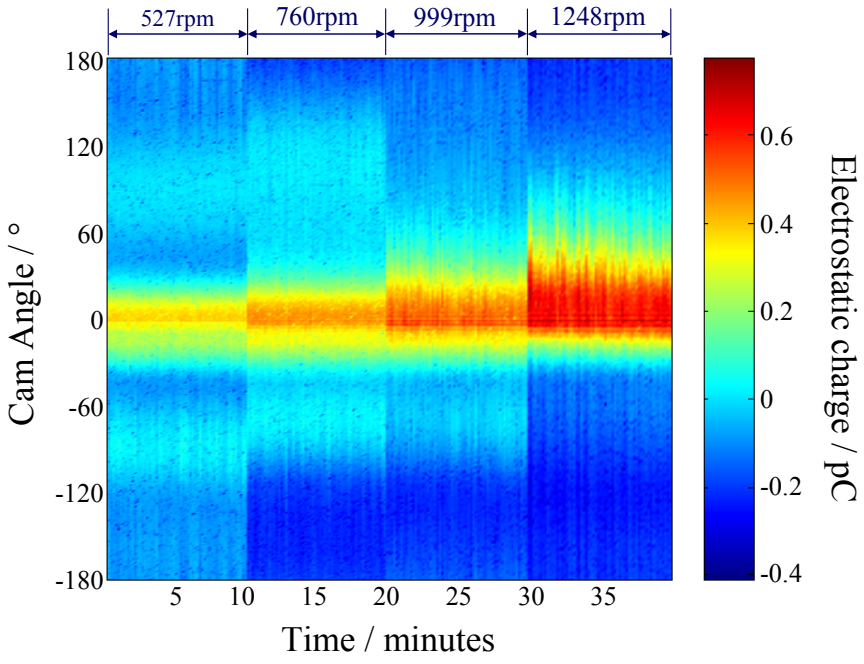

Figure 74. Charge colour map for camshaft rotation speed of 527, 760, 999, 1248 rpm at a constant lubricant temperature of 40°C.

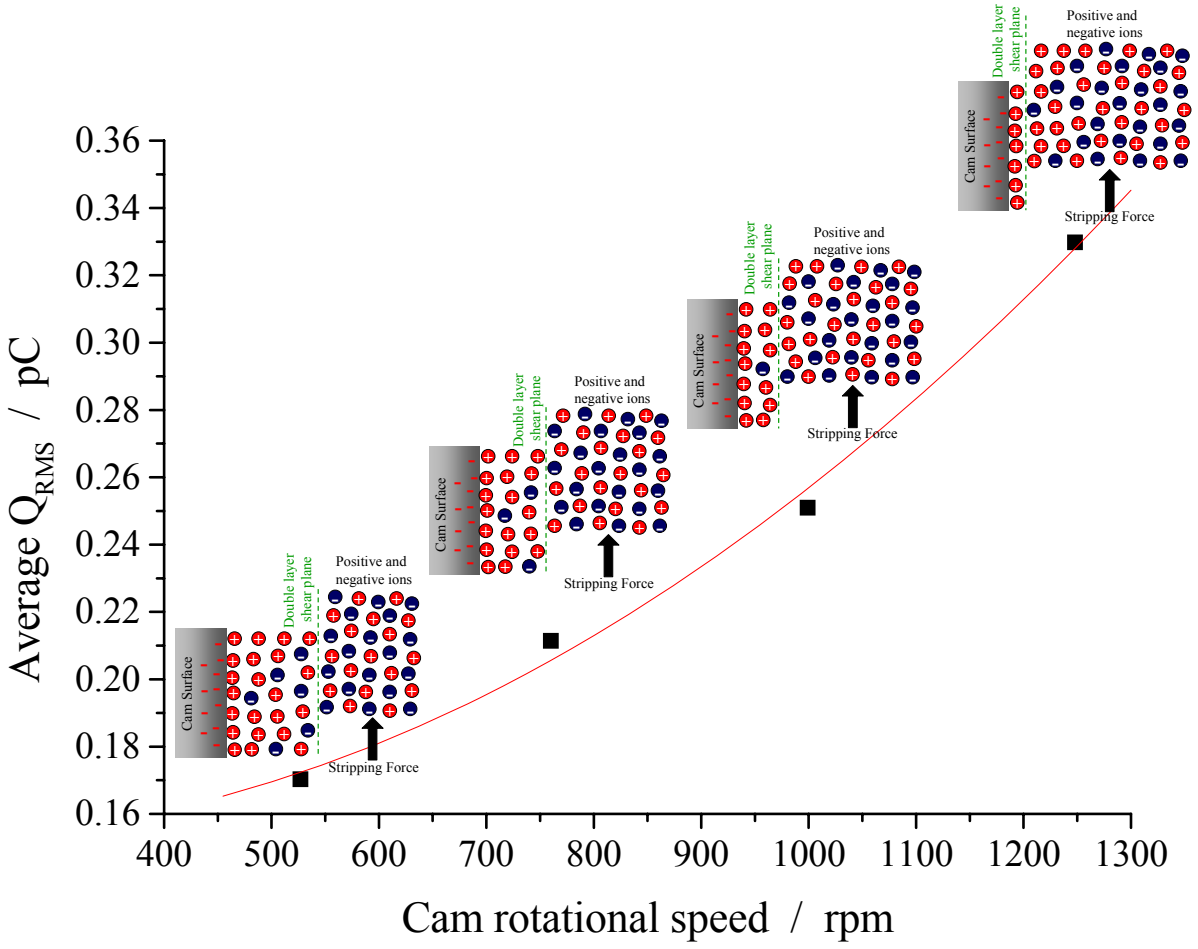

Figure 75. Schematic diagram depicting the distance between the double layer shear plane and cam decreasing with increasing rotational speed, and how this leads to a greater surface charge.

4.4 WEAR TESTS

The following Section discusses the charge data from a carbon black contaminated oil (CBCO) wear test and an oil starvation (OS) wear test. Detailed post-test analysis of the worn components was carried out to identify wear mechanisms and the charge generation mechanism which might result. The latter part of this Section pulls together real-time data and post-test analysis to relate charge measurements to the lubricant (tribocharging) or wear (CPD) and debris generation.

4.4.1 CARBON BLACK CONTAMINATED OIL (CBCO) TEST

4.4.1.1 RMS data

Figure 76 shows the electrostatic and lubricant temperature data for the CBCO test. After 330 minutes, highly dynamic charge signals were seen in real-time through the GE Aviation (formerly Smiths

Aerospace) software. Given the dynamics of the charge trace compared to the preceding signal a decision was made to stop the test. Visually inspecting the cam and follower confirmed that scuffing had occurred.

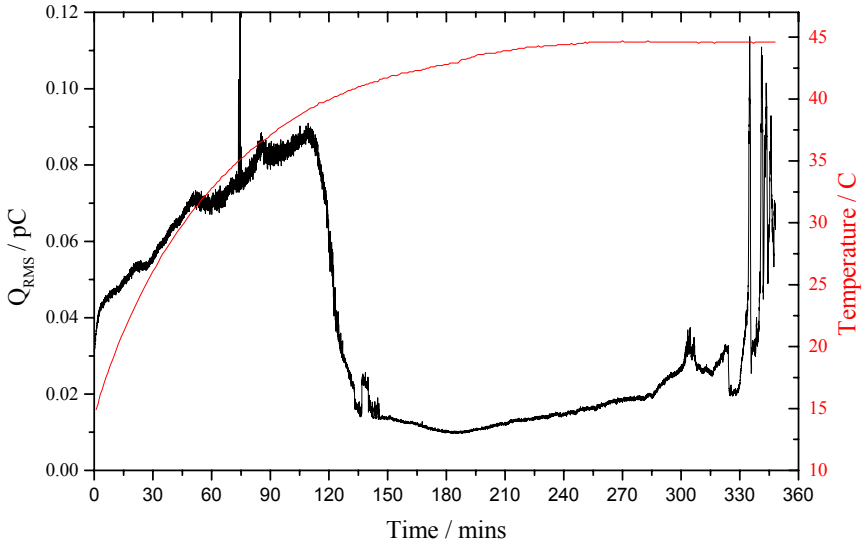

Figure 76. Charge RMS and sump oil temperature data for the entire duration of the carbon black contaminated oil wear test run at 400 rpm.

At the beginning of the test, charge increased almost linearly, which generally correlates with the increase in temperature. From the SCVLT test (see Figure 74), charge increases with increasing temperature due to the increased mobility of the charge species [291]. As the temperature starts to level out, the charge drops from 0.08pC to 0.01pC. There are two possible explanations for this: temperature induced charge relaxation and a reduction in roughness, reducing tribocharging. Electrostatic charging has been observed to increase with temperature to a maxima, then decrease due to charge relaxation through leakage [345,347,348]; high temperatures can promote charge recombination (see Figure 52(a)). This was not seen in the SCVLT tests, but the lubricant chemistry is significantly different and therefore may affect this response. Indeed numerous authors [324,342,343,349] did not report such maxima and some have observed both types of behaviours over the temperature range of 25–60°C [344]. As the cam and follower run-in their surfaces become conformal [54,66], resulting in a reduction in roughness, reducing tribocharging as observed by Harvey et al. [291] (See Figure 52(b)). A reduction in roughness reduces the actual surface area reducing the number of charge species that can be stripped. A reduction in roughness also reduces the microturblance which facilitates charge removal from the double layer.

The charge signal from 110 minutes onwards follows the idealised bathtub wear curve (see Figure 10) shape of running-in, mild wear and failure. Although no steps were taken to directly relate charge and wear rate, it has been observed by Harvey et al. [25] and Wang et al. [313] that electrostatic charge signals can be related to wear rate.

4.4.1.2 Charge colour maps

Figure 77 shows a positive peak (red) around 0° which increases in magnitude and spread over the initial period (0-110 minutes); in a similar manner to the SCVLT test (see Figure 72). This peak then decreases in magnitude and spread. At approximately 200 minutes the charge peak changes from a faint positive charge to a faint negative charge, which increases in magnitude and width as the test progresses. The appearance of a strong negative charge on the cam nose was not seen in the system characterisation tests.

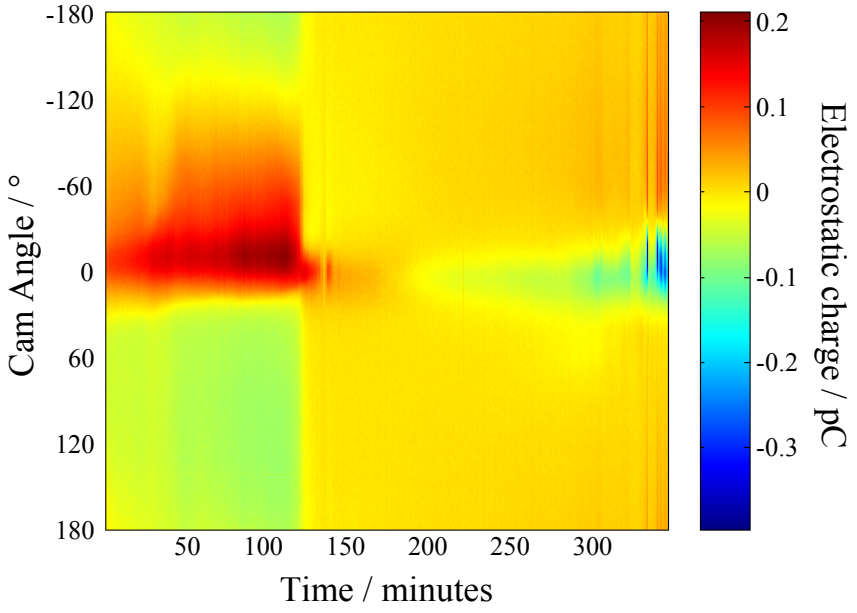

Figure 77. Charge colour map for the entire duration of the carbon black contaminated oil wear test run at 400 rpm.

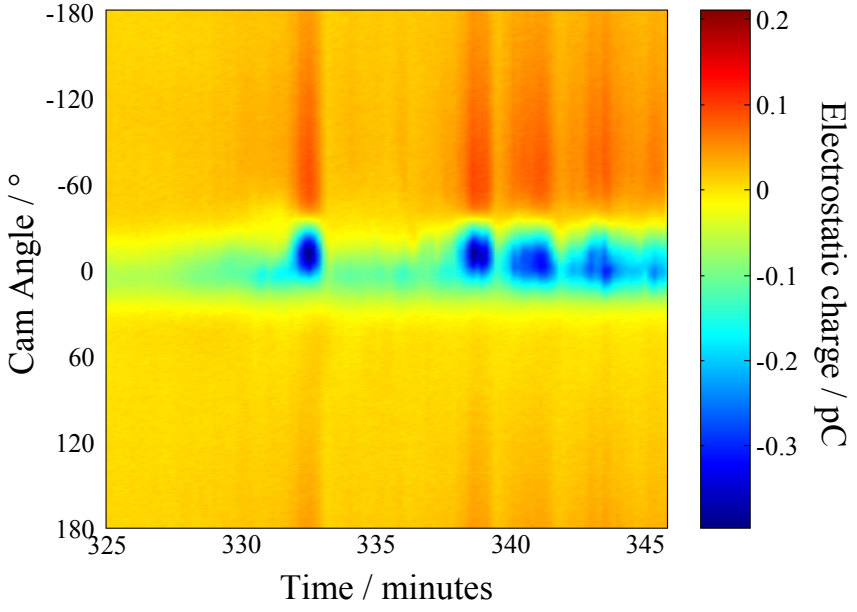

Figure 78. Charge colour map of the carbon black contaminated oil wear test, from minute 325-346.

Figure 78 shows a colour map of the end of the test, which is an expansion of Figure 77 between 325 and 345 minutes. This clearly shows four highly negative charge features between 1 and 2 minutes in duration. The cam surface is closest to the sensor at 0° on the colour maps and it is this position that produces the highest positive charge level (see discussions in Section 4.3). However, the first two high magnitude negative peaks occur between -6° and 26°, the centre of the feature is positioned at 10° (see Figure 78). This can be explained by comparing the colour map to Figure 25(b), which shows the film thickness between the TU3 cam-follower contact for different viscosity oils; this shows that the point of minimum film thickness appears at a point -12° away from the centre of the cam nose, where the oil entrainment velocity between the cam-follower contact is small [58]. It is likely that if film break-down occurs, wear will initiate at this position. It was observed that after the first two high negatively charged peaks (see Figure 78), the negative charge levels remain high and further peaks are positioned closer to the cam nose. This is believed to be an indication of the progression of wear around the cam surface.

4.4.1.3 Raw data traces

Raw data traces for the CBCO test are shown in Figure 79. The initial raw signal (see Figure 79(a)) shows a high, broad positive peak, which is thought to relate to the adsorption of Dispersant 1 onto the cam surface promoting tribocharging and/or surface charge mechanisms. The dispersant will acquire a positive charge via reaction with an acidic surface site, thus forming an acid-base pair [350]. The raw data trace half-way through the test, where the charge level is at its lowest, is relatively flat (see Figure 79(b)). Just before the end of test, where scuffing is thought to be occurring, a high magnitude negative peak of approximately -0.15 pC is observed (see Figure 79(c)). This charge peak is more symmetrical than at the beginning of this test; probably due to discrete regions of (high) wear around the cam surface. At the beginning of the test, wear is thought to be minimal and therefore the surface charge generated by tribocharging, in comparison to discrete regions of wear, is relatively uniform over the cam surface. Thus the sensor mainly detects charge related to cam geometry, which is asymmetric because of the position of the sensor, below the cam centre line, thus the sensor sees the rise side of the cam for longer than the fall side (see Figure 79(a)). Wear on the cam surface is not uniform and therefore leads to a non-uniform charge distribution over the cam surface, which results in a charge profile which is no-longer dominated by geometry, but rather geometry and discrete regions of wear around the cam nose.

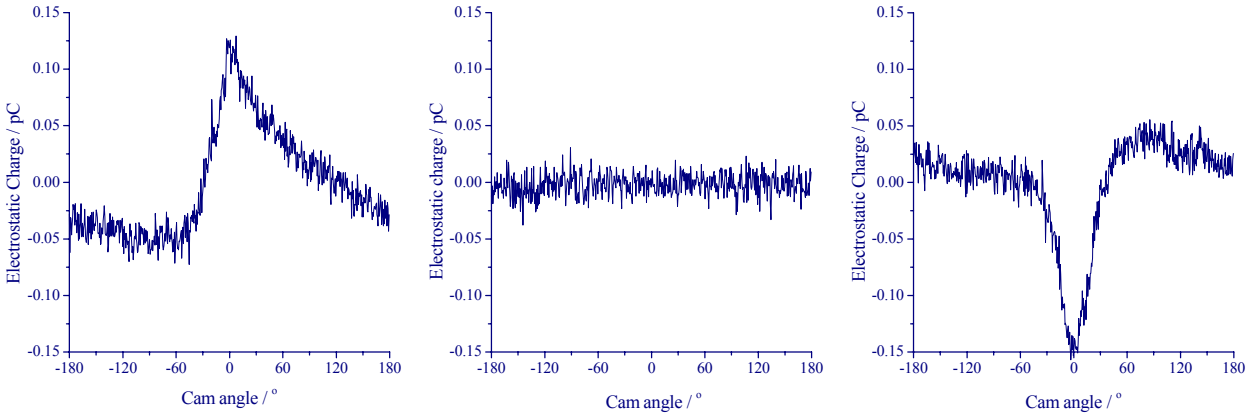

(a) (b) (c)

Figure 79. Electrostatic charge raw data for one rotation of the cam for the carbon black contaminated oil test at: (a) 10 minutes, (b) 170 minutes and (c) 340 minutes.

4.4.2 OIL STARVATION (OS)

The charge colour maps and raw data for the CBCO test show that the charge signal goes through a sign inversion. To gain a better understanding of the charge mechanisms involved, which are believed to be tribocharging of the lubricant and CPD due to wear, a second wear test under oil starvation conditions was performed to remove the lubricant/tribocharging effect.

4.4.2.1 RMS data

Figure 80 shows the charge (Q_{RMS}) for the OS test. The test starts with a low charge (around 0.015 pC), lower than observed for the majority of the CBCO test (0.04 pC). However, these charge levels are similar to the middle stage of the CBCO test. After 10 minutes, there is a steady increase in charge (to 0.055 pC) as the test progresses. This is about half the maximum level reached by the CBCO test. The charge signal for the OS test does not exhibit the same dynamics as the CBCO tests (compare Figure 80 to Figure 76); instead there are a number of charge oscillations over longer time durations.

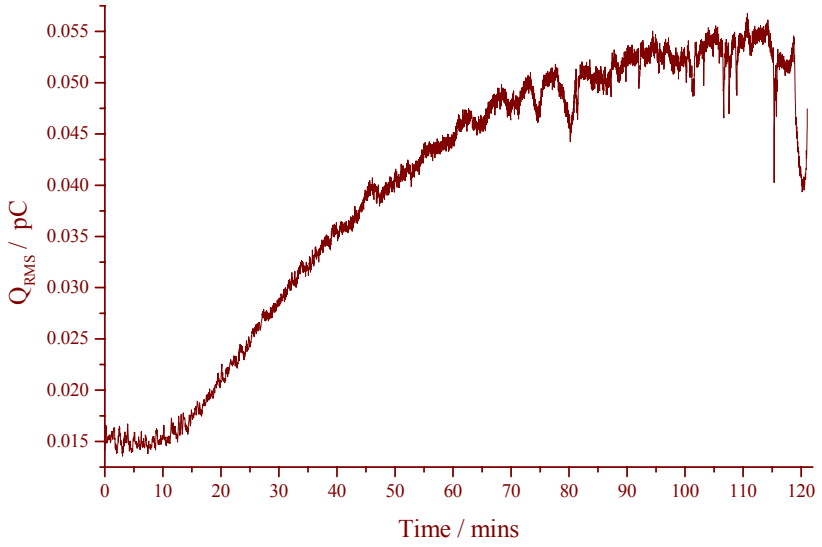

Figure 80. Charge RMS levels for oil starvation test.

4.4.2.2 Charge colour maps

The charge colour map (see Figure 81) shows the development of a strong negative region at around 0°. Unlike the CBCO test, wear does not initiate around the side of the cam nose. The absence of a positive charge peak indicates that the source of the positive charge in Figure 76 was related to the presence of the lubricant and the negative charge was produce by wear.

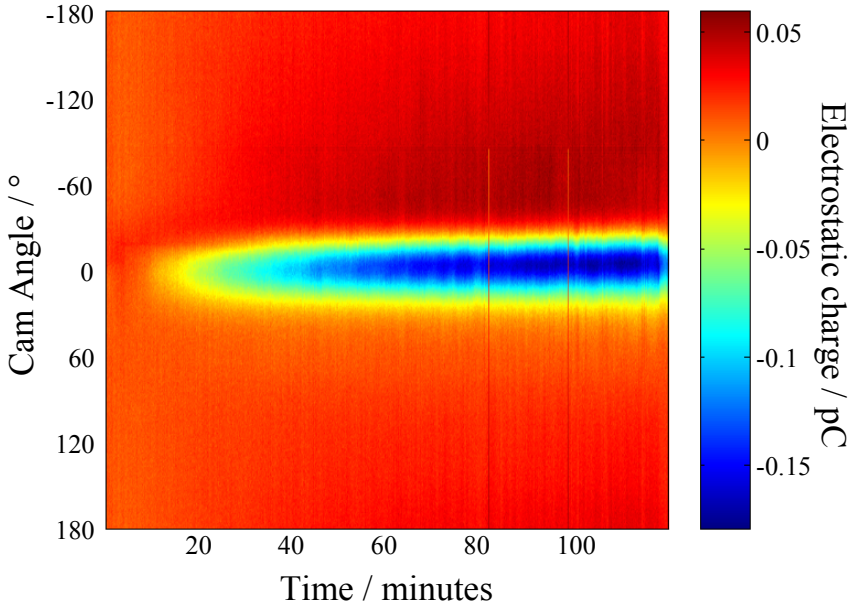

Figure 81. Colour map for oil starvation test.

4.4.2.3 Raw charge data

The raw signal for the initial part of OS test (see Figure 82(a)) exhibited a small magnitude negative charge peak (approximately –0.015 pC). As can be seen, towards the end of the test (see Figure 82(b)) the negative peak has increased in magnitude to approximately -0.125 pC. If Figure 82(a) & (b) are compared to the CBCO test Figure 79(b) and (c) a clear similarity in sign, shape and magnitude can be seen, indicating that for the two wear tests the charge generation mechanism, are comparable.

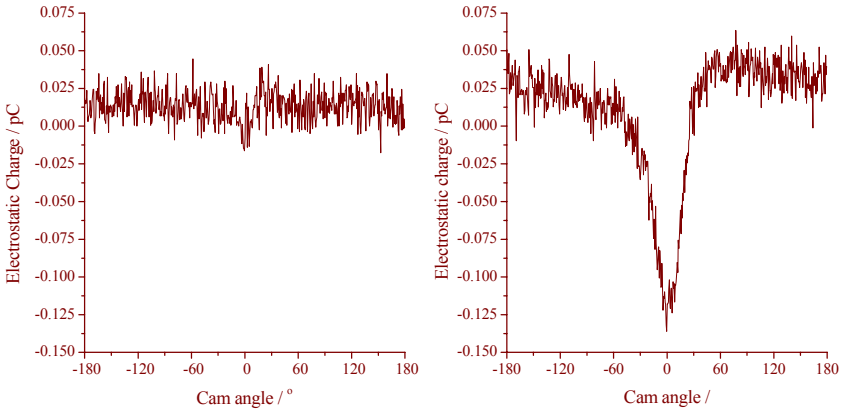

(a) (b)

Figure 82. Electrostatic charge raw data for one rotation of the cam for the oil starvation test at: (a) 10 minutes (b) at 120 minutes.

4.4.3 POST-TEST ANALYSIS

The cam and followers for both wear tests were examined by SEM and their surface topography measured using a Taylor Hobson 120L Talysurf. This information was used to identify wear mechanisms and the severity of wear so that charge generation mechanisms as a result of wear could be revealed. Energy dispersive x-ray analysis (EDX) identified areas of different chemical composition.

4.4.3.1 Carbon black contaminated oil test (test 4.4.1)

Figure 83 (a) shows that wear occurred from the nose of the cam, round to the base circle. However wear on the base circle and flanks was minimal compared to the nose; in general, small adhesive tears in the direction of sliding were observed (see for Figure 11 illustration). Around both flanks of the cam are areas of embedded material (see Figure 83(b)), which are high in carbon, oxygen and iron content (see Table 25). It is thought that this substance is a mixture of carbon black and wear debris which 'clumped' together and has been entrained through the cam-follower contact. Towards the cam nose, greater surface deformation was observed as well as the removal of carbides at the surface (see Figure 83(c)). Repeated contact between the follower and cam could have loosened the carbides, resulting in ejection and/or pulled out when surface material is plucked away. Figure 83 (d) is typical of the type of greater adhesive

material removal seen around the cam nose. EDX analysis identified that there is a large difference in surface composition between point 2 (which mainly contains carbon and could be carbon black) and points 3 and 4, which have both a higher iron concentration, but differ in carbon concentration (see Table 25). These differences in chemical composition will drive CPD and thus charge generation.

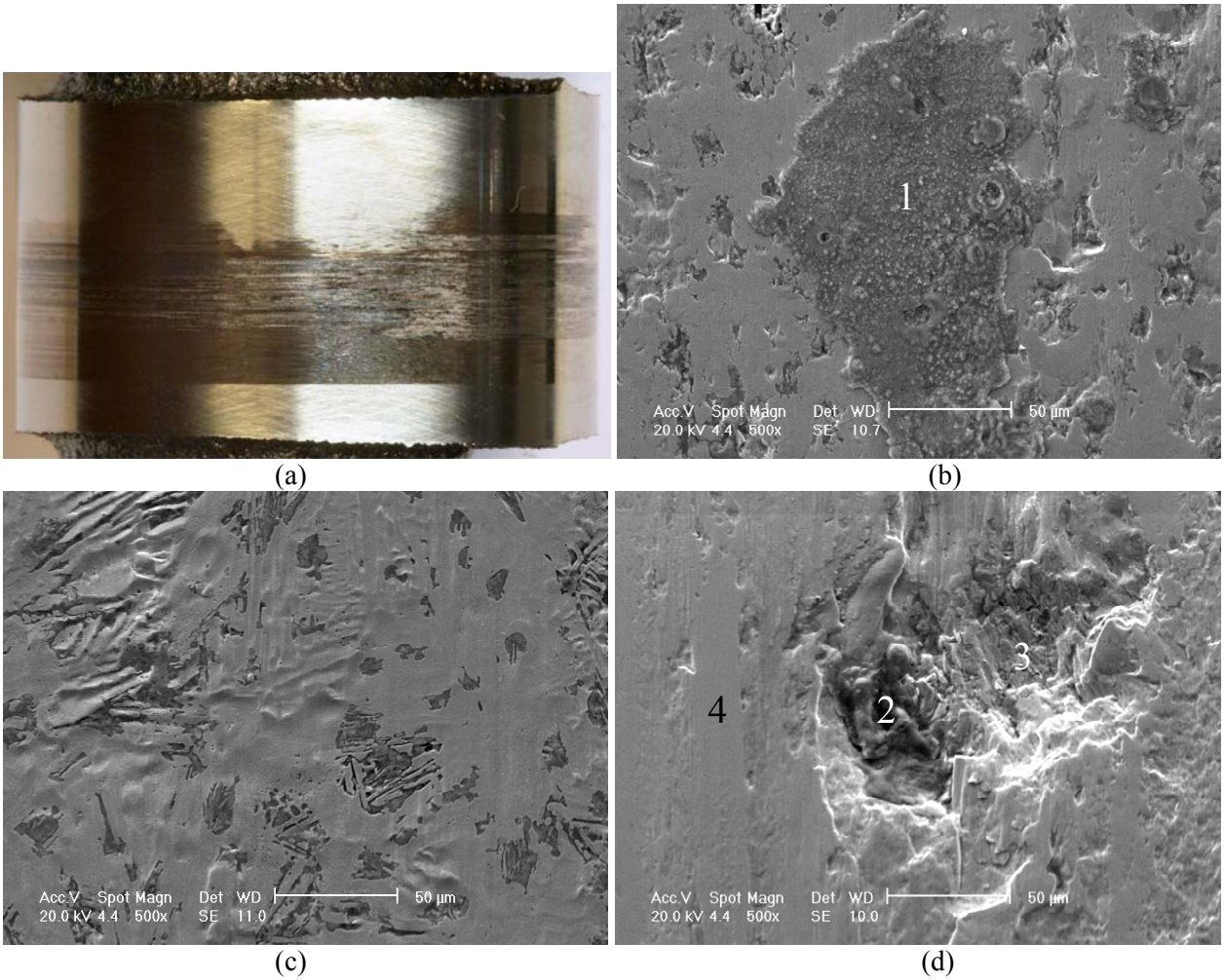

Figure 83. Images of the CBCO test cam surface: (a) entire cam surface (b) material embedded all over the flanks of the cam (c) deformation and carbides pulled out with material removal, and (d) showing large material transfer with three regions of differing surface composition.

The greatest adhesive wear was shown around the rise flank, close to the cam-nose, as indicated by surface topography measurements, which show the greatest amount of wear at 15° before the cam nose (see Figure 84). This correlates with theoretical oil film thickness and charge colour map data, which indicated that wear initiated at approximately 10° before the cam nose.

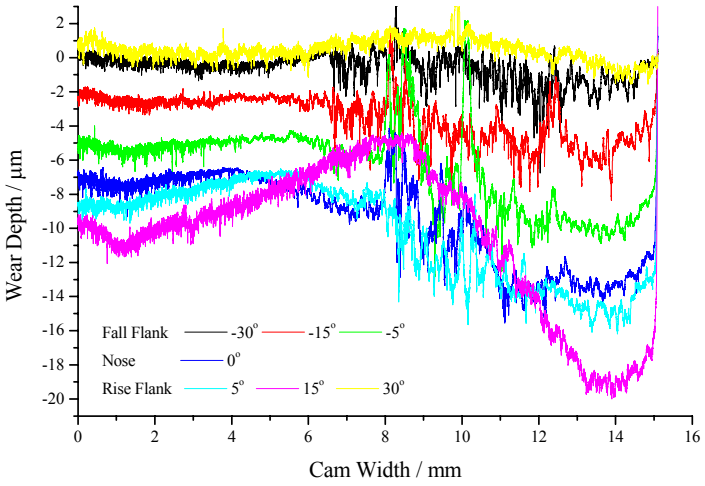

Figure 84. Surface topography of cam from carbon black contaminated oil test.

Figure 85(a) shows the region of wear on the follower. Closer inspection shows that surface cracks are present throughout the wear area and tend to connect to regions where large pieces of material have been ejected (see Figure 85(b)). A cross-section of the follower shows that the cracks are subsurface (see Figure 85(c)). Fatigue is indicated by large debris (large voids) ejected through surface and subsurface cracks. The follower surface shows signs of adhesion, which is symptomatic of high localised temperatures that can generate subsurface strain. A high localised stress caused by load applied through carbon black particles or rough asperities could cause subsurface cracking to initiate and then propagate to the surface (see Section 2.1.1.2 & Figure 14). This type of wear mechanism is seen on the follower rather than the cam because it is harder and has a shorter contact path (sliding distance per revolution).

It is widely thought by other researchers that plastic deformation is one of the main mechanisms which initiate scuffing. Typically, once the cam-follower elastic shakedown limit is exceeded, the contacts pass through an intermediate stage of plastic deformation wear, which accelerates the roughening of the surface, and this accelerated roughening finally causes scuffing [61]. Although some micrographs in this study show plastic deformation, due to the short duration at which scuffing occurred and that abrasive particles were present, plastic deformation is not thought to be the dominant mechanism that initiated scuffing. Rather it is thought that abrasion or contact starvation by carbon black initiated scuffing. Carbon black may cause roughening and enlargement of valleys, by abrasion, leading to increased localised hydrodynamic pressure and collapse of the oil film by a mechanism of the type proposed by Evans and Snidle [351], as a result of the increasing area of individual valleys. Alternatively agglomerated carbon black particles of approximately the size of the dynamic film thickness could starve the contact, causing local asperity contact, deformation and increase the localised surface temperature. After a set number of cycles where the contact has been starved of oil separating the cam and follower surface, high localized temperature will lead to asperity welding and the onset of severe adhesion ensues. Although it is possible that follower fatigue (surface cracking and ejection of large wear debris) led to

increased surface roughening and oil film collapse, the high localised temperature required to produce high subsurface stresses suggests that fatigue was a secondary mechanism to adhesive wear.

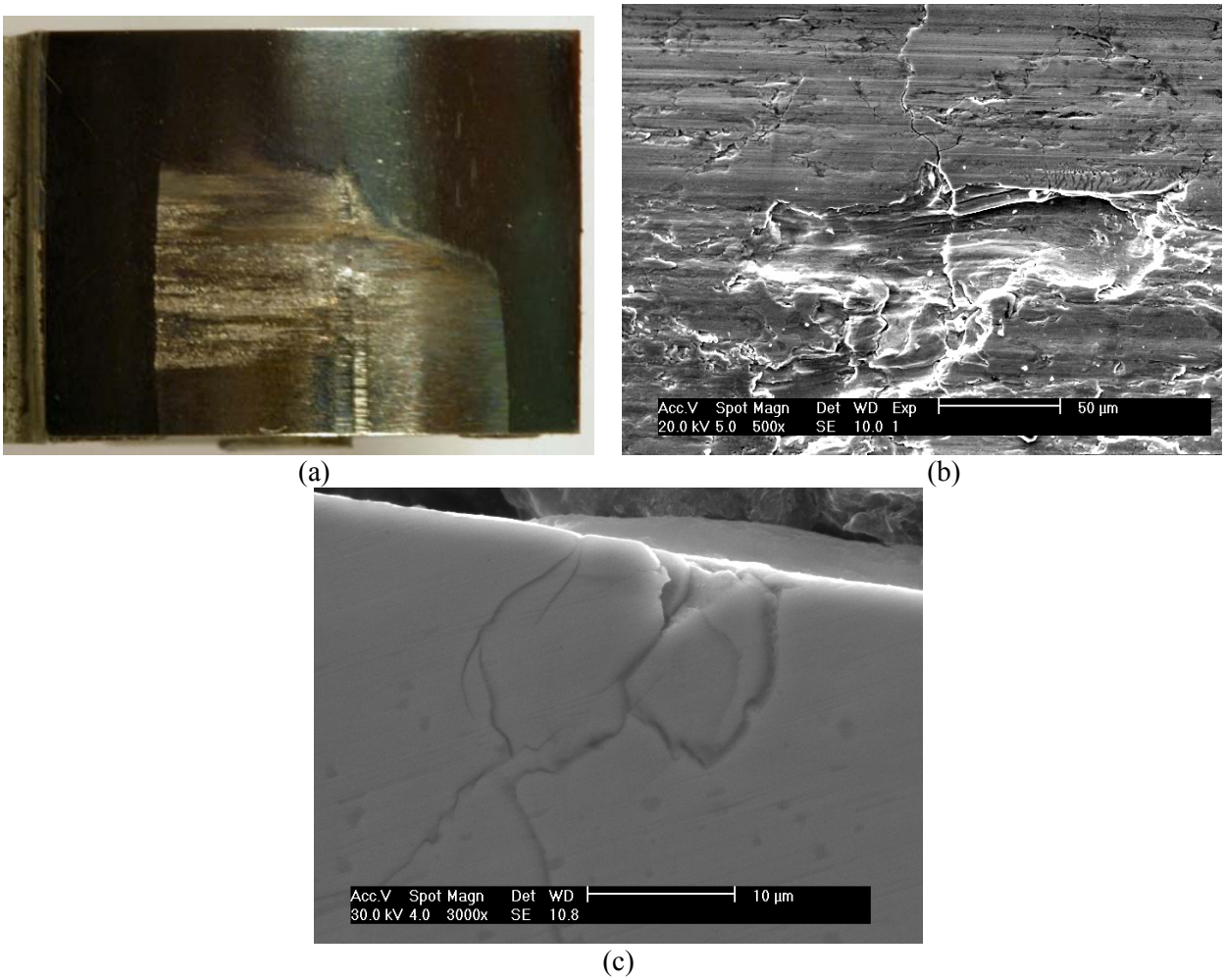

Figure 85. Follower micrographs, from the carbon black contaminated oil test, of; (a) plastic deformation, adhesive material removal and surface cracking; (b) material ejection and surface cracks, and (c) a cross-section showing subsurface cracks.

4.4.3.2 Oil starvation test (test 4.4.2)

Severe adhesive failure is seen on the cam surface (see Figure 86(a)); material has been plucked-out and debris has been embedded. There were also signs of deformation, where once sharp edge protrusions are displaced laterally, smoothing the edges. Figure 86(b) shows gross material removal. The flat dark areas are not believed to be the original surface of the cam as they are significantly below the unworn plane. This infers that the micrograph only represents one of many cycles of material removal, a layer at a time. The plate-like wear debris (see Figure 89) produced also supports this theory. EDX analysis of regions 5 and 6 of Figure 86(b) shows that the uppermost surface (dark grey) is oxidised and the surface below is fresh, un-oxidised (see Table 25). Figure 86(c) also shows that there are smaller oxidised and un-oxidised regions. Figure 86(d) shows that the OS test exhibited a greater severity of carbide loosening and removal

than the CBCO test. Loose carbides in the contact could also be responsible for the abrasion observed on the protruding surface in Figure 86(b).

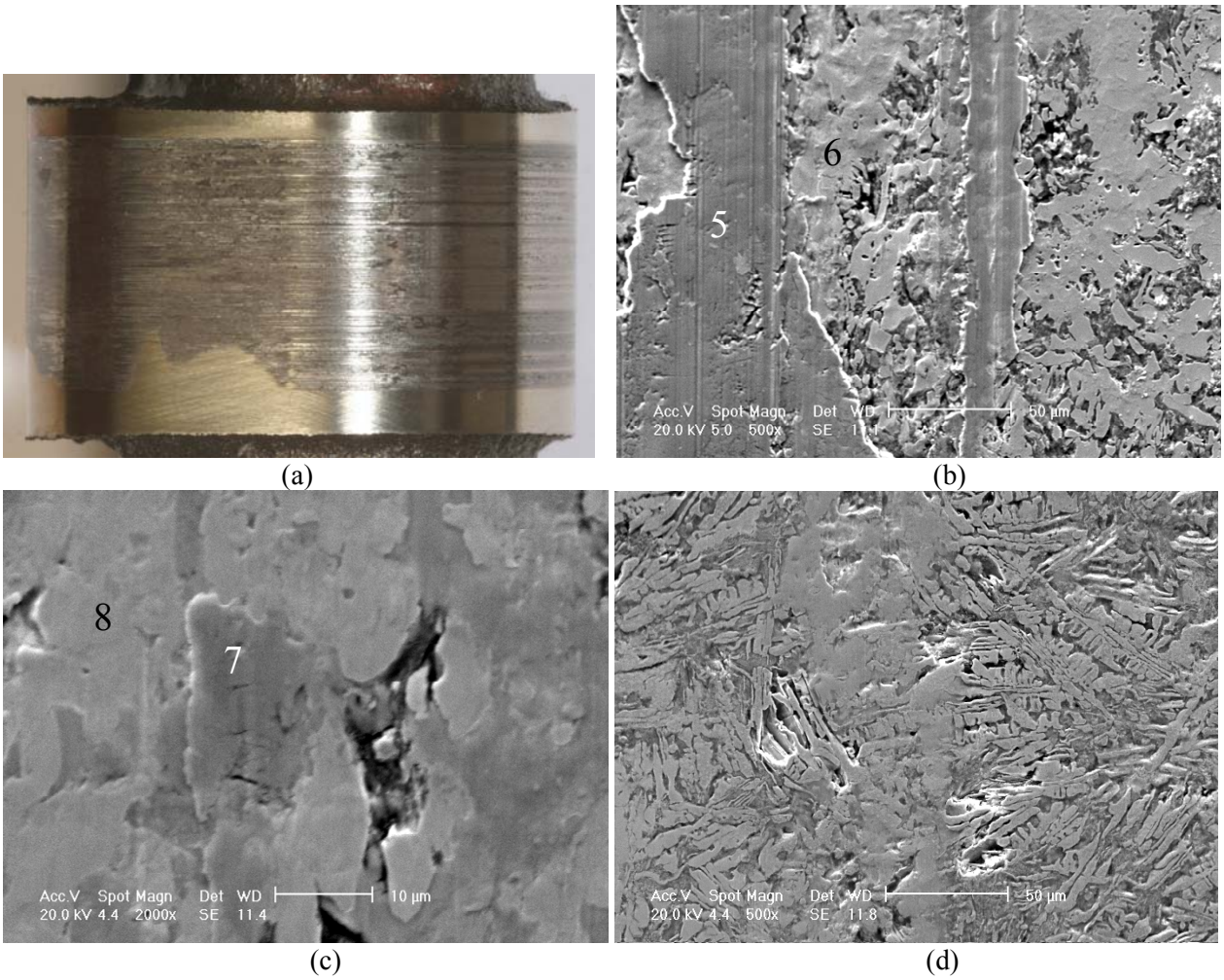

Figure 86. Images of OS test cam; (a) one side of cam surface (b) material removal leaving large fresh material (un-oxidised) large oxidised regions, (c) smaller scale oxidised and un-oxidised regions, and (d) carbide loosening and removal.

Surface profilometry shown in Figure 87, identifies the greatest wear on the cam in the region 15° before the nose (on the rise flank of), which was also observed for the CBCO test.

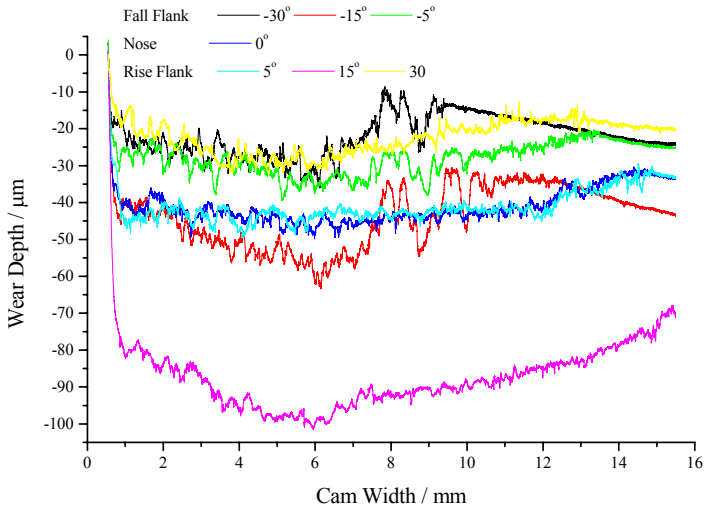

Figure 87. Surface topography of cam from oil starvation test.

The worn follower surface is shown in Figure 88(a); the area near the worn/unworn boundary shows indications of adhesive material removal and some plastic deformation. In severely worn areas, this adhesive wear and deformation creates a *'wavy'* surface which is quite rough in places (see Figure 88(b)), there are also some protruding areas with evidence of material transfer; embedding of debris contributes to abrasion, as shown by Figure 88(c).

Wear during the OS is dominantly plastic deformation and adhesion. There are some differences between the two wear tests. The area, on both the follower and cam, affected by adhesive wear was significantly larger for the OS test. The levels of surface and subsurface cracks on the OS test follower (see Figure 88 (c)); are lower than those observed in the CBCO test (see Figure 85 (b)), which could be due to removal of the original surface, along with any signs of initial surface fatigue. The extent of cam adhesive material removal for the OS test can be seen through comparison of Figure 86(c) with Figure 83(c). There is also greater carbide removal from the cam during the OS test. These differences could be due to the period of oil starvation being much shorter for the CBCO test. Despite these differences the wear from both tests was principally adhesive and the predominant charge mechanism is CPD generated between areas which are oxidised and un-oxidised.

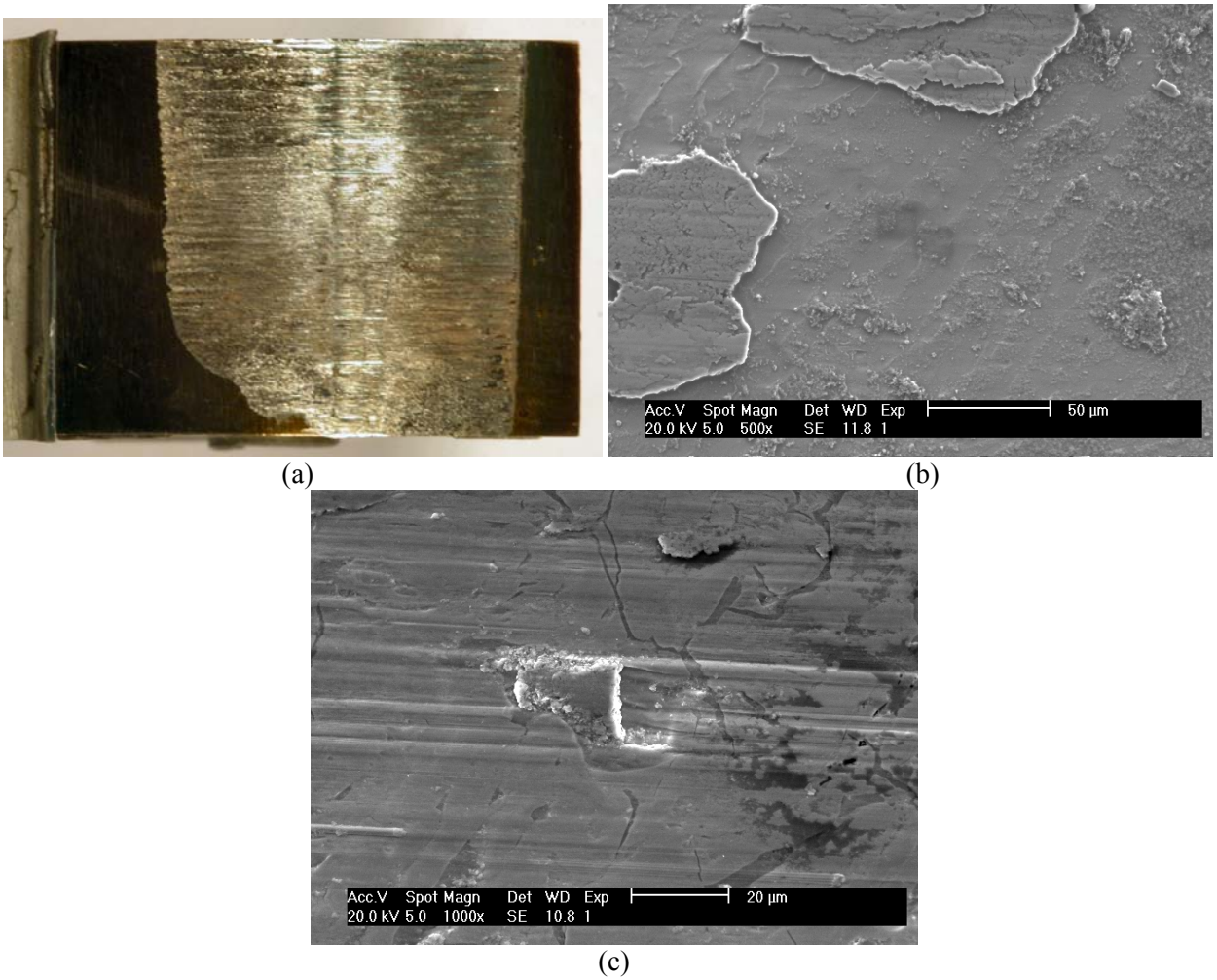

(a) (b)

(c)

Figure 88. Oil starvation test follower micrographs of: (a) adhesive material removal, debris embedded and plastic deformation; (b) adhesive material removal leaving a wavy/rough finish with (c) debris from cam embedded into follower surface (material transfer).

Wear debris was collected from the oil wells close to the cam. Figure 89(a) shows a follower debris particle (as indicated by the high chromium content measured by EDX), which is a similar shape to the protruding material shown in Figure 88(b). There are abrasion marks on the debris particle which could be a surface feature prior to detachment or due to subsequent entrainment into the tribo-contact. Figure 89(b) shows a rougher, oxidised cam debris particle. Adhesion of these highly oxidised particles onto the nascent cam surface (e.g. Figure 86 (b)) would create a CPD, due to the difference in oxygen and iron concentration.

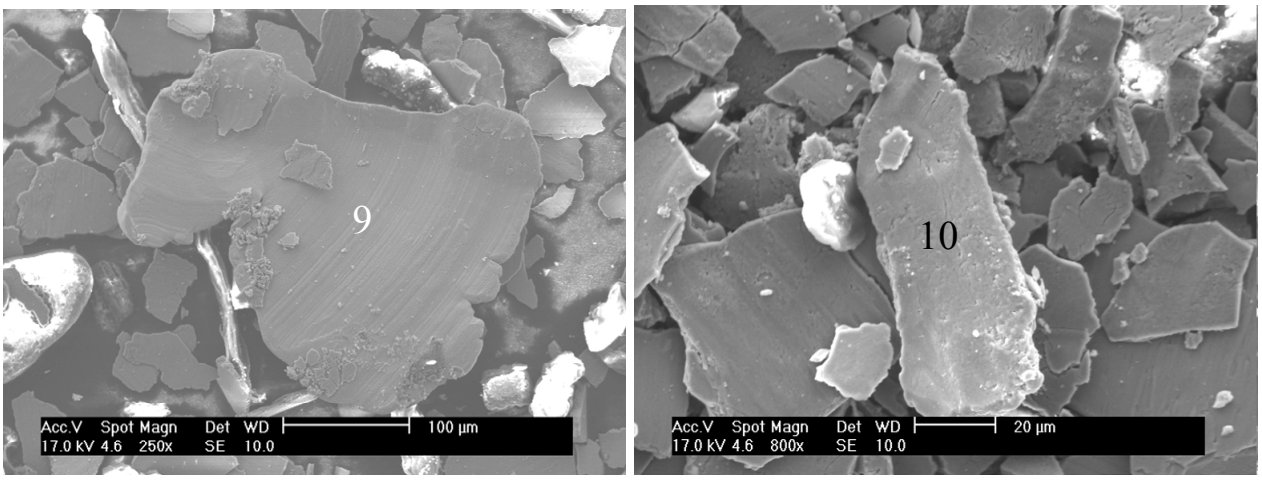

(a) (b)

Figure 89. Wear debris from a) follower b) cam.

Spot	Atomic concentration %											
Number	C	O	Si	Cr	P	S	Cl	Ca	Mn	Zn	Ni	Fe
1	29.16	37	1.87	0.17						1.25		30.56
2	59.57	10.83	2.02		0.18	0.32	0.14	0.24	0.29	0.85		25.56
3	4.28	4.49	2.76						0.73			87.73
4	13.62	5.75	0.62	0.41							2.76	76.84
5	7.63	56.63	1.6	0.34								33.8
6	28.29		0.8						0.76			70.14
7	6.36	51.78	2.38						0.47			39
8	22.48	8.41	1.69						0.67			66.75
9	37.6	12.96	0.68	14.22		0.12		0.03	0.63	0.14		34.35
10	8.86	43.86	1.45	0.48	0.06	0.1	0.05	0.17	0.45	0.09	0.4	44.02

Table 25. Summary of EDX elemental composition analysis.

4.4.3.3 Topographical comparison across wear tests

As discussed above the greatest cam wear (as measured by surface profilometry, identified by colour map, and theoretically predicted) for the CBCO and OS tests occurred around 15° before the cam nose, on the cam flank. Figure 90(a) and (b) show the surface profiles of the two worn cams and an unused cam perpendicular and parallel to the sliding direction respectively. The wear generated in the OS test was significantly larger than the CBCO test. It was also noted that the regions of greatest wear along the follower (see Figure 90(b)) are similar to those predicted by Coy [40] and Bell [52,61], notably the wear at the 0 mm position, which corresponds to the minimum entrainment velocity (see Figure 24 of theoretical and experimental follower wear profiles). (This region of maximum wear at the centre of the follower can be seen on the macro images of the follower, see Figure 85 and 88). It has been observed that failure most frequently initiates towards the end of the contact path closest to the pivot of the follower, which is the position of maximum contact duration in the main loaded part of the cycle and is believed to be due to the inherent asymmetry of the rocker-follower system causing dwell times to be greater at the pivot end of

the contact path [61]. Although both tests artificially induce wear, the surface topography of the cam and follower shows good correlation with results reported by researchers studying long term engine wear.

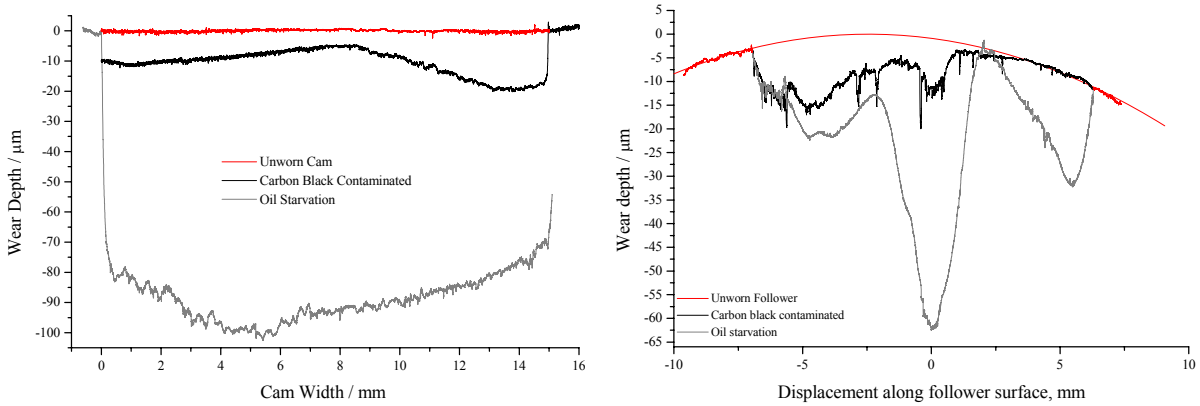

(a) (b)

Figure 90. Surface topography of unused, carbon black contaminated oil test, oil starvation test specimens; (a) cam perpendicular to sliding direction at 15° before the nose, and (b) along the centre of the follower, parallel with sliding direction; 0 mm refers to the centre of the follower.

4.4.4 EXPLANATION OF CHARGE CHARACTERISTICS DURING WEAR TESTING

The following Section pulls together all the real-time data and post-test analysis of the system characterisation tests and the oil starvation test to fully explain the charge data from the CBCO test; which is also representative of generic component life. The system characterisation test produced charge signals similar to that of the first half of the carbon black contaminated oil test – a predominantly positive charge signal. The oil starvation test, like the second half of the carbon black contaminated oil test produced a predominantly negative charge. The main charge mechanisms are thought to be tribocharging followed by CPD. By decoupling the tribocharging and CPD charge mechanisms into the system characterisation tests and oil starvation tests, greater insight into the charge produced by a lubricated contact undergoing adhesive wear (scuffing) was gained.

Although debris generation is generally an important charging mechanism, it is not thought to be a dominant mechanism in this study for the following reason; the rotation of the cam could lead to a synchronous generation of debris that should appear in electrostatic charge colour maps [25], but such signals are not observed.

4.4.4.1 Running-in

The initial part of the CBCO test exhibited an increase in charge which appears to be closely associated with the lubricant temperature (see Figure 76). If this is compared to the SCVLT tests (see Figure 72),

there is clear similarity. Both show the development of a strong positive charge feature associated with the camshaft nose. For the characterisation test the increase in charge with increasing temperature was associated with the decrease in lubricant viscosity, increasing hydrodynamic entrainment and ionic mobility, thus increasing tribocharging. This confirms that tribocharging is an important charge mechanism during the first half of the contaminated CBCO test. After the first 110 minutes, there is a drop in surface charge while the temperature continues to increase. This can be explained by either a reduction in roughness (running-in), reducing tribocharging (a smaller surface area with adsorbed charged species), or increased temperature promoting charge recombination and therefore charge relaxation.

It should be noted that the charge magnitude is dependent on the lubricant used (see Figure 91). The charge magnitude of the OS test (no lubricant) was about half the maximum level reached by the CBCO test. The system characterisation tests show a charge magnitude over 3 times higher than the soot contaminated lubricant test. The fully formulated oil used for the characterisation tests contains between 10-25% wt. of additives, many of which are extremely mobile and surface active. This increase in mobile charge species will enhance tribocharging levels.

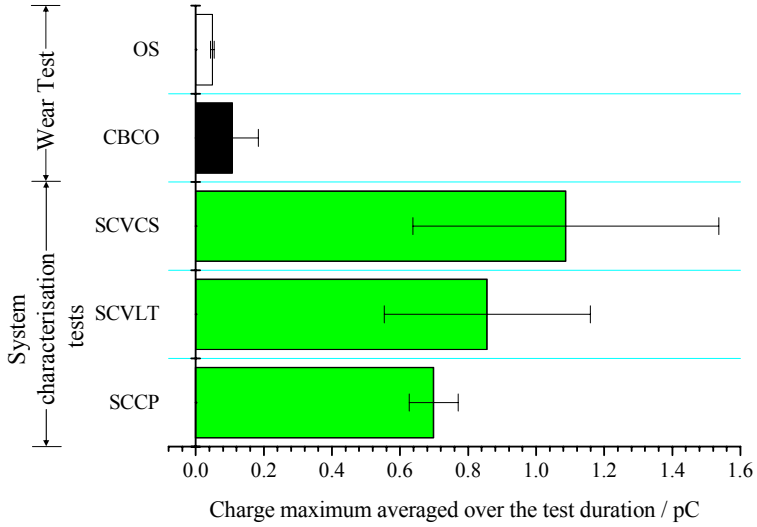

Figure 91. Bar chart showing the charge maximum average over the test duration for system characterisation and wear testing.

4.4.4.2 Mild wear / transition to high wear

From 130 minutes the charge level decreases further, which is thought to relate to a low wear rate regime (see Figure 10), until 180 minutes at which point it starts to increase slowly (see Figure 76). During this period the positively charged cam nose gradually changes to a negative charge (see Figure 77). This signifies a transition from tribocharging to CPD. The onset of adhesion (and abrasion) will reveal nascent material. The work function difference between the oxidised and un-oxidised surface can produce surface

charge; charge will increase as the surface roughens/valleys get deeper (see Figure 76, between 180-300 minutes).

4.4.4.3 Adhesive failure

The oil starvation test produced a dominantly negatively charge, this was of the same sign as the charge features produced at the end of the CBCO test. This negative charge is related to a CPD driven by the areas of the cam with differences in chemical composition. Common to both tests were adhesively worn areas which contained regions of oxidised and un-oxidised material. Also the removal of carbides from certain areas could also produce a CPD effect. It is noteworthy that, rotation of the worn cams without the follower present shows that a negative charge is still persistent, if at a fraction of that during the wear test. Retention of charge on an adhesively worn surface was also seen on FZG gears [284,308].

There were some subtle differences between the two wear tests, such as: surface chemical composition, angle of charge peak, and charge dynamics. In addition to the regions of oxidised and un-oxidised, on the flanks of the carbon black contaminated test cam a high-carbon and iron substance was observed; this will also produce a CPD effect. This material is thought to be embedded agglomerations of carbon black and wear debris.

During the last 15 minutes of the carbon black contaminated test, there are 4 periods of heightened negative charge activity (see Figure 76 & Figure 78), whereas the oil starvation test exhibited relatively constant negative charge (see Figure 81). The transient signals are indicative of scuffing, where the lubricant may re-enter the contact resulting in discrete periods of adhesive wear. With no lubricant to re-enter the contact in the oil starvation test, adhesion is continual.

The charge rms data, 65 minutes onwards for the oil starvation test exhibited oscillations (see Figure 80). These oscillations are thought to be closely related to the mechanism proposed by Morris et al. [8] of oxidation, de-lamination, re-oxidation (see Figure 92). Figure 86 (b) shows regions of oxidised and nascent cam material, well below the non-worn area, and thin wear debris Figure 89 (b) suggest that numerous cycles of oxidational wear have occurred. Layers of material are removed through, plastic deformation and repeated contact, leading to high surface temperature and to oxidation of surface material, followed by plucking of oxidised material leaving an un-oxidised surface. As the areas of oxidised and un-oxidised change during the cycles so the CPD between these areas, and thus charge, varies.

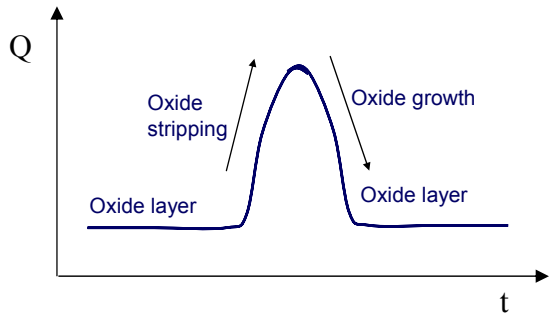

Figure 92. A schematic relating surface charge to oxide stripping and growth.

4.5 CONCLUSIONS

This Chapter has presented work from a feasibility study into the investigation of electrostatic condition monitoring of valve-train wear. A series of tests were carried out to investigate the charge generated between TU3 cam and follower contacts under conditions simulating various stages of component life.

System characterisation tests revealed that cam surface charge is affected by lubricant temperature and rotational speed; two factors consistent with the tribocharging mechanism. The charge polarity inverted during the CBCO test. The charge signals at the early stages of the test were similar to the system characterisations tests (no wear) and the charge signals at the latter part of the test were similar to the OS test. This demonstrated that the change in polarity corresponds to a transition between tribocharging of the lubricant under running-in and mild wear, and CPD generated at the onset and progression of adhesive wear. Both the CBCO test and OS test showed adhesive material removal and plastic deformation. These mechanisms left oxidised and un-oxidised regions on the cam surface, which produced a CPD on the cam surface. In addition, for the carbon black contaminated test, a carbon black / wear debris agglomeration was found embedded on the rise and fall flanks, which may have produced an additional CPD. Electrostatic charge signals identified that wear initiated approximately 15° from the cam nose (on the cam rise flank), which also correlated with oil film thickness calculations and the region of greatest wear, as identified from surface topography measurements.

Overall it is clear that electrostatic condition monitoring is a useful tool in the detection of the onset and progression to severe adhesive cam-follower failure, with specific reference to the mechanism. If a lubricant formulation does not meet the wear requirements, information about whether this excessive wear occurred over the entire duration of the test or whether it occurred in a small fraction of the test, such as at the beginning or end, could be valuable. For example this could mean that the lubricant formulator needs to: a) change the antiwear additives (in the case of overall poor wear); b) select a antiwear additive which is particularly good during running-in (in the case of rapid wear at the beginning of the test), or c) select and additive that doesn't readily deplete (in the case of failure at the end of test).

5 THE FEASIBILITY OF USING ELECTROSTATIC MONITORING TO IDENTIFY DIESEL LUBRICANT ADDITIVES AND SOOT CONTAMINATION INTERACTIONS BY FACTORIAL ANALYSIS

5.1 INTRODUCTION

In chapter 4 the highest charge levels were produced by a test with a fully formulated, which produced no wear and the lowest charge was produced by a test without a lubricant which produced the greatest wear. This inferred that lubricant chemistry has a major influence on charge generation, even under high wear conditions. There were charge features during the system characterisation test which may relate to additive activation or interactions of additives at the surface of the cam. Work presented in this Chapter was designed to investigate whether electrostatic monitoring is sensitive to more subtle changes in lubricant chemistry than the vast difference between a fully formulated oil and a carbon black contaminated base oil. This study focuses on interactions between three additive components commonly found in fully formulated oils, namely detergent, dispersant and zinc dialkyldithiophosphate (ZnDTP), as well as their interactions with carbon black (a soot surrogate) contamination.

5.1.1 AIM

The aim of this Chapter is to investigate additive-additive and additive-contaminant interactions by measuring on-line electrostatic charge; friction and wear performance. Of particular interest is the ability of dispersants to prevent carbon black from agglomerating (causing adverse wear), whether sufficient anti-wear films are formed at low temperature, and if so how carbon black affects the tribofilm formation.

5.2 EXPERIMENTAL PROCEDURE

Figure 93 (a) shows the basic set-up of the pin-on disc rig, without any instrumentation. The advantage of the PoD rig is that it can simulate, to a degree, contact conditions of an industrial component – in this case valve-train – in a cost effective and experimentally controlled manner. Advantages of this particular in-house PoD tribometer are the high load (0-250N) and sliding speed ranges (0-12m/s) compared to commercially available tribometers. The main limitations of this equipment are that temperature is not controlled and that sliding speed and applied load are manually controlled.

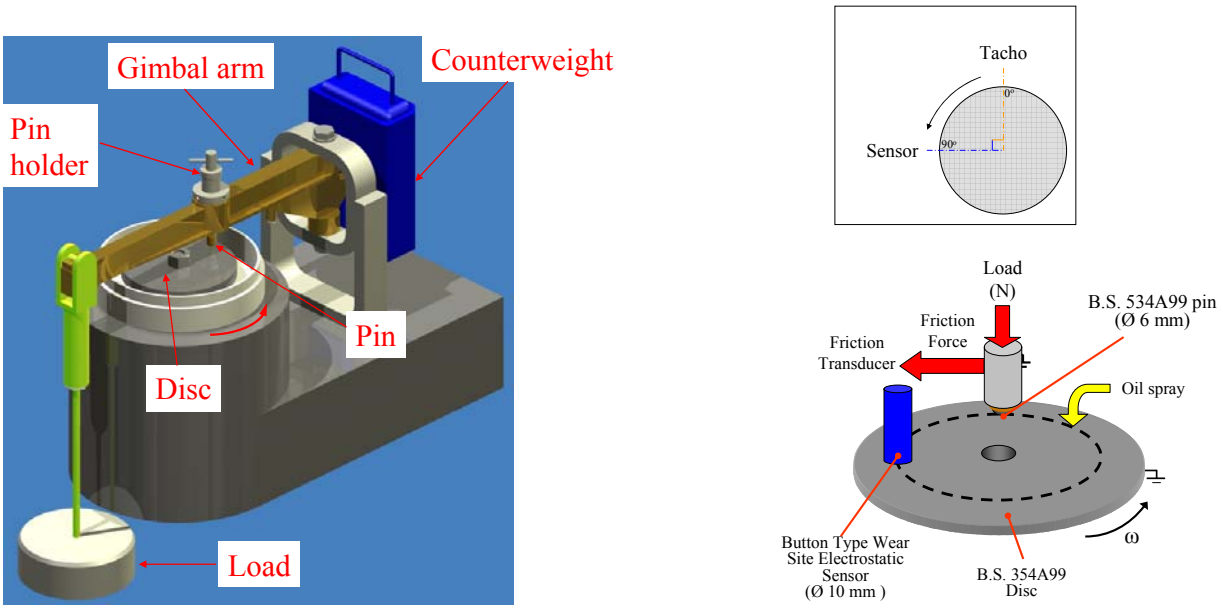

Figure 93. (a) Schematic of the PoD test set-up (b) PoD instrumentation and position of electrostatic sensor.

The pin consists of a 6 mm steel bearing ball, held in a brass ball holder (see Section 3.2). This is fixed in the pin holder, which is height adjustable to ensure that the Gimbal arm (and thus pin) is perpendicular to the disc (see Figure 93 (a)). The load is applied at the end of the Gimbal arm and a counter-weight is used to offset the load carrier. The PoD rig was adapted to employ a hydro-loading system, replacing the original dead weight system. The dead weight system encounters problems during load increments, the operator manually lowers the weight onto the load carrier, which can produce shock loading and cause unexpected damage and even premature failure. The dead weight system employs a high initial load (10 N). To avoid these problems a water-loading system was invented and adapted in this research work. The contact was lubricated by a pneumatic spray.

Figure 93 (b) shows a schematic of the 'in-house' (University of Southampton) pin-on-disc wear test rig with the associated instrumentation used. The electrostatic probe was positioned 90 degrees away from the pin/disc contact and 0.5 mm above the disc wear track. The friction force acting on the Gimbal arm was measured using a calibrated strain gauge force transducer. A data acquisition system and GE software (see Section 3.5) were used to collect and process the electrostatic charge and coefficient of friction (COF) signals in real-time.

5.2.1 TEST CONDITIONS AND PROCEDURE

The pin-on-disc (PoD) tribometer described above was used to simulate the wear of diesel engine valve-train components. Experiments were carried out under ambient conditions (temperature = 15-23°C, relative humidity = 20-60%) at a sliding speed of 5 m/s and load of 30 N (2.05 GPa initial contact

pressure). Hertzian contact stress within the valve-train in the range of 1.7-2.07 GPa has been reported for low emission diesel engines [352]. Thus the PoD conditions are mildly accelerated compared with typical valve-train entrainment velocities and contact pressure (see Table 22). Tests were carried out with a bearing steel ball loaded against a bearing steel disc, lubricated by different oil blends containing various additive combinations in a Group I base-stock (see Section 3.3). The half factorial test matrix is shown in Table 26. The properties of the test material BS534A99 (pin and disc) are given in Table 18 & 19; these are similar properties to the valve-train components of interest.

The test started with rotating the disc without contacting the pin for two minutes in order to record background signals before the oil was sprayed onto the disc using a pneumatic spray at a rate of 120 ml/hour. Five minutes later, once the disc surface was fully lubricated, the pin was brought into contact with nominal initial load. This load was then ramped up to the maximum load of 30 N; using a hydraulic loading system, over a period of about 12.5 minutes. This was considered sufficient running-in and once the maximum load was reached the tests were run for one hour.

5.2.2 OIL CHEMISTRY AND TEST MATRIX

This Chapter investigated the interactions between 4 additives and carbon black. Oil blends were prepared from baseline formulations that contained 7.3 percent viscosity index improver (see Appendix D) concentrate (ethylene/propylene copolymer) with an API Group I base oil. The four additives included one detergent, two dispersants and one type of ZnDTP. The concentrations of each factor, under investigation, are as follows:

- Carbon black (see Section 3.3.3) – 2% wt
- Detergent (see Figure 34(d)) – 50 milli-molar calcium (about 2% wt).
- Dispersant 1 (see Figure 31(b)) and Dispersant 2 (a polymeric succinimide) – 8% wt. However, when the two dispersants were used together, they were blended at an equal percent of 8% wt in total.
- ZnDTP 1 (see Figure 42(a)) – 0.1% phosphorus

Chemical and physical properties of the additives and base oil are shown in Table 21. The blending process can also be found in Section 3.3. The test matrix was designed, taking into account *A*- & *D*-optimality (see Section 3.7), to enable analysis of main effects and two factor interactions.

	1	2	3	4	5	6	7	8	9	10	11	12	13	14	15	16
Detergent		x		x		x		x		x		x		x		x
Dispersant 1			x	x			x	x			x	x			x	x
Dispersant 2					x	x	x	x					x	x	x	x
ZnDTP 1	x			x		x	x			x	x		x			x
Carbon black									x	x	x	x	x	x	x	x

Table 26. Factorial matrix oil blends.

5.2.3 OFF-LINE ANALYSIS

The volume loss for the pin and disc were measured by TaiCaan 3D laser Profilometry (see Section 3.6.2.1). Post-test XPS analysis was carried out on three worn pin samples (see Section 3.6.4.2).

5.2.3.1 Electrokinetic sonic amplitude (ESA)

The separation of charge which exists at the particle liquid interface gives rise to several dynamic phenomena associated with colloidal systems. The driving force for electrokinetic phenomena is the net charge at the interface between the liquid; which is (hydrodynamically) bound to the particle, surface and the bulk fluid. The potential of the interface; known as the plane of shear, is the zeta potential. When an alternating electric field is applied to a colloidal dispersion, the particles will move in the electric field because of their net zeta potential. If there is a density difference between the particles and the liquid, this oscillatory motion of the particles will result in the transfer of momentum to the liquid and the development of an acoustic wave (see Figure 94). Electrokinetic Sonic Amplitude (ESA) is the pressure amplitude generated by the colloid per unit electric field strength and is analogous to electrophoretic mobility.

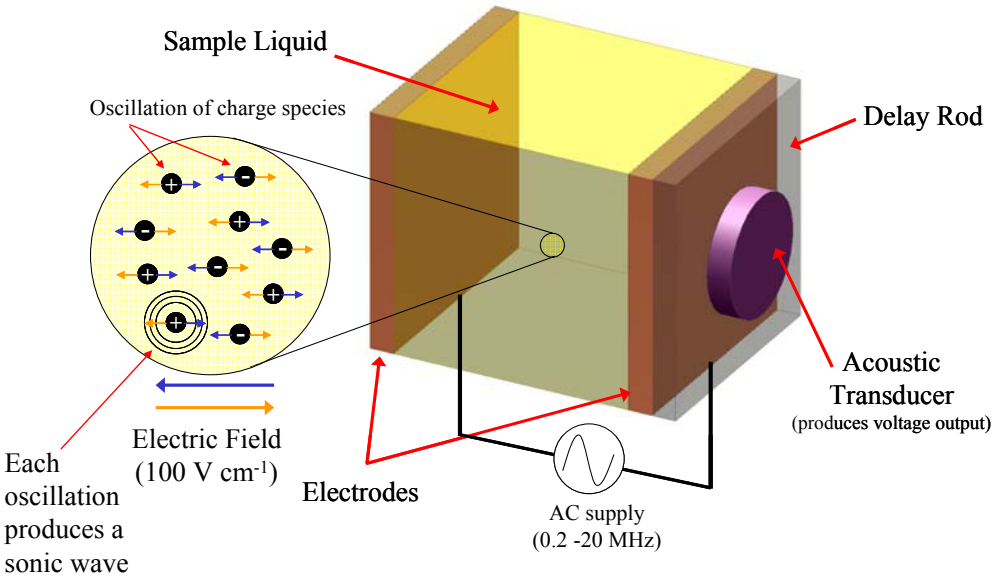

Figure 94. Principle operation for measuring ESA.

A Matek Instruments MBS 8000 system was used to measure the electrokinetic sonic amplitude (ESA) of the 16 oils. The instrument was configured for non-aqueous measurement, and the phase was referenced to a used diesel engine oil that contained approximately 6% wt. of soot by thermogravimetric analysis. Ten measurements were performed for each sample and the results averaged.

5.2.4 STATISTICAL ANALYSIS

All real-time and off-line data was statistically analysed in the manner described in Section 3.7.

5.3 RESULTS

The results for the measured on-line and off-line parameters are shown graphically in Figure 95- 97. ANOVA was carried out on both the on-line and off-line parameters. Only a few interactions (additive-additive and additive-contaminant) were identified for the 60 minute electrostatic charge average. Electrostatic monitoring is sensitive to dynamic events and thus when ANOVA was carried out for each 5 minute interval of the 60 minute period, interactions were found, and in some cases persisted for the duration of the test. The statistical analysis yielded many interactions and therefore narrowing down these statistical results was necessary. This was achieved by focusing on the electrostatic results and calculating the significance of such interactions, *p-values* (see Table 27).

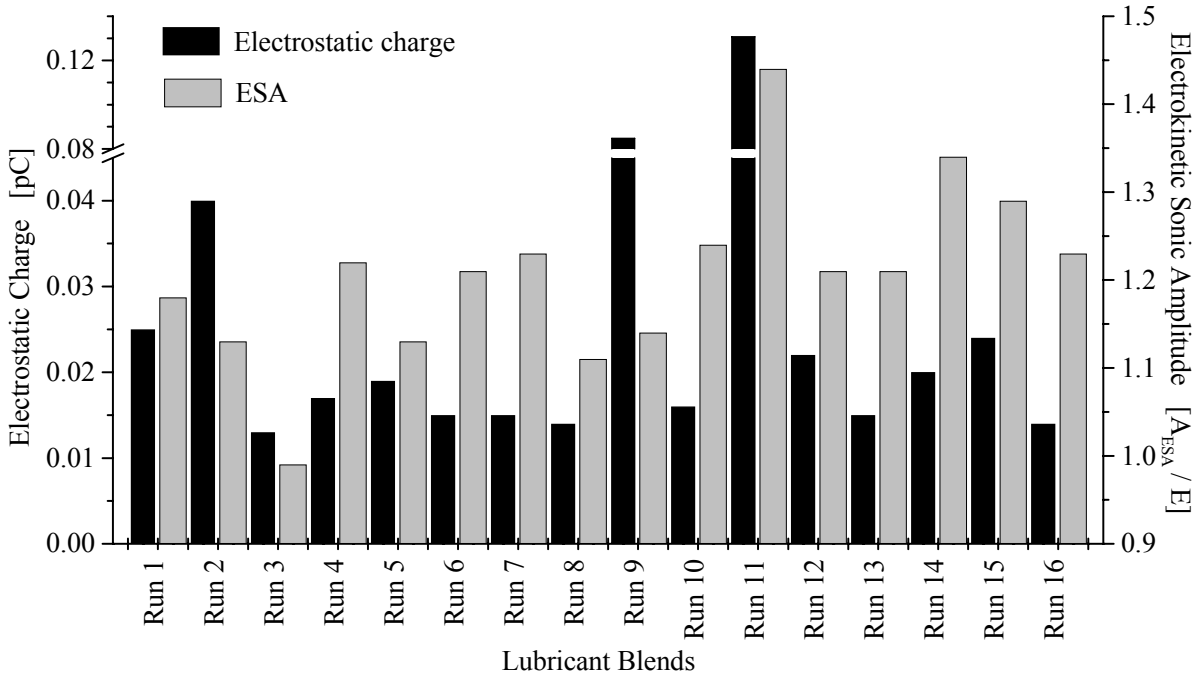

Figure 95. Bar chart of the 60 minute average electrostatic charge values and the off-line ESA measurements.

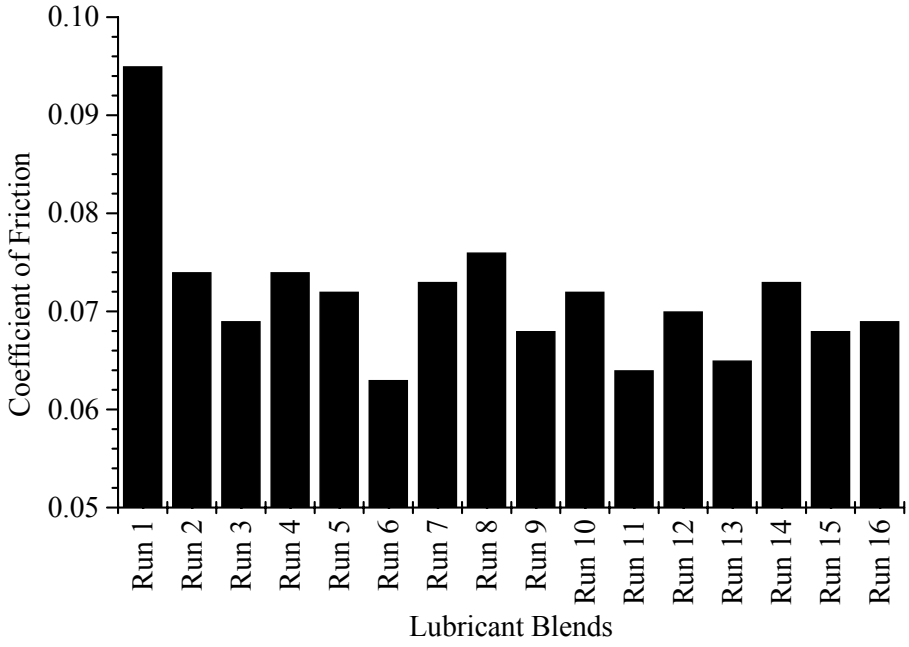

Figure 96. Bar chart of the 60 minute COF average.

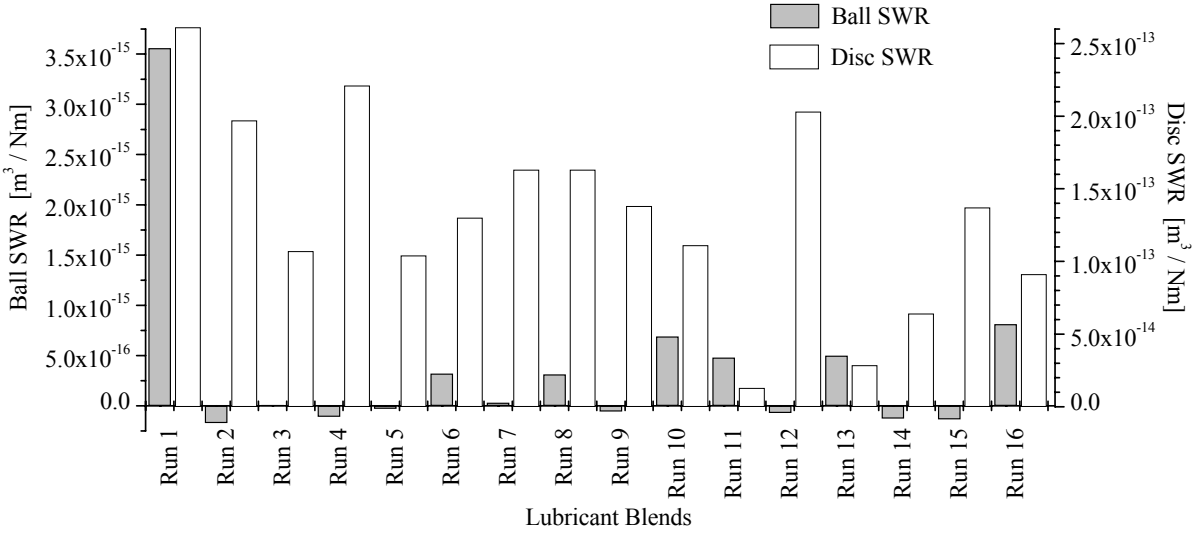

Figure 97. Bar chart of disc and ball SWR.

Factor	Variable	Response	*p-value*
Carbon black	Average charge	increase	0.13
Dispersant 2 without Detergent	Interval charge	decrease	<0.05
ZnDTP 1 with Dispersant 2	Interval charge	increase	<0.05
Carbon black without Detergent	Interval charge	increase	<0.05
Carbon black without Dispersant 2	Interval charge	increase	<0.05

Table 27. Statistical results from ANOVA for On-line parameters.

Factor	Variable	Response	*p-value*
ZnDTP 1	Ball SWR	increase	0.06
Carbon black with ZnDTP 1	Disc SWR	decrease	0.01
Dispersant 2 without Dispersant 1	Disc SWR	decrease	0.04
Carbon black	ESA	increase	0.01
ZnDTP 1 without Dispersant 2	ESA	increase	0.04
Detergent with Dispersant 1	ESA	decrease	0.09
ZnDTP 1 with Dispersant 1	ESA	increase	0.12

Table 28. Statistical results from ANOVA for post-test parameters.

5.4 DISCUSSIONS

A marginal correlation between ESA and 60 minute average surface charge was suggested by a relatively high *p-value* of 0.15. Although both are charge related techniques, ESA is a measurement of the pre-existing charge in the oil, whereas the electrostatic sensor detects the total charge as a result of tribological activity. Thus the correlation is marginal rather than significant. The following sections discuss charge response in relation to additive behaviour, the effect carbon black had on wear, and where possible draw some links between the two.

5.4.1 CARBON BLACK INTERACTIONS WITH OTHER ADDITIVES AND THE EFFECT ON CHARGE RESPONSE

Carbon black increased the electrostatic charge detected and ESA measured (see Table 27 and Table 28). This could be due to the fact that carbon black particles are known to be chargeable (see Section 2.3.8.2). In oil containing 2%wt of carbon black, considering an average diameter of 300 nm for spherical carbon black agglomerates, there would be 7×10^{12} carbon black particles in one ml of oil sample. Agglomerated particles (see Figure 47), if large enough, could retain a localised charge to be detected by the electrostatic sensor. Some agglomerated carbon black particles may adhere to the disc surface, but the correlation between ESA and electrostatic charge, for carbon black, suggests that the charge characteristics are a result of suspended (agglomerated) carbon black particles.

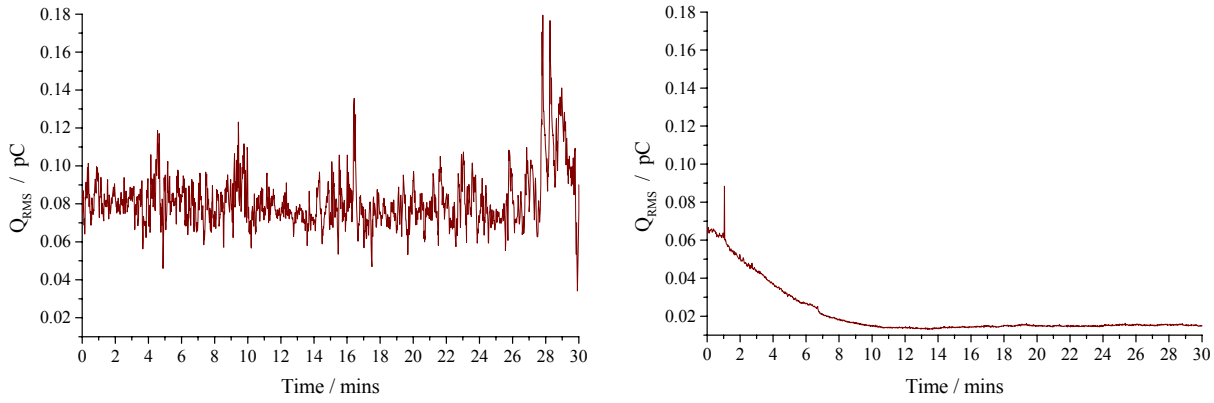

Figure 98. Real-time electrostatic charge for (a) Run 9 (carbon black) (b) Run 14 (Detergent, Dispersant 2, carbon black).

Figure 98 illustrates the statistical findings (see Table 27) that both Dispersant 2 and Detergent reduce the effect that carbon black contributes towards increasing electrostatic charge; Dispersant 1 does not have this effect. For dispersed carbon black to acquire a charge, Dispersant (1 & 2) and/or Detergent must desorb or be stripped from the surface taking a charge with it and leaving an equal but opposite charge on the aforementioned surface. As the dispersants employed are amine-based they acquire a positive charge from the formation of an acid-base pair at the soot surface (see Figure 32). Relative to Dispersant 2, Dispersant 1 is more surface active, and as there are fewer polar-regions per non-polar hydrocarbon tails – there are 2 hydrocarbon tails per polar-region in Dispersant 1 – it is more likely to desorb and/or strip from carbon black as it goes through the contact. Dispersant 2 contains about 10 polar-regions per molecule and a ratio of polar to non-polar regions of about 1:1, which means it is less likely to desorb or be stripped from carbon black. In addition Dispersant 1 can form multiple layers (many adsorption and potential desorption sites), whereas Dispersant 2 can only form a monolayer (fewer adsorption and potential desorption sites)). For these reasons, Dispersant 2 does not support charge formation as well as Dispersant 1. Thus lower charge from carbon black may suggest a more stable suspension.

Detergents generally employ organic acid based surfactants, which are negatively charged [350]. As there may be both positive and negative charges present when Dispersant and Detergent are used, these positively charged particles serve to offset, or neutralize the measured static charge.

5.4.2 SPECIMEN WEAR

Figure 99 (a - d) shows 3D topographical ball maps grouped in relation to the presence or absence of ZnDTP 1 and carbon black, which have historically had the greatest impact on wear performance. The four maps are representative of the four different ball scar shapes seen for all 16 tests, but with varying severity. For oils without either ZnDTP 1 or carbon black (e.g. run 5, see Figure 99 (a)) the ball SWR was

small and conformal. Oils containing carbon black, but no ZnDTP 1 exhibit slightly greater (abrasive) ball wear (see Figure 99 (b)), the SWR for run 9 is double that of run 5. For oils which contain ZnDTP 1 and carbon black the ball shoulders are severely worn leaving a *'Mohawk'* type feature in the middle of the ball (see Figure 99 (c)). Run 16 showed 14 times greater ball SWR than run 9. All oils containing both ZnDTP 1 and carbon black exhibited this *Mohawk* feature; but with varying widths. The *Mohawk* width for run 16 (see Figure 99 (c)) is 220 μm; this is larger than the initial maximum Hertzian contact pressure (see Section 2.1.1.1) diameter of 167 μm. For all other oils which contain ZnDTP 1 and no carbon black, the ball scar is approximately flat, with small ridges and has the greatest ball SWR, a fact shown in the statistical analysis (see Table 28). Run 1 (see Figure 99 (d)) has the highest ball SWR out of the 16 test oils, which is 4 times more wear than run 9 and over 100 times more wear than run 5. The effect of ZnDTP 1 to exacerbate wear is contrary to what is generally thought of as an antiwear additive; in the following sections this negative effect is termed *'pro-wear'*.

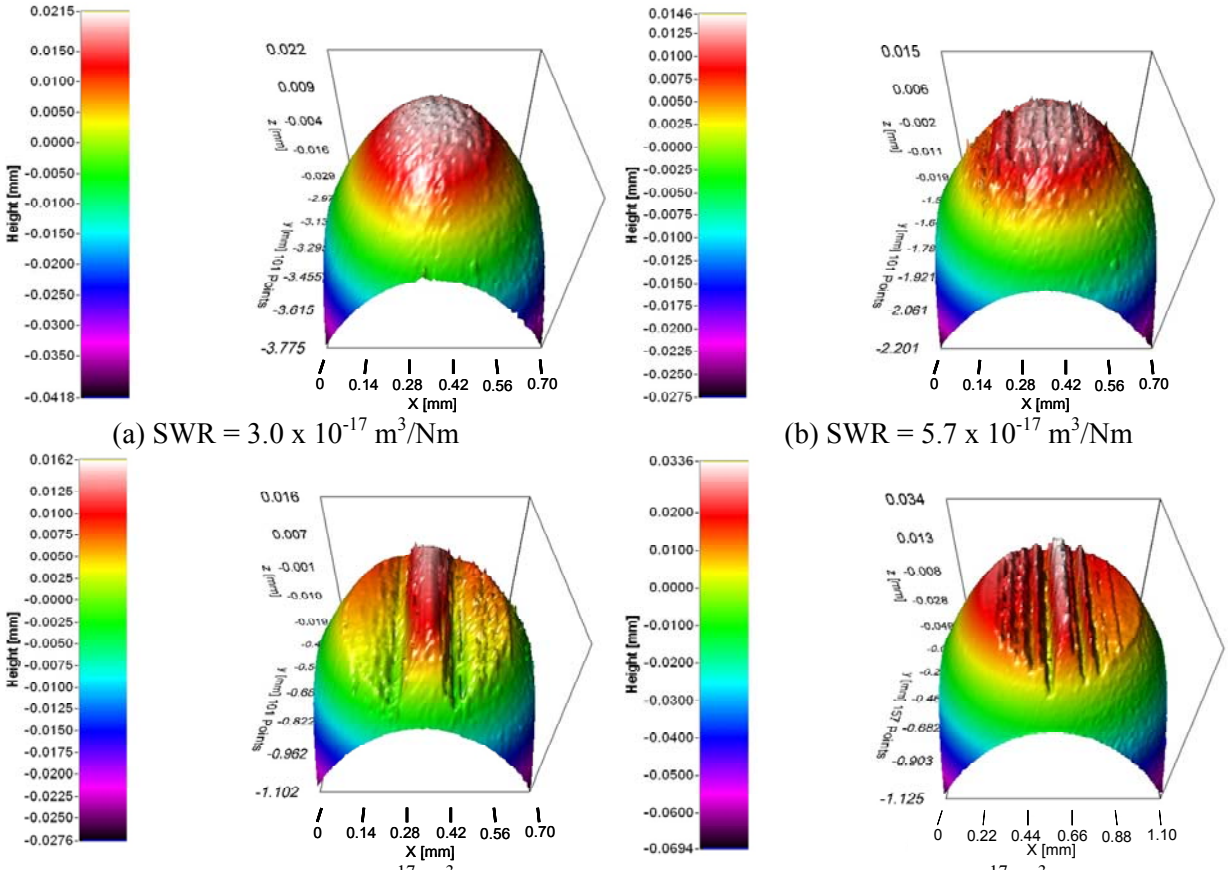

(a) SWR = 3.0 x 10^{-17} m^3/Nm (b) SWR = 5.7 x 10^{-17} m^3/Nm

(c) SWR = 81.2 x 10^{-17} m^3/Nm (d) SWR = 356.0 x 10^{-17} m^3/Nm

Figure 99. *(a) Run 5 (Dispersant 2), (b) Run 9 (carbon black), (c) Run 16 (Detergent, Dispersant 1, Dispersant 2, carbon black, ZnDTP 1) and (d) Run 1 (ZnDTP 1).*

The wear scar shapes, in particular those oils containing carbon black and ZnDTP 1, can be explained by elastohydrodynamic theory (see Section 2.1.3). In sliding elastohydrodynamic point contacts, deformation of the (originally) spherical surface (see Figure 5(a)) will cause a constriction in the oil film with an associated pressure spike (see Figure 5(b)), towards the downstream end and around the side of the contact, forming a '*horse-shoe'* shaped constraint [353], producing areas of minimum film thickness [354] (see Figure 5(c)).

Wear for run 1 started around the area of maximum pressure/minimum film thickness and progresses to the centre of the ball, flattening the spherical surface. For oils containing other additives and/or contaminants the *pro-wear* effect of ZnDTP 1 is slowed – preventing the progression of wear from the ball shoulders to the centre.

5.4.2.1 ZnDTP 1's '*pro-wear*' effect

The following sections discuss reasons behind the *pro-wear* effect and how this is minimised due to interactions with other additives, in particular dispersants. X-ray Photoelectron Spectroscopy (XPS) was

conducted on three worn ball surfaces and an *unusual* tribo-film was found for those surfaces run with oils containing ZnDTP 1. Table 29 shows the elemental compositions of these films. The results show low concentrations of zinc, sulphur and phosphorous compared to other ZnDTP antiwear films [355] (also see Chapter 6). The low phosphorous level especially relatively to sulphur indicates that a minimal amorphous-polyphosphate layer had formed. This layer is critical for effective ZnDTP antiwear performance; it shears preferentially to the metal component under boundary lubrication conditions, or provides a wear resistant barrier.

Ball specimen	C	N	O	Na	Si	P	S	Cl	K	Ca	Fe	Zn	Pb
Run 5	40.2	2.0	40.9	0.8	1.8	-	-	0.6	0.5	1.1	10.3	1.0	0.9
Run 7	39.8	1.7	40.9	0.7	1.3	0.9	0.4	0.4	-	0.8	10.0	2.5	0.7
Run 16 (centre)	35.5	0.4	44.1	0.9	-	0.2	0.5	0.4	-	0.6	13.2	3.6	0.7
Run 16 (side)	34.8	0.7	43.4	0.8	0.9	0.4	0.6	0.8	-	0.5	13.2	3.1	0.8

Table 29. Surface chemistry identified by XPS for run 5, 7 and 16.

The *pro-wear* effect of ZnDTP 1 is due to the formation of an under-developed anti-wear film – minimal polyphosphate layer. Primary ZnDTPs, like ZnDTP1, have high thermal stability (see Section 2.3.4.4.1) and at the test temperature (approximately 20°C) there is limited thermal decomposition of primary ZnDTP, hence the formation of an under-developed antiwear film. However, the reaction of sulphur within ZnDTP, with iron to form iron-sulphide is less temperature dependent. Active sulphur has a significant influence on promoting wear [103]. The polyphosphate layer normally creates a barrier against access of sulphur and oxygen, thus reducing the rate of the tribochemical wear caused by uncontrolled sulphide and oxide growth, as the amorphous phosphate film structure develops [111]. However under these conditions, low temperature and high sliding speed, the thin phosphate layer is easily stripped away leaving an iron sulphide layer, which is also readily sheared leaving nascent metal surface (see Figure 100). This nascent metal surface is able to form iron oxide which reacts with sulphur to form iron sulphide. This tribochemical (see Section 2.1.4.2 & Figure 15) process repeats to promote ball wear.

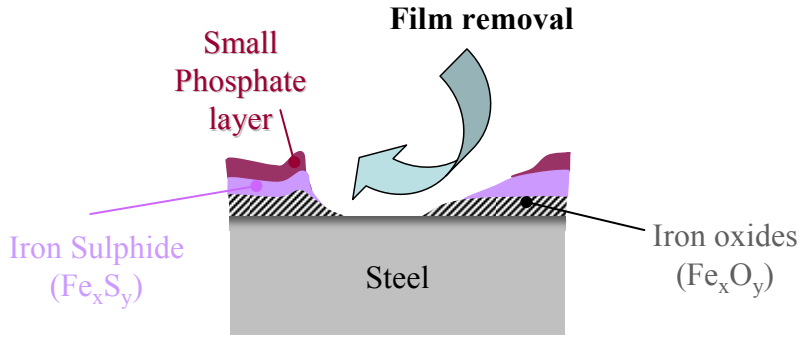

Figure 100. Schematic diagram of proposed under-developed film which leads to a pro-wear characteristic – ZnDTP 1 reacts with the surface to form initial stage of tribofilm but constant removal of this iron rich film will promote wear (tribochemical wear).

5.4.2.2 Interactions between ZnDTP 1 and Dispersant

The ball and disc SWR clearly showed that other factors (additives and carbon black) reduce the *pro-wear* effect of ZnDTP 1 (see Figure 97). Both Dispersants in particular show a reduction in the ball *pro-wear* effect of ZnDTP 1. The interaction of Dispersants and Detergents with ZnDTP has been investigated by other researchers [112,165,356-358].

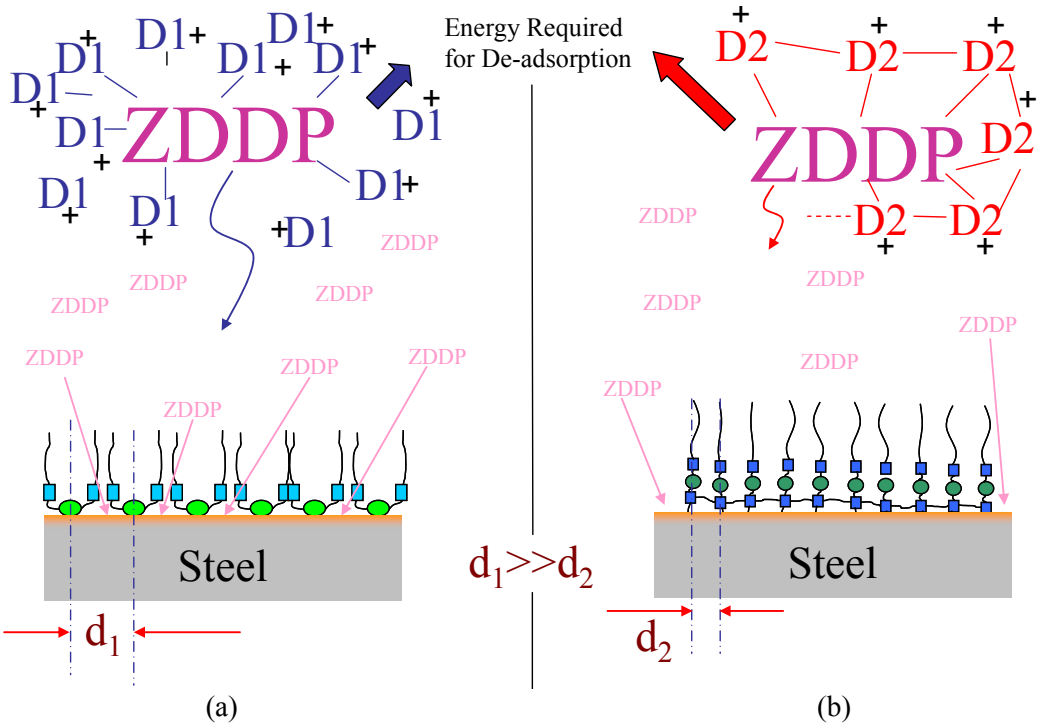

Figure 101. Schematic of the (a) Dispersant 1 and (b) Dispersant 2 interaction with ZnDTP 1 which leads to a reduction in the pro-wear effect of ZnDTP 1.

The ZnDTP 1-Dispersant interaction is thought to be a combination of three mechanisms: increasing the thermal stability of ZnDTP 1, suspension of ZnDTP 1 and ZnDTP 1 decomposition products, and competition for surface sites. Figure 101 shows a simplified schematic of three mechanisms associated with ZnDTP 1-Dispersant interaction. The formation of a complex between ZnDTP and succinimide Dispersants has been observed by other researchers [359,112] and has been proposed as a reason for reduced antiwear performance [360,361]. Harrison et al. [362] reported that the basic nitrogen from the Dispersant was shown to form a stable complex with ZnDTP. It has been demonstrated that this ZnDTP-amine complex makes the ZnDTP more resistant to thermal degradation [363] by retarding the rate of peroxide decomposition [112]. Usually a reduction in ZnDTP decomposition products would reduce the ability of ZnDTP to form an effective film to minimise wear. However, under the test conditions in this

study a reduction in the amount of ZnDTP 1 decomposition products, especially sulphur containing, is beneficial as it minimises the *pro-wear* effect.

In addition, Dispersants suspends undegraded ZnDTP 1 and ZnDTP 1 decomposition products. This prevents sulphur containing decomposition products from reacting with the steel surface, further reducing the *pro-wea*r effect of ZnDTP 1. Bartha et al. [364] postulated that the strength of ZnDTP-Dispersant interaction is dependent on the dispersing efficiency.

Surface catalysed decomposition of ZnDTP 1 is also reduced by surface competition between the Dispersant molecules and ZnDTP 1 decomposition products [365,366]. The more adsorbed Dispersant molecules on the steel surface, the fewer ZnDTP 1 decomposition products can reach the surface. This effect is discussed in Section 5.4.2.3.

The interaction between ZnDTP 1 and both Dispersants is also shown by electrostatic charge and ESA (see Table 27 & 28) and is thought to be related to the same interaction discussed for ball SWR. Figure 102 illustrates the statistical finding that ZnDTP 1 with Dispersant 1 increases interval electrostatic charge. The interaction between ZnDTP 1 and Dispersant 2 is shown by the statistical analysis to be only significant for ESA. However, on-line electrostatic data shown in Figure 102 (b) indicated that there is a marginal reduction in electrostatic charge due to the presence of Dispersant 2. This follows the marginal correlation between ESA and electrostatic charge discussed earlier.

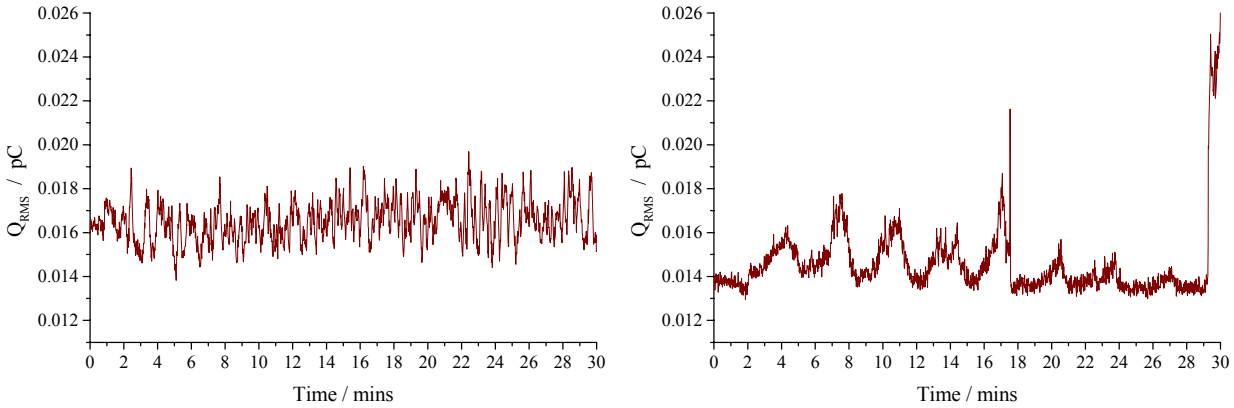

Figure 102. Real-time electrostatic charge for (a) Run 4 (Detergent, Dispersant 1, ZnDTP 1), (b) Run 6 (Detergent, Dispersant 2, ZnDTP 1).

The suspension of ZnDTP 1 and ZnDTP 1 decomposition products by Dispersant 2 and the corresponding reduction in charge is believed to relate to the reasons discussed for the carbon black-Dispersant 2 interaction. The tenacious bond formed between the 10 polar-regions of Dispersant 2 and ZnDTP 1

requires more energy to desorb than for Dispersant 1. Thus the suspension of ZnDTP 1 by Dispersant 2 is more stable as shown by the lower ESA measurement. Dispersant 1 in the presence of ZnDTP 1, increased the charge detected by both electrostatic sensor and ESA, because it can form multiple layers that are more easily desorbed, resulting in a higher localised charge, even if comparatively unstable.

Through comparison of Figure 102 (a) & (b) it can be seen that the presence of Dispersant 2 produced oscillating charge features. Interval charge averages (5 minute duration) were used to try and identify the transient nature of the surface charge. However this statistical analysis does not take into account the oscillating characteristic that only occurs in a few experiments, neither does it assess if the oscillations have different periods. It is thought that Dispersant adsorption/desorption (or stripping) is responsible for this behaviour. Dispersant 2 has a significantly higher molecular weight than Dispersant 1, therefore when it desorbs or is stripped from the surface, it takes longer to re-adsorb. Subsequent Chapters address this observation in more detail.

5.4.2.3 The effect of dispersants on wear

For the oils which did not contain ZnDTP 1, it appears that the additives in particular dispersants provided a film which minimised the wear on the ball (see Figure 99 (a)). Both dispersants employed in this study are expected to form surface films capable of small wear reductions. The surface packing efficiency of the two dispersants is very different. A molecule of Dispersant 1 has two hydrocarbon tails standing out from the surface. Each of these tails occupies space at the surface based on the area occupied by the polar-region, and the volume filled by the motion of the hydrocarbon tail in the oil medium, this limits packing efficiency. For Dispersant 2, the hydrocarbon tails are linked together through polar-regions; the distance between these *anchor* points for the hydrocarbon tails is of the order of several carbon-carbon single bonds. These molecules are expected to form comb-like adsorbed layers [367]. The close packing of the hydrocarbon tails serves to thicken the surfactant layer in the contact (relative to Dispersant 1) and reduce wear. When both dispersants were employed, the anti-wear effect of Dispersant 2 was not observed (see Table 28); indicating a competition for surface sites, which favours the lower molecular weight and more mobile Dispersant 1.

5.5 CONCLUSIONS

This study has demonstrated the use of electrostatic sensors and ESA to detect changes in charge associated with the presence of additives and a contaminant, as well as detecting binary interactions on a PoD tribometer. Electrostatic sensors that correlate or show anti-correlation with off-line electrokinetic measurements such as ESA, could be extremely useful for lubricant performance evaluation. By comparing the pre-existing charge in the lubricant (measured by ESA) with the electrostatic charge

detected from the tribo-contact, further understanding of additive and contaminant interactions could be gained.

The presence of carbon black was found to increase average electrostatic charge and ESA. Where steric or electrical barriers are insufficient to keep carbon black particles dispersed, agglomeration will occur; these large particles could retain a high enough charge to be detected by the electrostatic sensor. Dispersant and Detergents can also charge carbon black through a desorption mechanism. Both Dispersant 2 and Detergent in the presence of carbon black were found to reduce the interval electrostatic charge, which are known to bind tightly to the carbon black surface; minimising charge formation through desorption.

Ball wear increased in the presence of ZnDTP 1. Investigations using XPS analysis identified that under the test conditions used in this study, the presence of primary ZnDTP (ZnDTP 1) did not generate a fully developed antiwear film. Instead, the formation and stripping of iron sulphide promoted ball wear.

The majority of electrostatic charge observations in the Chapter discuss charge species in the bulk of the lubricant – hence the correlation with ESA – with a few observations about surface charge generation. This suggests that future experiments need to move away from testing in EHL and into more severe (boundary) lubrication, to be able to more closely relate charge generation to additive-surface behaviour, plus many additives such as ZnDTP 1 are more surface active under more severe conditions. Another possible reason, that few direct surface charge / additive-surface behaviour observations were made, is that the tribofilm will be made-up, to varying degrees, as many surface active additives are present in the oil. Perhaps under these conditions no-one additive dominated the film, thus the statistical analysis failed to pick-up on these effects because only main effects and two factor interactions could be identified.

6 MINI-TRACTION-MACHINE TESTS TO ASSESS THE EFFECT OF BASE OIL AND ADDITIVE INTERACTIONS ON SURFACE CHARGE AND FRICTION.

6.1 INTRODUCTION

Although Chapter 5 identified some interesting additive-additive and additive-contaminant interactions related to charge, direct observations were confounded by the fractionated nature of the matrix. In addition, there was a limitation in interpreting additive-additive interactions related to charge because single additive charge behaviour was not fully understood. In this study single additive oils were used, so that electrostatic charge signatures could be directly related to single additive behaviour, without the added complication of trying to decouple additive-additive or additive-contaminant interactions.

Six surface active additives were chosen; these represented the wide range of additives used in IC engine oils. The nature of the surface interaction of these additives is quite different. This enabled the sensitivity of electrostatic monitoring to these significant differences in additive chemistry and surface behaviour to be assessed. Additives were blended into three base oils with differing impurity levels, which affects the solubility of additives and results in different additive-surface interactions; this enabled the assessment of the sensitivity of electrostatic monitoring to subtle differences in surface behaviour of the same additive.

Testing was carried out on a MTM tribometer, under conditions designed to simulate the valve-train contact. One of the main limitations with the 'in-house' PoD tribometer used in Chapter 5 is that lubricants cannot be used at elevated temperature. In addition, manual loading and speed control meant that testing was subject to human error, which may compromise repeatability. This is a major consideration when statistical analysis is being used to identify subtle changes in additive behaviour. The MTM enabled elevated lubricant temperatures to be used and contact load and sliding speed to be programmed.

A full factorial matrix was carried out to assess the effect of dependent variables (additives and base oils) on measured parameters (electrostatic charge, COF, ball wear, disc wear and conductivity). Due to the size of the data set, which included 9 dependent variables (6 additives and 3 base oils) and 5 measured parameters (charge, COF…etc.), the following systematic approach was taken;

- All measured parameters were averaged over each test duration, to produce a single value which was statistically analysed using ANOVA (see Section 3.7).

  - Correlations between the measured parameters were assessed (e.g. whether charge related to wear, friction related to wear…etc.) to identify which measured parameters to focus on.
  - Statistical analysis was used to identify the affect that different additives and base oil–additive interactions had on the measured parameters. This enabled information about the overall additive friction and/or charge performance to be obtained.
- Real-time data was examined to give additional insight into the statistical findings for the averaged data. The real-time data, in addition to off-line measurements and additive adsorption studies, were complied to form hypotheses about additive-surface interaction.
  - This approach was used to discuss differences between additives (in the same base oil) and the effect that different base oils had on the same additive.
- The interpretation of additive-surface interaction through real-time data, for one additive (ZnDTP) in one base oil, was investigated through additional tribological testing and extensive surface chemistry analysis. (The cost of the surface chemistry analysis required to verify all real-time data discussions was beyond the financial constraint of this work.)

Additive absorption onto iron oxide powder was investigated through XPS analysis to show that adsorption relates to additive solubility; thus the difference in charge levels produced by the same additive in different base oils could be compared to the solubility of the additive.

Charge features produced by ZnDTP were thought to relate to the breakdown of the antiwear film. To investigate this hypothesis, a series of tests were carried out to investigate the tenacity of the antiwear film by running a ZnDTP containing oil followed by a base oil. Many similar tests reported in the literature stopped the experiment to change the oils and found that it took more than 12 hrs before the ZnDTP film broke-down [206]. This observation has led many researchers to state that ZnDTP is extremely tenacious and does not readily break down. However, while developing a test procedure to test the hypothesis, it was found that exchanging oils while the pin-on-disc were still in contact and moving relative to each other significantly decreased the tenacity of the ZnDTP antiwear film. Although this is not fully understood, it is thought that the reduction in tenacity is a result of the removal of physically adsorbed ZnDTP.

When a test is stopped and cleaned it is extremely difficult to remove all of the un-reacted ZnDTP. Thus, residue (physiadsorbed) ZnDTP may enable further film formation or replenishment. However, by not stopping the test the changing of oils (flushing) occurs at high temperature where the physically adsorbed ZnDTP is more readily desorbed from the surfaces (see Section 2.3.3.1). Another important point is that if the test is stopped, cleaned and re-started important data is not recorded; data logging only starts once the test is started. While developing a test procedure to test the hypothesis it was noticed that there were important transient signals not detected if the test is stopped.

6.1.1 AIMS

The aims of the work presented in this Chapter were to;

- Relate electrostatic charge to additive-surface behaviour, and to assess whether;
    - The absence or presence of a film can be detected
    - Charge features correspond to additive-surface interactions, e.g. adsorption and desorption/stripping
    - Charge can be related to chemical composition of the tribofilm
- Investigate how base oil – additive interaction affects surface film formation.

6.2 EXPERIMENTAL PROCEDURE

6.2.1 SAMPLES, TEST CONDITIONS AND PROCEDURE

The MTM was run in pin-on-disc mode; a 6 mm ball was loaded onto a standard MTM disk (both AISI 52100 steel, see Table 18 &19). Details of the MTM and instrumentation deployed can be found in Section 3.1.1 & 3.5 respectively. A maximum contact pressure of 1.2GPa was used. The test was split into two stages; during the first stage the sliding speed changed incrementally from 5-1 m/s over 2.5 minutes, and the second stage was run at constant speed of 0.8 m/s for 25 minutes (see Table 22). Experiments were carried out at an oil temperature of 100°C.

6.2.2 BASE OIL AND ADDITIVE CHEMISTRY

Six additives (see Table 30) were blended into three API base oils: Group I, Group II and poly alpha olefin (PAO) base oils at 1% wt., to minimise any rheological changes (see Table 20). The additives included a Detergent, Dispersant 3, ZnDTP 2 and three different friction modifiers (see Table 21 for more details). For the Glycerol Mono-oleate (GMO) approximately 70% of the GMO is made up of mono oleate; for the Modified Glycerol Mono-oleate (MGMO) this is around 90%. A full factorial matrix was constructed (6 x 3) and each base oil test (non-additized) was repeated, giving 24 runs in total.

Additive type	Hereafter referred to as	Additive description
Detergent	Detergent	Overbased sulphurised calcium phenate, Branched C20-28, 450 Mwt (Figure 34 (d))
Dispersant	Dispersant 3	Mono-polyamine succinimide, 1200 Mwt (50Å in length) (see Figure 31(a))
ZnDTP	ZnDTP 2	Secondary Alcohol zinc dialkyldithiophosphate (see Figure 42(b))
Friction modifier	GMO	Glycerol Mono-oleate (see Figure 39)
	MGMO	Modified Glycerol Mono-oleate (chemical structure is unavailable)
	MoDTC	Molybdenum dithiocarbamate (see Figure 40)

Table 30. Description of additives used in a full factorial matrix.

6.2.3 POST-TEST ANALYSIS.

Ball and disc wear volume loss were measured by laser profilometry (see Section 3.6.2.1). XPS elemental depth profiling analysis was carried out in a manner described in Section 3.6.4.3. Test oil conductivity measurements were also taken (see Section 3.6.1).

6.2.4 STATISTICAL APPROACH

The measured parameters (dependent variables) obtained from running the full factorial matrix were disc wear, ball wear, conductivity, and real-time data. The real-time data, including coefficient of friction (COF) and rms charge, were averaged for the duration of stage 2, for each test. The effect of additive and additive-base oil interaction on measured parameters was identified using ANOVA (see Section 3.7).

6.2.5 ADSORPTION STUDY

Oils were mixed with iron oxide powder and were subjected to heat (100^{o}C) and stirring for 1hr. The iron oxide was then removed from the oils, rinsed multiple times with solvent and dried. The iron oxide powder was then examined using XPS analysis (see Section 3.6.4.1). The strength of the iron and oxygen peaks were compared between samples to assess the adsorption of additives onto the iron oxide powder; the lower the iron concentration, the greater the adsorption.

6.2.6 ZNDTP 2 TRIBOFILM TENACITY EXPERIMENTAL PROCEDURE

Tests were run under the same contact conditions as for the full factorial matrix, except that 20 minutes into stage 2 the ZnDTP 2 containing oil was replaced by Group I base oil. This oil change was carried out while the test was running – ball and disc were in contact and moving relative to each other. The ZnDTP 2 containing oil was drained and 500 ml of base oil (pre-heated to 100^{o}C) was flushed through the system. During flushing the oil reservoir volume was maintained at approximately 50 ml to ensure that the contact was not starved. The entire flushing procedure lasted approximately 1 minute. Multiple tests were carried out using this procedure with the base oil only stage run for differing durations.

6.3 STATISTICAL ANALYSIS RESULTS AND DISCUSSIONS

This Section interprets base oil and additive significant findings for friction, electrostatic charge, conductivity and wear. The statistical observations are discussed in terms of general additive-surface behaviour.

6.3.1 CORRELATION BETWEEN MEASURED PARAMETERS

Previous work has tried, with varying degrees of success, to relate electrostatic charge with: wear, COF and oil conductivity (see Sections 2.4.4.1 & 2.4.4.2). It was therefore important to assess whether the electrostatic charge detected is purely a function of wear, friction or conductivity; if it was, then electrostatic monitoring of tribofilms would be a superfluous technique to the measurements already being deployed. This study showed there was no statistical correlation between electrostatic charge and ball or disc wear. There was a 20% correlation between average COF and LnQ_{RMS}, which was significant (*p-value* = 0.02), (see Figure 103(a)). Similarly conductivity was significantly (*p-value* = 0.00) correlated with LnQ_{RMS}; 52% of the charge detected related to the oil blend conductivity (see Figure 103(b)). This left a significant proportion of the total charge unaccounted for and is thought to be related to surface chemistry.

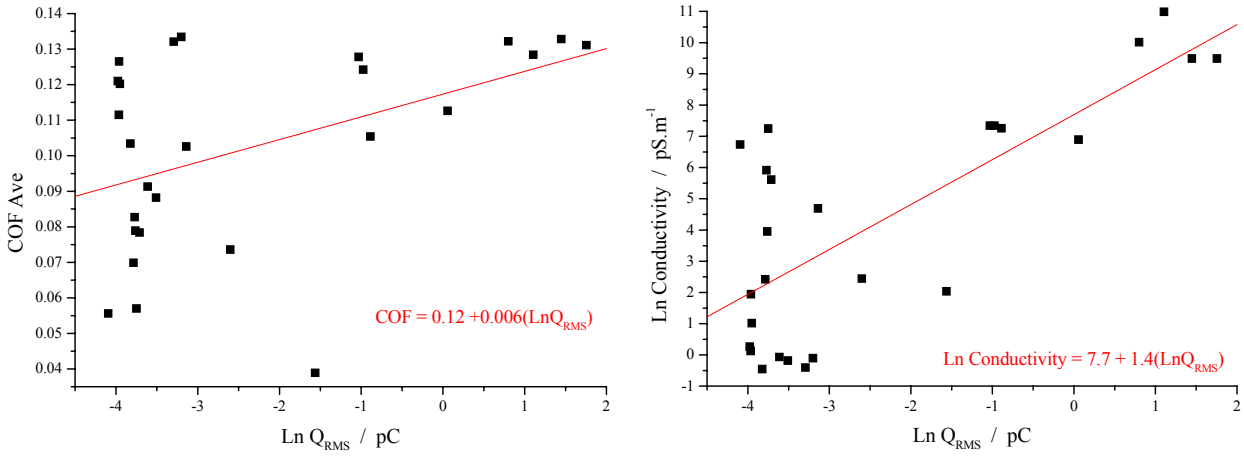

(a) (b)

Figure 103. Correlation between electrostatic charge and (a) COF, (b) conductivity.

6.3.2 COEFFICIENT OF FRICTION

Across all base oils, the Detergent and ZnDTP 2 produced significantly (*p-value* ≤ 0.03) higher COF than the friction modifiers: GMO, MGMO and MoDTC (see Figure 104). These findings are consistent with the literature. In general ZnDTP and detergent produce rough tribofilms, which effectively increase the severity of boundary lubrication conditions (reduce lambda ratio, see eq(32)). Also ZnDTP and detergent films may offer resistance to the relative motion of pin and disc (see Sections 2.3.4.4.5 for more details about ZnDTP friction behaviour). All three FMs produce tribofilms which easily shear and offer little resistance to the relative motion of pin and disc. GMO and MGMO form physically adsorbed films consisting of closely packed multi-molecular layers; the outer layers are easily sheared from the tribofilm (see Section 2.3.4.3.1). MoDTC forms a chemical film, containing MoS_2 (see Section 2.3.4.3.2) sheets with weak van der Waals interactions between layers, enabling the lattice layers to be easily sheared.

Figure 105 illustrates the tribofilm characteristics, for all 6 additives, which dominated friction performance.

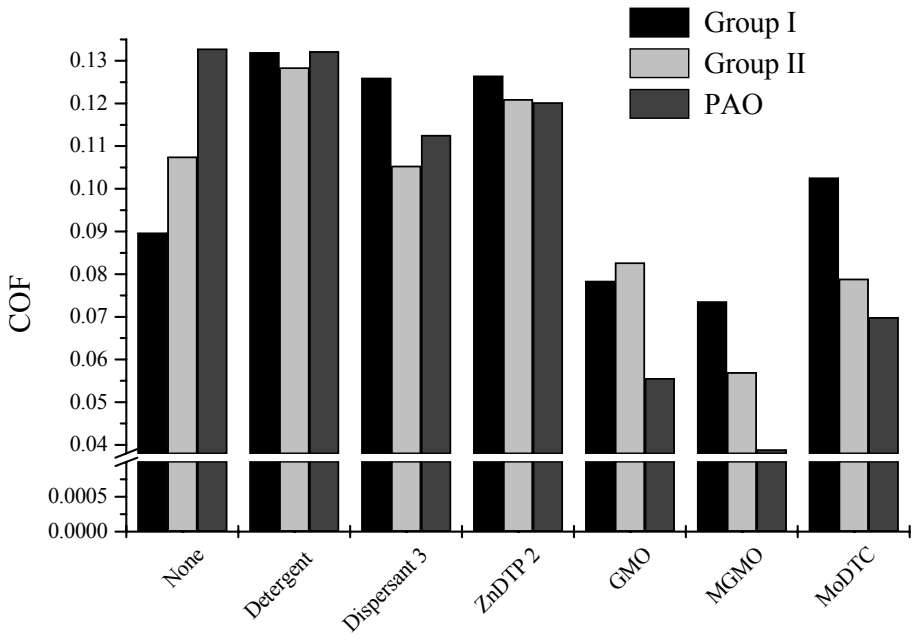

Figure 104. Coefficient of friction average for the full factorial test matrix.

Although it has been reported that detergents produce lower COF than ZnDTP [158,357,368], no statistical difference was found between the two. There were no statistical findings for base oil only; this is due to the large variation in COF produced by the three different base oils (see Figure 104).

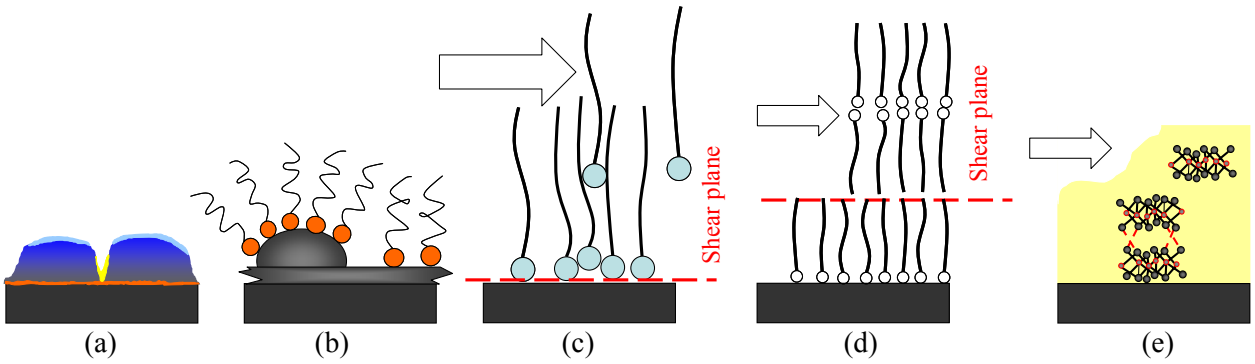

Figure 105. Schematic diagrams showing friction characteristics for additive tribofilms of: (a) ZnDTP (b) Detergent (c) Dispersant 3 (d) GMO & MGMO (e) MoDTC.

Partial friction differences between additive and base oil groups

Another interesting statistical finding was that MoDTC had significantly lower COF standard deviation than the Dispersant 3 (*p-value* = 0.03); and GMO and base oil alone had a marginally lower COF standard

deviation than the Dispersant 3 (*p-values* < 0.06). This variation in COF may be an indication of tribofilm stability – an unstable film will produce variable friction. The FMs produce tribofilms which can be sheared off in layers and easily rebuilt, due to the strong orienting forces (see Section 2.3.4.3.1). Whereas the Dispersant 3 tribofilm requires more time to re-form due to its considerably greater molecular weight. The greater variability in friction for Dispersant 3 is explored further in Section 6.4.3.3.

6.3.3 ELECTROSTATIC CHARGE

Across all base oils, Detergent and Dispersant 3 produced a significantly (*p-value* < 0.001) higher charge than MGMO, MoDTC, GMO and ZnDTP 2 (see Figure 106). This significant difference in surface charge is now discussed in relation to the proposed mechanism of additive adsorption, whether physical or chemical.

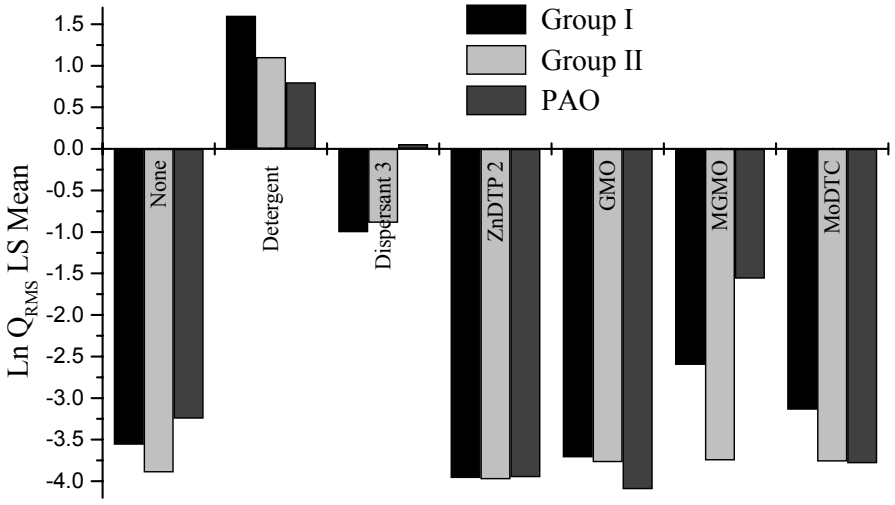

Figure 106. LnQ_{RMS} LS Mean for the full factorial test matrix.

6.3.3.1 Dispersants & detergents

Dispersant 3 and Detergent surfactant physically adsorb onto ferrous surfaces. Detergents and dispersants have the ability to form acid-base pairs with the ferrous surface. Detergent surfactants are acid (in order to suspend excess base) and adsorb onto a basic site on the surface; dispersants contain excess base and adsorb onto an acidic site (see Figure 107 (b) & (c) respectively). Adsorption of dispersants and detergent to the surface will generate a surface charge. Ionic separation, through desorption or mechanical stripping could result in charge retained on the surface.

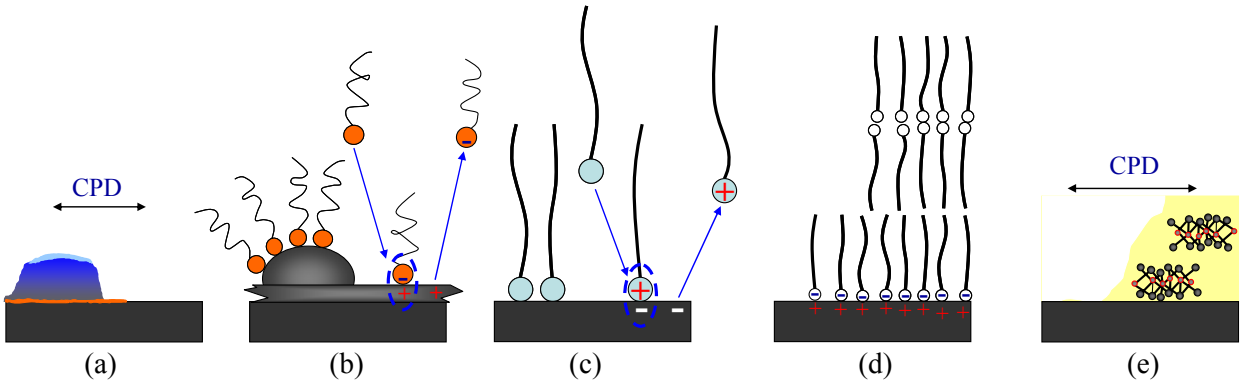

Figure 107. Schematic diagram showing charge generation for additive tribofilms of (a) ZnDTP (b) Detergent (c) Dispersant 3 (d) GMO & MGMO (e) MoDTC.

6.3.3.2 Detergent & Dispersant 3 vs. GMO & MGMO

Although GMO, MGMO, dispersants and detergents all physically adsorb onto the surface, the surface charge generated by the organic FMs was significantly lower than Dispersant 3 and Detergent is (*p-values* ≤ 0.00, see Figure 106). The explanation for this observation is the difference in charge carriers and the mode of adsorption. Dispersants and detergents containing oils contain a greater number of ions – although Dispersant 3 does not contain as many cations as the Detergent anions, (as evidenced by the conductivity (see Section 6.3.4)) – that form acid-base pairs with the surface. GMO and MGMO are very weak bases and are unlikely to form an acid-base pair with the surface in their original form; typically adsorption will arise from the sharing of charges (hydrogen bonding), rather than charge separation (see Section 2.3.4.3.1).

Preferential shearing at the hydrocarbon tail interface of the FMs, rather than at the polar-head/ferrous surface interface (see Figure 45 (d)), means there is little charge separation through stripping. Although alignment of the FM hydrocarbon tails is caused by electrostatic and van der Waals forces, shearing of theses layers does not have the same likelihood to generate surface charge as desorption of Dispersant 3 and Detergent polar-head from the surface.

6.3.3.3 Surface charge generation by chemical film forming additives (ZnDTP 2 & MoDTC)

The additives which form chemical films such as ZnDTP 2 and MoDTC produced a lower charge than dispersants (*p-values* 0.00, see Figure 106) which physically adsorb. The reaction of the chemical film forming additives, with the surface, is irreversible. Thus charge generation from contact potential difference (CPD) is most likely; where the chemical tribofilm has a different work function to the steel, which drives charge separation. In addition, the surface coverage by chemical and physical adsorption is likely to have an affect on surface charge. These chemical films occur in the wear track, where as dispersants and detergents physically adsorbed onto the entire surface (see Section 2.3.4). The Detergent

contains elements which physically adsorb (surfactants) and chemically adsorb (calcium carbonate); the high surface charge produced by Detergent is a result of the physical adsorption, rather than the chemical film, although CPD from the chemical film will contribute to the surface charge detected.

6.3.3.4 Detergent vs Dispersant 3

For Group I and Group II base oils, the Detergent exhibited a greater charge than Dispersant 3 (*p-values* 0.00 for both, see Figure 106). This may be contrary to expectations, when considering charge generated through desorption – Dispersant 3 has a greater molecular weight than Detergent, which makes desorption of Dispersant 3 more likely than Detergent. Three aspects could explain this, detergents have: a greater surface packing efficiency, greater number of charge species present, and contribution of a chemical film.

6.3.4 CONDUCTIVITY

Across all base oils, the Detergent had a significantly ($0 < p\text{-value} < 0.05$) higher conductivity than the other additives (see Figure 163 in Appendix E). Dispersant 3 exhibited a significantly ($0 < p\text{-value} < 0.05$) higher conductivity than MoDTC and ZnDTP 2. These observations are related to the concentration of ions present in oils. As discussed above, Detergent contains the greatest number of ions, followed by Dispersant 3. The poor correlation between conductivity and electrostatic charge is a result of the pre-existing charges in the oils (conductivity) compared to the production of additional charge carriers in the tribo-contact and the extent to which these charge carriers are present in the bulk oil or adsorb to the surface.

6.3.5 SPECIMEN WEAR

There were no significant additive or base oil effects on ball wear volume. However, there were some significant findings for disc wear volume loss, but none were consistent for additives across base oils. For the non-additized oils, the PAO exhibited significantly greater disc volume loss than the Group I and II base oils (*p-values* 0.00 & 0.01 respectively (see Figure 164 in Appendix E)). The greatest wear came from MoDTC in Group II base oil, which was significantly greater than that from MoDTC in PAO and Group I base oils ($p\text{-value} = 0.01$, for both).

6.4 RESULTS & DISCUSSIONS OF REAL-TIME DATA

This Section examines the significant findings from the real-time data. Dynamics in the real-time data, which are not handled by the statistical approach (see Section 6.3) are also discussed.

6.4.1 DIFFERENCES BETWEEN NON-ADDITISED BASE OILS

The COF for PAO base oil was significantly higher than Group II (*p-value* = 0.05) (see Figure 108(b)). The PAO base oil exhibited significantly greater disc volume loss than the Group I and II base oils (*p-values* 0.00 & 0.01 respectively) (see Figure 164, in Appendix E). Thus the high COF seen for PAO is due to the abrasive wear of the disc surface, and Group I and Group II base oils were capable of forming low shear strength tribofilms which produced a stable COF and low wear. In addition to the significant difference between PAO and Group II, Group II produced a significantly higher COF than Group I (*p-value* = 0.05), thus the ranking of friction levels followed the impurity concentrations (see Table 20). It is interesting to note that for the first 7, minutes the charge levels also follow the impurity concentrations of the base oils (e.g. PAO < Group II < Group I). However, over the whole duration of the test, the charge produced by PAO was marginally higher than Group II (*p-value* = 0.06). It is therefore thought that the progression of the high charge for PAO corresponds to wear. It is noteworthy that for the remainder of the test the charge levels for Group I and Group II continued to correspond to the impurity levels. Wear, friction and charge results indicate that the impurities in the Group I and II base oils are able to form a weak tribofilm which reduces wear and maintain a constant friction level.

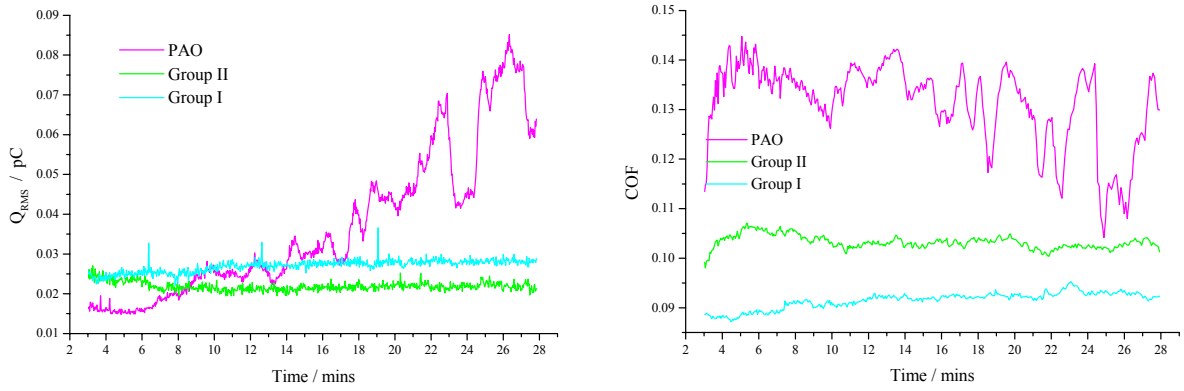

(a) (b)

Figure 108. Real-time (a) electrostatic charge and (b) coefficient of friction data for non-additized: Group I, Group II and PAO base oils.

6.4.2 DIFFERENCES BETWEEN ADDITIVES WITHIN BASE OIL

This sub-section details the statistical and real-time data differences between different additives within the same base oil.

6.4.2.1 FMs in PAO

All FMs in PAO produced tribofilms with friction reducing properties compared to PAO alone (*p-value* = 0.00, also compare Figure 108(b) 109(b)). MGMO produces a significantly lower COF than MoDTC (*p-*

value = 0.02). The MGMO started the stage at a low COF and then progressed to an even lower friction level; indicating an induction period was required for full film formation (see Figure 109 (b)). The electrostatic charge for the MGMO was an order of magnitude higher than that of MoDTC (*p-value* = 0.00) (see Figure 109 (b)), yet the conductivity for MoDTC was higher than MGMO (*p-value* = 0.02). This observation indicates that the charge generated by the MGMO was related to surface interaction rather than bulk electrical properties of the oil. The high charge level by MGMO infers that there is a full film on the disc surface; this corresponds to the low friction.

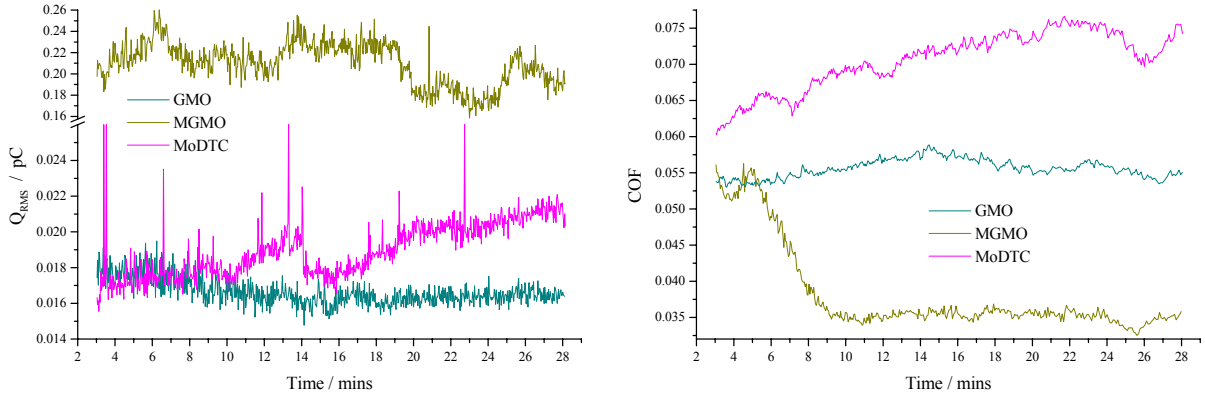

(a) (b)

Figure 109. Real-time (a) electrostatic charge and (b) coefficient of friction data for GMO, MGMO and MoDTC in PAO base oil.

Although there was no statistical difference between the GMO and MGMO average COF (*p-value* = 0.23, see Figure 104), Figure 109 shows there is a large difference in COF and charge, particularly at the end of test. This difference is believed to be related to the concentration of mono oleate in the two additives; mono oleate is the component principally responsible for friction reduction. For the GMO approximately 70% of the GMO is made up of mono oleate; for the MGMO this closer to 90%.

6.4.2.2 ZnDTP 2, Detergent and Dispersant 3 in Group I base oil

Detergent, Dispersant 3 and ZnDTP 2 COF traces compared to the Group I base oil alone were significantly higher (*p-values* 0.00, 0.00 and 0.01 respectively), which suggests that a film was present from the beginning of the test (compare Figure 108 & 110). The charge and friction data indicated that the kinematics of the films produced by these three additives were quite different. The charge traces show that Dispersant 3 adsorption/desorption was extremely dynamic; Detergent exhibited periodic features and ZnDTP 2 exhibited some periodic features that became more dynamic as the test progressed (see Figure 110 (a)). The COF traces for Dispersant 3 and Detergent were also dynamic.

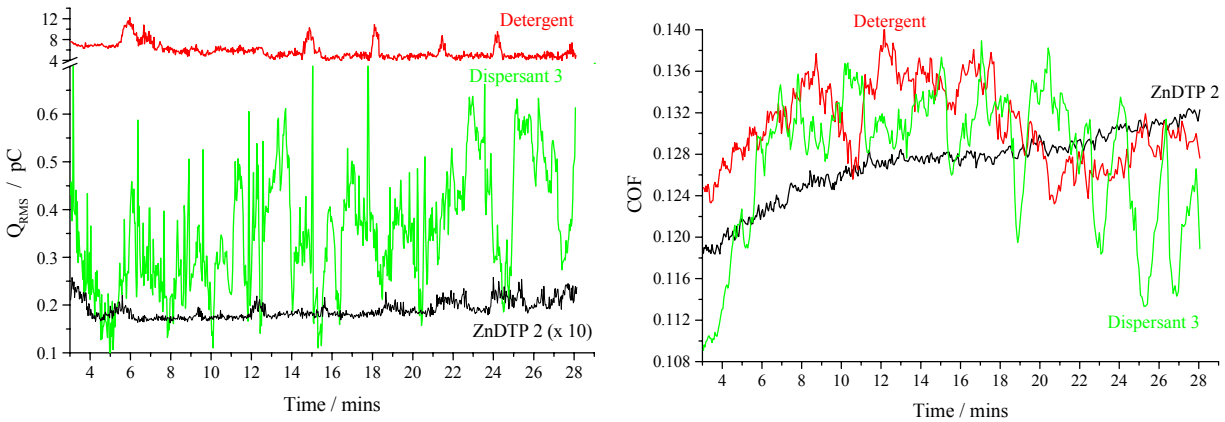

Figure 110. Real-time (a) electrostatic charge and (b) coefficient of friction data for Detergent, Dispersant 3 and ZnDTP 2 in Group I base oil.

The charge oscillations and the variability in the COF (see Figure 110) for Dispersant 3 and Detergent relate to the dynamic process of additive adsorption and desorption/partial film removal. Dispersant 3 exhibited dynamic charge features which were irregular. By comparison, Detergent exhibited short duration semi-regular periodic features which occurred 5 times during the 25 minute stage. This might be due to the fact that the Detergent was not as susceptible to stripping as the Dispersant 3, or that adsorption is much quicker and equilibrium is therefore restored more quickly. The superior solubility of the high molecular weight Dispersant 3, compared to the Detergent, accounted for the continually variable charge and friction; the charged dispersant cation is more easily desorbed than detergent. Similarly, the length (70 Å vs. 30 Å, for Dispersant 3 and Detergent molecules respectively) of Dispersant 3 relative to the Detergent makes Dispersant 3 more likely to be sheared from the surface compared to Detergent.

In comparison to Detergent and Dispersant 3, the ZnDTP 2 exhibited a relatively stable COF and charge trace, although COF steadily increased over the duration of the test. The electrostatic charge signal for ZnDTP 2 exhibited some charge dynamics, especially towards the end of the test.

6.4.3 Differences between additives among base oils

The statistical analysis indicated that the base oil had an effect on Q and COF. The real-time friction and charge data are used in this section to interpret base oil and additive interactions.

6.4.3.1 MGMO

MGMO exhibited a significantly lower COF in PAO compared to Group I (*p-value* = 0.01). The low solubility of MGMO in PAO, as evidenced by a hazy solution, may have increased the surface activity of MGMO and resulted in a greater surface coverage. It is believed this is related to the higher charge

observed for MGMO in PAO compared to other base oils indicating denser coverage (see Figure 111). For the PAO and Group II base oils, MGMO exhibited a significantly lower COF than the respective base oils only (p = 0.001, 0.00 respectively) (see Figure 104). The reduction in friction between MGMO in Group I base oil and Group I alone was not significant (p value 0.16). The formation of a full friction modifying film was inhibited as a result of the higher solubility of, and competition with, impurities in the base oil. It is not fully understood why Group II exhibited the lowest charge of the MGMO containing oils.

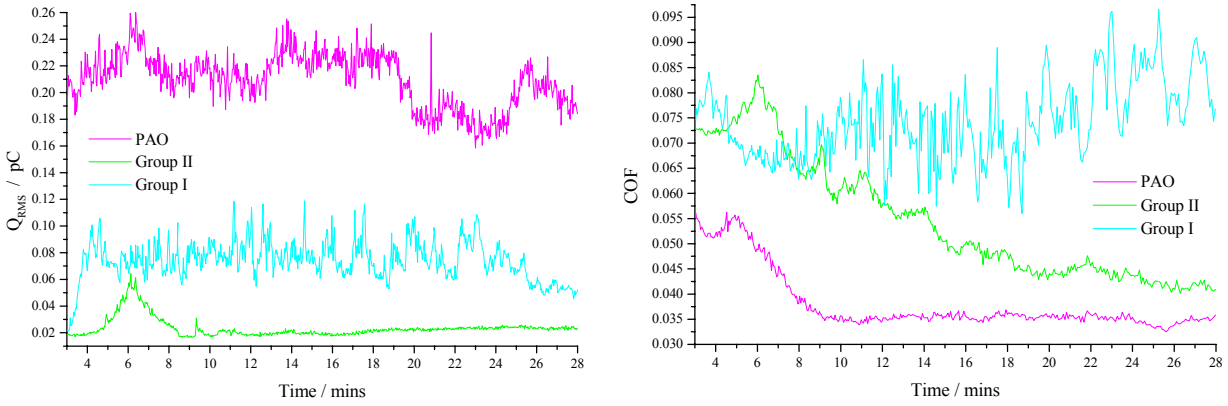

(a) (b)

Figure 111. Real-time (a) electrostatic charge and (b) coefficient of friction data for MGMO in Group II, Group I and PAO base oil.

Figure 111 (b) shows a peak in COF around 5-6 minutes followed by a decrease in friction for both MGMO in PAO and Group II base oils, which appears to correlate with a charge peak at the same time. This infers that the film present at the beginning is stripped and then re-formed with a greater covering (see Figure 111).

6.4.3.2 MoDTC

MoDTC in Group I base oil exhibited higher and more dynamic electrostatic charge and COF than Group II or PAO (see Figure 112). MoDTC produced significantly lower COF in PAO and Group II than the respective base oils alone (*p-values* 0.00, 0.02 respectively). For MoDTC in Group I, compared to Group I base oil only there was no statistical difference (*p-value* = 0.32) in COF average. Through comparison of Figure 108 and Figure 112 the MoDTC in Group I only formed a friction reducing tribofilm after the 21st minute.

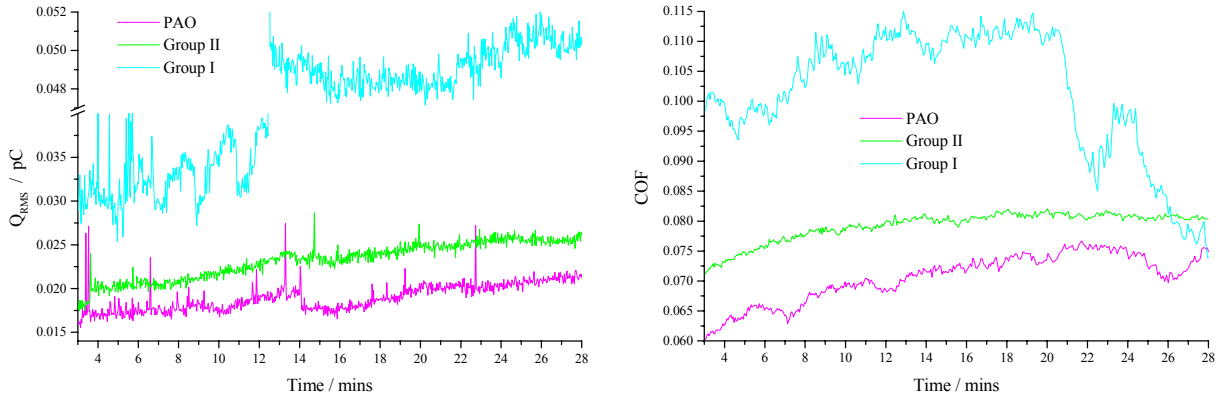

(a) (b)

Figure 112. Real-time (a) electrostatic charge and (b) coefficient of friction data for MoDTC in Group II, Group I and PAO base oil.

It has generally been observed that MoDTC film formation occurs in two phases: the initial phase produces high friction and is called the induction phase. The subsequent phase produces a film which reduces friction. It has been observed that there is no molybdenum in the tribofilm during the induction phase [172]. During this stage, metal-metal contact removes the oxide layer facilitating breakdown of MoDTC [171] to react with the surface to form FeS_x which reduces friction [233,369,370]. The tribofilm formed during the induction phase was reported to reduce wear and promote formation of the friction reducing MoS_2 tribofilm [218]. However, in this study MoDTC in Group I exhibited significantly greater disc wear volume loss than MoDTC in Group II or PAO (*p-value* = 0.01, for both). This suggests that the delayed progression (i.e. after 21 minutes) from high to low COF resulted in high wear. It has been reported that once a (low friction) MoDTC tribofilm is formed it needs continuous replenishment from MoDTC additive in the bulk oil to maintain the low friction and if MoDTC is removed from the lubricant an instantaneous increase in friction can occur [371]. The higher levels of impurities in the Group I base oil may compete for surface sites, hindering the formation of a MoDTC tribofilm, or the high solubility of MoDTC in Group I may prevent MoDTC getting to the surface. This is confirmed by an XPS adsorption study carried out on MoDTC in the three base oils, which showed that MoDTC in Group I base oil produced the least coverage of the adsorbant (FeO) (see Figure 113). It is proposed that up until this time breakdown of iron oxide and formation of FeS_x followed by removal caused tribochemical wear (see Section 2.1.4.2) similar to that seen for primary ZnDTP (ZnDTP 1) in Chapter 5. The cause of the transition to friction reducing tribofilm is not fully understood, but a change in contact conditions as a result of wear – increasing contact area and therefore reducing contact pressure – may have promoted the formation of a fully developed MoDTC film. It is noteworthy that the friction levels at the end of the test are the same for all base oils with MoDTC (see Figure 112).

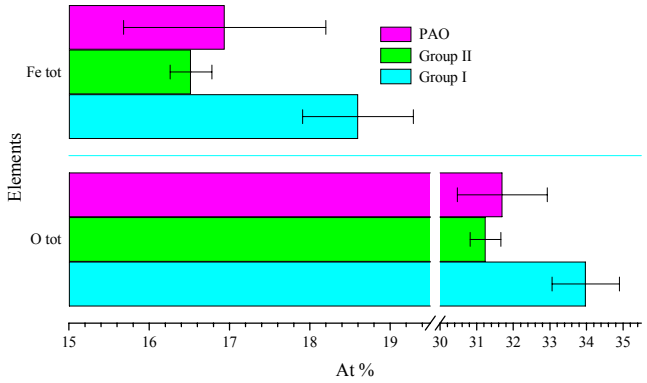

Figure 113. XPS results from a adsorption study involving MoDTC in Group I, Group II and PAO base oils.

6.4.3.3 Dispersant 3

In Group I base oil, Dispersant 3 exhibited a significantly higher COF than the base oil alone (*p-values* 0.00); for PAO this was marginally significant (*p-value* = 0.07), and for Group II there was no statistical difference (*p-value* = 1) between base oil and Dispersant 3 containing base oil. If the real-time data is examined a more complex picture emerges (see Figure 114 (b)). All the friction traces start at a low level (similar to base oil only) then increase to higher friction levels at different rates. This behaviour does not appear to follow simple impurity and solubility relationships, but appears to be more complex and will be explored later in Section 6.4.3.6.

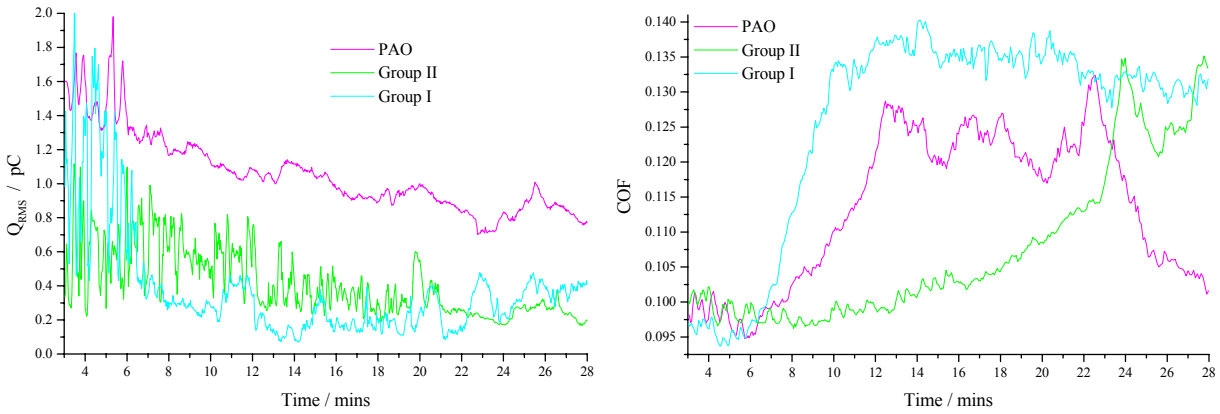

(a) (b)

Figure 114. Real-time (a) electrostatic charge and (b) coefficient of friction data for Dispersant 3 in Group II, Group I and PAO base oil.

Dynamic electrostatic charge signals were observed for all three oils, prior to the increase in friction (see Figure 114), which may be associated with tribofilm formation. For example, Group I showed dynamic charge signals up to the 7th minute, by the 9th minute the friction has reached the higher level. For Group II, the charge dynamics persist until 21st minute, by the 24th minute the COF has reached the higher level. These charge dynamics are thought to be related to the initial instability of a Dispersant 3 tribofilm, where the film is partially formed then removed. As discussed in Section 6.3.2, dispersants produced a significant to marginally significantly higher COF standard deviation than (MoDTC, GMO and) base oil alone; which infers tribofilm instability. The observed difference in positive and negative charge data supports this explanation (see Figure 115). Dispersant 3 can become positively charged at the amino group by a reaction with the surface. It is believed that upon desorption, an opposite charge may remain on the surface [350]. Dispersant 3 in Group II compared to Group I exhibited oscillating positive and negative charge signals, with a short periodicity (compare Figure 115 (c) & (b) respectively). The dominance of positive and negative charge varies over these oscillations, which is thought to indicate Dispersant 3 adsorption and desorption, which also suggests an unstable film was produced. This reinforces the view that an unstable film was produced by Dispersant 3 in Group II.

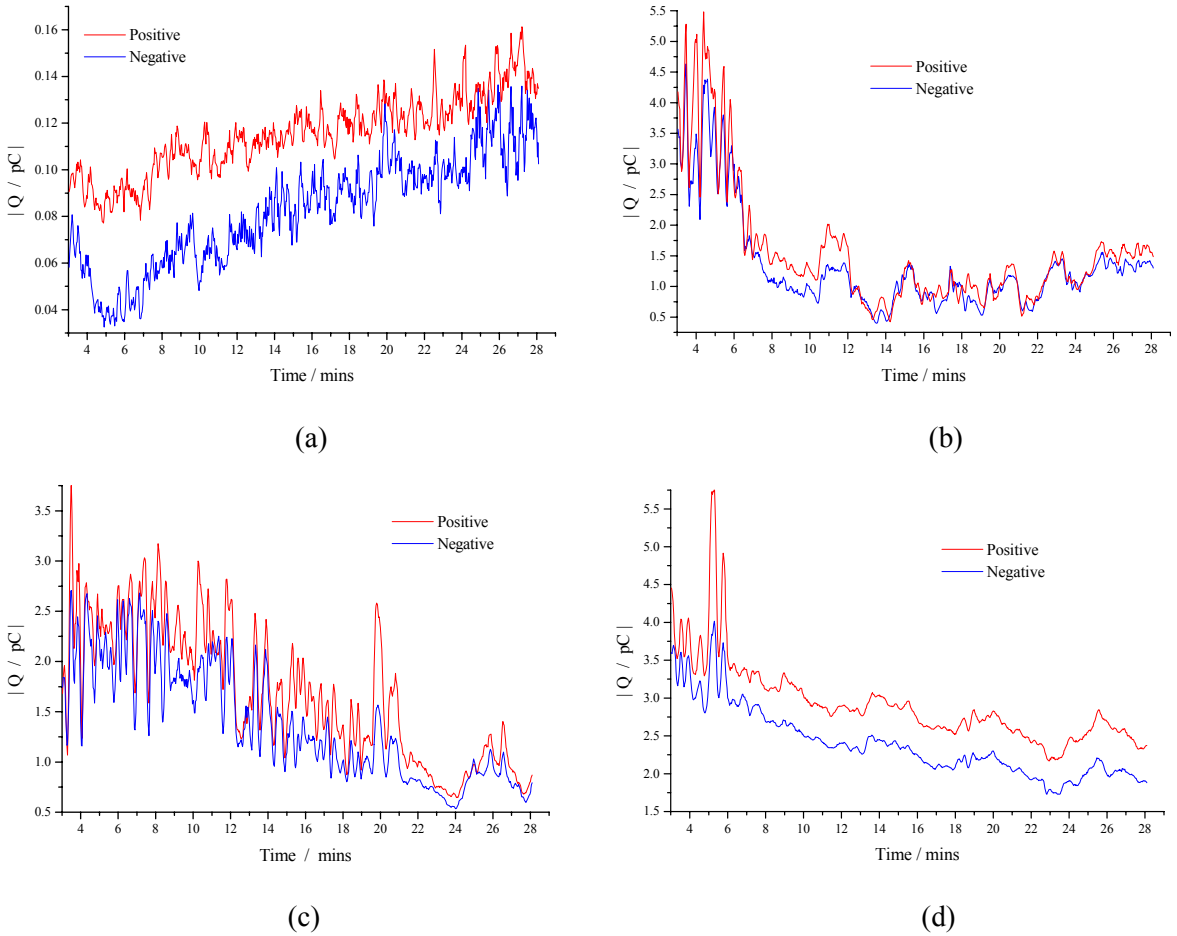

Figure 115. Real-time positive and negative charge data for (a) Group II base oil only; (b) Dispersant 3 in Group II, (c) Dispersant 3 in Group I, and (d) Dispersant 3 in PAO.

This inability for Dispersant 3 to form a full stable film, until the 24th minute, probably explains the higher wear observed for Group II than Group I (*p-value* = 0.05). This might suggest that these charge dynamics are related to wear, however, there was no significant difference in wear between Group II base oil with and without Dispersant 3 (*p-value* = 0.92), but the positive and negative charge data is very different, not only in magnitude but more importantly in the oscillations (compare Figure 115 (a) & (c) respectively).

Dispersant 3 produced a significantly higher electrostatic charge in PAO base oil when compared to Group I (*p-values* 0.02) and marginally higher electrostatic charge than Group II (*p-value* = 0.06). This can be explained by examining the positive and negative charge data for PAO. Figure 115 (d) shows that from 5 minutes onwards there were fewer charge dynamics between positive and negative charge, which is believed to be related to the lower solubility of Dispersant 3 in PAO base oil, as evidenced by the directionality of the adsorption data (see Figure 116). The adsorbed positively charged Dispersant 3 molecules are less likely to desorb into bulk PAO than Group I and Group II producing a greater density of adsorbed dispersants, which yielded a greater surface charge.

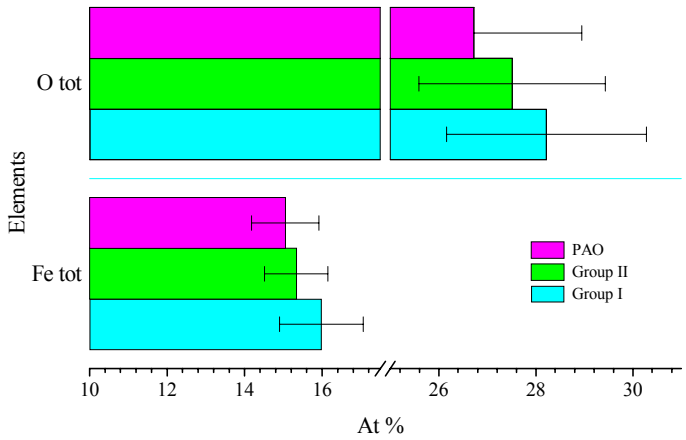

Figure 116. XPS results from an adsorption study involving Dispersant 3 in Group I, Group II and PAO base oils.

6.4.3.4 Detergent

The Detergent in PAO and Group I (see Figure 117) both increased in COF to a peak at around 12 minutes followed by a drop to the initial levels. The electrostatic charge data shows periodic features for Detergent in PAO and Group I. This periodicity, like Dispersant 3, is thought to relate to adsorption and stripping/desorption that cause variable COF. By contrast, Detergent in Group II showed less fluctuation in COF and increased in magnitude over the duration of the test; the charge signal was also more stable.

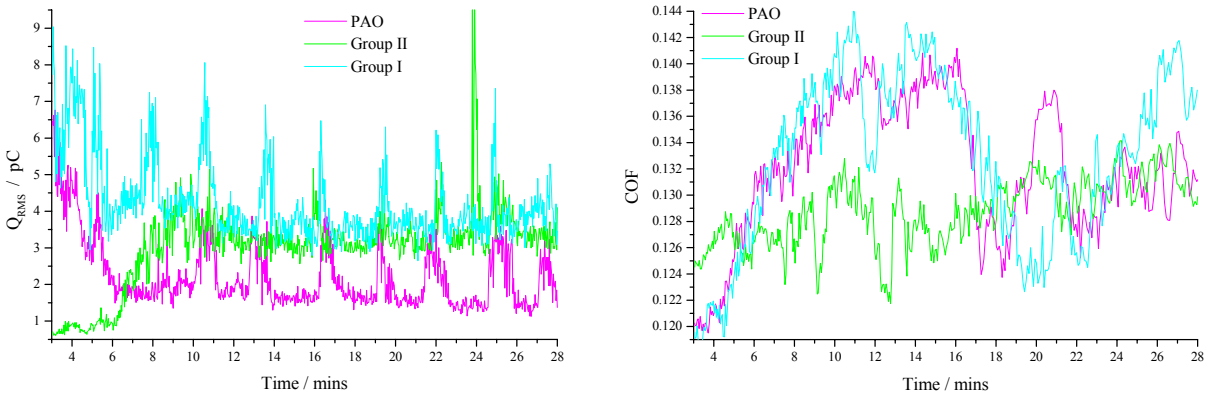

(a) (b)

Figure 117. Real-time (a) electrostatic charge and (b) coefficient of friction data for Detergent in Group II, Group I and PAO base oil.

The positive and negative charge data showed periodic signals which are predominantly negative for Group I and PAO (see Figure 118 (a) & (c) respectively). For Group I and PAO the charge signals contained peaks, with the negative charge at a greater level than positive charge at the peak; this was not as pronounced for the Group II. An overbased sulphurised calcium phenate detergent was used in this study employing an organic based surfactant, which is negatively charged. It is thought that adsorption of the surfactant gives rise to this negative peak.

Figure 119 shows a magnification of a single charge peak typically seen for Group I and PAO. During the dwell periods the surface is thought to be made up of CaO, adsorbed $CaCO_3$ and adsorbed surfactant, yielding equal positive and negative charge (see Figure 119 *A* & Figure 120(a)). Changes in the contact result in the adsorption of $CaCO_3$ micelles and mass adsorption of free surfactants which generate negative charge [350] (see Figure 119 *B* & Figure 120 (b)). Over many passes through the contact the surfactants are sheared/stripped resulting in equal positive and negative charge (see Figure 119 *C* & Figure 120(c)).

The Detergent contained an excess amount of surfactant to ensure that all the base is suspended in the oil; consequently there were free surfactants in solution. These free surfactants can adsorb to the surface, producing a negative charge. However, the reason for the initiation of mass surfactant adsorption is not fully understood. Surfactants have a greater affinity for nascent metal than oxides, therefore breakdown of CaO or iron oxide layers to reveal nascent metal could result in mass adsorption of surfactant molecules.

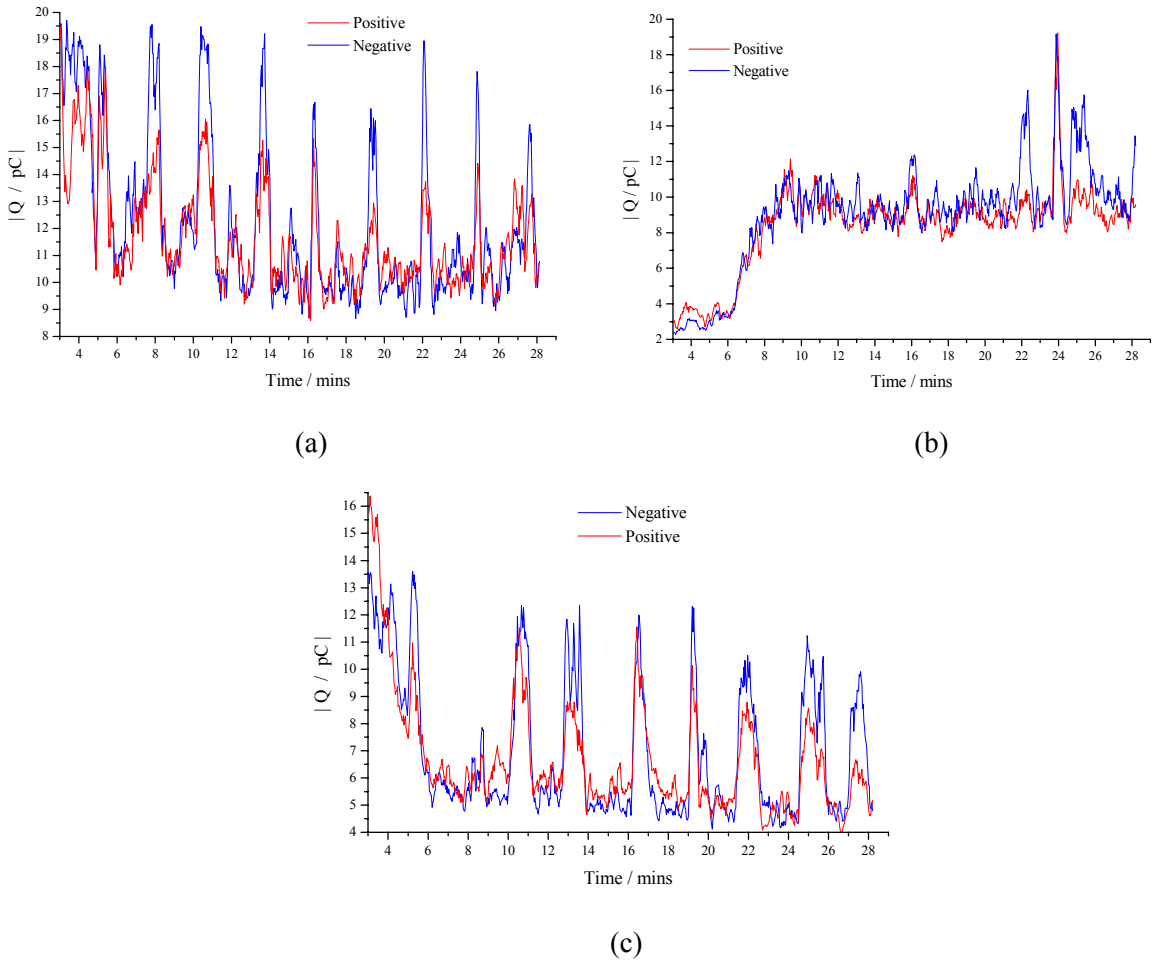

Figure 118. Real-time positive and negative charge data for Detergent in (a) Group I, (b) Group II and (c) PAO.

Shearing of surfactants has been observed by comparing adsorbed surfactants on and off the wear [155]. Cizaire et al. [156] carried out more detailed analysis and found that the stripping of surfactant from the surface can result in the splitting of hydrocarbon chains and/or the ionic bonds between sulphur and calcium. Although this observation was for calcium sulphonate detergent, calcium phenate could be split in a similar manner.

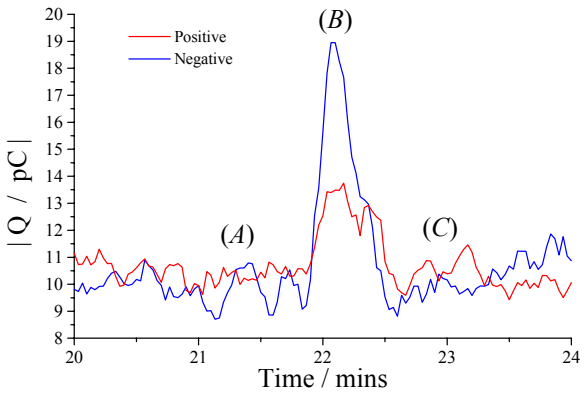

Figure 119. Positive and negative charge data for Detergent in Group I highlighting the negative charge peak between 21.8 & 22.5 minutes.

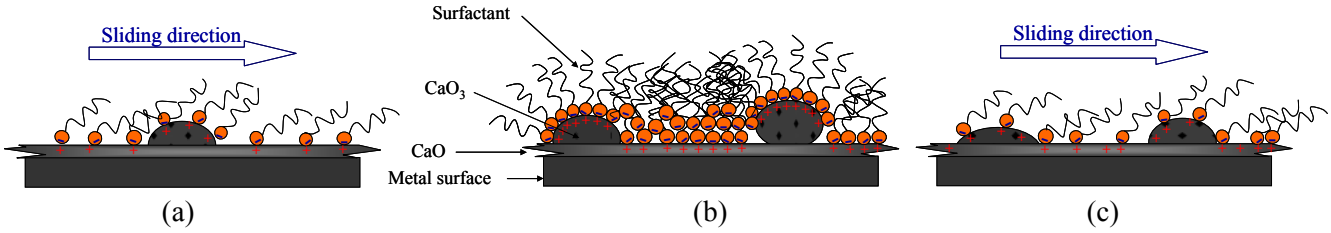

Figure 120. Schematic describing how the charge features seen in Figure 118 & Figure 119 can be explained; (a) CaO, adsorbed $CaCO_3$ and some adsorbed surfactant produce equal positive and negative charge, (b) changes in the contact result in the mass adsorption of surfactants which generate negative charge, and (c) surfactant is sheared from the surface resulting in equal positive and negative charge.

This interpretation of charge data and Detergent surface interactions links with the observed fluctuating friction and intermittent adsorption of $CaCO_3$ micelles [154]. It is believed that Detergent in Group II produced a stable tribofilm, which was not susceptible to the mass adsorption and stripping seen for the Detergent in Group I and PAO, as evidenced by the comparatively stable friction and charge data.

6.4.3.5 ZnDTP 2

The high friction observed for ZnDTP 2 in Group I base oil also produced the most dynamic charge trace (see Figure 121), which is similar to charge dynamics seen for Dispersant 3 and Detergent, and associated with a non-steady state tribofilm, or more specifically film stripping and formation. The positive and negative charge data showed that the oscillations seen on the RMS charge graph (see Figure 121) were a result of periodic negative charge features (see Figure 122 (a)). It is also noted that the positive charge did not follow the negative charge oscillations, which is different to dynamic features associated with Dispersant 3 and Detergent tribofilms. A possible explanation for this difference is the tenacity of ZnDTP

2 film. The oscillations seen for ZnDTP 2 could relate to the partial removal of the polyphosphate layer, creating a patchy surface and temporary CPD effect (which is observed in Figure 165 (d) which shows a patchy ZnDTP 2 tribofilm), followed by replenishment by organic ZnDTP decomposition products. Partial film removal could also explain the higher friction levels seen for ZnDTP 2 in Group I, compared to PAO or Group II, as the patchy film equates to a rougher surface and thus, higher friction (see Section 2.1.3). Partial ZnDTP 2 tribofilm removal and tenacity of these films is explored further in Section 6.5.

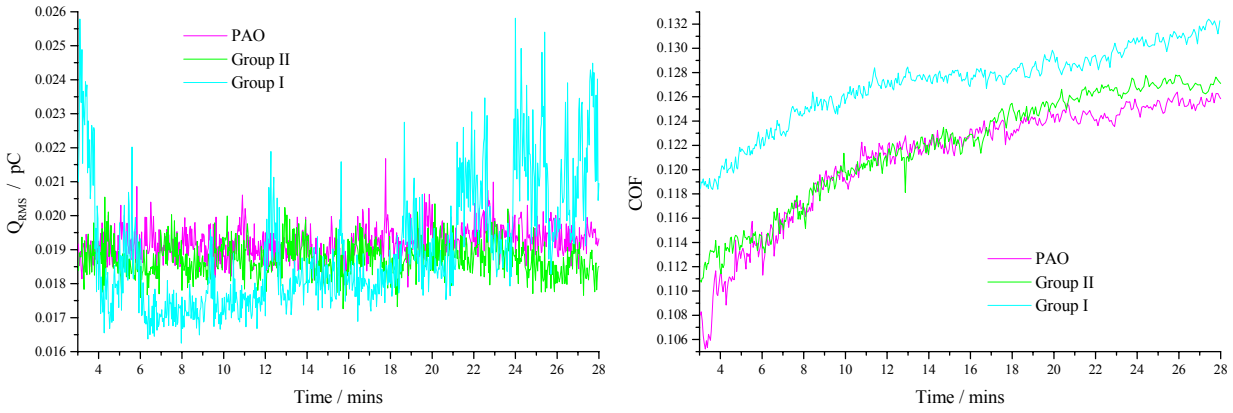

(a) (b)

Figure 121. Real-time (a) electrostatic charge and (b) coefficient of friction data for ZnDTP 2 in Group II, Group I and PAO base oil.

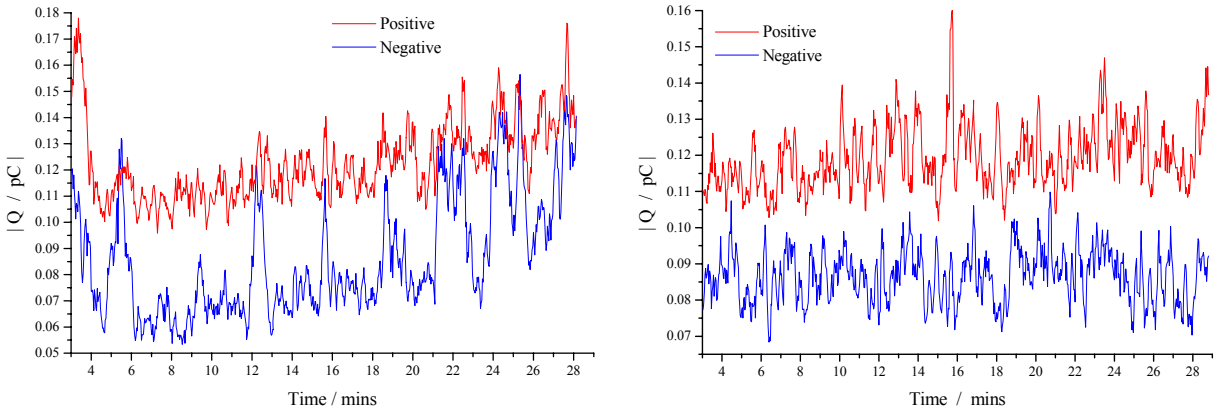

(a) (b)

Figure 122. Real-time positive and negative charge data for ZnDTP 2 in (a) Group II and (b) Group II.

6.4.3.6 Base oils

It is clear from the charge and friction data that the duration for additive film formation and the extent of coverage was related to the solubility of various additives in the three different base oils. However, the solubility of these additives in the three base oils did not simply follow the impurity concentration (Group I > Group II > PAO, see Table 20); instead the polarity or structure of these base oils (solvents) were the dominant factors.

The FMs and ZnDTP 2 exhibited friction and charge results which suggest that the tribofilm formed by these additives either takes longer, or is less tenacious, in Group I base oil than Group II and especially the PAO (see Figure 111,112 & 121). Group I contains the most polar hydrocarbon species, followed by Group II and then PAO. All the FMs (GMO, MGMO and MoDTC) and ZnDTP 2 are highly polar species. Thus FMs and ZnDTP 2 are more soluble in Group I, which means that they do not readily come out of solution to form a tribofilm. In addition, the highly polar nature of some of the impurities present in Group I base oil, means that impurities compete with the FMs and ZnDTP 2 for surface sites, inhibiting film formation further. The FMs in PAO produced the lowest friction films with the least instability. Similarly, Costello [118] reported that GMO is most effective in the least polar base oil and least effective in the most polar base oil, but no explanation was given. It is because FMs are the least soluble in PAO and there are fewer polar species in PAO to compete with the FMs for surface sites. Although this resulted in a significantly better friction performance for the tests in this study, it must be realised that there is an issue for additives which readily fall out of solution in a particular base oil for long term engine use – although this might give greater performance initially, additive depletion could occur over a unacceptable period of time.

Dispersant 3 and Detergent in Group II produced different results to the two additives in PAO and Group I base oil. A tribofilm was formed more readily for dispersants in Group I and PAO base oils, whereas it took considerably longer for Dispersant 3 in Group II (see Figure 114 (b)). Detergent in PAO and Group I base oil produced dynamic charge signals and variable COF traces, whereas Detergent Group I yielded a steady charge and friction trace (see Figure 117). The proposed reason for this is that dispersants and detergents are less polar than FMs and ZnDTP 2 and are therefore more soluble in a less polar base oil, which makes them more soluble in Group II. This meant that Dispersant 3 did not as readily come out of solution in Group II compared to PAO and Group I and it therefore took longer for the film to build. The greater solubility of Detergent in Group II, or more specifically the surfactant, meant that the surfactant did not come out of solution and adsorb onto the surface ‘en mass’ like Detergent in Group I and PAO.

6.5 ZnDTP 2 TRIBOFILM TENACITY EXPERIMENT

It was hypothesised in Section 6.4.3.5 that the negative charge peaks produced by ZnDTP 2 in Group I base oil are related to partial stripping of the tribofilm. This hypothesis was investigated through a series

of tests which artificially induced wearing/stripping of the ZnDTP 2 tribofilm through changing the ZnDTP 2 containing oil to a base oil 20 minutes into the test. Different test durations were run to assess the extent of ZnDTP 2 tribofilm stripping so that tribofilm thickness would be a function of time to which charge signals could be compared. However, the test variability proved to be too poor to be able to plot test duration as a function of tribofilm wear/stripping. Despite this, some interesting observation can be made through comparison of electrostatic charge data with tribofilm XPS elemental depth profiling.

Figure 123 (a) shows the positive and negative charge data for the test with no base oil flushing (F0). Although there are some dynamics at 5.5 and 14.5 minutes, this test showed a predominant positive charge and will be used as a comparison for the other tests. Test F1 (Figure 123 (b)) shows that after base oil flushing, the negative charge dominates the charge level. Test F2 (see Figure 123 (c)) shows an increase in charge when the ZnDTP 2 oil is exchanged for base oil only; in this test negative charge was only slightly dominant. Test F4 yielded a high negative charge during and immediately after the changing of oils (see Figure 123 (d)). The negative charge levels then reduce to a level below the positive charge and similar to that seen for at the beginning of the test.

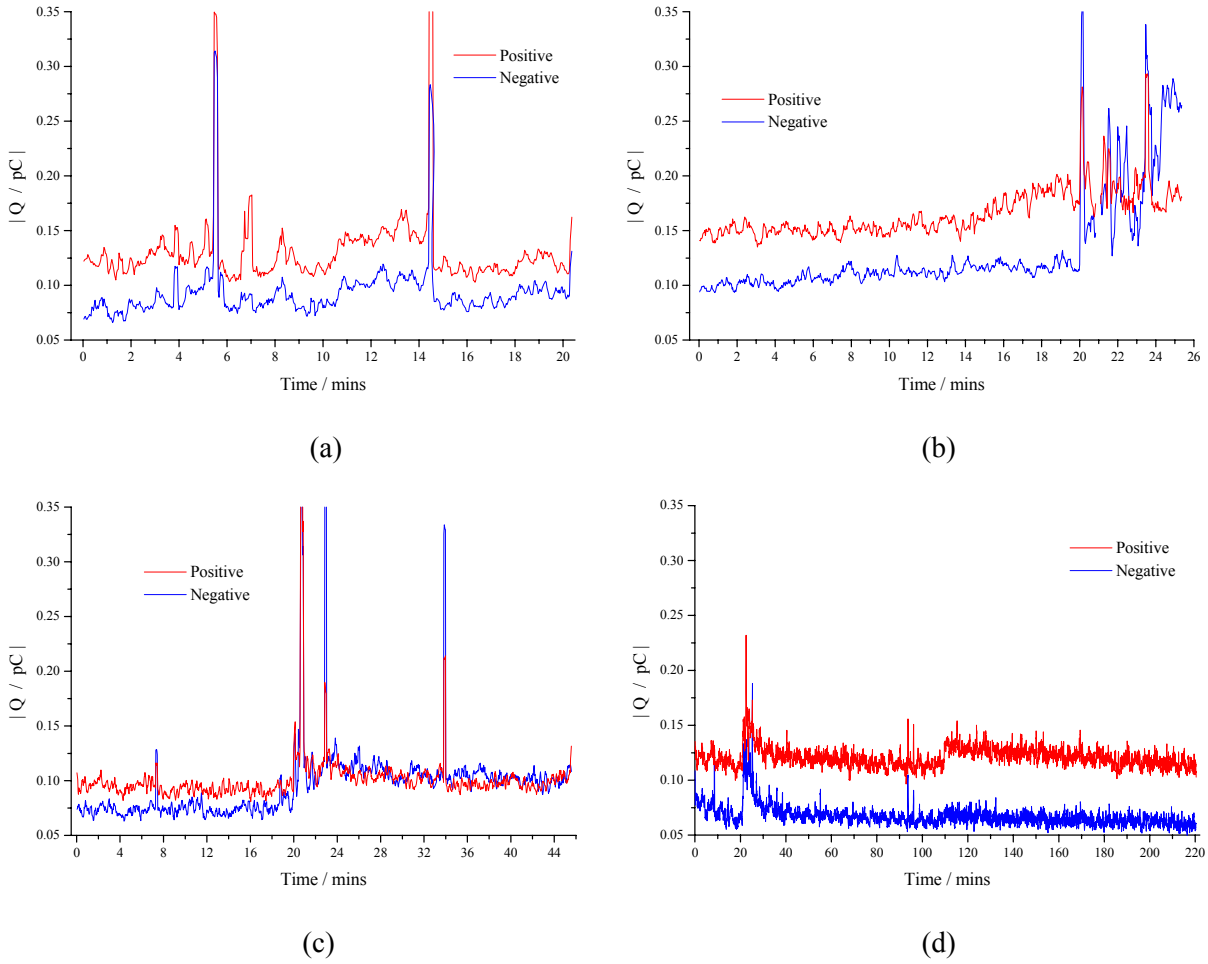

Figure 123. Real-time charge positive and negative data for tests (a)F0 (b)F1 (c) F2 and (d) F3. Base oil flushing occurred at 20 minutes.

A summary of four of the tests, in terms of dominant charge sign and tribofilm thickness is reported in Table 31. Comparisons between the dominants of a positive and negative charge to tribofilm thickness demonstrated that a significant increase in negative charge appears to relate to ZnDTP 2 tribofilm removal.

Test reference	Duration of test run with Base oil / minutes	Tribofilm thickness / nm	Positive/negative charge observation
F0	0	25	Dominant positive charge
F1	5	5	Dominant negatively charge
F2	25	25	Equal positive and negative charge
F3	200	30	Dominant positive charge

Table 31. ZnDTP 2 followed by base oil experiments; positive and negative charge observations, and tribofilm thickness as measured by XPS.

The main charge species thought to be present in a ZnDTP 2 tribofilm are zinc cations (Zn^{2+}), phosphate anions (PO_4^{3-}) and sulphate anions (SO_4^{2-}). XPS elemental depth profiling was carried out to examine changes in surface chemistry that might have led to the change in charge polarity (see Figure 124). Test F0, which yielded a dominant positive charge, had the highest levels of Zn in the tribofilm. The concentration of Zn in the tribofilms decreased from high to low with charge polarity from positive (F0), comparable positive and negative (F2), and predominantly negative charge (F1). There was also a reduction in phosphorous and sulphur concentration from the tests with predominantly positive to negative charge, but the change was not as great as that for zinc. The reduction of the Zn, which will include Zn^{2+} ions, meant that there were substantially less positively charge species in the tribofilm, thus leading to a dominance of negatively charge species.

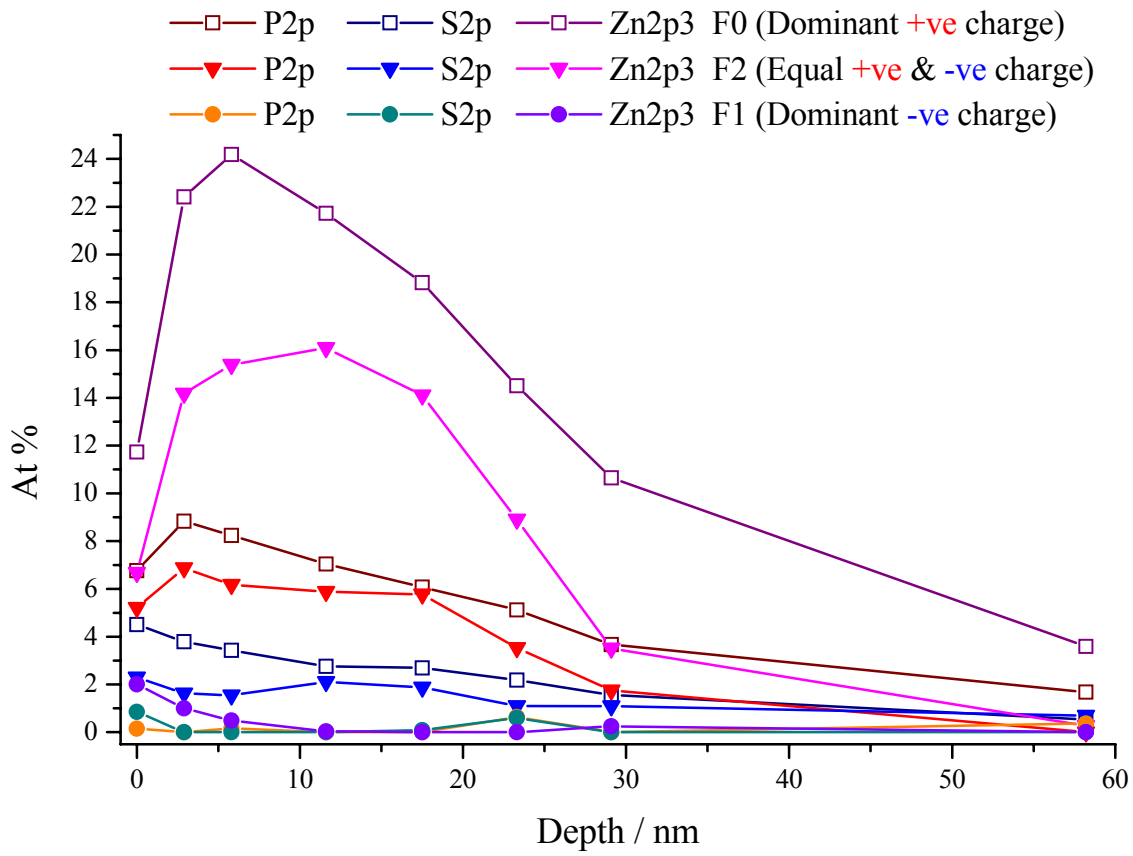

Figure 124. XPS elemental depth profiling for test F0, F1 and F2.

Figure 125 shows the ratio of tribofilm elements which are likely to be positively charge (zinc) against elements which are likely to be negatively charged (e.g. phosphate and sulphate). It was found that those tests which produced a tribofilm that contained more zinc than phosphate and sulphate produced a dominantly positive charge (e.g. F0). Those tribofilms which contained a greater concentration of phosphate and sulphate than zinc produced either a negative charge or an equal positive/negative charge (e.g. F1 and F2). This analysis indicates that the negative peaks seen for ZnDTP 2 in Group I (see Section 6.4.3.5) relate to partial removal of the tribofilm and the source of the negative charge is a reduction of Zn.

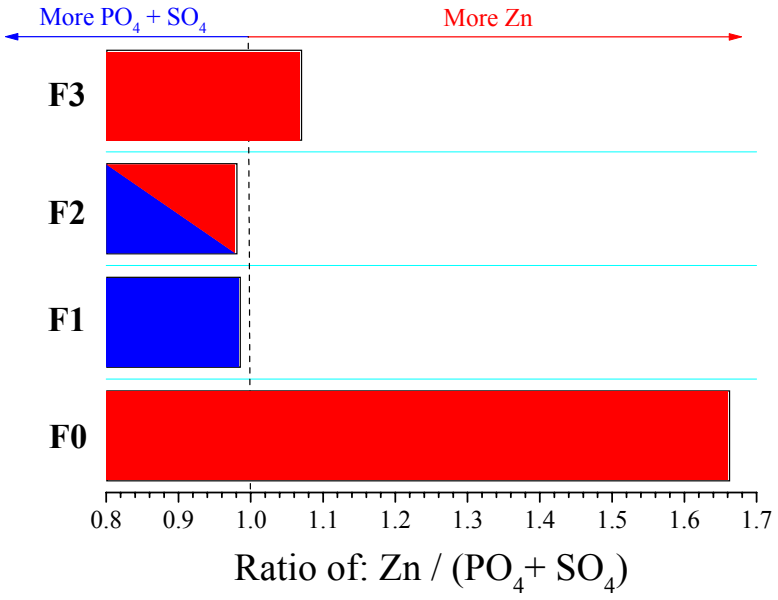

Figure 125. Ratio of the major positive (Zn) and negative charges (PO_4 and SO_4) thought to be present in ZnDTP 2 tribofilms for test F0, F1, F2 and F3.

As discussed previously, many of the tenacity experiments were discarded because they were difficult to plot ZnDTP 2 film wearing/degradation as a function of time. Re-examination of these tests show the same findings as discussed above. One of the most interesting tests was F3 which showed a separation between positive and negative charge prior to the change from ZnDTP 2 oil to base oil (see Figure 123 (d)). During and shortly after the oil change the negative charge increased to a greater extent than the positive charge. After 10 minutes (30 minutes from start) the positive and negative charge levels separated and returned to that seen in the first 20 minutes and seen for test F0 which did not involve a change to base oil. This infers that during the change of oils, the ZnDTP 2 tribofilm is stripped and then re-built, which was further substantiated by the near identical elemental depth profiles for F0 and F3 (see Figure 126).

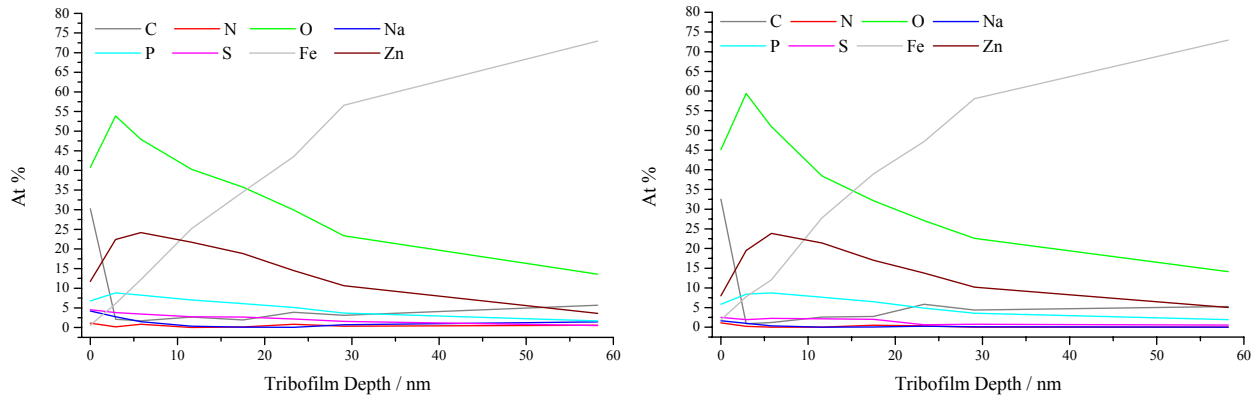

Figure 126. XPS elemental depth profiling for test (a) F0 and (b) F3.

Despite the difference that F0 was run for a short period of time in a ZnDTP 2 containing oil and F3 was run in base oil, after the ZnDTP 2 oil, for two hours, the wear of the two samples were very similar. This suggests that ZnDTP 2 could break-down and reform with very little effect on wear. This is at odds with many researchers who suggest that low wear produced by ZnDTP is evidence that the tribofilm it forms is extremely tenacious and not readily removed. This series of ZnDTP 2 tenacity experiments have demonstrated, through electrostatic monitoring and XPS analysis, that films could partially break-down and quickly reform again with minimal effect on wear.

The detailed cross-correlation between electrostatic charge and surface chemistry further substantiates the dynamic additive-surface interactions inferred from electrostatic charge, friction, wear and adsorption data.

6.6 CONCLUSIONS

This study assessed the effect of three base oils and 6 additives on friction, wear and electrostatic surface charge. A full factorial matrix was carried out, under conditions designed to simulate the valve-train contact.

Electrostatic charge generation from additive-surface interaction has been discussed. The charge generation was found to be dependent on the mode of adsorption (chemical or physical) and the charge carriers existing in the additive (whether acids or bases). Physical adsorption is thought to generate charge through adsorption, particularly through the formation of acid-base pairs, as well as desorption (charge separation). Detergent and Dispersant 3 produced charge levels two orders of magnitude greater than the FMs and ZnDTP 2. Dispersant 3 is basic and therefore promotes positive charge formation through adsorption. Due to the excess base present in the Detergent, there is a significant amount of acid surfactant molecules which keep the base soluble, adsorption of these surfactant molecules containing acidic sites, promotes negative surface charge formation. The Detergent produced a higher charge in Group I and Group II base oils because there is a greater number of acidic surfactants in the Detergent compared to the basic dispersants. The organic FMs (GMO and MGMO) produced a low charge compared to detergents and dispersants, because they physically adsorb, through sharing of electrons rather than charge separation (formation of an acid-base pair). In addition, FMs preferentially shear at the hydrocarbon tail interface rather than at the polar-head/metallic surface interface, which produces less charge.

ZnDTP 2 and MoDTC, which adsorb at the surface then, chemically react to produce a surface film which has a different work function to the bulk steel and this drives charge separation. The charge generated by these chemical films is lower than that produced by additives which only physically adsorb, because

chemical films cannot desorb (creating charge separation). Chemical films are also often only found in and just outside the contact, whereas physically adsorbed films adsorb on the entire surface; the surface area to sensor area ratio is smaller for chemically adsorbed films, hence a lower charge is detected.

Real-time charge and COF signals have been used to discuss tribofilm kinematics, with particular reference to the affect the base oil has on additive film formation (additive solubility). Charge and friction signals indicate that the higher molecular weight Dispersant 3 is more susceptible to stripping/desorption than Detergent. Electrostatic charge signals have been related to the partial stripping of the ZnDTP 2 film as well as the chemical composition of the tribofilm; the reduction of zinc relative to phosphate and sulphate resulted in an increase in negative charge.

This work has an impact on formulating, as additive selection could be, in part, based on additive-surface charge and additive tribofilm kinematics. Additives which are known to produce different charge levels and sign could be optimised to attract absorption of another additive, or alternatively additives that are not desired at the surface could be repelled. The tribofilm kinematics could also be managed to promote the desired tribofilm composition, or more correctly minimise antagonistic surface competition – a point, to the knowledge of the author, that has not been realised in the literature. Understanding the kinematics of tribofilm formation for surface active additives could enable lubricant formulators to achieve their goal of achieving low friction and low wear.

7 EVALUATION OF THE TRIBOLOGICAL PROPERTIES OF DISPERSANT AND FRICTION MODIFIERS WITHIN A SIMULATED AUTOMATIC TRANSMISSION TRIBO-COUPLE

7.1 INTRODUCTION

Work presented in Chapter 6 showed that different additives produced different charge levels – the difference between physical and chemically forming additives was significant – and charge features were also related to additive-surface interaction. With this advance in understanding, the work presented in this Chapter investigated single additive-surface charge generation, as well as how additive interactions affect surface charge. This work shows an incremental increase in test complexity, to push understanding of additive-surface charge generation further.

Two physically adsorbing additives, dispersant and FM, which are found in automatic transmissions, were chosen. These additives affect the frictional performance in wet clutches in automatic transmissions; dispersants are used to maximise torque capacity and FMs are used to minimise shudder. These requirements are conflicting as FMs lower torque capacity, and dispersants increase friction, making shudder more likely. In industry, an iterative approach is taken to identify the type and concentration of these two additives which optimise these two characteristics, but it is usually a trade off between the two. Interaction between these additives and how this affects film formation, in most cases, is identified through frictional behaviour; there is very little known about the chemical and physical properties of the film produced by these two additives, and how this leads to the friction characteristics seen.

The tests detailed in this Chapter represent a challenge for the interpretation of electrostatic charge. Both additives are quite similar in chemical and physical structure (both are succinimides) and electrostatic monitoring has not previously been employed to monitor the charge on wet friction material.

7.1.1 AIM

The work presented in this Chapter investigated the tribological behaviour of dispersant and friction modifier containing oils on a steel-paper tribo-couple through; real-time friction and surface charge measurements, and off-line wear and XPS analysis. The work aimed to assess;

- Monitoring of wet friction material surface charge.
- Whether electrostatic monitoring was sensitive enough to small changes in additive chemistry.
- Whether electrostatic monitoring can offer new insight into dispersant and FM interaction.

7.2 EXPERIMENTAL PROCEDURE

A PCS instruments MTM was employed in Pin-on-Disc mode, under pure sliding (see Section 3.1.1 & Figure 60). Details of the instrumentation, data acquisition and signal processing can be found in Section 3.5.

7.2.1 WEAR SPECIMENS AND TEST PROCEDURE

In order to simulate FM and dispersant interactions found in clutch pack contacts of modern automatic transmissions, it was important to try to mimic the wet friction clutch materials and contact conditions.

The test specimens consisted of a 380 μm thick paper bonded to a coated standard MTM disk with an epoxy resin, and a 6mm AISI 52100 steel ball (see Figure 127). The physical properties of these components are shown in Table 19. The wet friction material was supplied by an automotive fibre composites manufacture.

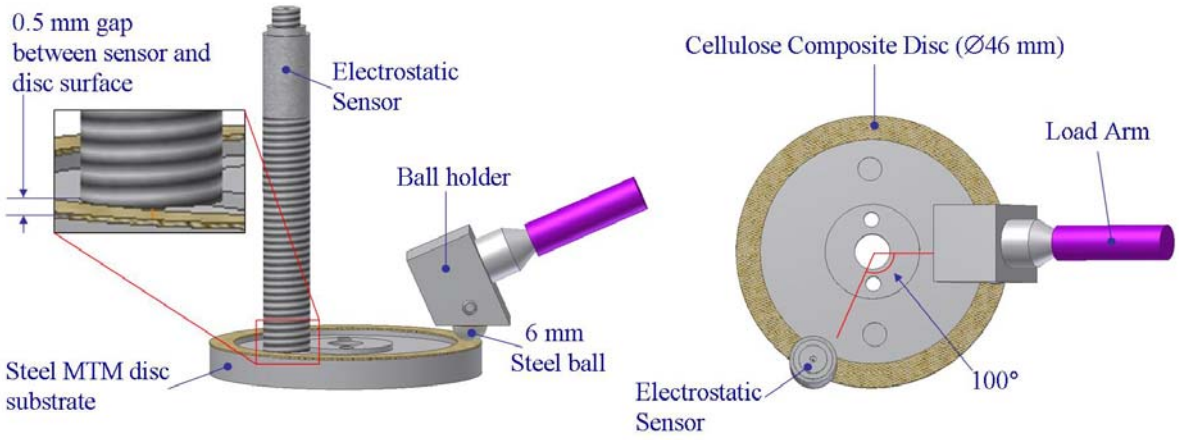

Figure 127. Schematic showing brass disc and the position of the sensor relative to the steel ball.

Oil (50 ml) was added to the MTM oil reservoir. The reservoir was heated until the oil reached the test temperature of 100°C (considered normal operating temperatures for transmission components [76]), which typically required 15 minutes. During this period the disc was rotated at 0.8 m/s, without the pin in contact. Once thermal equilibrium was achieved the test was started. A constant load of 3 N was employed, which produced a contact pressure higher than normally experienced by the clutch pack, 400 MPa was found to be the lowest pressure that produced repeatable results. Contact pressure has a moderate influence on clutch friction compared to the influence of temperature and sliding velocity [76]. The test consisted of two stages (see Table 22); the first stage employed sliding speeds between 4.5 m/s and 0.6 m/s over a period of 2 minutes for running-in; the second stage employed a constant sliding velocity of 0.2 m/s for a period of 33 minutes. A sliding speed of 0.2 m/s has been found to be the upper range for investigating friction-induced vibration from automatic transmission clutches [74].

7.2.2 BASE OIL RHEOLOGY AND ADDITIVE CHEMISTRY

In this study, an API Group II base oil (see Table 20), dispersant and an ATF friction modifier were used. The choice of base oil was based on good repeatability identified in Chapter 6. A conventional mono-succinimide dispersant (Dispersant 3), made from polyisobutene, had one polar-head/molecule and according to molecular modelling[‡‡‡‡‡] was 70Å in length (tail-head) (see Figure 31(a)). The friction modifier (FM 1) was a bis succinimide with 2 tails/polar-head with dimensions of 28Å tail-head[‡‡‡‡‡] and 41Å tail-tail[‡‡‡‡‡] (see Figure 31(b)). For both FM 1 and Dispersant 3 the polar-head was attached to the hydrocarbon tail via an alkylation reaction. The FM 1 contained about one amine functional group and the Dispersant 3 typically contained more than 3 amine functional groups. Dispersant 3 and FM 1 were tested individually and in mixtures (1:1) at 1% wt. (in total), to minimise changes in oil rheology (see Table 32); also it was reported that the friction behaviour of dispersants, when used alone, saturates above 1% - concentrations above 1% do not significantly alter the friction characteristics compared to the friction characteristics at 1% [83,84]. Blended at an equal percent weight the FM 1 containing oil has a higher concentration of nitrogen than Dispersant 3 containing oil.

Test order	Oil
1	Base oil
2	Base oil + 1% Dispersant 3
3	Base oil + 1 % Friction Modifier 1
4	Base oil + 0.5% Dispersant 3 + 0.5% Friction Modifier 1

Table 32. Oil test matrix.

7.2.3 OFF-LINE ANALYSIS

On/off wear scar surface composition analysis was carried out on worn wet friction material sample (see Section 3.6.4.1). The ball wear scars were measured using an optical microscope (see Section 3.6.2.3). Due to the elliptical nature of the wear scar, it was characterised by two measurements; the first in the direction of sliding and the second perpendicular to sliding. The wet friction material surface wear was impossible to image through laser profilometry; even with tactile profilometers, the wear track is not discernable. Given these problems with quantification methods, a qualitative approach was taken, which compared optical macro and micro images between test specimens. Although this method is not without subjective error, some general visual observations about the difference in wear can be made. Conductivity measurements (see Section 3.6.1) were carried out on test oils 1-4 (see Table 34).

[‡‡‡‡‡] Minimum energy conformations, and molecular dimensions, for additives were determined using Cambridgesoft Company CSChem3d Pro software version 7.0.0. Conformations were minimised to an RMS gradient of 0.05.

7.3 RESULTS

7.3.1 ON-LINE DATA

7.3.1.1 Coefficient of friction

The highest COF was produced by the Dispersant 3 containing oil followed by base oil, FM 1 + Dispersant 3, and then FM 1 alone (see Figure 128). All friction traces were relatively stable, apart from the FM 1 + Dispersant 3; that starts at 0.17, which is in-between FM 1 and Dispersant 3 levels (0.16 and 0.19 respectively), and as the test progressed the friction level increased in magnitude and dynamics. By the end of the test, the FM 1 + Dispersant 3 COF level was similar to that of Dispersant 3 alone.

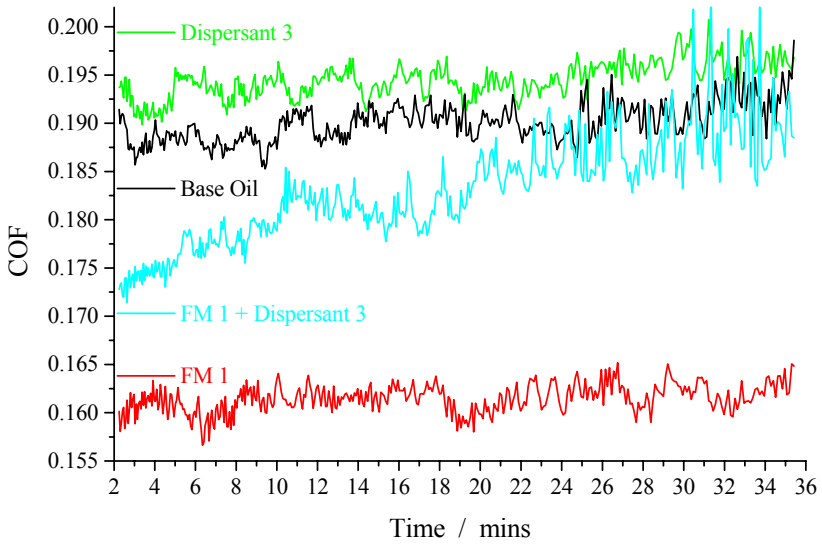

Figure 128. COF traces for base oil, Dispersant 3, FM 1, and FM 1 + Dispersant 3.

7.3.1.2 Electrostatic charge

The base oil electrostatic charge levels were fairly constant around 1.2 ± 0.2 pC for the majority of the test, but after 29 minutes the charge level doubled (see Figure 129). Dispersant 3 varied around similar charge levels to the base oil, but did not increase in magnitude towards the end of the test. The FM 1 produced a lower charge level than base oil and Dispersant 3 alone, in addition the FM 1 charge trace was more stable than the other test oils, and exhibited a steady increase in magnitude over the entire duration of the test. The FM 1 and Dispersant 3 mixture yielded initial charge levels half way between Dispersant 3 and FM 1 only. At approximately 6 minutes the charge dropped to a level slightly above that of the FM 1 only. Between 9th and 11th minutes the level increased to be around that of Dispersant 3 only, where it remained until the 16th minute. Around the 20th minute, the charge signals returned to a low level, close to that for the FM 1 only. From this time onwards, the charge signals became more dynamic in terms of amplitude and spikiness, alternating between Dispersant 3 and FM 1 levels.

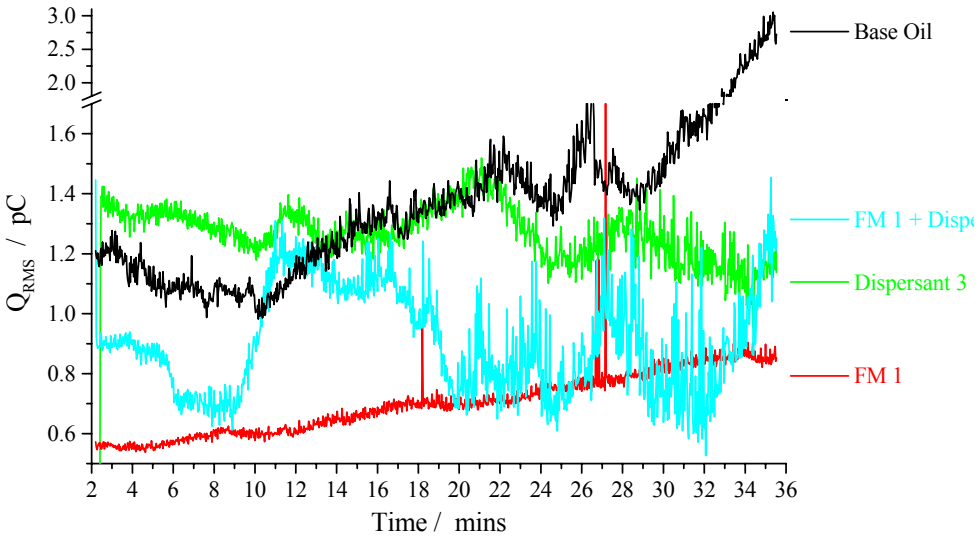

Figure 129. Electrostatic charge traces for base oil, Dispersant 3, FM 1, and FM 1 + Dispersant 3.

7.3.2 OFF-LINE ANALYSIS

7.3.2.1 Disc wet friction material wear

The paper surface from the Dispersant 3 + FM 1 run shows the most damage (see Figure 130), followed by the base oil. It is not possible to clearly distinguish whether FM 1 or Dispersant 3 individually was better at minimising paper surface damage.

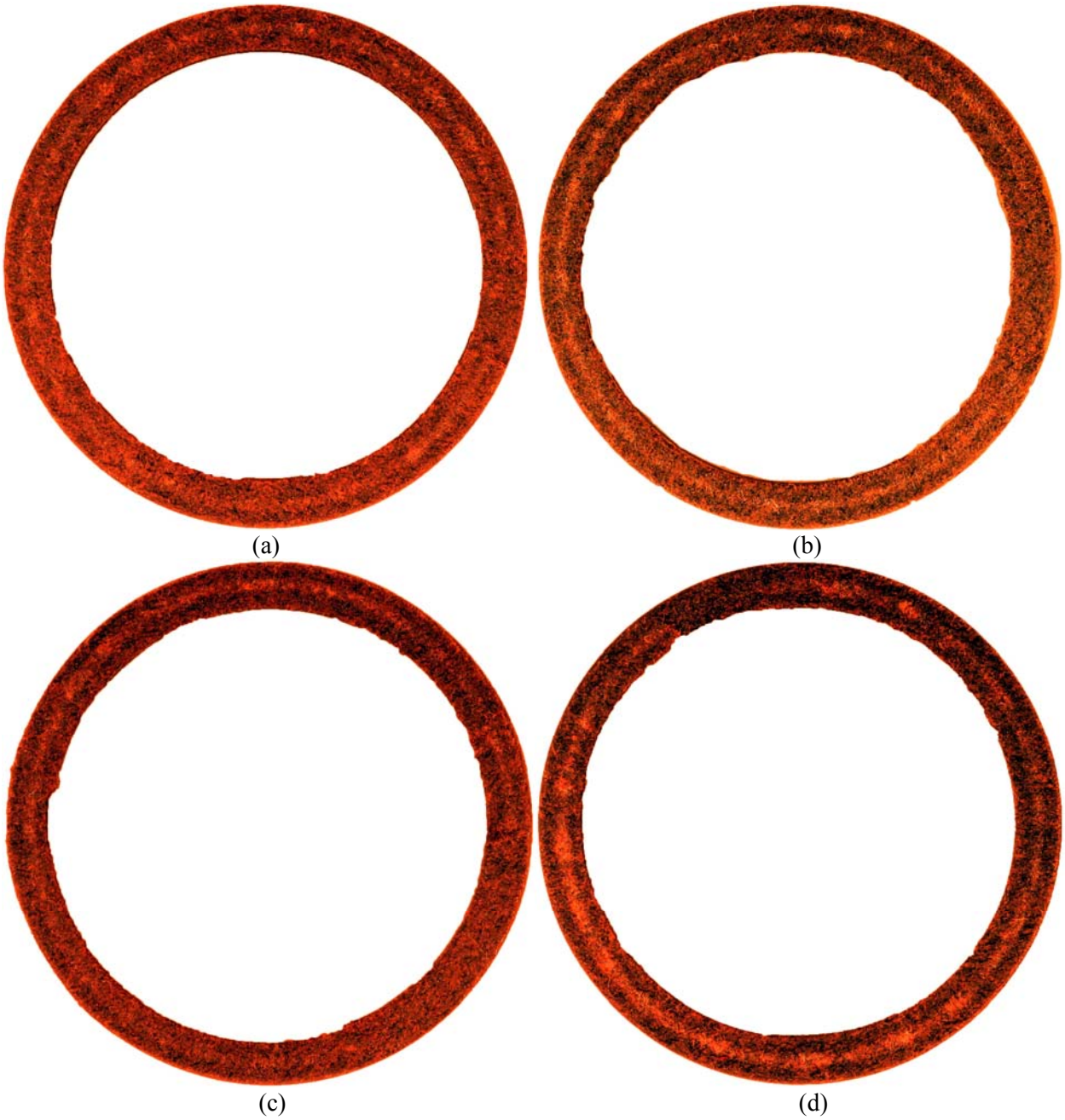

Figure 130. Macro images of worn disc (46 mm diameter) wet friction material for: (a) base oil (b) Dispersant 3 (c) Friction Modifier 1 and (d) Friction Modifier 1+ Dispersant 3. Images are processed in Adobe Photoshop to give greater definition to the worn areas.

7.3.2.2 Ball wear scar analysis

The ball surface was characterised using a macroscope. The ball wear scars are large and acutely elliptical (see Figure 131 (a)). The ball scar width for base oil is over 15 times larger than the Hertzian contact width and 20 times that for an equivalent steel-steel contact. Eguchi et al. [372] reported that the real contact area of wet friction material on steel compared to steel/steel is different by 1-2 orders of magnitude. The friction material deforms to take the shape of the ball; the compliances of the friction material in the direction of sliding is different to that perpendicular to sliding, hence the elliptical wear scar. The ball wear scar was not flat; the ball contact surface remained fairly spherical, but exhibited

groves in the sliding direction, indicating that only mild abrasion had occurred on the ball surface. A degree of caution is required when viewing the ball wear scar results, because the wear scars are not flat, the same wear volume could arise from a small wear scar with deep groves and a wide wear scar with shallow groves. Despite this, the methodology employed gave a general indication of test oil wear performance. Taking into account a certain degree of error, the single additive containing oils showed the best wear resistance (see Figure 131 (b)). The combination of Dispersant 3 + FM 1 exhibited the worst wear performance, significantly worse than base oil alone.

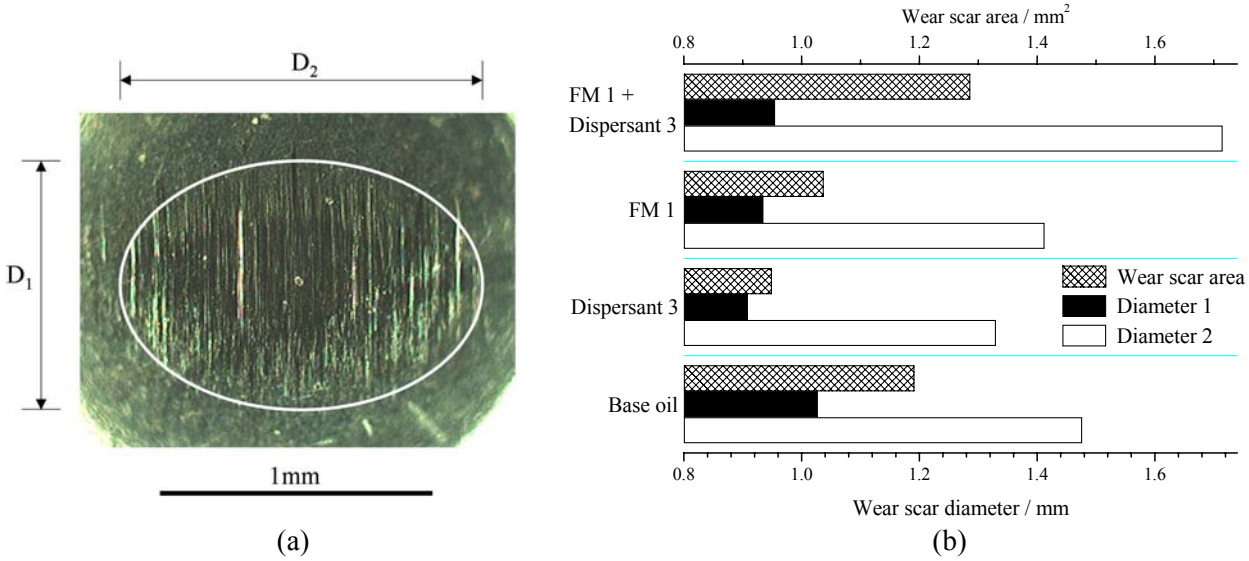

Figure 131. Ball wear scar analysis (a) characterisation of wear scar (b) wear scar results for the test oils.

7.3.2.3 Disc XPS analysis

Figure 132 shows the results from XPS analysis performed on five friction material discs: base oil only, Dispersant 3, FM 1, FM 1 + Dispersant 3, and an unused sample (as a control). Elemental analysis was carried out on the wear track and off the wear track (for the unused sample the analysis was performed in similar radial positions). The unused disc exhibited the highest oxygen, but lowest hydrocarbon and nitrogen concentrations of all the samples analysed (see Figure 132). The source of nitrogen could be the phonic resin (see Figure 46 (b)). The base oil only sample showed a lower oxygen concentration and higher hydrocarbon concentrations than the base oil, indicating the presence of a weak tribofilm from the '*impurities'* in the oil. Of the additive containing oils, FM 1 yielded the highest oxygen concentration and Dispersant 3 exhibited the highest hydrocarbon concentration. Hydrocarbon and Oxygen levels for the FM 1 + Dispersant 3 mixture were in-between that of Dispersant 3 and FM 1 alone. The most significant result is that the Nitrogen levels for the FM 1 + Dispersant 3 and Dispersant 3 only are similar.

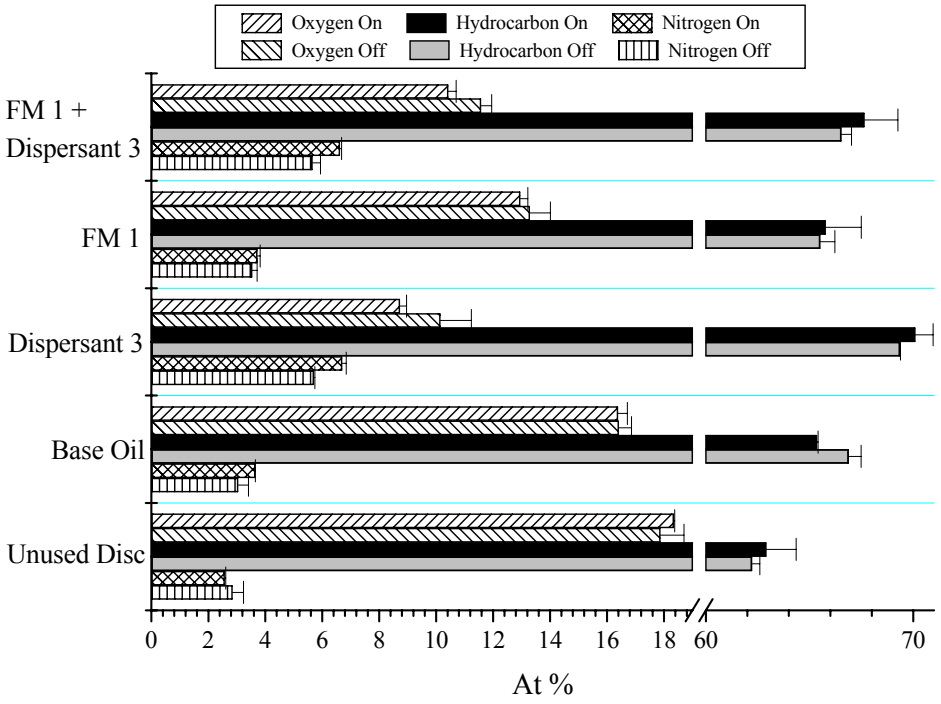

Figure 132. Disc wet friction material XPS analysis for worn and unused surfaces.

7.3.2.4 Conductivity measurements

Figure 133 shows the conductivity results for the test oils. Dispersant 3 has the highest conductivity and the base oil the lowest. The conductivity of the Dispersant 3 + FM 1 oil is half that of Dispersant 3 alone, which is not surprising considering that Dispersant 3 is present at 0.5% wt..

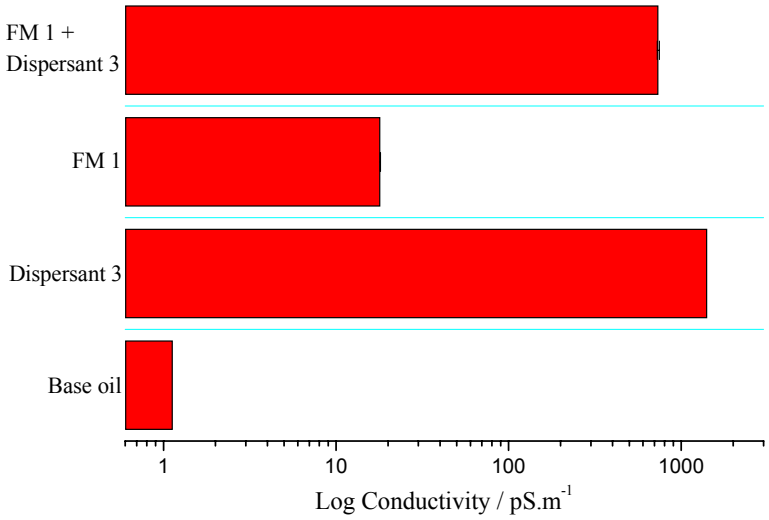

Figure 133. Conductivity of test oils.

7.4 DISCUSSIONS

7.4.1 WET FRICTION MATERIAL

The charge and COF levels for friction-material/steel contacts lubricated with base oil and Dispersant 3 containing oils are significantly higher than those produced when the same oils were used on steel/steel contacts (see Table 33). The paper surface compared to the steel is considerably rougher; rough surfaces generally reduce the lambda value and thus increase asperities contact (see Section 2.1.3). However classical EHL may not strictly apply to paper/steel contacts; adhesion and deformation between the paper disc and steel ball may play a role. The rubbing of a rough insulator (disc friction material) against a conducting material (steel ball) will lead to a major contribution of contact charging to the total charge detected. The majority of published work on electrostatic monitoring has concentrated on tribo-contacts, which have been conducting; thus contact charging has not previously been considered a major charge mechanism. Contact charging is thought to predominantly affect the DC levels (steady state magnitude) as load and sliding speed are kept constant; the two main contact conditions affecting contact charging levels. However, if the contact area of the surface increased through either wear or deformation of the composite surface, it may lead to an increase in contact charging. This could be an explanation for the high charge seen at the end of the base oil test (see Figure 129).

The FM 1 produced a lower charge than Dispersant 3; this corresponds to similar studies involving steel/steel contacts (see Section 6.3.2). However, the same studies showed that base oil produces a lower charge than Dispersant 3 and FMs. In this study the base oil charge level is similar to that of Dispersant 3. It is thought that this observation relates to the influence of the additives on contact charging. The base oil test charge level (29 minutes onwards) is the closest to charge generated by dry sliding of organic polymer against a conductor; it is thought that the high charge level is a consequence of increased contact charging during wear. The FM 1 provided a sufficient film (as indicated by the significantly low COF levels) which minimised contact charging. The similar charge levels between base oil and Dispersant 3, up until the 29th minute, suggests that the larger Dispersant 3 molecules did not cover the entire friction material; therefore contact charging was not significantly reduced. The relatively similar COF levels of Dispersant 3 and base oil compared to FM 1 also suggest this. However, the COF level is slightly higher for Dispersant 3 compared to base oil; this does infer an adsorbed Dispersant 3 film was present, even if only a minimal covering, and this reduced wear. The charge level of the FM 1+ Dispersant 3 tests was lower than the base oil, even though the wet friction material wear was greater. It is thought that the additives partly covered the friction material, even if the dominance of one additive over another is changing and antagonises wear, the presence of these additives still minimise contact charging relative to the base oil test. Further explanations of additive charge characteristics are discussed below.

	COF		Electrostatic charge /pC	
	steel / steel Ave, Std	paper / steel Ave, Std	steel / steel Ave, Std	paper / steel Ave, Std
API Group II base oil	0.103, 0.002	0.190, 0.002	0.022, 0.001	1.396, 0.348
Mono-succinimide dispersant	0.105, 0.010	0.194, 0.002	0.411, 0.192	1.266, 0.122

Table 33. Comparison of COF and electrostatic charge results from the same or similar oils tests on friction - material/steel and steel/steel (from Chapter 6) contacts under similar test conditions.

7.4.2 FRICTION MODIFIER

In order for FM 1 to significantly reduce the COF compared to base oil alone (see Figure 128), multiple layers of FMs must have adsorbed onto the fibre and resin surface. Due to the severe boundary conditions, on a nanometre scale the FMs are unlikely to form multiple layers on asperities' tips even allowing for re-arrangement of the flexible hydrocarbon tails, but they will form in the pores/valleys, effectively smoothing the surface. The presence of FMs in the pores may explain the low COF seen from the beginning of the test (see Figure 128). The FMs would be able to form multiple layers, even if the shear plane crosses the top of two adjacent asperities (see Figure 134). The roughness of the disc surface changed from 9µm at the start of the test to 5 µm on the track at the end of the test; microscopic analysis revealed that this was predominantly as a result of plastic deformation (compression of the porous surface) rather than asperity removal. This change in roughness over the duration of the test will reduce the severity of boundary conditions, which will promote greater adsorption of FMs further along asperities towards the tip, not increasing film thickness as such, but increasing surface coverage and hence the surface charge increased with time (see Figure 129).

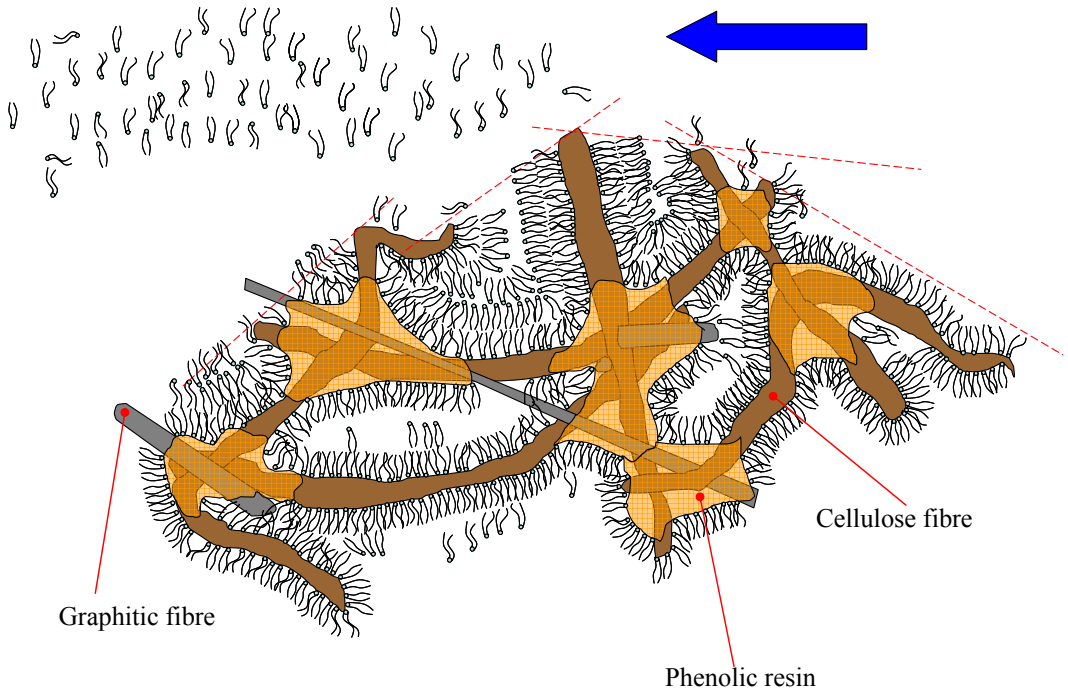

Figure 134. Schematic depicting the adsorption of FMs on wet friction material.

7.4.3 DISPERSANT

The slightly higher COF for Dispersant 3 compared to base oil infers that an adsorbed Dispersant 3 film has formed on the contacting surfaces. Previous studies with Dispersant 3 have shown that dispersant film formation on steel-steel contacts resulted in an increase in COF (see Chapter 6, when the film forms it is higher). Other researchers have used similar dispersants in wet friction material / steel tribological testing and reported that dispersants increase COF relative to base oil [83,84,254,373,374]. The base oil and Dispersant 3 COF and charge levels are quite similar, especially when compared to the FM 1 (see Figure 128 & 129), the data implies that Dispersant 3 does not form multiple layers and/or does not cover the contacting surfaces completely. The charge level for Dispersant 3 and base oil coincide between 12 and 22 minutes. A possible explanation for this is that the contact conditions during this period are such that Dispersant 3, which has a higher molecular weight and stiffer hydrocarbon tail than FM 1, is unable to maintain a stable adsorbed film. On the whole the Dispersant 3 charge signal is more stable than the base oil; in previous studies this charge characteristic has been associated with a steady state process such as stable tribofilm, equilibrium of film formation and shear (see Chapter 6), or mild wear.

The base oil and Dispersant 3 tests showed very similar charge levels during the first two thirds of the test; from 22 minutes onwards the charge signals for the base oil and Dispersant 3 diverge. The charge levels were similar up to this point, but the ball and disc wear was significantly different; so the increase in charge for the base oil, at the latter stage of the test, could be related to the onset and progression of wear for the base oil. Figure 135 (a) shows that the top surface of the composite material has been disrupted and fibres have been pulled through or have broken away from the composite matrix. The movement of fibres against one another (tribo-electrification), or the breaking of insulating fibres (by breaking bonds), will generate surface charge. The production of fibrous debris may also contribute to the overall charge level. The disc track for the Dispersant 3 containing oil did not exhibit the same degree of disruption. Matsuoka et al. [256] reported that dispersants help retain the shear strength of cellulose fibres compared to base oil; however no explanation as to the mechanism by which shear strength increased was given.

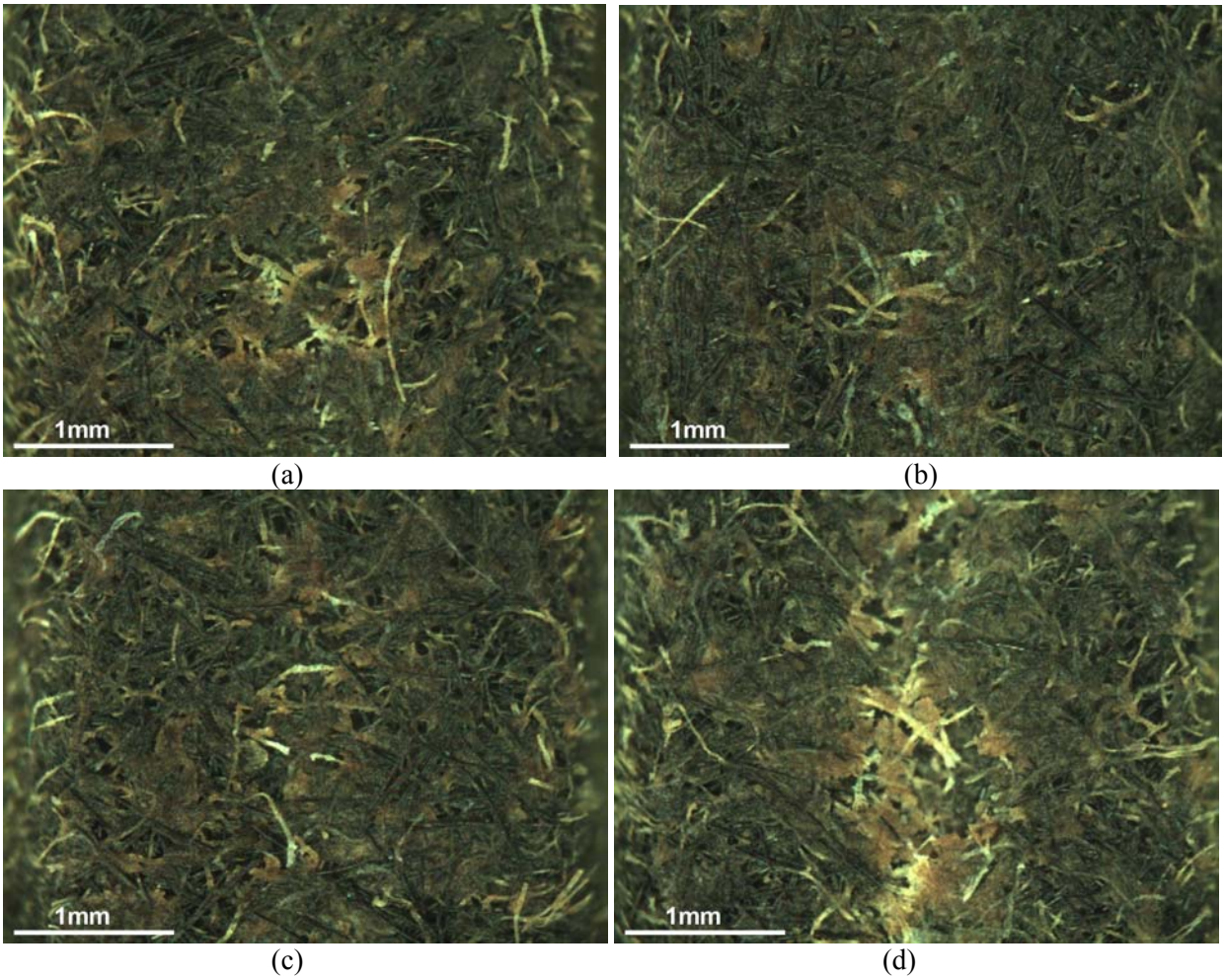

Figure 135. Macro images of worn wet friction material areas for (a) base oil, (b) Dispersant 3, (c) Friction Modifier 1 and (d) Dispersant 3 + Friction Modifier 1.

7.4.4 DIFFERENCES IN DISPERSANT 3 AND FRICTION MODIFIER 1 TRIBOLOGICAL AND SURFACE CHARGE BEHAVIOUR

FM 1 molecules have flexible hydrocarbon tails, while Dispersant 3 molecules have one stiff tail which increases viscosity locally and therefore COF. In addition, multiple layers of FM 1 molecules easily shear at the hydrocarbon tail interfaces, reducing COF, whereas Dispersant 3 molecules bind tightly to the surface and require a greater shear force to remove them (see Figure 136).

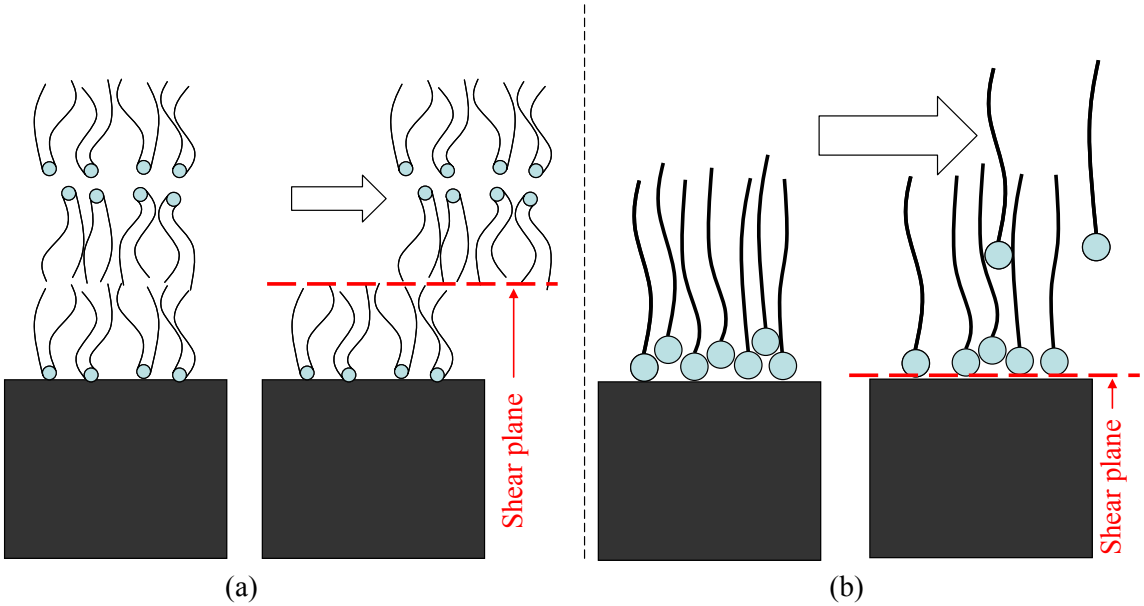

Figure 136. Shearing and corresponding friction behavior of (a) Friction Modifier 1 and (b) Dispersant 3.

Dispersant 3 or FM 1 will acquire a positive charge via reaction with an acidic surface site, thus forming an acid-base pair (see Figure 137 (a) & (b)). Desorption of the charged molecules results in a negative charge on the surface (see Figure 137 (c)). The superior solubility of the high molecular weight Dispersant 3 versus FM 1 can account for the increased charge detected; the charged Dispersant 3 cation is more easily desorbed. Similarly the high molecular weight and length of Dispersant 3 relative to the contact clearances make Dispersant 3 most likely to be sheared from the surface compared to FM 1. Although alignment of the FM 1 hydrocarbon tails is caused by electrostatic and van der Waals forces, shearing of theses layers does not have the same likelihood to generate surface charge as dispersants. The electrostatic charge stability also relates to the shearing and stripping of FM 1 and Dispersant 3 respectively. Due to the high mobility and strong orientation forces, sheared-off layers are quite easily rebuilt to their original state [103] hence the fairly linear charge trace. Dispersant 3 molecules are large and bulky compared to FM 1 molecules and take time to re-adsorb, so areas of the surface are left deficient of Dispersant 3 for a period of time, consequently the charge levels are more variable than FM 1. This follows observations for FMs and Dispersants 3 in Chapter 6.

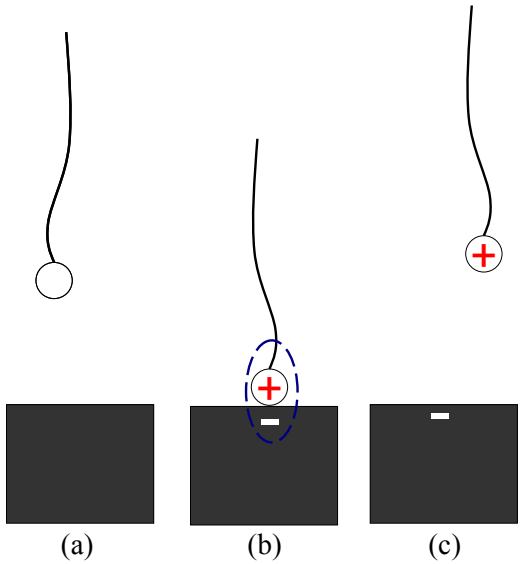

Figure 137. Mechanism for surface charge generation by succinimides (a) free dispersant (b) adsorption – creating an acid-base pair, and (c) desorption.

The nitrogen level on the paper surface indicates that, lubricated with Dispersant 3, the paper becomes nitrogen enriched (even though the nitrogen contained in Dispersant 3 is lower than FM 1). For this to occur the dispersant must decompose in the contact; this is probably through cleavage of a carbon-carbon bond near the hydrocarbon tail / polar-head linkage in the molecule, during shear. However it could also occur thermally via a reverse alkylation reaction of the succinimide portion of Dispersant 3 (see Figure 138). These processes would leave the nitrogen rich polar-head on the surface. Dispersant 3 has the possibility of forming 3 amide groups, whereas FM 1 only has one. Consequently, FM 1 is more likely to desorb intact (one surface bond versus 3).

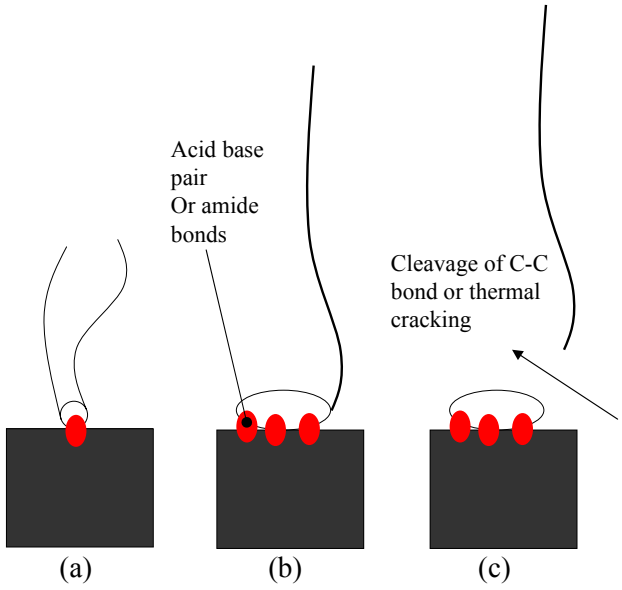

Figure 138. Schematic of additive adsorption showing (a) FM 1 forms one amide, (b) Dispersant 3 forms three amides, and (c) decomposition of Dispersant 3.

The difference in friction material wear for Dispersant 3 and FM 1 is indistinguishable (see Figure 135 (b) & (c) respectively). Conversely there appeared to be a difference in steel ball wear scar between the two additives. Dispersant 3 protected the ball better than the FM 1, because it is more polar and has stronger adsorption to the ferrous surface.

7.4.5 DISPERSANT 3 + FRICTION MODIFIER 1

For the combination of FM 1 and Dispersant 3, the COF and charge data indicated that the FM 1 dominated the tribofilm between 2 and 9 minutes. Kamada et al. [84], noted a similar finding – that FM exerts the controlling action over dispersant when blended at the same weight – for dispersant and a phosphorous based FM. The same authors also argued that this was an unlikely finding since the dispersant molecule is significantly larger than the FM, therefore the larger part of the sliding surface is coated with dispersant molecules; however this assumes that the dispersants are able to sufficiently cover the contact area. FM 1 is smaller, more mobile and flexible than Dispersant 3, which is preferential for FM 1 film formation under the test conditions, where clearances are likely to be small. During running-in, deformation of the paper material occurred, so the film thickness to composite roughness increased, allowing Dispersant 3 into the contact and competition between FM 1 and Dispersant 3 for surface sites ensued. Despite FM 1 being more mobile, Dispersant 3 is more polar and can therefore compete with FM 1 for surface sites. The charge trace shows Dispersant 3 dominates the tribofilm between 11 and 17 minutes. The charge level then drops, implying that the FM 1 is dominating the tribofilm content. It is possible in the preceding period that wear and sufficient roughening of the surface occurred to reduce the film thickness to composite roughness ratio, minimising Dispersant 3 adsorption. For the remainder of the test the charge level is highly dynamic, varying in-between levels similar to FM 1 and Dispersant 3 alone. By the end of the test the charge and COF levels are of the same magnitude as the Dispersant 3 only. In addition the XPS analysis showed that the nitrogen levels for the mixture was the same as for the Dispersant 3 only test. Therefore, charge, COF and XPS data all infer that Dispersant 3 dominated the tribofilm by the end of the test. Whether Dispersant 3 displaces FM 1 by the end of test or whether Dispersant 3 forms a substantial layer on top a FM 1 layer is not clear, but the displacement of FM 1 from the surface is more likely to result in an increase in friction (see Figure 139).

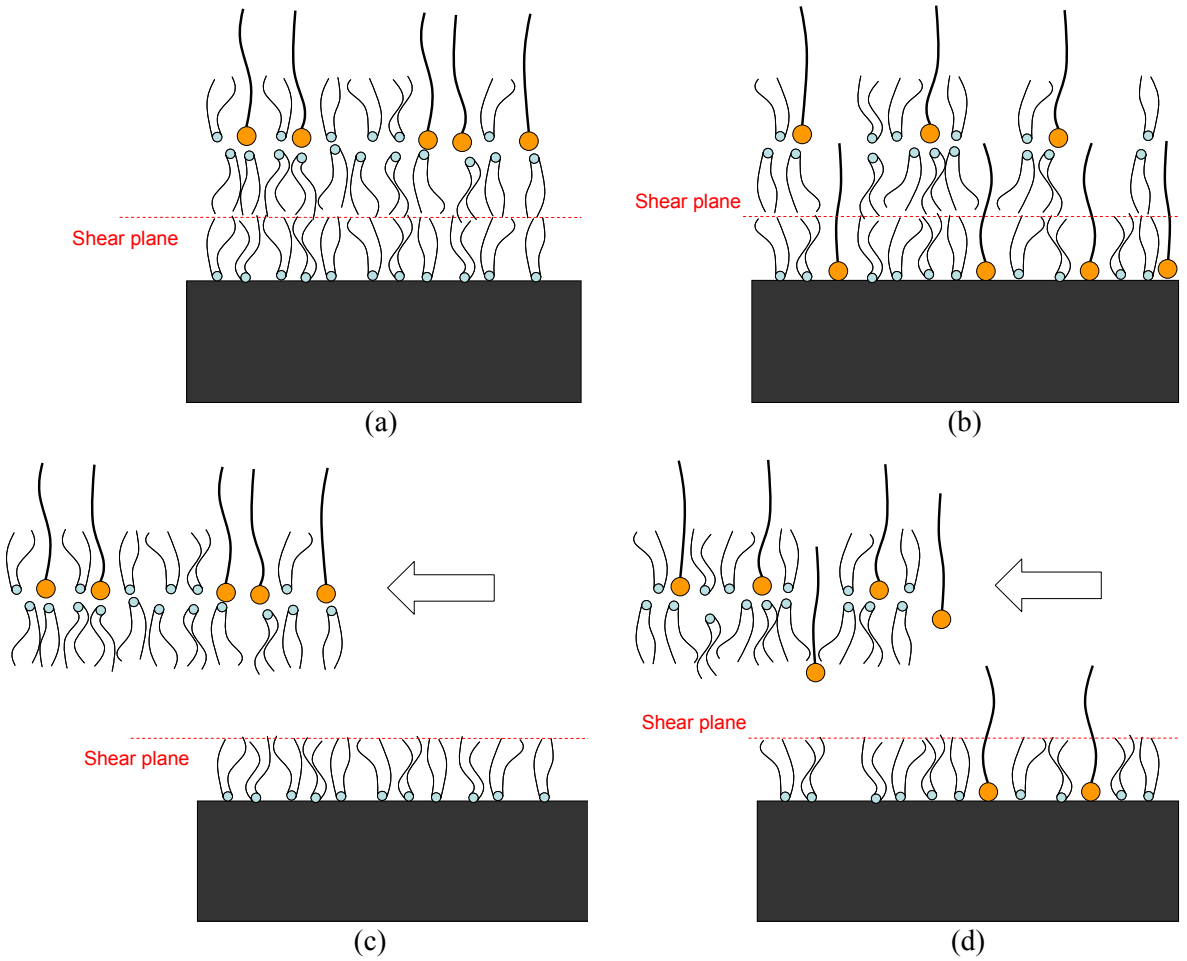

Figure 139. Schematic depicting the layering permutations of Friction Modifier 1 and Dispersant 3 molecules as a (a) dispersants on top of friction modifiers, and (b) dispersants mixed amongst the friction modifiers. The shearing of these two scenarios is shown in (c) and (d) respectively.

Other researchers have reported that during wear, the surface composition of wet friction material changes and this effects preferential absorption of one additive over another [375,376]. Although likely, evidence in this study suggests that it is the interaction between the two additives which produces wear. The disc and ball wear for the FM 1 + Dispersant 3 mixture was the greatest among the tests run, clearly showing antagonism between the two additives. Figure 135 (d) shows disruption of the paper surface, with fibres detached from the main composite matrix, leading to large holes/spaces along the wear track. The degradation of the surface is indicative of a *'fatigue'* like process. The charge data shows that the dominance of Dispersant 3 and FM 1 on the paper surface is continually changing. Also, as the COF levels increase so the peaks of the oscillations within the overall trend increase (see Figure 128). This perhaps leads to an oscillating high friction/low friction response resulting in a *'fatigue'* process/loosening and breaking of fibres.

Both FMs and dispersants are used in ATFs to minimise shudder and improve torque capacity respectively, yet they have resulted in the greatest amount of wear and the most unstable friction response. Clearly an incorrect balance of FMs and dispersants could have disastrous consequences for durability and

shudder. Guan et al. [377] suggested that the identification – through bench tests – of ATF-friction material interactions that accelerate friction material degradation may be related to ATF effects on the service life of AT clutches. Thus the test procedure described in this Chapter could be useful for FM and dispersant development in ATF additive packages.

7.5 CONCLUSIONS

FM 1 produced low friction and low surface charge, whereas Dispersant 3 exhibited high friction and charge characteristics. Both additives singularly were effective at reducing friction material and steel ball wear compared to base oil. XPS analysis revealed that when FM 1 and Dispersant 3 are combined the friction material nitrogen levels are similar to Dispersant 3 alone, indicating that by the end of test the Dispersant 3 is dominating the tribofilm content. The friction trace shows a gradual increase over the test duration, which infers that Dispersant 3 is steadily dominating the tribofilm content. The electrostatic charge data suggests that competition for surface sites is an extremely dynamic process, with each additive appearing to dominate surface coverage at different times. The dominance of one additive over the other is thought to be a function of friction material compression/deformation and wear. The competition between the two additives is thought to mechanically weaken the friction material. The information gained by these tests could enable the reactivity and concentration of these additives in a formulation to be tailored to suit ATF applications. Electrostatic charge monitoring could enable tests to be stopped at critical moments – as identified by charge features – so that detailed surface chemical analysis maybe carried out off-line. The real-time charge/film information may be a valuable tool for the optimisation of additive chemistry, and for the formulation of finished ATFs.

8 EVALUATION OF GEAR OIL ADDITIVES IN A SIMULATED MANUAL TRANSMISSION CONTACT

8.1 INTRODUCTION

The previous Chapter (7) investigated the interaction between surface active additives through real-time electrostatic charge and COF measurements as well as off-line wear analysis. Due to the success of real-time charge measurements to identify the dynamic nature of the interaction between two physically adsorbing additives (Dispersant 3 and FM 1) and the negative effect this has on wear resistance, a similar approach was undertaken for the work presented in this Chapter. The interaction between two chemical forming additives hydrocarbyl-polysulphide and dispersed potassium-borate, which are used to lubricate manual transmission synchronisers was investigated. The nature of a tribofilm which forms from a binary additive oil can be more complicated than the resultant/composite of the films which form when the additives are used singularly, especially for chemical film forming additives. Also of interest is, whether the interaction between these additives during film formation is dependent on surface chemical composition; synchronisers typically consist of a ferrous-brass pair. This Chapter presents a series of pin-on-disc wear tests, using a brass disc and steel ball, intended to mimic the metallurgy of synchroniser ring contacts in a manual transmission. Real-time surface charge and coefficient of friction (COF) measurements, along with off-line XPS (x-ray photoelectron spectroscopy) elemental depth profiling, are analysed with respect to film composition and formation mechanism.

8.1.1 AIMS

The work presented in this Chapter aimed to assess whether electrostatic charge monitoring could give insight into the nature of the films produced on brass and steel surface by hydrocarbyl-polysulphide and dispersed potassium-borate additives, and how interaction between the two additives affects film formation.

8.2 EXPERIMENTAL PROCEDURE

A PCS instruments MTM was employed in Pin-on-Disc mode, under pure sliding (see Section 3.1.1 & Figure 60). Details of the instrumentation, data acquisition and signal processing can be found in Section 3.5.

8.2.1 SAMPLES, TEST CONDITIONS AND PROCEDURE

The wear test specimens consisted of a brass MTM disk and a 6mm AISI 52100 steel ball. The chemical and physical properties of these materials are shown in Table 18 & 19 respectively.

The test consisted of two stages (see Table 22); the first involved a reduction of sliding speed from 4.5 m/s and 0.6 m/s over a period of 2 minutes 10 seconds, with decreases every 10 seconds. This stage was designed to replicate increasingly more severe boundary lubrication conditions experienced by the gear and synchroniser ring prior to equalisation of their peripheral speeds. The second stage employed a constant sliding velocity of 0.2 m/s for 33 minutes; the sliding velocity used was similar to other bench test transmission simulations [151]. For both stages a constant load of 7 N was employed; this produces a contact pressure of 964 MPa, slightly higher than normally experienced by the synchroniser.

8.2.2 BASE OIL RHEOLOGY AND ADDITIVE CHEMISTRY

As in the previous Chapter (7), an API Group II base oil (see Table 20) was used because of repeatability. A dual-component additive system was examined employing potassium borate and hydrocarbyl polysulphide gear oil additives (see Figure 45 & 44 respectively). The mean particle size of the colloidal potassium borate was 163 nm (as characterised using a Horiba Instruments LA920 – Laser Particle Size Analyser). The dispersant length was approximately 7 nm; therefore the potassium borate was 149 nm. More details of a similar potassium borate additive can be found in [243]. The hydrocarbyl polysulphide additive varies in molecular weight from 144 to 390, and has an average molecular size of about 9 Å.

The work presented in this Chapter studied individual components, the effect of combining them, as well as seeding additives mid-test (see Table 34). In order to understand how these additives interact and which one drives initial film formation, time-delayed introduction of each additive component (hereafter referred to as seeding) was carried out. The seeding experiments were conducted in a similar manner to the standard test, except that the second component of the binary system (borate or sulphur additive) was introduced approximately 16 minutes into the *'wear'* stage. Both permutations were tested. All test oils were blended to 1% by weight, to minimise changes in rheological properties; the mixed and seeded set at 0.5% by weight for individual additives (i.e. 1% by weight in total).

Test Number	Oil Blend
1	Group II Base oil
2	Group II Base oil + 1% wt. potassium borate
3	Group II Base oil + 1% wt. hydrocarbyl polysulphide
4	Group II Base oil + 0.5% wt. potassium borate + 0.5% wt. hydrocarbyl polysulphide
5	Group II Base oil + 0.5% wt. potassium borate + Seeded 0.5% wt. hydrocarbyl polysulphide
6	Group II Base oil + 0.5% wt. hydrocarbyl polysulphide + Seeded 0.5% wt. potassium borate

Table 34. Lubricant Test Matrix.

8.2.3 OFF-LINE ANALYSIS

Both, on/off wear scar surface composition and elemental depth profiling was carried out on worn brass disc and steel ball samples (see Section 3.6.4.1 & 3.6.4.3). The ball wear scars were measured using an optical microscope (see Section 3.6.2.3); wear scars were circular (measurements in direction of and perpendicular to sliding were similar), therefore wear scar diameter was deemed sufficient to characterise the worn ball. Brass disc wear, was analysed by performing 2D Taylor Hobson Talysurf profilometry (see Section 3.6.2.2) at four radial positions (typically at 0°, 90°, 180° and 270°); wear track depth and height were averaged across the four readings. Conductivity measurements (see Section 3.6.1) were carried out on test oils 1-4 (see Table 34).

8.3 RESULTS

8.3.1 ON-LINE DATA

8.3.1.1 Stage one

All the test oils exhibited an increase in COF, with decreasing sliding speed, during stage 1; this is associated with increasing asperity contact (see Figure 140). The potassium borate additive produced the highest COF, followed by base oil, the binary combination of additives, and then polysulphide additive. This suggests that the borate additive forms a COF increasing film; whereas the polysulphide film reduces COF. There was a large increase in COF when the sliding speed was decreased from 0.6 m/s to 0.2 m/s for the additive containing oils. The mixture of the borate and polysulphide additives yielded a COF level between that of its individual components; but still lower than base oil.

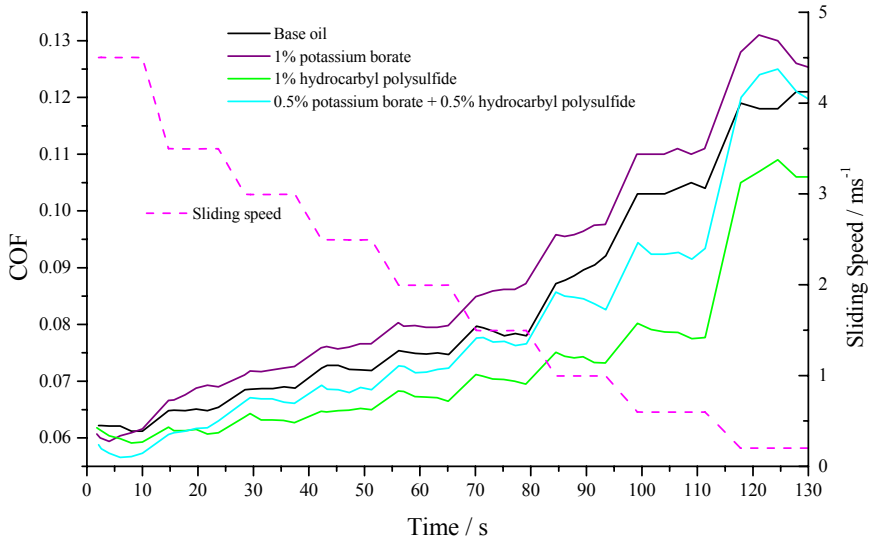

Figure 140. Stage one COF data for oils tested.

Base oil yielded the lowest charge level (the same observation as seen in Chapter 6) and charge remained low throughout stage 1 (see Figure 141). Initially (at high sliding speed), all the additive containing oils exhibited relatively high charge levels; these dropped to a baseline level as sliding speed decreased (time increased). Both the borate additive and the combination showed a stepped increase in charge with decreasing sliding speed below 1.5m/s (70s) and 0.8m/s (100s) respectively. Like the COF trace, the largest increase in charge was seen for sliding speeds 0.6 m/s to 0.2 m/s; but whereas this was seen for all additives for the COF, an increase in charge was only seen for the borate additive containing oils.

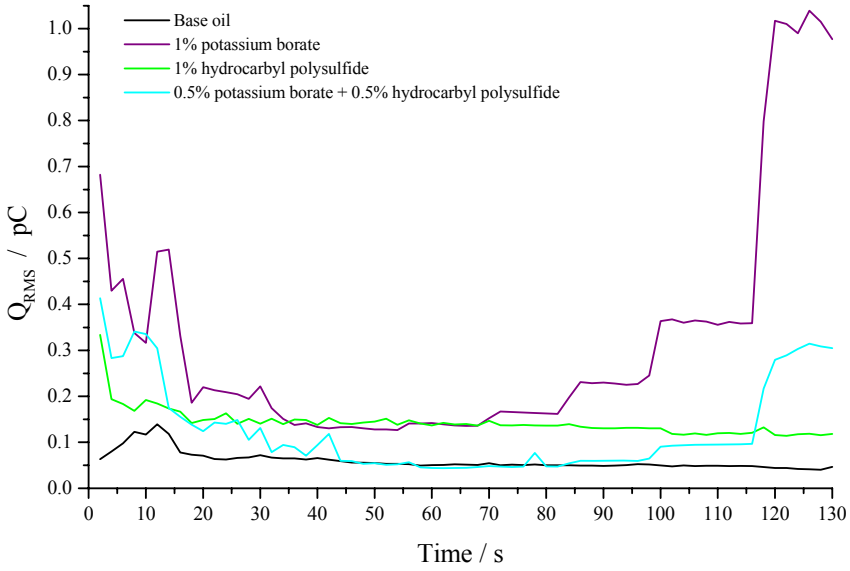

Figure 141. Stage one charge data for oils tested.

8.3.1.2 Stage 2 non-seeded

The base oil COF exhibited a steady and relatively linear increase over the test duration (see Figure 142). The polysulphide additive exhibited the lowest and most variable COF of all the oils tested. The borate additive produced a relatively high COF level and it reached stable behaviour 8 minutes onwards, whereas the polysulphide additive does not appear to have exhibited stable behaviour until 22 minutes onwards. The friction trace for the borate additive and base oil cross at approximately 20 minutes. Combining the borate and polysulphide additives produced a COF trace that more closely resembled the borate additive than polysulphide, and it was more stable than the polysulphide.

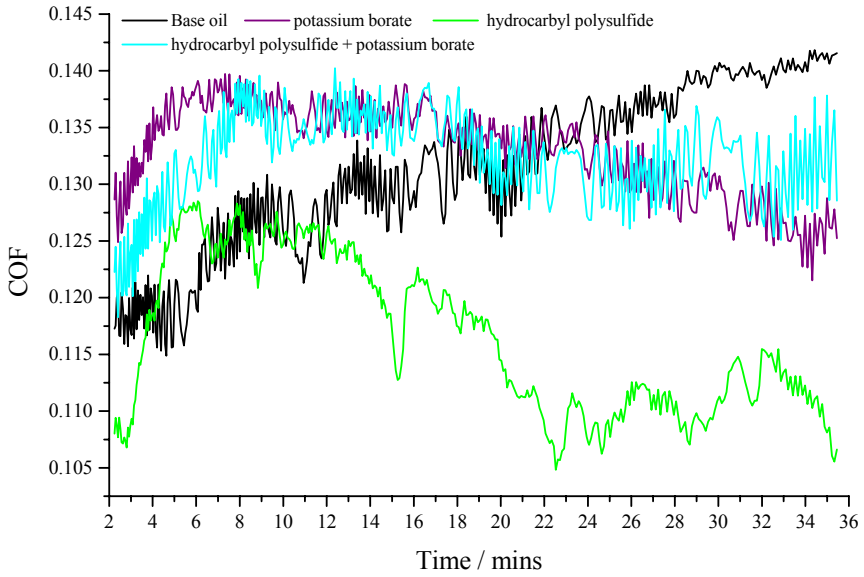

Figure 142. Stage two coefficient of friction traces for base oil, potassium borate, hydrocarbyl polysulphide, and hydrocarbyl polysulphide + potassium borate.

The lowest surface charge (0.04 pC) was observed for base oil test (see Figure 143), which has been previous observed for steel/steel contacts under similar test conditions (see Chapter 5 & 6). The charge level for the polysulphide additive test, like the base oil, was low and stable. The most variable charge was observed for the borate additive; the charge trace contained regular small pulses that occurred on average every 13.8 seconds, which was not associated with the disc rotational frequency (1.57 Hz). The combination of additives produced a charge level less than 50% of the borate additive, but significantly higher than the polysulphide. In addition the charge signal was more stable when the polysulphide and borate were combined, than the borate additive alone. The individual additives and base oil exhibited a reduction in charge with time, whereas the charge level for both additives combined increased with time.

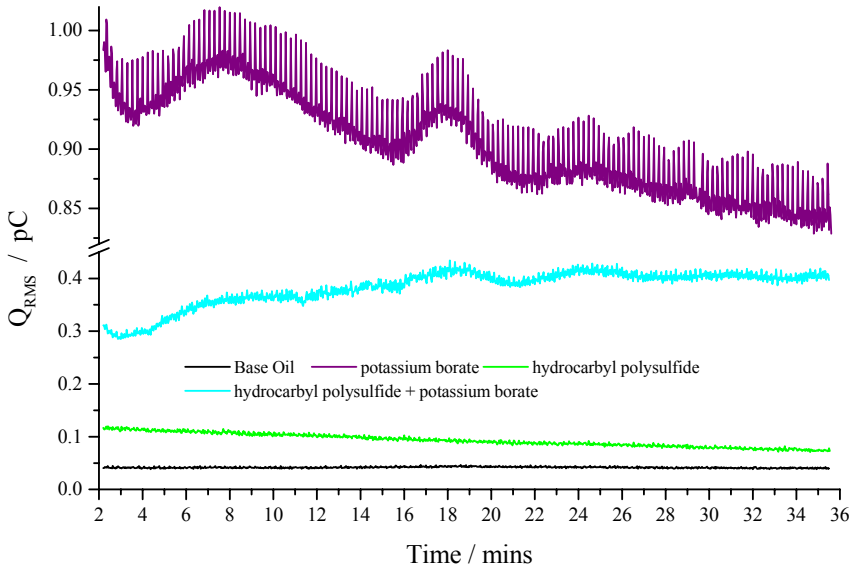

Figure 143. Stage two electrostatic charge traces for base oil, potassium borate, hydrocarbyl polysulphide, and hydrocarbyl polysulphide + potassium borate.

8.3.1.3 Stage 2 seeded

Both seeded tests created dynamic COF and charge traces and therefore have been plotted separately to the non-seeded tests. During the beginning of the test, where only the borate additive was present, a reduction in charge and peak in charge occurred at 4 and 7 minutes respectively (see Figure 144). These features also appeared in the borate additive only run (see Figure 143). Although the COF at the beginning of the test was similar to that of the borate additive only, the COF trace increased in a relatively linear fashion (over the first 16 minutes), rather than increasing, reaching a peak and then reducing as in the borate additive only run; possibly due to a longer induction time for film formation with one-half the borate concentration. After the point that the polysulphide additive was seeded into the oil, there was a step drop in charge level and an increase in COF that progresses to a COF of 0.15 at the end of the test; the highest seen for all tests in this study. The charge level was also the highest seen for all experiments in this study. Again, regular charge pulses occurred every 13.8 seconds; when the polysulphide additive was seeded, the pulses persisted.

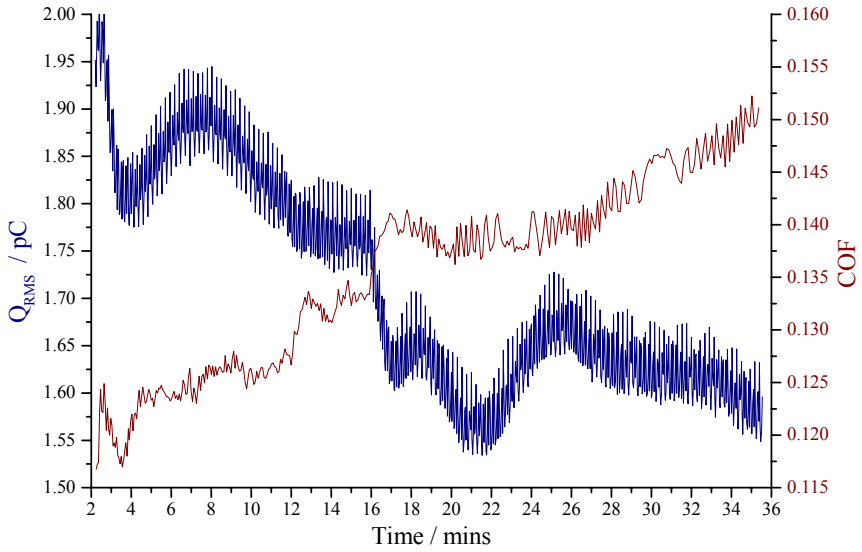

Figure 144. Stage 2 electrostatic charge and coefficient of friction results for test 5: 0.5% wt. potassium borate + 0.5% wt. hydrocarbyl polysulphide seeded in at 16 mins.

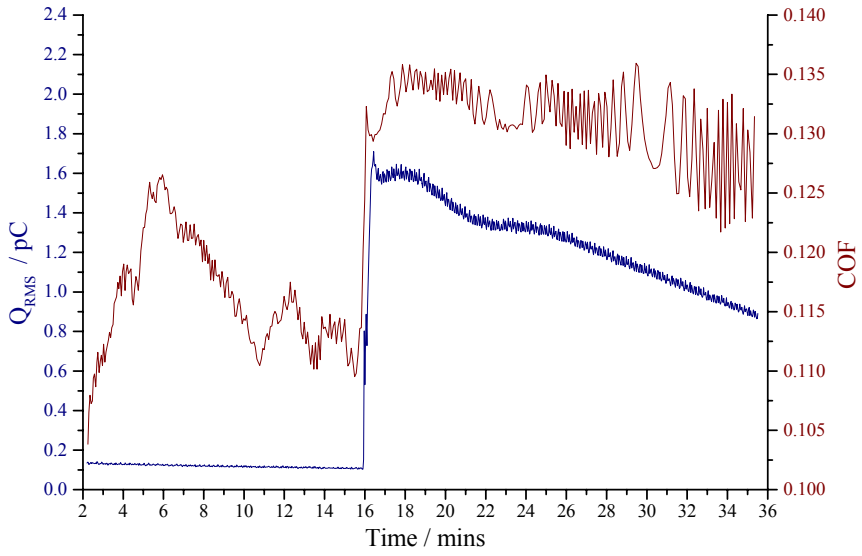

Figure 145. Stage 2 electrostatic charge and coefficient of friction results for test 5: 0.5% wt. hydrocarbyl polysulphide + 0.5% wt. potassium borate seeded in at 16 mins.

For the polysulphide + borate seeded experiment the COF level and variability (see Figure 145) was similar to the polysulphide additive only run (see Figure 142); during the first 16 minutes, the charge level was low, and dropped linearly from the start of the test. Seeding in the potassium borate additive yielded a 1.5 pC increase in charge and a 0.02 increase in COF. This step change in charge was more significant than the borate additive + the polysulphide additive seeded test. After seeding, the COF became more stable and both COF and charge decrease steadily over the remainder of the test. The charge pulses

appeared, once the borate additive is seeded into the polysulphide additive, but they are not as pronounced in magnitude as the borate additive alone, or borate + polysulphide seeded (see Figure 143 & 144).

8.3.2 POST-TEST ANALYSIS

8.3.2.1 Specimen wear

The base oil test yielded the highest steel ball wear and the polysulphide produced the greatest ball wear resistance (see Figure 146). The ball wear for the borate additive was only slightly larger than the polysulphide additive. It is interesting to note that the combination of borate and polysulphide produced a wear scar, greater than that produced by the additives singularly, indicating an antagonistic interaction between the two additives. Both permutations of seeding produce the same wear scar diameter, which was better than base oil, but worse than the polysulphide singularly, borate singularly and both additives in combination from the start.

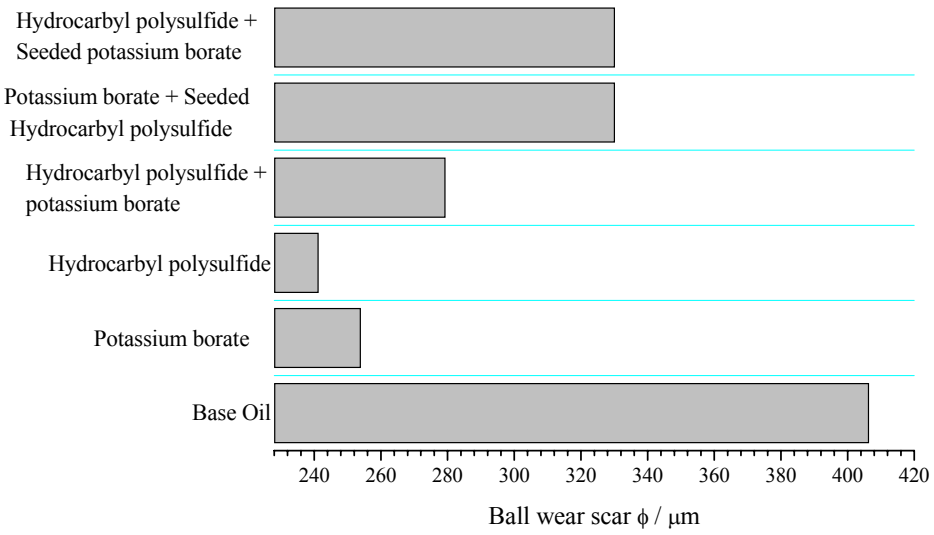

Figure 146. Steel ball wear scar diameter.

The borate additive with polysulphide seeded, borate singularly and base oil produced the greatest brass disc wear (see Figure 147). This indicates that the borate additive exhibited negligible brass disc anti-wear properties when employed as the only anti-wear additive, or when allowed to react first with the brass surface. The greatest brass disc wear resistance came from the polysulphide additive + borate additive seeded and polysulphide only test, suggesting that the polysulphide was the significant factor for brass disc anti-wear performance. However seeding of the borate additive after the polysulphide arguably produced lower wear than the combination from the start. This suggests that initial competition for the surface between the two additives at the start of the test antagonises wear resistance, and delaying the

introduction of the borate additive was beneficial for minimising brass disc wear. This infers that initial reaction of sulphur additive was beneficial for brass wear performance, and that a highly surface active sulphur compound is desirable such that the sulphur compound will adsorb and react before the borate.

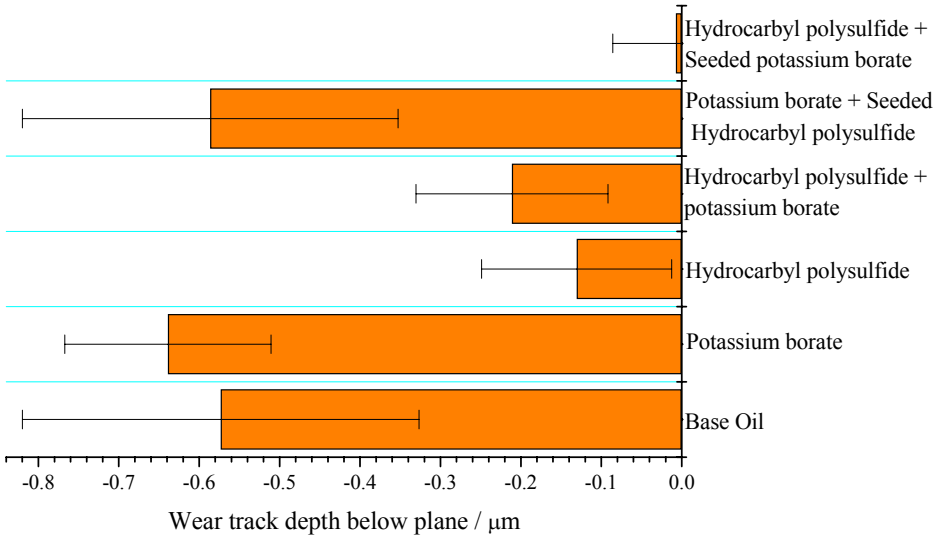

Figure 147. Brass disc wear track depth.

8.3.2.2 Conductivity

The oil containing the borate additive has the highest conductivity followed by: the combination, base oil and the polysulphide additive (see Figure 148). It is interesting to note that the polysulphide conductivity was nearly half that of the base oil, whereas the charge levels for the polysulphide were twice that of the base oil. This indicates that disc surface charge, as detected by electrostatic sensor, was related to additive-surface interaction rather than the bulk oil electrical properties; this is similar to findings in Chapters 6 & 7.

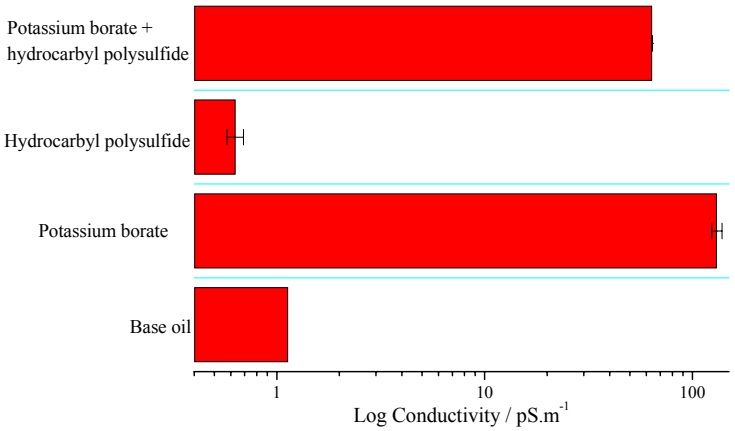

Figure 148. Conductivity of test oils.

8.3.2.3 Steel pin elemental depth profiling

Figure 149 showed the atomic concentration of various elements across the depth of the tribofilm for steel balls. The plateau in the iron atomic concentration was assumed to indicate the position of the steel surface and thus an indication of the tribofilm thickness. For the steel balls, the borate additive yielded the thickest film. The films produced by the polysulphide additive and the mixture were about half this thickness. All steel balls show evidence of material transfer (presence of copper), with the polysulphide additive having the greatest amount, followed by the borate additive and the mixture.

The tribofilm formed on the steel ball by the borate additive consisted of small concentrations of potassium and boron throughout the depth of the film (see Figure 149 (a)). The film formed by the polysulphide additive on the steel surface contained a high concentration of sulphur, which occurred near the top of the film (see Figure 149 (b) at 0 nm sputter depth). The boron concentration for the combination of borate and polysulphide was higher than the borate alone, despite the concentration being half of that used singularly (see Figure 149 (c)). Similarly, the potassium levels were higher for the mixture than for the borate additive alone. The film consisted of a mainly boron containing top layer with a predominately sulphur layer under it.

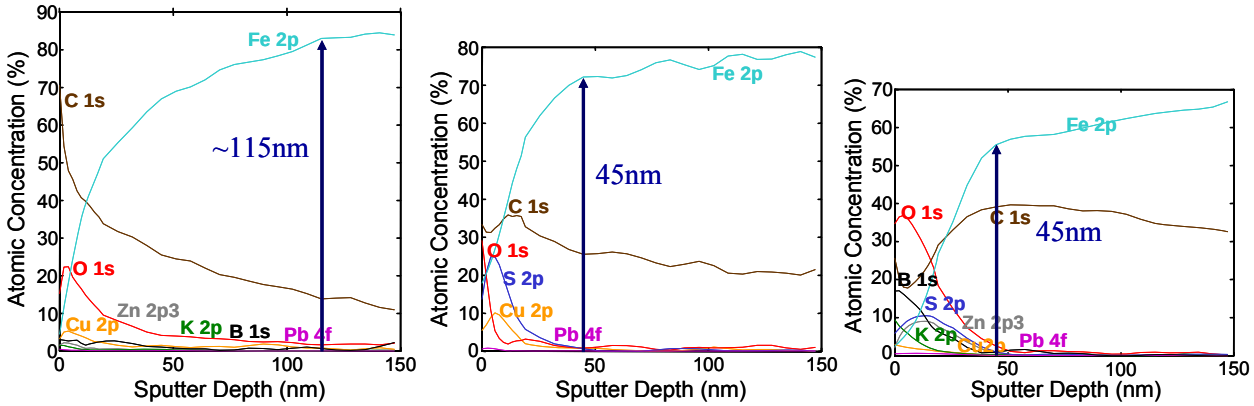

Figure 149. XPS elemental depth profiling of Steel pins (a) potassium borate (b) hydrocarbyl polysulphide (c) potassium borate + hydrocarbyl polysulphide.

8.3.2.4 Brass disc elemental depth profiling

Figure 150 showed the atomic concentration of various elements across the brass tribofilm, and like the steel elemental depth profiling, the plateau in the copper atomic concentration was assumed to indicate tribofilm thickness. The borate additive produced the thinnest film and the mixture the thickest film; the polysulphide additive thickness falls in-between these levels. The presence of iron on the brass discs was not detected; therefore material transfer was in one direction only (softer metal to the harder metal – similar to that seen in service).

The borate tribofilm formed on the brass surface was thinner than the steel surface (see Figure 150 (a) and Figure 149 (a) respectively). The brass surface also showed the presence of sulphur, which was not observed on the steel disc. Potassium was present at a much higher level on the brass surface than on the steel surface. Boron was present but not at a significant level to be detected in the depth profiling. The polysulphide tribofilm contained a high sulphur concentration at the top surface, which penetrated the depth of the film (see Figure 150 (b)). The mixture yielded the thickest tribofilm on the brass disc, but thinnest on the steel ball (see Figure 150 (c)). The tribofilm for the mixture has a lower concentration of sulphur than the polysulphide additive alone and the potassium concentration was lower than the borate additive only. These later observations are understandable given that the mixture has half the treat rate of the individual additive tests. However, despite the lower treat rate, boron was present in the tribofilm at much higher concentration than that produced by the borate additive only test (where it is present at twice the concentration). Like the polysulphide additive film, sulphur penetrated the depth of the film for the combination, whereas boron was predominately present at the top of the tribofilm; boron alternated across the depth of the film.

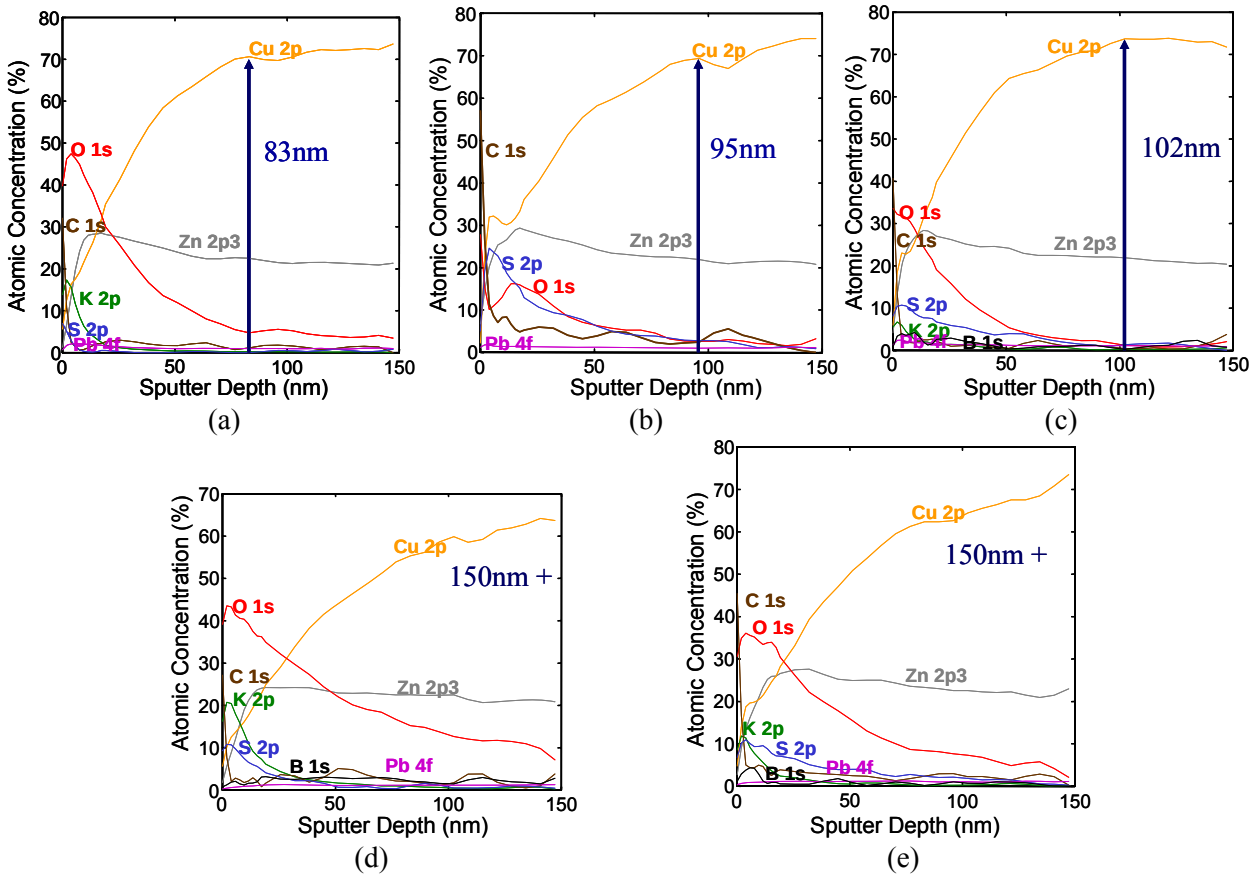

Figure 150. XPS elemental depth profiling of brass discs lubricated with; (a) potassium borate; (b) hydrocarbyl polysulphide; (c) potassium borate + hydrocarbyl polysulphide; (d) potassium borate + hydrocarbyl polysulphide seeded and (e) hydrocarbyl polysulphide + potassium borate seeded.

The tribofilms produced by the seeded experiments are thicker than those produced by single additives and the mixture (non-seeded). The borate additive + the polysulphide additive seeded film contained the highest concentration of potassium close to the top of the film (see Figure 150 (d)) of all the tests. There was a high concentration of sulphur at the top of the film again, but, like the borate additive only run, the sulphur concentration tailed off over a much shorter depth than the polysulphide additive only (see Figure 150 (e)). The polysulphide additive + the borate additive seeded produced a predominantly sulphur containing film (see Figure 150 (e)), which, like the hydrocarbyl polysulphide additive only (see Figure 150 (d)), has a higher concentration at the top of the film, but penetrated all the way to the brass surface. It is noteworthy that the maximum sulphur concentration, which occurred towards the top of the tribofilm, was the same for all binary additive oils, whether seeded or not.

8.4 DISCUSSIONS

8.4.1 XPS ANALYSIS

8.4.1.1 Polysulphide

The formation and nature of a tribofilm formed by organic sulphur containing compounds is fairly well characterised; sulphur reacts to form metal sulphides [103]. Formation is believed to be through physical adsorption onto the iron surface of *S–S(x)–S* group (see Figure 44), then cleavage of the sulphur–sulphur bond to give an inorganic sulphur containing layer. A similar film formation process was thought to occur on a brass surface. XPS analysis identified the presence of sulphur/sulphide and sulphate in the brass tribofilm (see Figure 151).

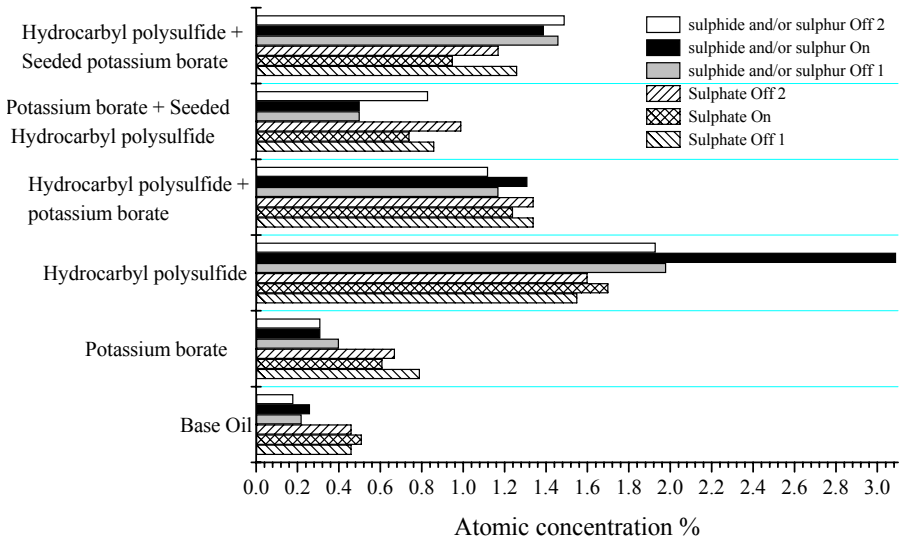

Figure 151. Test oils sulphide (and/or sulphur) and sulphate concentrations for the brass tribofilm.

8.4.1.2 Potassium borate

Dispersed potassium borate produced a thick boron containing film on the steel ball, but the presence on the brass surface was negligible in the elemental depth profiling (see Figure 150), and the lowest of all borate containing oils (see Figure 152). Similar to calcium sulphonate detergent (see Section 2.3.4.2), a sequence of processes, which resulted in a borate tribochemical film is proposed, based on that described by Hu et al. [238] for dispersed magnesium and lanthanum [236] borate on steel surfaces. Firstly dispersed potassium borate was adsorbed onto the scar/rubbing surface (see Figure 153). Shearing breaks-up the adsorbed micelles, resulting in an amorphous layer containing borate and potassium, as well as adsorbed dispersing agent. High contact pressure and temperature, as well as further shearing causes polymerisation (through dehydration) of the amorphous borate particles into a glassy film. The

tribochemical film may also contain small amounts of FeB [149,236,247], Fe_2B [247] and B-Fe-O [149]. Although the literature is not unanimous on the specific film formation mechanism, it was generally acknowledged that surface charge and electric field play a major role. Adams and Godfrey [378] suggested that the borate film was formed through electrophoresis; metal surfaces in contact and sliding relative to each other generate surface charge to which charged borate particles are attracted. Junbin et al. [379] thought the reactivity of borates may be due to the existence of electron-deficient p orbitals, which enables electron transfer between borate and iron, and acts as an electron carrier to lower the escape of exo-electrons. Low energy exo-emissions can cause lubricant degradation and can catalyze the degradation of some additives, the degradation products can react with a surface to form a tribofilm [380].

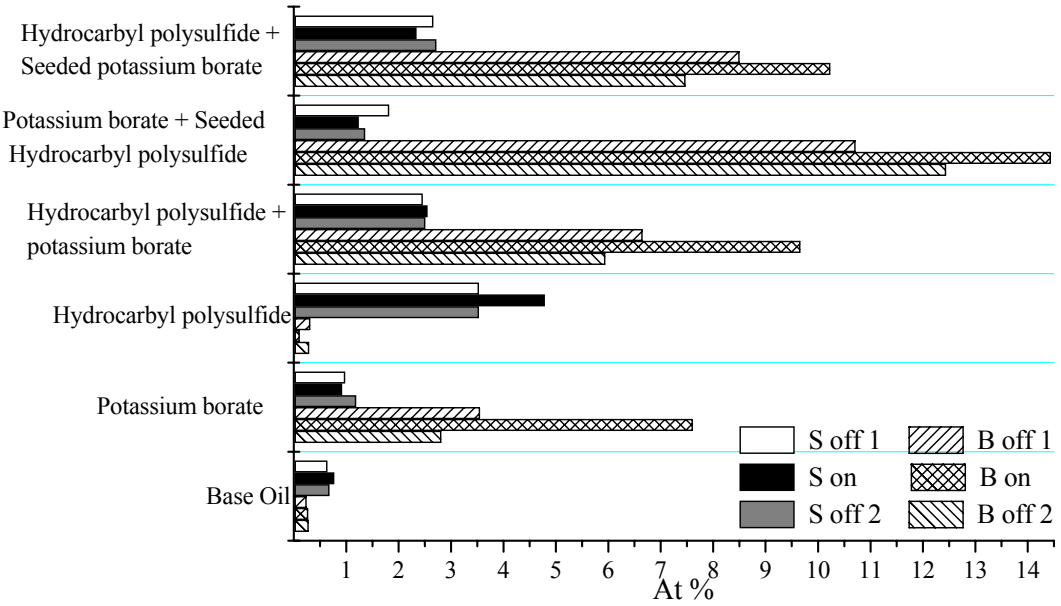

Figure 152. Sulphur and boron concentrations on and off the brass wear track for entire test matrix.

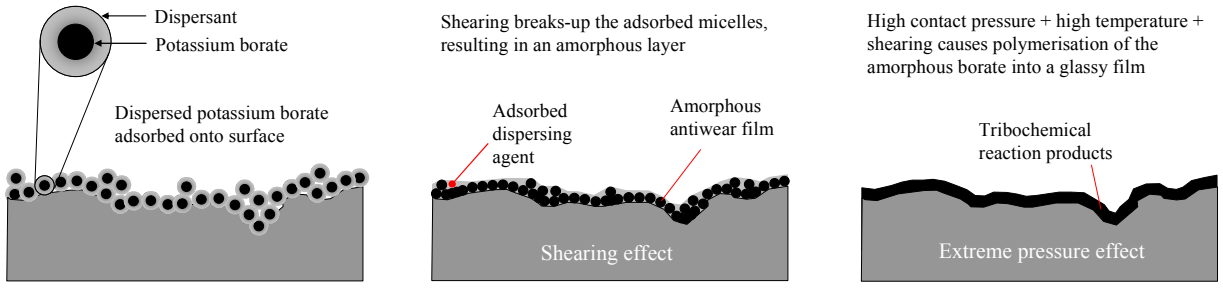

Figure 153. A schematic describing the anti-wear mechanism for dispersed potassium borate.

The elemental depth profiles show that boron preferentially accumulated on the steel surface over the brass surface (compare Figure 149 (a) with Figure 150 (a) and Figure 149 (c) with Figure 150 (c)). This is thought to be due to preferential transfer of boron containing species onto the steel surface from the brass; as a result of the two interlinking factors of chemical reactivity and contact conditions.

The contact minimum film thickness (see Table 22) was smaller than dispersed potassium borate micelle (see Table 21); therefore the borate additive must adsorb onto the disc surface and then transfer to the steel ball in the contact. Converse to the greater boron concentration on the steel surface rather than brass, there was a greater potassium concentration on the brass surface, which may relate to the electrophoresis mechanism for potassium borate film formation proposed by Adams [378]. The borate anion ($B(OH)_4^-$) preferentially collected on the predominantly iron surface, which has vacant d orbitals (can accept s orbital electrons), where as the Potassium cation (K^+) collected onto the predominantly copper surface, which has 1 s orbital electron that it can donate.

The physical conditions in the contact affected film formation. Morizur et al. [151] reported that with the potassium triborate additive a solid film of borate, bound to the steel, was only detected under conditions of severe wear when the steel friction surfaces have been activated by abrasion. Out of the two specimens, the steel ball fulfilled these characteristics better than the brass disc as it was under the greater continued mechanical stress. The adsorbed borate additive on the disc surface required successive disc cycles to promote the formation of a chemical film; whereas the steel ball was continually under extreme pressure and localised high temperature conditions that generated a tribochemical film. In Chapter 5 a difference between ball and disc were was observed – in that particular case both ball and disc were steel – which highlights that different tribological conditions experienced by pin and disc influences tribofilm formation. Figure 153 shows a significantly higher boron concentration in the brass tribofilm on the wear track than off, which emphasises the importance of high pressure, high temperature and abrasion for borate film formation.

8.4.1.3 Polysulphide + potassium borate

Insight into this interaction can be found by looking at the primary elements for these two additives, sulphur and boron, from the on and off the wear scar XPS analysis and elemental depth profiling (see Figure 151 & 150 respectively). For both steel and brass surfaces, the boron and potassium concentrations produced by the combination of borate and polysulphide additives, was higher than the borate alone, despite the treat rate used in the combination being half of that used alone. This suggests that the combination of borate with polysulphide was beneficial for high boron concentration in the tribofilm. The sulphide film produced by the polysulphide additive could either promote or protect the inclusion of boron in the tribofilm. The borate additive may have a greater affinity to adsorb/react with the electron rich iron sulphide and copper sulphide surfaces than the nascent iron and copper surfaces. Conceivably, the reaction of sulphide with the surfaces activates a reaction with potassium borate in a manner similar to activation through abrasion. Alternatively, the polysulphide additive could form a shear resistant film, which prevents the borate additive from being stripped from the surface.

The boron and sulphur concentrations across the depth of the tribofilm and on/off the wear scar concentrations (see Figure 152) for the combination of both additives from the start was very similar to the polysulphide + borate additive seeded. Whereas the boron and potassium concentrations were much higher for the borate additive + polysulphide additive seeded case. It therefore appears that artificially delaying the introduction of the borate additive into the oil, and therefore the contact, produced the same film composition and structure as the combination from the start. This suggests that the polysulphide additive was driving initial film formation.

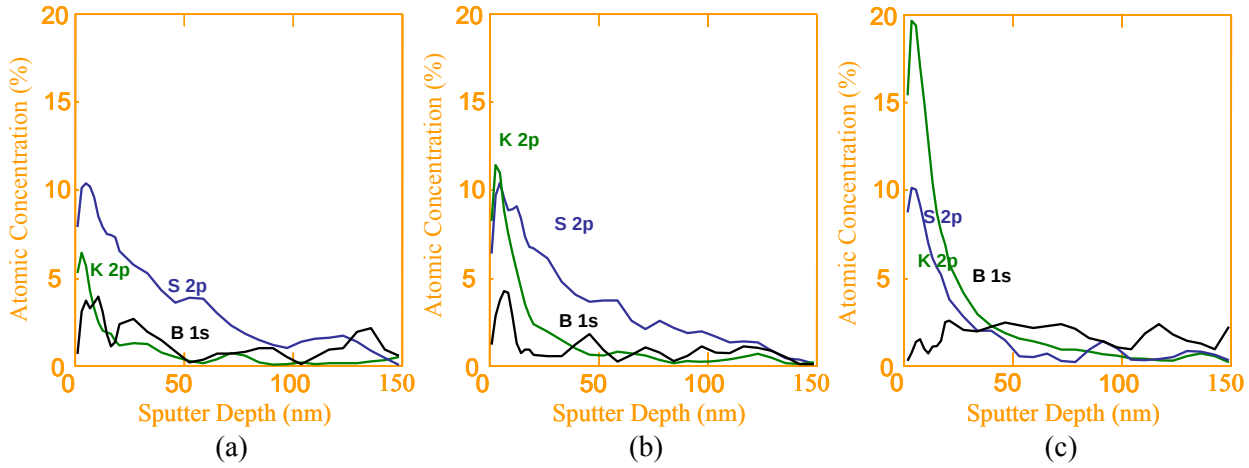

Figure 154. XPS elemental depth profiling of brass disc tribofilm, re-plotted to look at B & concentration of: (a) potassium borate + hydrocarbyl polysulphide, (b) hydrocarbyl polysulphide + potassium borate seeded, and (c) potassium borate + hydrocarbyl polysulphide seeded.

Figure 154(b) shows that boron was present close to the brass surface (between 100-150 nm), even though the borate additive was introduced after the polysulphide additive. It is thought that this is due to the small atomic diameter of boron, which allows it to penetrate into the sublayer [381]. For the borate additive + polysulphide additive seeded film, the boron concentration was consistently much higher throughout the depth of the tribofilm than for any other tests. Clearly the interaction between the polysulphide and borate additives was complex; the polysulphide additive was required to either promote/protect the formation, but the more constant boron concentration and higher potassium concentration was produced when the borate additive does not compete with the polysulphide additive for initial film formation. Perhaps polysulphide affected the growth of the boron containing tribofilm rather than the initial film formation. When polysulphide was seeded into the borate additive, the greatest concentration of sulphide was detected on the surface. Although the ordering of additive addition affected the film structure the interaction between boron and sulphur promoted film formation. This can be explained by the electron rich nature of sulphur, and the availability of an empty p orbital in boron. A layering of boron (an electron acceptor) and sulphur (an electron donor) films is anticipated, and is evidenced in the depth profiles (see Figure 154 (a) & (b)).

8.4.2 ELECTROSTATIC CHARGE

The triboelectric series shows that the brass disc should charge negatively when rubbed against steel (see Table 14, also see Figure 55). However, the positive and negative charge data for the base oil shows a slightly stronger positive surface charge than negative (see Figure 155). The base oil contains impurities that are easily polarisable. Migration of these impurities can cause a charge sign inversion. Harvey et al. [319] found that base oils have a tendency to charge positively (see Section 2.4.4.2.1).

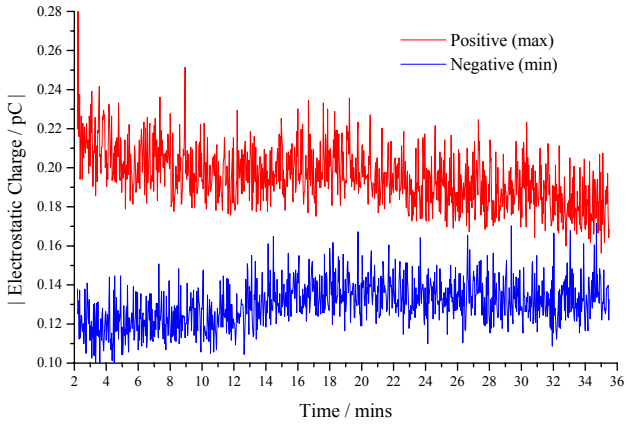

Figure 155. Positive and negative electrostatic charge data for base oil.

Polysulphide and potassium borate have distinctly different charge characteristics. The charge generated by the polysulphide was low and stable, whereas the borate additive produced a high variable charge. These charge signatures do not appear to be related to wear or conductivity of the oil. These two observations infer that charge signals relate to additive-disc surface charge generation – this conclusion was also made in Chapters 6 & 7. Thus the difference in surface charge activity between the borate and polysulphide additives indicates different physical and/or chemical processes occurred on the brass disc.

8.4.2.1 Polysulphide

The polysulphide additive exhibited distinctly different charge characteristics to base oil and the borate additive. It produced a notable surface charge as indicated by the higher charge level for polysulphide than base oil, despite the lower or comparable conductivity of polysulphide compared to base oil. In addition, the wear for the base oil was higher than the polysulphide additive. Both these observations infer that wear generated surface charge and tribocharging are insignificant compared to the surface charge generated by polysulphide film formation. Previous experience in Chapters 5,6 & 7 have shown high and dynamic charge signals for film formation – stripping/shearing processes. However, additives that exhibit a high dynamic charge through film formation and removal are able to desorb (e.g. dispersants

and detergents) – leaving a surface charge in the process. The small sulphur additives quickly adsorb and react with the surface; this reaction is not reversible. Therefore, the likely way that a sulphur (only) containing film gains charge is oxidation followed by sulphate ion transfer between the surfaces. Figure 151 shows a significantly greater sulphate concentration in the tribofilm for polysulphide containing oils than base oil. The decrease in charge level for the polysulphide additive (see Figure 143 and the first 16 minutes of Figure 145) may be related to the relative increase of sulphide, rather than sulphate in the tribofilm due to decreasing friction from tribofilm maturation, decreased contact temperature, and thus a decrease in the oxidation of the sulphide film.

8.4.2.2 Potassium borate

Potassium borate is a salt of potassium cations and borate anions. The borate anion ($B(OH)_4^-$) preferentially collected on the steel surface, whereas the Potassium cation (K^+) preferentially accumulated on the brass surface (compare Figure 149 (a) with Figure 150 (a) and Figure 149 (c) with Figure 150 (c)). The positive and negative charge data for the brass disc with the potassium borate additive showed that the disc charged significantly more positively than the base oil (see Figure 156 and 155 respectively). Since concentration of potassium ions onto the brass disc surface will lead to positive surface charge, the elemental depth profiling and electrostatic charge data appear correlated.

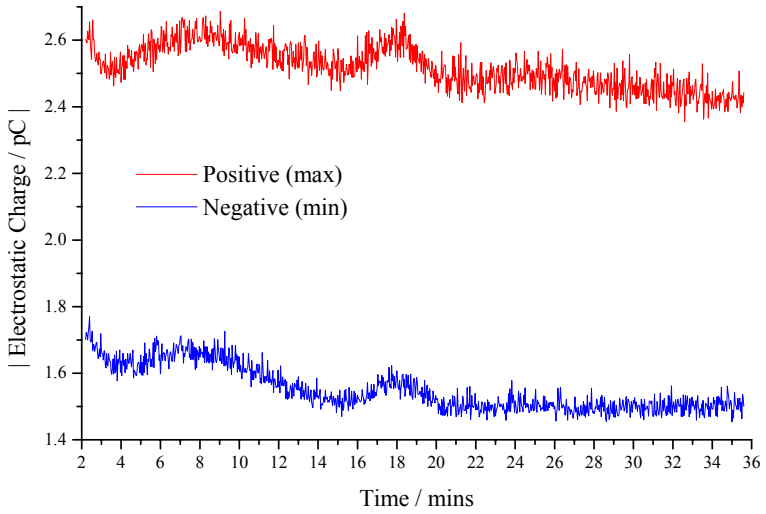

Figure 156. Positive and negative electrostatic charge data for the potassium borate additive.

In addition to the transfer of borate and potassium ions that generated surface charge, the dispersing agents can contribute to surface charge generation; as shown in Chapters 4-7. To achieve complete dispersion of the potassium borate particles, succinimide dispersants and sulphonate detergents are present at levels higher than the critical micelle concentration. This means there are free dispersant and detergent

molecules in solution. Dispersing agents in chapters 4-7, similar to those used to disperse the potassium borate, have been found to yield a high electrostatic charge.

The stage one electrostatic charge data showed that for the borate additive alone, and the binary combination, the charge level starts to increase with decreasing sliding speed; the polysulphide additive and the base oil charge levels remained unchanged (see Figure 141). This increase in charge could be related to tribofilm formation. As the sliding speed decreased, so the contact temperature and level of asperity contact increases; these factors are thought to be important for borate film formation.

The potassium borate additive alone and in both seeded experiments generated the most complex charge response, with semi-regular dynamics lasting tens of seconds and other dynamics lasting between 5 and 10 minutes (see Figure 143 - 145). This is thought to relate to the constituent parts of the additive; large potassium borate core (149 nm) which is dispersed by a significantly smaller, and therefore more mobile, sulphonate surfactant (7 nm). Borate film formation is a dynamic process involving adsorption, shearing of micelles and polymerisation, which could generate variable surface charge; the small surfactant is more likely to give rise to short duration transient processes (adsorption/stripping) compared to the larger potassium borate particle. Whereas polysulphide film formation requires adsorption followed by chemical reaction; this is a more straightforward process.

8.4.2.3 Polysulphide + potassium borate

The highest charge was seen when the polysulphide additive was seeded into the borate additive (see Figure 144). This test also produced the greatest potassium and boron concentrations, both of which are thought to be the main charge sources. The charge data for the polysulphide additive + borate additive seeded showed the most dramatic change in COF and charge (see Figure 145). Positive and negative charge data showed a change from a predominantly positive charge before seeding to a mainly negative charge after seeding (see Figure 157). This change in dominance of disc positive and negative surface charge was not seen in any of the other tests; the other test oils produced a positive surface charge, to varying degrees. This real-time data also lends insight into the film formation mechanism. The positive and negative charges look to be converging, possibly relating to a tribochemical reaction that would have brought the system to the same state as the other binary experiments, if the test was allowed to run on. Thus, the observed sulphur boron interaction created a borate rich negatively charged top-layer on the sulphur film (similar to the observed layering of boron) when the borate additive was seeded. This reverse film appeared to be less stable than the other films and may be approaching a charge inversion (as indicated by the convergence of positive and negative charge signals, see Figure 157) as a result of a change in film composition (e.g. an additional sulphur layer on top of the borate layer).

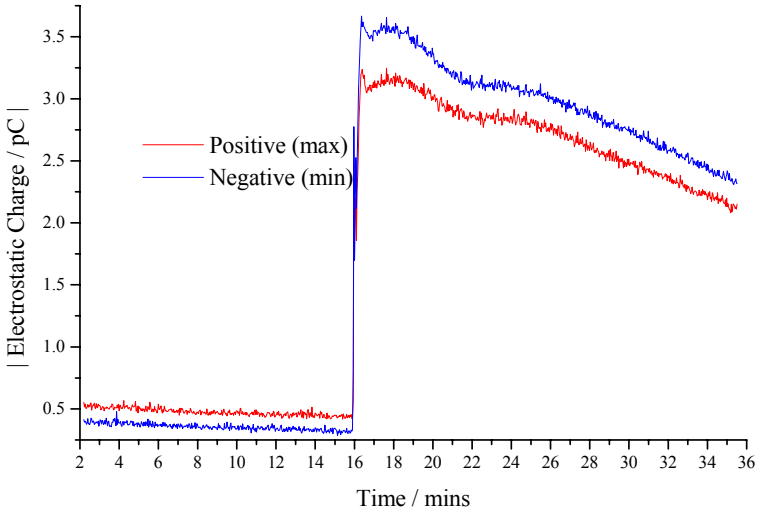

Figure 157. Minimum and maximum charge data for the polysulphide additive + borate additive seeded test, which infers whether the disc surface charge was predominantly negative or positive.

8.4.3 FRICTION

8.4.3.1 Polysulphide

The friction properties of iron sulphide are fairly well known; sulphide films are more easily sheared than the metallic asperity junctures under extreme pressure conditions [382]; hence the lower COF seen for the polysulphide additive compared to base oil and the borate additive in both stage one and two of the test (see Figure 140 & 142). However, the COF trace is not entirely explained by the iron sulphide film. The physical properties of a copper-sulphide film are not as well understood as iron sulphide. It could be similar to the low shear nature of iron sulphide, but the twice as thick sulphide film observed on brass shows there is a difference (compare Figure 149 (b) with Figure 150 (b)). Sakurai et al. [383] noted a similar finding and concluded that the greater formation of sulphide for the brass versus steel, suggests that the reactivity of the copper with sulphur on the friction surface was greater than that of the iron. However, the tribofilm thickness is not solely explained by the reactivity of the surface. It is possible that the different type of sulphide film on brass was more shear/wear resistant than the iron sulphide, and this allowed the formation of a thick, possibly rough or patchy, sulphur containing film. This could explain the variable friction seen for the polysulphide additive; copper sulphide may require more energy to shear and was therefore a transient process rather than constant shearing, hence the dynamics seen in the friction trace.

8.4.3.2 Potassium borate

Although borate films have been reported to be friction reducing [240,241], the literature is not clear on the friction performance. Morizur et al. [151] reported that borate films displayed increasing friction levels with boron content. The borate additive in this study produced a high friction film, which over the duration of the test, dropped to below the base oil COF level. The high COF produced by the borate additive over the first 20 minutes of the test can be explained by the process of borate film formation. The adsorbed layer of potassium borate, as well as the amorphous phase it develops into, created a high friction surface, predominantly because of the presence of adsorbed dispersing agent, which was shown to increase COF in Chapter 6. After 20 minutes the COF levels of the base oil and borate additive crossed-over. This change in friction characteristics could be a result of tribochemical reactions between borate and iron, producing a glassy surface, which was smoother than the amorphous film. This change in COF for the boron additive compared to base oil during a wear tests was also observed by Hu et al. [384] for titanium borate.

8.4.3.3 Polysulphide + potassium borate

The polysulphide additive COF trace was low and the most dynamic/variable (see Figure 142) and at the beginning of polysulphide + borate additive seeded test (see Figure 145). The polysulphide additive alone would not provide friction magnitude and stability required for the synchromesh to achieve quick and smooth gear changes. When the borate additive was present with the polysulphide, and when introduced after the polysulphide additive, it increased the stability of the COF. This may be a result of relatively high boron concentrations at various points across the tribofilm depth effectively 'pinning' the shear planes, or the amorphous layer of adsorbed borate and dispersant on top of the copper sulphide layer, modifying COF behaviour.

8.4.4 SPECIMEN WEAR

Previous discussions have identified the composition and possible mechanisms for tribofilm formed by polysulphide and borate additives, singularly, combined and seeded one-into another. Having understood film composition, it was important to relate this with properties that produce anti-wear performance. It is worthy of note that there was no correlation between film thickness and brass disc wear.

8.4.4.1 Polysulphide

The polysulphide additive produced the greatest steel ball wear resistance. Sulphur containing oils can be detrimental to wear; high sulphur activity results in faster formation of the metal sulphide and has been reported to result in higher wear [103]. However, provided the rate of tribofilm regeneration is similar to that of the film stripping, reduced wear should result (see Section 2.3.3.3). In addition, the tendency for

brass disc wear is reduced further by the thicker, more shear resistant sulphide film, which minimises film stripping that resulted in wear.

8.4.4.2 Potassium borate

The ball wear scar was small and the disc wear was large compared to the other test oils. Thus suggesting that the predominantly boron containing tribofilm on the steel ball was more wear resistant than the potassium enriched film on the brass disc.

8.4.4.3 Polysulphide + potassium borate

When both additives were used in combination, seeded or non-seeded, steel ball anti-wear performance was not as good as when the additives are used singularly, indicating an antagonistic interaction between the two additives. However, it should be noted that all additives, singularly, mixed or seeded, produce lower steel ball wear than base oil.

Polysulphide formed the most wear resistant tribofilm on brass; the mixture of polysulphide and borate additives produced a good anti-wear film, but it was not as wear resistant as polysulphide alone. Even though polysulphide was thought to be more surface active than the borate additive, the borate additive may still offer significant competition with the polysulphide to antagonise film formation. This was supported by the very low brass wear for seeding the borate additive after the polysulphide additive (see Figure 147). Sulphur, and a varying composition of boron in the tribofilm produced by the combination and borate additive seeded into the polysulphide additive, minimised wear. Whereas a high and constant boron/potassium concentration, produced by the borate additive + polysulphide additive seeded, did not exhibit any brass anti-wear properties.

An interesting observation from both the brass disc wear and XPS analysis was the significance of sulphur. The highest sulphur concentration in the tribofilm was produced from the polysulphide additive only run, which also saw the lowest wear. The worst anti-wear performance came from the films that contain the least sulphur: base oil, borate additive and borate additive + polysulphide seeded. This infers a relationship between the brass tribofilm sulphur content and brass disc wear, such a relationship does not exist for boron (see Figure 158). Baldwin [385] examined the anti-wear efficiencies of a series of sulphur-containing borates and suggested that the sulphur and not the boron, plays a major role in the anti-wear properties of such compounds. The dispersed potassium borate produced a tribofilm which contained greater sulphate than sulphide (see Figure 151); the origin of this was the sulphonate detergent used to disperse the potassium borate particle. The polysulphide additive produced a mainly sulphide and/or sulphur containing film, however it also produced the highest sulphate concentration as well. When the borate and polysulphide are combined, equal quantities or sulphide and sulphate are produced.

The three lowest brass wear producing oils had a higher sulphide and/or sulphur content than sulphate, whereas the three highest were predominantly sulphate containing. Such a relationship is tentative, but warrants further investigation.

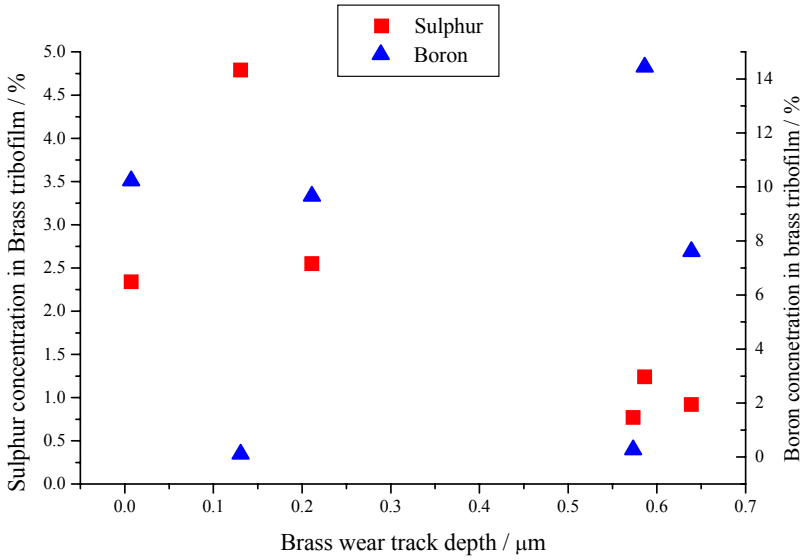

Figure 158. Shows a possible relationship between brass tribofilm sulphur content and brass disc wear performance, no relationship exist between boron tribofilm content and brass disc wear.

8.5 CONCLUSIONS

A series of pin-on-disc wear tests, using a brass disc and steel ball to mimic the synchroniser ring contacts, were carried out to investigate the nature of the tribofilms produced on these surfaces by hydrocarbyl-polysulphide and potassium borate additives.

The polysulphide additive exhibited good brass and steel anti-wear performance, but low and unstable friction behaviour. Both brass disc and steel ball tribofilms contained sulphide, but the thicker film on the brass surface and the variable friction levels are thought to indicate that sulphide formed on the brass surface is more shear resistant. The potassium borate exhibited good steel ball anti-wear performance and high stable friction, but negligible brass disc anti-wear performance. Boron was found at a higher concentration on the steel surface compared to brass and vice versa for potassium; suggesting preferential adsorption of potassium to brass and borate to steel. The combination of the two additives produced good steel ball anti-wear and high steady friction (necessary for synchroniser contacts). The tribofilm formed by this combination indicated that polysulphide with potassium borate promotes and/or protects boron inclusions in the brass tribofilm. Seeding one additive into another additive solution mid test illustrated

that the polysulphide drives initial film formation, when in combination with the potassium borate additive.

Real-time charge measurements identified distinctly different charge levels and dynamics for the potassium borate additive and the polysulphide additive. Surface charge related to polysulphide film formation was related to the generation of sulphate. The highest charge levels were correlated to the tribofilm which contained the greatest inclusion of charge carriers. The charge data for the polysulphide additive and borate additive seeded shows a change from predominantly positive charge before seeding to a mainly negative charge, thought to relate to the adsorption of negative borate charge species, inferring a amorphous borate layer.

The experiments presented in this Chapter illustrate that the interaction between polysulphide and borate may be beneficial or antagonistic depending on the conditions, i.e. the order of reaction of the additives with the surface. The polysulphide with seeded potassium borate produced the best brass wear protection, moderate wear on the steel, as well as the needed stable friction required for a synchroniser. The information gained by these tests could enable the reactivity and concentration of these additives in a formulation to be tailored to suit various applications. The real-time charge/film information may be a valuable tool for the optimisation of additive chemistry, and for the formulation of finished lubricants.

9 CONCLUSIONS

9.1 MOTIVATION

The engine power-train design is continually evolving to meet environmental demands of lower emissions and increased fuel economy. These design improvements are often to the detriment of tribological performance. The lubricant formulator must mitigate the severity of the contacts by blending additive packages which increase fuel economy, reduce environmental impact and minimise wear for lengthened service intervals. Formulating lubricants is a difficult process because additive-surface behaviour and interactions between additives is not well understood. A review of the literature identified that an absence of real-time technology has hindered understanding of additive behaviour and interactions between additives in tribo-contacts. The work presented in this thesis assessed whether electrostatic charge monitoring, which is sensitive to changes in surface chemistry, can offer insight into additive film formation and additive-additive interactions and how these affect tribological performance.

9.2 METHODOLOGY

Electrostatic sensors were deployed on a range of tribological tests apparatus: TU3 valve-train, in-house pin-on-disc (PoD) and a PCS instruments Mini-Traction-Machine (MTM). Specific test conditions were used to simulate: engine valve-train, manual transmission synchroniser, and automatic transmission frictional clutch tribo-contacts. A range of additives were tested including: dispersants, detergents, friction modifiers, antiwear and extreme pressure. The interaction of these additives with: bearing steel, brass and paper materials was assessed. Also additive-additive and additive contaminant interactions were investigated. This was achieved by assessing surface charge generation, as well as analysing friction and wear performance and, where appropriate, cross-correlated with one another and off-line XPS analysis.

9.3 SENSITIVITY OF ELECTROSTATIC MONITORING TO WEAR AND LUBRICANT CHEMISTRY

A series of tests were carried out to investigate the charge generated between TU3 cam and follower contacts under conditions simulating various stages of component life. Charge signals underwent a sign inversion during a simulated wear test; this was due to a transition between tribocharging of the lubricant under running-in and mild wear, and contact potential difference generated at the onset and progression of adhesive wear. Electrostatic charge signals identified that wear initiated at point of minimum film thickness on the cam and post-test correlated to position of greatest wear.

Although electrostatic monitoring was originally developed to monitor wear, experiments on the TU3 valve-train revealed that the highest charge was produced by a test with a fully formulated which produced no wear and the lowest charge was produced by a test without a lubricant which produced the greatest wear. Clearly lubricant chemistry had a significant effect on charge generated. Two statistical studies (Chapter 5 & 6) investigated the correlation between electrostatic charge, wear and lubricant electrokinetic properties. Both studies showed no correlation between wear and electrostatic charge; there was a poor correlation between electrostatic charge and lubricant electrokinetic properties. The low degree of correlation is explained by the electrokinetic techniques measuring the pre-existing charge in the oil, whereas electrostatic charge is generated as a result of tribological action and additive-surface interaction.

9.4 ADDITIVE-SURFACE INTERACTION

Results (Chapters 6 & 8) have shown that additives which can physically adsorb (e.g. Dispersants, Detergents) produced a greater surface charge than additives which principally chemically adsorb (e.g. ZnDTP 2, MoDTC and polysulphide). The charge generation mechanisms are different for the two types of additives; Detergents and Dispersants form acid-base pairs with the surface, whereas chemical films generate charge through contact potential difference.

9.5 ADDITIVE-CONTAMINANT AND ADDITIVE-ADDITIVE INTERACTIONS

Work in Chapter 5 showed statistically that carbon black, compared to base oil alone, increased electrostatic charge. Both Dispersant 2 and Detergent in the presence of carbon black were found to reduce the interval electrostatic charge. The charge data indicated that Dispersant 2 and Detergent provided sufficient barriers to prevent agglomeration and therefore minimise charge generation. The interaction between dispersants and ZnDTP 1 was found to reduce electrostatic charge because dispersant complexes with ZnDTP 1 making it less reactive; thus the number of free charges is reduced.

9.6 ADDITIVE FILM COMPOSITION RELATED TO ELECTROSTATIC CHARGE

Across the different experimental studies electrostatic charge measurements were related to tribofilm chemical composition, as identified by XPS. To the author's knowledge no real-time technique has shown a correlation with tribofilm composition.

Changes in zinc, phosphate and sulphate concentrations in a ZnDTP 2 tribofilm (Chapter 6) affected charge polarity. For the polysulphide additive (Chapter 8) higher electrostatic charge measurements were found for tribofilms which contained a higher ratio of sulphate to sulphide; the most likely way for polysulphide to generate surface charge is through oxidation (sulphide to sulphate). In Chapter 8 the

highest charge was seen when the polysulphide additive was seeded into the borate additive. This test also produced the greatest potassium and boron concentrations, both of which are thought to be the main charge sources (borate anions and potassium cation). The charge data for the polysulphide additive + borate additive seeded showed a transition from being predominantly positive to predominantly negative. This correlated with the observed borate rich (anions) layer on top of the sulphur film.

9.7 TRIBOFILM KINEMATICS

Cross-correlation between electrostatic charge and tribofilm thickness showed that dynamic charge peaks related to the stripping of the ZnDTP 2 antiwear film. The source of this charge peak was found to be due to an increase in negative charge, which correlated with a dominance of phosphate and sulphate (anions) compared to zinc (cations), as the film was worn away.

When FM 1 and Dispersant 3 were combined, XPS analysis and friction data indicated that Dispersant 3 dominated the tribofilm composition; nitrogen levels and friction levels were similar to Dispersant 3 alone. The electrostatic charge data revealed that competition for surface sites is an extremely dynamic process, with each additive dominating surface coverage at different times; as indicated by charge levels which alternate between the levels of the FM 1 and Dispersant 3 alone.

Adsorption of Detergent surfactants leads to negative surface charge and adsorption of Dispersant 3 produces positive surface charge; thus the dynamic variation between the dominance of positive and negative surface charge is thought to be related to Dispersant 3 and Detergent adsorption and stripping.

Organic friction modifiers (Chapters 6 & 7) produced a low and stable surface charge compared to Dispersants and Detergents. This is because organic FMs preferentially shear at the hydrocarbon tail / hydrocarbon tail interface rather than the polar-head / surface interface, thus minimising charge generated through desorption and/or stripping.

Cross-correlation of surface charge and tribofilm composition has demonstrated the ability of electrostatic sensors to detect the tribofilm kinematics. This is a significant finding; no current real-time technique used to monitor tribofilm kinematics derives its measurements from the tribofilm chemical composition. The tribofilm kinematics could also be managed to promote the desired tribofilm composition – a point, to the knowledge of the author that has not been realised in the literature. Additives selection could be based on the time it takes to re-form a tribofilm. During this dwell period it might allow other additives that are required at the surface to adsorb, thus enabling a composite tribofilm made up off additives with different functions. Antiwear additives and friction modifiers in particular – although other additives will be important – could be optimised in this way.

9.8 NON-CHARGE RELATED OBSERVATIONS

Through investigation into additive-surface charge behaviour, there have been many additional tribological discoveries; many of these findings are, in their own right, original.

9.8.1 WEAR

In Chapter 5 statistical analysis revealed that ball wear was increased in the presence of ZnDTP 1; contrary to the expected antiwear behaviour of ZnDTP. XPS analysis indicated that primary ZnDTP (ZnDTP 1), which has a high thermal stability, did not form a fully developed antiwear film under the low test oil temperature. The source of the *pro-wear* effect was the reaction of sulphur, from ZnDTP 1 (which is less temperature dependent), with iron, which promoted a tribochemical wear process. This supports the theory that thermal decomposition of ZnDTP does have a role in the formation of a ZnDTP antiwear film, which has been disputed by some researchers. Dispersants were found to minimise the *pro-wear* effect of ZnDTP 1, by forming a complex and increasing the thermal stability.

The greatest friction material disc and steel ball wear was observed when the FM 1 + Dispersant 3 were combined, which clearly shows antagonism between the two additives. This is an important finding as both these additives are widely used in ATFs to fulfil two different functions; FMs minimise shudder and dispersants improve torque capacity. However, this study has demonstrated that an incorrect balance of FMs and dispersants could have disastrous consequences.

When both polysulphide and potassium borate additives were used in combination (seeded or non-seeded) steel ball anti-wear performance was not as good as when the additives were used singularly; thus indicating an antagonistic interaction between the two additives.

9.8.2 ADDITIVE PREFERENTIAL SURFACE ADSORPTION

XPS carried out on brass and steel wear specimens lubricated with potassium borate and polysulphide identified the effect surface chemistry has on film formation. For the potassium borate additive alone; potassium (cation) preferentially adsorbed to brass, and borate (anion) preferentially adsorbed to steel. For the polysulphide additive alone, both brass disc and steel ball tribofilms contained sulphide, but the film on the brass surface was thicker, which may explain the variable friction performance; polysulphide is generally known as a stable friction educing additive.

9.8.3 THE EFFECT OF BINARY ADDITIVE SYSTEMS ON TRIBOFILM COMPOSITION

The combination of the borate additive with polysulphide additive was beneficial for high boron concentration in the tribofilm – higher than the borate additive alone. The sulphide film produced by the polysulphide additive either promotes or protects the inclusion of boron in the tribofilm.

Artificially delaying the introduction of the borate additive into the oil (seeding), and therefore the contact, produced the same film composition and structure as the combination from the start. This suggests that the polysulphide additive was driving initial film formation. Seeding is an extremely powerful technique, but its use is almost absent in the literature.

9.9 CONCLUDING REMARKS

With reference to the original aim, the work presented in this thesis has demonstrated the benefits of using electrostatic monitoring for the purpose of wear testing and additive screening. It is clear that electrostatic condition monitoring is a useful tool in the detection of the onset and progression to severe adhesive cam-follower failure, with specific reference to the breakdown of the oil film and wear mechanism. This in itself is valuable information to the lubricant formulator. It has been shown that additive-surface interaction dominates charge levels even in a wearing contact. Electrostatic monitoring is sensitive to the type of additive-surface adsorption, interactions between additive and additive or contaminant, and tribofilm kinematics. The charge sign and magnitude produced by additive-surface adsorption could be useful criteria on which to select an additive, or combinations of additives. Also tribofilm kinematics – identified by electrostatic charge monitoring – could also be managed to promote the desired tribofilm composition. The information gained by using electrostatic monitoring in tribological testing has great potential to streamline the additive screening process. Although interpretation of electrostatic charge data is currently an intensive process, in the long term, lubricant development could see a move towards charge informed formulation.

10 FUTURE WORK

The directions of future work is split into work that is short term, the next step from the work presented in this thesis, and in the long term, more fundamental approach of looking at additive by electrokinetic techniques, as well as applying electrostatic monitoring to full scale fired engines.

10.1 FUTURE INVESTIGATION BORN DIRECTLY FROM THIS WORK

10.1.1 ELECTROSTATIC CHARGE BASED WORK

There is a great deal of electrostatic monitoring work that could immediately follow on from work presented in this thesis. Understanding of the relationship between charge and additive film formation could be furthered through testing of a greater range of additives. Financial restriction limited the extent to which tribofilm chemical compositions were analysed; any future advances in understanding surface charge generated by tribofilm formation, will be best served with extensive XPS analysis, as well as other surface techniques. This would enable a model to be built which relates electrostatic charge parameters with film composition and film kinematics; to improve the accuracy of this model information about friction and wear performance would also be required. The natural progression of single additive testing is to add complexity through binary, tertiary and so on, up to complete additive package systems with additives at different concentrations. This model could enable the interactions of a blend of additives previously not tested to be predicted. Such a model could also aid the development of new additives.

One of the most important findings reported in this thesis is the correlation between electrostatic charge features and ZnDTP 2 film removal and formation, through base oil flushing experiments. There is an absence of technology which monitors tribofilm kinematics in real-time, let alone derives its measurements from film chemical composition. Therefore it is important to continue this work to further understand tribofilm formation, removal and replenishment. Given more time, using this flushing technique on detergent and potassium borate would have been useful as comparatively very little is known about the kinematics of their films. Detailed XPS analysis of the tribofilm elemental composition would be integral to this work.

It is envisaged that the post-test analysis used to examine absorbed additives (namely XPS) may have limitations when examining physically adsorbing additives. Because by the time the sample surface is examined the surface chemical composition may have change due to re-adsorption or desorption of additive(s) (as it takes time to remove the sample from the lubricant. For chemical film forming additives this is not really a problem as physical adsorption of this additive is different in to the tribofilm they

produce. However for physically forming additives it is difficult to distinguish between additives adsorbed during tribological testing and additives adsorbed after. A new approach to analysing physically adsorbing additives is required so that kinematics of physically adsorbing additives can be better characterised and therefore enable confidence in corroboration with electrostatic charge signals.

It is acknowledged that fairly basic charge parameters have been used during this work. Despite this, a correlation between charge and additive-surface interaction has been made. Of particular value was the use of maximum and minimum (positive and negative) charge data, in conjunction with known additive chemistry this enabled electrostatic charge signals to be correlated with additive-surface interactions. For the physically adsorbing dispersants and detergent surfactants, charge polarity was related to their adsorption and desorption. However, it is intuitive that if a dispersant which forms a positive charge upon adsorption and a detergent surfactant which forms a negative charge upon adsorption are combined, interpretation of positive and negative charge data may be difficult. More sophisticated charge parameters are required to better characterise the complexity that multiple additive systems might create. The ultimate goal would be to develop an artificial intelligence system which incorporates many real-time and off-line parameters, but is predominantly driven by electrostatic charge data to yield information such as: tribofilm thickness, tribofilm composition, tribofilm tenacity factor, time for tribofilm formation, interaction with other additives etc.

10.1.2 NON-EXCLUSIVE ELECTROSTATIC CHARGE BASED WORK

Although the main focus of this thesis has been electrostatic monitoring of tribo-contacts, there have been a number of interesting tribological and surface chemistry observations which are in their own right extremely interesting. The main two are preferential adsorption of one additive over another and the preferential adsorption of an additive for a particular surface.

XPS analysis of tribofilms produced by artificially delaying the introduction of an additive into the contact (seeding) has found to be very useful in identifying which additive drives film formation of the additive mixture. This seeding technique is an extremely powerful technique which is surprisingly unused. A possible reason that this technique may not have seen widespread uses is that wear may differ between the different permutations of seeding. However, wear could be used as another parameter to identify which order of seeding best represents the additive system when not seeded. Its application is not limited to binary additive systems; a four additive system could be assessed, although this would require a large number of tests (2^4), although the information gained would be extremely valuable.

The preferential adsorption of an additive onto one surface over another was identified; when a series of test run with a steel ball on a brass using a potassium borate additive, it was found that the potassium (ions) preferentially adsorbed onto the brass surface and borate preferentially adsorbed onto the steel

surface. It was postulated that this was driven by electron orbital interactions between the adsorbate and surface. Alternatively it has been suggested that potassium borate only forms a film once the surface has been activated by abrasion, which general occurs more rapidly on the (steel) ball as it is in continuous contact. To determine which mechanism is the driving factor in tribofilm formation it is suggested that a brass ball on steel disc test should be run. If the film composition on the brass ball is the same found for the brass disc and likewise the steel components, then surface chemistry drives preferential adsorption. However, if the tribofilms for the balls (and discs) for the two tests are the same the contact conditions drives preferential adsorption.

The wear of wet friction material was found to increase when friction modifier and dispersant additives were blended together. It is believed that this requires further work to understand the antagonistic interaction between these two additives and if a fatigue-type process, induced by the different friction performance of the additives, is responsible. Alternative suggestions for the increase wear rates are that the adsorption weakens the material.

10.2 WIDER REACHING WORK

The work presented in this thesis has wider reaching implications and would see a move from electrostatic monitoring of PoD contacts to fundamental additive charge investigations and tribological testing of more complex components to acknowledge the various experimental levels (see Figure 159).

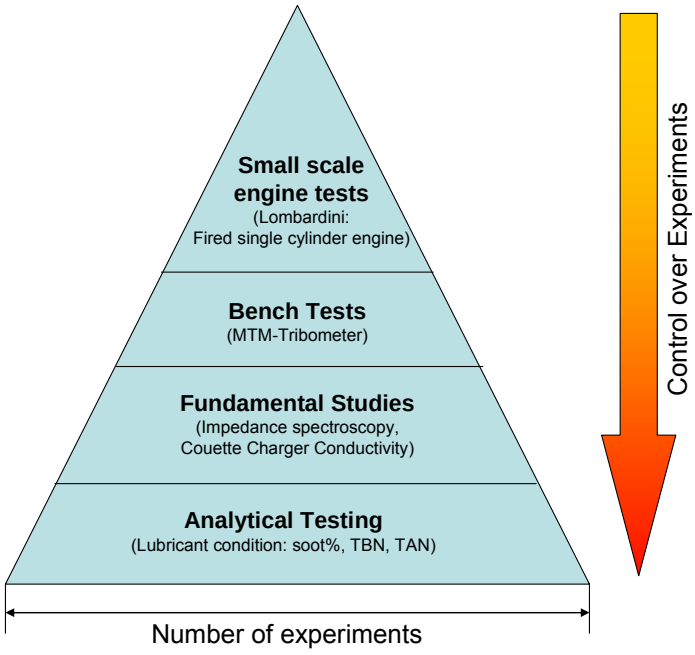

Figure 159. Schematic describing the various experimental levels of lubricant testing.

10.2.1 FUNDAMENTAL ELECTRO-KINETIC WORK

A fundamental approach to understanding additive charge and additive-surface interactions is thought to be obtained through electrokinetic techniques, such as impedance spectroscopy or electrokinetic sonic amplitude. For both techniques apply an AC field to the colloid sample; impedance spectroscopy measures the response as a lag (impedance) associated with frequency, while ESA measures electrophoretic motion of the particle by the associated sound wave. Both techniques enable information about particle size, zeta potential and charge sign to be determined. Zeta potential is the electrical potential that exists in the shear plane of the double layer of a particle. This is important, as it directly relates to tribocharging. It is also a function of the surface charge of a particle, any absorbed layer at the interface and the nature and composition of the surrounding medium in which the particle is suspended. Although ESA was used in this thesis, it was of limited use, because analysis was only carried out at one frequency (due to the use of dated equipment). Most modern electrokinetic measurement techniques operate over a range of frequencies, allowing more information to be obtained. These fundamental electrokinetic experiments could be extremely insightful for understanding the interaction between additives and soot; surfactants and metal salts for calcium phenate detergent and potassium borate. Information gained from these fundamental experiments would help add further insight into the charge generated by a lubricated contact.

10.2.2 FULL-SCALE TESTING

Pin-on-disc tribometers have been the main apparatus for additive testing in this thesis. Tribometers are used to try and replicate power-train components; it is therefore important to transfer the advances made on electrostatic monitoring of PoD additive tests to actual power-train component. The success of being able to monitor cam surface charge has been proven in Chapter 4. The same test oils as those used in Chapter 6 could be run in the motorised engine test to assess whether similar findings are found in full scale contacts. It would also be interesting to run a series of additive-base oil flushing experiments similar to those carried out for ZnDTP 2 in Chapter 6.

Ultimately there should be a long-term aim to use electrostatic monitoring on full scale fired engines, as this is where a large proportion of lubricant development costs are consumed. If additive interactions could be determined then this would greatly aid the lubricant development process. Attempts have been made to deploy electrostatic sensors to monitor the cams of a single cylinder diesel engine have unfortunately not been successful, because the location of the camshaft in the crankcase meant that the sensor was susceptible to a great deal of noise from other rotating components in the crankcase as well as oil splatter (see Figure 160). Although fraught with difficulties, electrostatic monitoring of full scale, real-life components should be attempted.

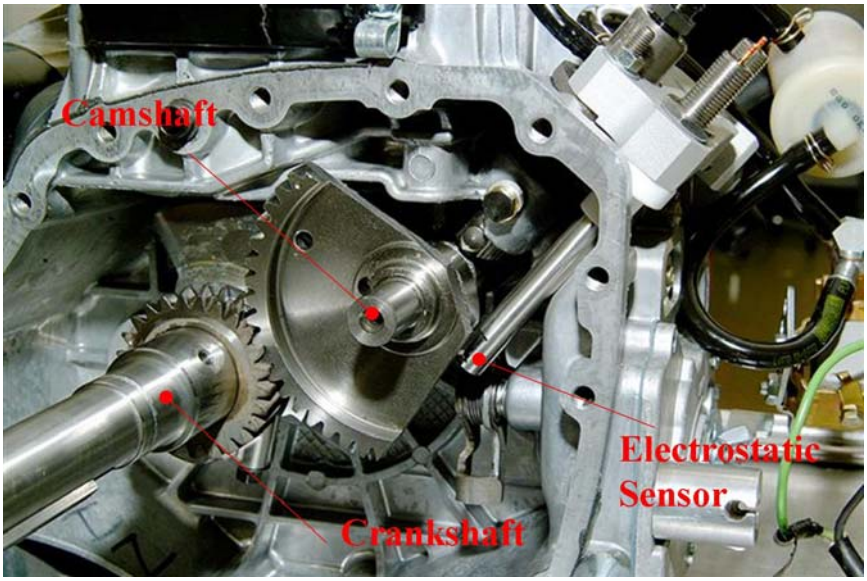

Figure 160. Electrostatic sensor positioned to monitor cam wear in a fired single cylinder diesel engine.

APPENDIX

Appendix A. Valve-train design

There are a wide range of valve-train mechanisms e.g., push rod, pivoted follower, direct acting (DAT), roller follower and desmodromic; more details of these can be found in [57,386]. Table 35 shows a summary of the advantages and disadvantages of different valve-train designs. The type of valve-train of interest is the pivoted finger follower and DAT system; however it is important to have an appreciation of a range of valve-trains.

	Valve-train Configuration		Advantage	Disadvantage
Over-head Valve	Push-Rod		• Simple camshaft drive-gear • Low engine height • Simpler head design • Single camshaft use for V-engine	• High reciprocating mass • Low Valve-Train Stiffness
Over-Head Camshaft	Finger follower		• Low reciprocating Mass • High Stiffness	• High friction • Pure sliding – requires positive lubrication – prone to wear
	Compound valve head		• Reduced reciprocating Mass • Increased valve-train stiffness	• Small tappet diameter constrains cam profile design
	Roller	Finger Follower	• High stiffness (although not as stiff as direct acting) • Lower friction than sliding contact • Low cost pressed steel	• Higher contact stress than sliding and therefore requires a more expensive re-entrant cam
		Rocker Arm	• Low engine height compared with DAT and finger followers • Low friction	• Low stiffness compared to DAT and finger follower • Die cast aluminium requires more machining
	Direct Acting	External Shim	• High system stiffness • Optimum material choice for shim	• Requires adjustment on initial engine build and service checks there after • Cam contact is less than tappet diameter
		Internal Shim	• High system stiffness • Full tappet diameter for cam contact • Optimum shim material	• Adjustment on initial engine build and services thereafter • Limited material choice for tappet face
		Hydraulic Lash adjuster	No lash adjustment on initial build Full tappet diameter available for cam contact Compensates for valve seat wear	• Not as stiff as mechanical adjustment • Limited material choice for the tappet face

Table 35. Advantage and disadvantage of different valve-train designs.

Many of the problems with the finger follower valve-trains have been over come through the use of DAT valve-train systems. In part, this has been due to the move to double over-head cam (DOHC) gasoline engines, which have inclined valves to give a pent roof combustion chamber, which is more desirable. DAT designs are highly suitable for this type of arrangement. However, finger follower valve-trains are

still used in diesel engines. Diesel engines require vertical valves for optimum combustion which makes the DOHC DAT system infeasible, because the camshafts would be too close together.

Appendix B. Other degradation processes

There are other lubricant degradation process such as oxidation, corrosion and shear. However these are not dealt with directly in the experimental work presented in this thesis. Therefore their discussions about these processes are treated briefly.

The rate of oxidation is affected by the operating conditions, such as temperature and aeration. The tendency towards oxidation is affected by the basestock; highly unsaturated basestocks have a greater tendency to oxidize. The use of sulphur in either the basestock or in the additive system is influential as it is an antioxidant. All oxidative processes have a common reaction pattern due to the bi-radical nature of oxygen. Oxidation degradation can be measured by oxygen number, a change in viscosity, acid number build up, and an increase in polar materials. The formation of organic acids can be corrosive to some engine components. Oxidation is always detrimental to the performance of a lubricant and can result in the formation of sludge, which can block oilways and filters. At advanced stages reactions of high molecular weight intermediates results in products (precipitates) which are no longer soluble in the hydrocarbon called sludge. Varnish-like deposits are formed on the metal surface under thin-film conditions [387].

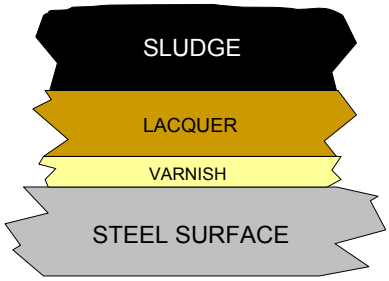

Figure 161. Schematic of the deposits that can occur on the engine surface as a result of oxidation.

As discussed above some of the products of incomplete combustion are nitrogen oxides and sulphur oxides; these can react with water to form nitric and sulphuric acids (eq (16)), which causes corrosion within the engine.

$$S + 1.5O_2 \Rightarrow SO_3 \quad \text{and then} \; SO_3 + H_2O \Rightarrow H_2SO_4 \qquad (16)$$

Rust refers to the oxidation of ferrous metals, catalyzed by water and acids through the following reaction (eq (17)).

$$2Fe + 1.5O_2 \Rightarrow Fe_2O_3 \qquad (17)$$

There is also corrosion of non-ferrous metals such as copper and lead (see eq(18) & (19)).

$$Cu + S \Rightarrow CuS \qquad (18)$$

$$Pb + acid \Rightarrow Pb - salt \qquad (19)$$

Appendix C. Shear

When a polymer is stretched the maximum energy is concentrated in the middle of the molecule. Thus when a polymer breaks due to mechanical shearing, the resulting fragments are predicted to be about half of the molecular weight of the starting polymer. The higher the molecular weight, the more likely a polymer is to break. However the mechanical degradation process is limited by the molecular weight. At some point, whatever the application, a molecular weight is reached where the energy concentration during coil distortion is insufficient to break further bonds. Viscosity loss during use is thus characterized by a rapid initial decrease as the bigger molecules break, followed by a slower loss and finally a plateau as the equilibrium molecular weight is reached, however this final viscosity maybe insufficient to prevent surfaces from wearing.

Permanent loss in molecular weight can also occur through chemical degradation (e.g. by acids), oxidative and thermal; although the processes are quite different the outcome is the same. Chemical degradation is a totally random process. Thus a significant viscosity loss will only come as a result of the chemical reaction in the middle of the polymer. If the reaction occurs at the end of the polymer then no real change will occur to the viscosity. However when the last scenario happens there are deposit implications. As the fragments produced from such a reaction are reactive and may contribute to sludge formation.

Appendix D. Viscosity index improver

The primary function of viscosity index improvers (VIIs) is to increase viscosity at high temperature, more than at low temperature (see Figure 162). Oil viscosity is defined by the SAE J300 classification, which specifies viscosity at low temperatures to define the W (winter) grade and at 100^{o}C. Oils containing VIIs are known as multi-grade oils.

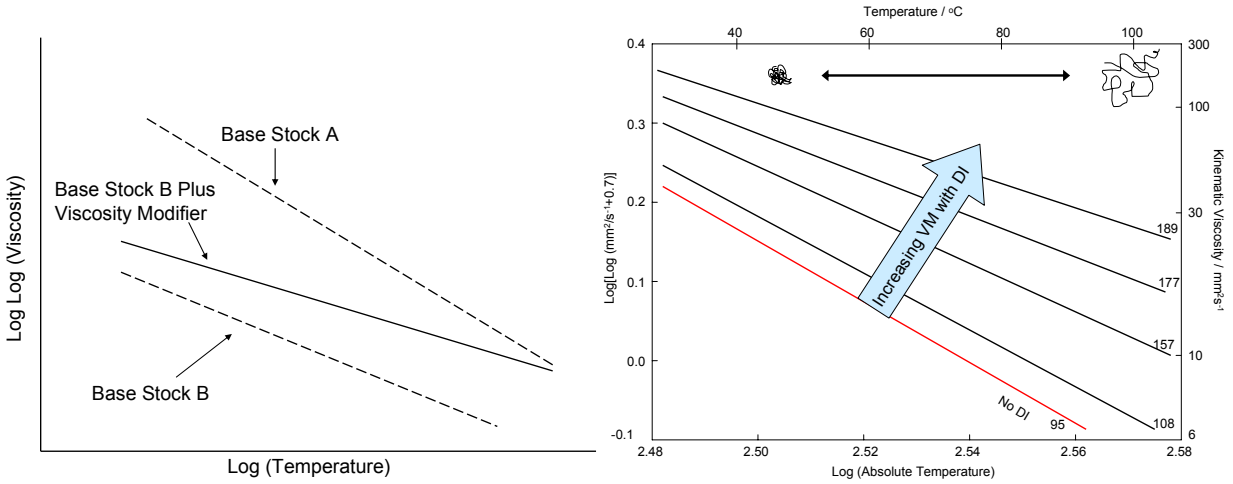

(a) (b)

Figure 162. (a) How viscosity modifiers affect the viscosity/temperature response, (b) Function of viscosity modifiers.

Types of VIIs include Olefin Copolymers (OCPs), poly methacrylates (PMA) and Styrene-butadienes. OCPs typically cause considerable thickening of oil at low temperatures as well as at high temperature. The side chains of the polymer have little effect on the viscosity; it is mainly affected by the length of the back bone. Styrene-butadiene, polyisoprene and poly methacrylate (PMA) are attractive VII components as they retain improve viscosity at high temperature behaviour but reduced at low temperature.

Appendix E. Additional figures for Chapter 6

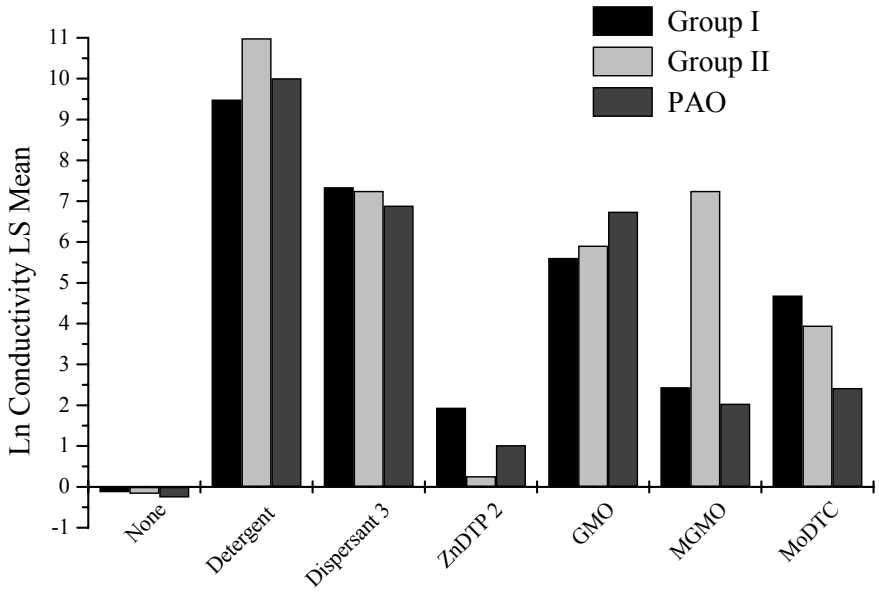

Figure 163. Conductivity for the all oils in the used in the test matrix.

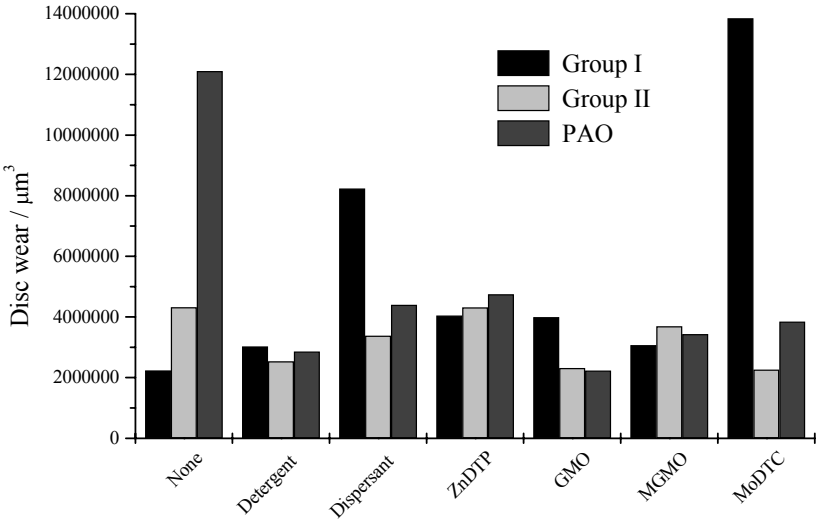

Figure 164. Disc wear average for the entire test matrix.

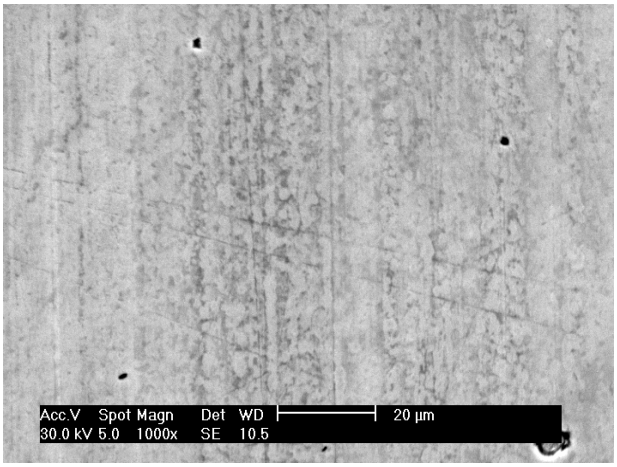

(a)

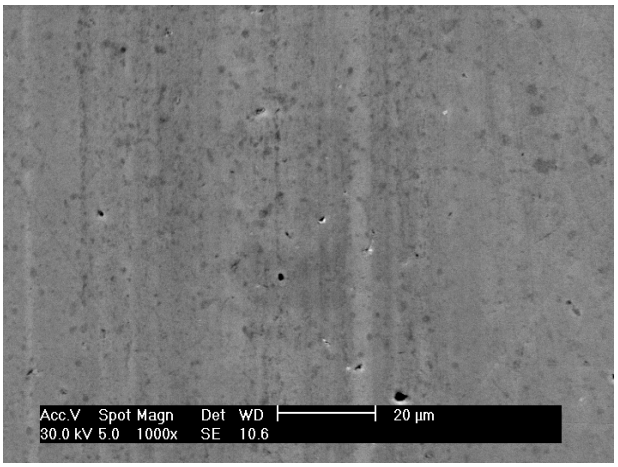

(b)

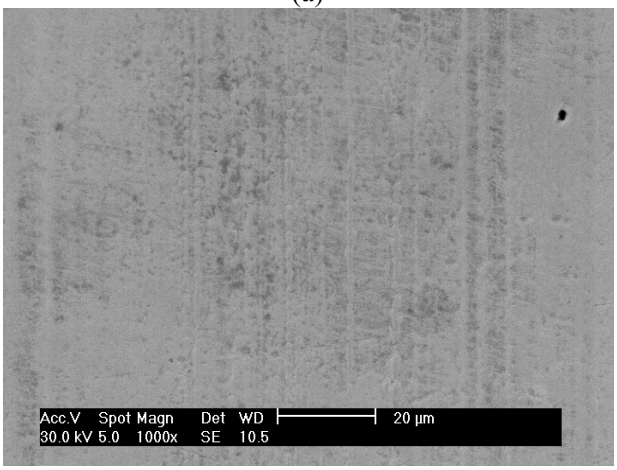

(c)

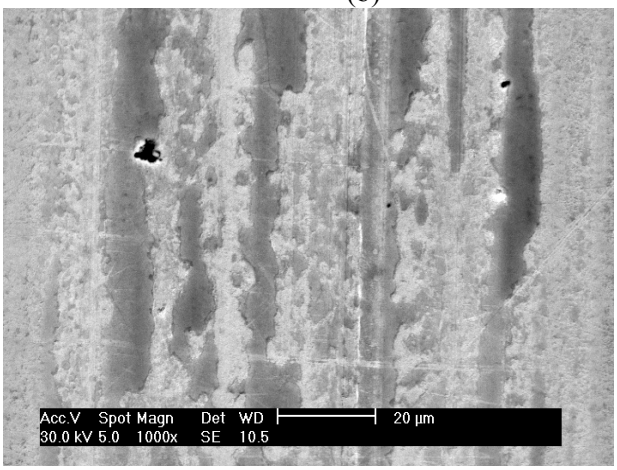

(d)

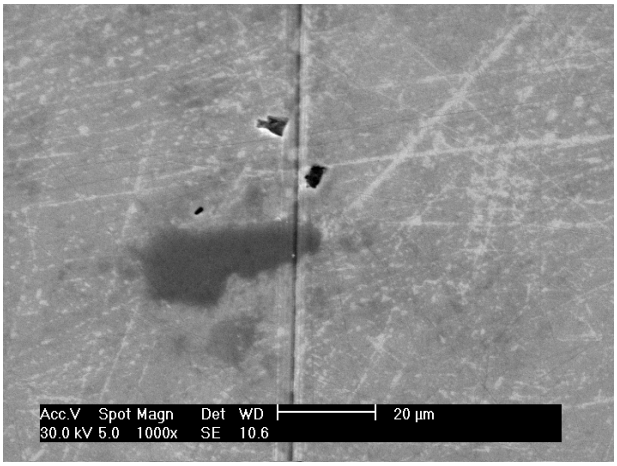

(e)

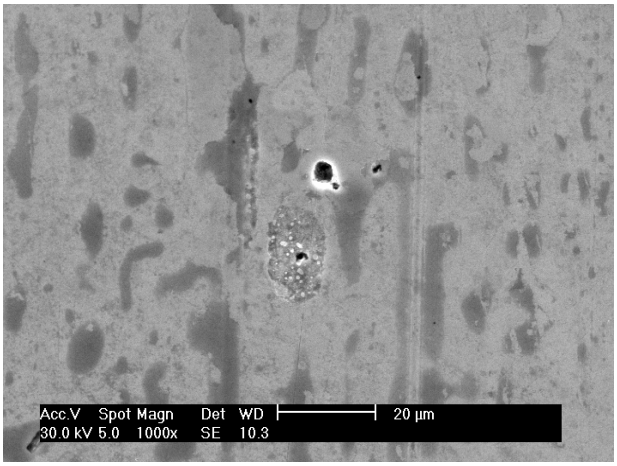

(f)

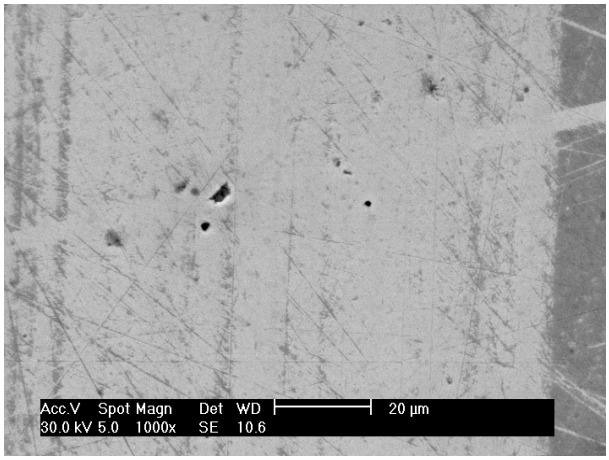

(g)

Figure 165. Micrographs of disc wear track for (a) Group II Base oil, (b) Detergent, (c) Dispersant 3, (d) ZnDTP 2, (e) GMO, (f) MGMO and (g) MoDTC.

References

[1] Howarth S. A century in oil: The shell transport and trading company 1897-1997. Weidenfeld & Nicolson, 1997. ISBN 0 297 82247 0.

[2] Co-ordinating European Council for the Development of Performance Tests for Lubricants and Engine Fuels. Gasoline engine scuffing test. CEC L-38-A-94.

[3] Moore AJ. Automotive lubricants: Today's choice, tomorrow's possibilities. The tribology of internal combustion engines. Mecanical Engineering Publications Limited, 1997:93. ISBN 1 860580718

[4] Powrie HEG, McNicholas K. Gas path condition monitoring during accelerated mission testing of a demonstrator engine. American Institute of Aeronautics and Astronautics Paper 97-2904.

[5] Nurse J, Petch C, Fisher CE. Engine gas path integrity monitoring. Aerotech Paper 1994, C470/6/052.

[6] Powrie HEG, Fisher CE. Monitoring of foreign objects ingested into the intake of a gas turbine aero-engine. Proceedings of the International Conference on Condition Monitoring 1999:175-190.

[7] Wood RJK, Harvey TJ, Morris S, Powrie HEG. Electrostatic monitoring of boundary and mixed lubrication. Proceedings of the 2nd World Tribology Congress, Proceedings of 28th Leeds-Lyon Symposium on Tribology 2001. ISBN 0-444-50969-0.

[8] Morris S, Wood RJK, Harvey TJ, Powrie HEG. Electrostatic charge monitoring of unlubricated sliding wear of a bearing steel. Wear 2003;255:430-443.

[9] Williams J. Engineering Tribology. Oxford University Press, 1994:166-341. ISBN 0521609887.

[10] Bhushan B. Principles and applications of tribology. John Wiley & Sons, 1999. ISBN 0-471-59407-5

[11] Rabinowicz E. Friction and wear of materials. John Wiley & Sons, 1965.

[12] Meriam JL, Kraige LG. Engineering Mechanics: Volume 2 Dynamics 5th Ed. John Wiley & Sons, Inc., 2001. ISBN 0 471 40645 7.

[13] Grubin AN. Investigation of the contact of machine components. Central Scientific Research Institute for Technology and Mechanical Engineering, 1893. DSIR Translation No. 337.

[14] Hamilton GM, Moore SL. Deformation and pressure in an elasto-hydrodynamic contact. Proceedings of the Royal Society A 1971;322:313-330.

[15] Gohar R. Elasto-hydrodynamics. Ellis-Horwood, Chichester 1988. ISBN 1-86094-170-2.

[16] Jacobson B. Rheology and elastohydrodynamic lubrication. Elsevier, 1991. ISBN 0444881468.

[17] Evans HP, Snidle RW. The ehl of point contacts at heavy loads. Proceedings of the Royal Society A 1982;382:183-189.

[18] Dowson D, Higginson GR. A numerical solution to the Elastohydrodynamic problem. Journal of Mechanical Engineering Science 1959;1:6-20.

[19] Dowson D. Higginson GR. Elastohydrodynamic lubrication. Pergamon Press, 1977. ISBN-0-08-021303-0.

[20] Dowson D. History of Tribology. Professional Engineering Publishing, 1998:768. ISBN 186058070X.

[21] Masuda M, Ujino M, Shimoda K, Nishida K, Marumoto I, Moriyama Y. Development of titanium nitride coated shim for a direct acting OHC engine. JSAE Review 1997;18(2):191-191.

[22] Bell JC. Reproducing the kinematic conditions for automotive valve train wear in a laboratory test machine. Proceedings of the Institution of Mechanical Engineers, Part J: Journal of Engineering Tribology 1996;212(J2):135-144.

[23] Morris S. Real-time electrostatic charge monitoring of the wear surfaces and debris generated by sliding bearing steel contacts. PhD Thesis, University of Southampton, 2003.

[24] Trezona RI, Allsopp DN, Hutchings IM. Transitions between two-body and three-body abrasive wear: Influence of test condition in the microscale abrasive wear test. Wear 1999;225:205–214.

[25] Harvey TJ, Morris S, Wood RJK, Powrie HEG. Real-time monitoring of wear debris using electrostatic sensing techniques. Proceedings of the Institute of Mechanical Engineers, Part J: Journal of Engineering Tribology 2007;221(1):27-40.

[26] Needelman WM, Madhavan PV. Review of lubricant contamination and diesel engine wear. SAE Technical Paper 881827. ISSN 0148-7191.

[27] Archard JF. Contact and rubbing of flat surfaces. Journal of Applied Physics 1953;24:981-988.
[28] Preston FW. Theory and design of glass polishing machines. Journal of the Society of Glass Technology 1927;11:214-256.
[29] Bueche F. Mechanical degradation of high polymers. Journal of Applied Polymer Science 1960;4(10):101-106.
[30] Briant J, Denis J, Parc G. Rheological properties of lubricants. Gulf Publishing Company, 1991. ISBN 2710805642.
[31] Kramer DC, Lok BK, Krug RR. The evolution of base oil technology: Turbine lubrication in the 21st century. Herguth WR, Warne TM, Edditors. American Society for Testing and Materials STP 2000;1407:25-39.
[32] Roelands CJA, Vlugter JC, Waterman HI. The viscosity-pressure-temperature relationship of lubricating oils. Transactions of the American Society of Mechanical Engineers. Journal of Basic Engineering 1963;85:601-607.
[33] Bayrakceken H, Ucun I, Tasgetiren S. Fracture analysis of a camshaft made from nodular cast iron. Engineering Failure Analysis 2006;13:1240–1245.
[34] Anderson BS. Company perspectives in vehicle tribology: Volvo. Proceedings of the 17th Leeds–Lyon Symposium on Tribology, Tribology Series 1991;18:503–506.
[35] Priest M, Taylor CM. Automobile engine tribology – approaching the surface. Wear 2000;241:193-203.
[36] Dowson D. Developments in lubrication – the thinning film. Journal of Physics D: Applied Physics 1992;25:A334–A339.
[37] Heyes AM. Automotive component failures. Engineering Failure Analysis 1998;2:129–141.
[38] Dowson D, Taylor CM, Zhu G. An experimental study of the tribology of a cam and flat faced follower. Proceedings of the 2nd International Conference, Combustion Engines – Reduction of Friction and Wear IMechE, 1989;C375/025:97-108.
[39] Taylor CM. Automobile engine tribology – design considerations for efficiency and durability. Wear 1998;221:1-8.
[40] Coy RC. Practical applications of lubrication models in engines. Tribology International, 1998;31(10):563-571.
[41] Chen FY. Mechanics and design of cam mechanics. Pergamon Press, 1982. ISBN 0 08 028049 8.
[42] Ball AD, Dowson D, Taylor CM. Cam and follower design. Proceedings of the 15th Leeds-Lyon Symposium on Tribology – Tribological design of machine elements, Tribology Series 1989;14: 111–130.
[43] Brooks AC. Developments in camshaft and follower technology: The tribology of internal combustion engines. Mechanical Enginerering Publication Limited, 1997:53. ISBN 1 86058 0718.
[44] Smith WF. Principles of materials science and engineering. 2nd Ed. McGraw-Hill International Editions, 1990.
[45] Haque T, Morina A, Neville A, Kapadia R, Arrowsmith S. Non-ferrous coating/lubricant interactions in tribological contacts: Assessment of tribofilms. Tribology International 2007;40(10-12):1603-1612.
[46] Michalski J, Marszalek J, Kubiak K. An experimental study of diesel engine cam and follower wear with particular reference to the properties of the materials. Wear 2000;240:168–179.
[47] Gautam M, Chitoor K, Durbha M, Summers JC. Effect of diesel soot contaminated oil on engine wear: Investigation of novel oil formulations. Tribology International 1999;32:687–699.
[48] Humbert D, Basset JJ, Vaisseyre JJ, Weston JPC. Valve train wear - Report on CEC IGL-17 Activities. SAE Technical Paper 861513.
[49] Roylance BJ, Wang G, Bovington CH, Hubbard A. Running-in wear behaviour of valve train systems. Proceedings of the 17th Leeds-Lyon Symposium on Tribology – Vehicle Tribology. Tribology Series, Elsevier, Amsterdam 1991;18:143-147.
[50] Test Method for Evaluation of Automotive Engine Oils for Inhibition of Deposit Formation and Wear in a Spark-Ignition Internal Combustion Engine Fueled with Gasoline and Operated Under Low-Temperature, Light-Duty Conditions. ASTM Method D5302.

[51] Shannon I, Bell JC, Cadu J. The effect of engine operating temperature on valve train wear: Mechanistic understanding through used oil analysis. Institution of Mechanical Engineers, Part J: Journal of Engineering Tribology 1996;210(J2):145-152.

[52] Bell JC. Gasoline engine valve train design evolution and the antiwear requirements of motor oils. Proceedings of the Institution of Mechanical Engineers, Part J: Journal of Engineering Tribology 1998;212:243-257.

[53] Colgan T, Bell JC. A predictive model for wear in automotive valve train systems. SAE Technical Paper 892145.

[54] Dyson A. Kinematics and wear patterns of cam and finger follower automotive valve gear. Tribology International 1980;13(3):121–132.

[55] Zhu G, Taylor CM. Tribological analysis and design of a modern automobile cam and follower. Engineering research series 7. The Cromwell Press Limited, 2001. ISBN 1 86058 203 6.

[56] Williamson BP, Bell JC. The effects of engine oil rheology on the oil film thickness and wear between a cam and rocker follower. SAE Technical Paper 962031.

[57] Taylor CM. Valve train lubrication analysis. Proceedings of the 17th Leeds-Lyon Symposium on Tribology - Vehicle Tribology. Tribology Series 1991;18:119-131.

[58] Bell JC, Davies PT, Fu WB. Prediction of automotive valve train wear patterns with a simple mathematical model. Proceedings of the 12th Leeds–Lyon Symposium on Tribology, Tribology Series 1985:323-335.

[59] Lancaster JK. Dry bearings: A survey of materials and factors affecting their performance. Tribology 1973:6(6);219–251.

[60] Childs THC. The sliding wear mechanisms of metals, mainly steels. Tribology International 1980;13(6):285-293.

[61] Bell JC, Willemse PJ. Mid-life scuffing failure in automotive cam-follower contacts. Proceedings of the 1st World Tribology Congress. Institute of the Mechanical Engineers, Part J: Journal of tribology 1997:259-269.

[62] Roper GW, Bell JC. Review and evaluation of lubricated wear in simulated valve train contact conditions. SAE Technical Paper 952473.

[63] Harrison P. A study of the lubrication of automotive cams. PhD Thesis, University of Leeds, 1985:281.

[64] Zhu G. PhD. A theoretical and experimental study of the tribology of cam and follower. PhD Thesis, University of Leeds, 1988:236.

[65] Williamson BP, Perkins HN. The effects of engine oil rheology on the oil film thickness between a cam and rocker follower. SAE Technical Paper 922346.

[66] Coy RC, Dyson X. A rig to simulate the kinematics of the contact between cam and finger follower. Lubrication Engineering 1983;39(3):143–152.

[67] Bell JC, Willemse PJ. The development of scuffing failure in an automotive valve train system. World Tribology Congress, 1997.

[68] Kapoor A, Williams JA, Johnson KL. The steady state sliding of rough surfaces. Wear 1994;175:81-92.

[69] Webster MN, Sayles RS. A numerical model for the elastic frictionless contact of real rough surfaces. Transaction ASME, Journal of Tribology 1986;108(3):314-320.

[70] Tura JM, Traveria A, de Castellar MD, Pujadas J, Blouet J, Gras R, Magham HG, Belair P, Hanau T, Romero A. Frictional properties and wear of a molybdenum coating and a bronze (Cu-10%Sn) with friction modifier fillers. Wear 1995;189:70-76.

[71] Callister WD. Materials science and engineering an introduction, 4th Ed. John Wiley & Sons, Inc. 1997. ISBN 0 471 13459 7.

[72] Elleucha K, Elleuch R, Mnif R, Fridrici V, Kapsa P. Sliding wear transition for the CW614 brass alloy. Tribology International 2006;39:290–296.

[73] Mang TH, Dresel W. Lubricants and Lubrication. 2nd Ed. Wiley 2007;763. ISBN 987-3-527-31497-3.

[74] Ko PL, Taponat MC, Pfaifer R. Friction-induced vibration – with and without external disturbance. Tribology International 2001;34:7-24.

[75] Devlin MT, Tersigni SH, Li S, Turner TL, Jao T, Yatsunami K, Cameron T. Fundamentals of anti-shudder durability: Part II - Fluid effects. SAE Technical Paper 2003-01-3254.

[76] Måki R. Wet clutch tribology – friction characteristics in limited slip differentials. Luleå University of Technology, Division of Machine Elemets, 2005.
[77] Kato Y, Shibayama T. Mechanisms of automatic transmissions and their requirements for wet clutches and wet brakes. Japanese Journal of Tribology 1994;39(12):1427-1437.
[78] Yamamoto T. The present and future state of tribological research into wet friction materials. Japanese Journal of Tribology 1994;39:1419-1425.
[79] Gil JJ, Sugiyama H, Arai T. Visualization of cavitation phenomena in wet clutch engagement process. JSME International Journal, Series C 1997;40(1):144-149.
[80] Kato Y, Akasaka R, Shibayama T. Experimental study on the lock-up shudder mechanism of an automatic transmission. Japanese Journal of Tribology 1994;39.
[81] Matsumoto T. Friction materials and lubricating oils. Petrotech 1988;11(2):111.
[82] Lu Y. Friction performance of phenolic binders. Proceedings of the International SAMPE Symposium and Exhibition 2002;47:236-41.
[83] Kugimiya T. Effects of additives of ATF and components of friction material for AT on mu-v characteristics. Japanese Journal of Tribology 2000;45(3):215-227.
[84] Kamada Y, Araki M, Yoshida T, Wang N, Mukaida K. Effects of adsorption of ATF additives to wet friction materials on friction performance at the low sliding velocity range. Japanese Journal of Tribology 1999;44:127-139.
[85] Lu Y. A combinatorial approach for automotive friction materials: Effects of ingredients on friction performance. Composites Science and Technology 2006;66:591-598.
[86] Matsumoto T. Wet-type friction materials and lubricating Oils. Petrotec 1988;11(12):111.
[87] Chiba N, Kano M, Inoue M. Mechanism of compression fatigue of wet friction materials. Journal of Society of Automotive Engineers Review 2001;22:169-174.
[88] Watts RF, Nibert RK, Tanson M. Anti-shudder durability of automatic transmission fluids: mechanism of the loss of shudder control. Tribotest 1997;4:29-50.
[89] Haycock RF, Hillier JE, Caines AJ. Automotive lubricants reference book 2nd Ed. Professional Engineering Publishing, 2004;277. ISBN 1 86058 471 3.
[90] Li S, Devlin MT, Tersigni SH, Jao T-C. Fundamentals of anti-shudder durability Part I – Clutch plate study. SAE Technical Paper 2003-01-1983.
[91] Watanabe N, Ichihashi T, Kato M. The requirements for the latest ATF and problems of Commercially Available ATF. Proceedings of the 8th Annual Fuels and Lubrication Asia Conference and Exhibition 2002.
[92] Piper D. Automatic transmissions – an American perspective. Berichte VDI, 1995. ISBN 1175 25-39.
[93] Nyman P, Mäki R, Olsson R, Ganemi B. Influence of surface topography on friction characteristics in wet clutch applications. Wear 2006;261:46-52.
[94] Kugimiya T. Development of automatic transmission fluid for slip-controlled lock-up clutch systems. SAE Technical Paper 952348.
[95] Nakada T, Nomura T, Yoshioka T, Nonoyama M. A study of additive effects on ATF frictional properties using new test methods. SAE Technical Paper 902150.
[96] George S, Balla S, Gautam M. Effect of diesel soot contaminated oil on engine wear. Wear 2007;262:1113–1122.
[97] Smith GC. Surface analytical science and automotive lubrication. Journal of Physics Part D: Applied Physics 2000;33:187–197.
[98] Willermet PA. Some engine oil additives and their effects on antiwear film formation. Tribology 1998;Letters 5:41–47.
[99] Mortier RM, Orszulik ST. Chemistry and technology of lubricants, 2nd Ed. Blackie Academic & Professional, 1997. ISBN 0 7514 0246 X.
[100] Dornte RW. Oxidation of white oils. Industrial and Engineering Chemistry 1936;28:26.
[101] American Petroleum Institute Base stock categories. API Publication 2007;1509:82-83
[102] Mandakovic R. Assessment of EP additives for water miscible metalworking fluids. Journal of Synthetic Lubrication 1999;16(1):13-26.
[103] Rudick LR. Lubricant additives chemistry and applications. Marcel Dekker LR, 2003. ISBN 0-8247-0857-1.

[104] Bowden FP, Tabor D. The friction and lubrication of solids. Oxford University Press, 1950 (republished 2001). ISBN-10: 0198507771.
[105] Podgornik B, Hren D, Vižintin J, Jacobson S, Stavlid N, Hogmark S. Combination of DLC coatings and EP additives for improved tribological behaviour of boundary lubricated surfaces. Wear 2006;261(1):32–40.
[106] Neville A, Kollia-Rafailidi V. A comparison of boundary wear film formation on steel and a thermal sprayed Co/Cr/Mo coating under sliding conditions. Wear 2002;252(3-4):227-239.
[107] Equey S, Roos S, Mueller U, Hauert R, Spencer ND, Crockett R. Tribofilm formation from ZnDTP on diamond-like carbon. Wear 2008;264(3-4):316-321.
[108] Neville A, Morina A, Haque T, Voong M. Compatibility between tribological surfaces and lubricant additives: How friction and wear reduction can be controlled by surface/lube synergies. Tribology International 2007;40:1680–1695.
[109] Korcek S, Jensen RK, Johnson MD, Sorab J. Fuel efficient engine oils, additive interactions, boundary friction, and wear. Proceedings of the 25th Leeds–Lyon Symposium - Tribology, Lubrication at the Frontier, Tribology Series 1999;13-24.
[110] Lin YC, So H. Limitations on use of ZDDP as an antiwear additive in boundary lubrication. Tribology International 2004;37:25–33.
[111] Morina A, Neville A. Tribofilms: Aspects of formation, stability and removal. Journal of Physics Part D: Applied Physics 2007;40:5476–5487.
[112] Inoue K, Watanabe H. Interactions of engine oil additives. American Society of Lubrication Engineers Transactions 1983;26(2):189-199.
[113] Rizvi SQA. Additives and additive chemistry. Fuels and Lubricants Handbook: Technology, Properties, Performance, and Testing. American Society for Testing and Materials Manual Series 2005;37:199-248.
[114] Smiechowski MF, Lvovich VF. Characterization of non-aqueous dispersions of carbon black nanoparticles by electrochemical impedance spectroscopy. Journal of Electroanalytical Chemistry 2005;577:67–78.
[115] Han N, Shui L, Lui W, Xue Q, Sun Y. Study of the lubrication mechanism of overbased Ca sulfonate on additives containing S or P. Tribology Letters, 2003;14(4):269-274.
[116] Marsh JF. Colloidal Lubricant Additives. Chemistry and Industry 1977;20:470-473.
[117] Riga AT, Hong H, Kornbrekke RE, Calhoon JM, Vinci JN. Reactions of overbased sulfonates and sulfurized compounds with ferric oxide. Lubrication Engineering 1993;49(1):67-71.
[118] Costello MT. Effects of basestock and additive chemistry on traction testing. Tribology Letters 2005;18(1):91-97.
[119] Luisi PL, Staub BE. Reverse Micelles. Plenum Press New York 1984:21-36. ISBN 0306416204.
[120] Pileni MP. Structure and reactivity in reverse micelles. Elsevier, 1989:13-43. ISBN 0444881662.
[121] Martin JM, Vacher B, Ponsonnet L, Dupuis V. Chemical bond mapping of carbon by image-spectrum EELS in the second derivative mode. Ultramicroscopy 1996;65(3):229.
[122] Mansot JL, Hallouis M, Martin JM. Colloidal antiwear additives – Part I: Structural study of overbased calcium alkylbenzene sulfonate micelles. Colloids and Surfaces A: Physicochemical and Engineering Aspects 1993;71:123-134.
[123] Ottewill RH, Sinagra E, Macdonald IP, Marsh JF, Heenan RK. Small-angle neutron-scattering studies on nonaqueous dispersions Part 5: Magnesium carbonate dispersions in hydrocarbon media. Colloid and Polymer Science 1992;270(6):602-608.
[124] Roman J-P, Hoomaert P, Faure D, Biver C, Jacquet F, Martin JM. Formation and structure of carbonate particles in reverse microemulsions. Journal of Colloid and Interface Science 1991;144:324-339.
[125] Kandori K, Konno K, Kitahara A. Formation of ionic water/oil microemulsions and their application in the preparation of CaCO, particles. Journal of Colloid and Interface Science 1988;122:78-82.
[126] Delfort B, Daoudal B, Barre L. Particle size determination of (functionalised) colloidal calcium carbonate by small angle x-ray scattering-relation with antiwear properties. Tribology Transactions 1999;42:296-302.

[127] Belle C, Beraud C, Faure D, Gallo R, Hornaert P, Martin JM. Rey C. Polyphasic reaction mechanism: Kinetic of overbased Calcium sulfonate synthesis in non-polar medium. Journal of Chemical Physics 1990;87:93-104.
[128] Hunt MW. Overbased alkali metal sulfonates. US Patent 4.867891, 1989.
[129] Hudson LK, Eastoe J, Dowding PJ. Nanotechnology in action: Overbased nanodetergents as lubricant oil additives. Advances in Colloid and Interface Science 2006;123–126:425–431.
[130] Inoue K, Nose Y. Solubilization by Sulfonates and Related Phenomena. Tribology Transactions 1987;31:76-82.
[131] Inoue K, Nose Y. Method for producing alkaline earth metal borate dispersions. US Patent 4,683,126, 1987.
[132] Galsworthy J, Hammond S, Hone D. Oil-soluble colloidal additives. Current Opinion in Colloid and Interface Science 2000;5:274-279.
[133] Bandyopadhyaya R, Kumar R, Gandhi KS. Modelling od $CaCo_3$ nanoparticle formation during overbasing of lubricating oil addictives. Langmuir 2001;17(4):1015.
[134] O'Connor SP, Crawford J, Cane C. Overbased lubricant detergents: A comparative study. Lubrication Science 1994;6(4):297-325.
[135] Griffiths JA, Bolton R, Heyes DM, Clint JH, Taylor SE. Physico-chemical characterisation of oil-soluble overbased phenate detergents. Journal of the Chemical Society Faraday Transactions 1995;91:687-696.
[136] Griffiths JA, Heyes DM. Atomistic simulation of overbased detergent inverse micelles. Langmuir 1996;12:2418-2424.
[137] Bearchell CA, Danks TN, Heyes DM, Moreton DJ, Taylor SE. Experimental and molecular modelling studies of overbased detergent particles. Physical Chemistry Chemical Physics 2000;2: 5197.
[138] Bearchell CA, Heyes DM, Moreton DJ, Taylor SE. Overbased detergent particles: Experimental and molecular modelling studies. Physical Chemistry Chemical Physics 2001;3:4774-783.
[139] Glavati OL, Kurilo SM, Kravchuk GG, Gordash YuT, Shilov VV, Tsukruk VV, Lokhonya OA. Structure of micelles of overbased salicylate lube oil additives. Chemistry and Technology of Fuels and Oils 1989;25:273-275.
[140] Bearchell CA, Edgar JA, Heyes DM, Taylor SE. Dielectric spectroscopy and molecular simulation evidence for aggregation of surfactant-stabilized calcium carbonate nonocolloids in organic media. Journal of Colloid and Interface Scinece 1999;210:231-240.
[141] Miller JF, Clifton BJ, Benneyworth PR, Vincent B, Macdonald IP, Marsh JF. Electrophoretic studies of calcium carbonate particles dispersed in various hydrocarbon liquids. Colloids Surfaces 1992;66:197-202.
[142] Hone DC, Robinson BH, Steytler DC, Glyde RW, Cleverly JA. Acid-base chemistry in high-performance lubricating oils. Canadian Journal Chemistry 1999;77:842-848.
[143] Hone DC, Robinson BH, Steytler DC, Glyde RW, Galsworthy JR. Mechanism of acid neutralisation by overbased colloidal additives in hydrocarbon media. Langmuir 2000;16(2):340-346
[144] Koch P, Serio AD. Compounds useful as detergent additives for lubricants and lubricating compositions. US Patent 5,021,174, 1991.
[145] Giasson S. Formation mechanism of boundary film obtained with overbased calcium sulfonates. PhD Dissertation, University of Paris VI, 1992;78-93.
[146] Mansot JL, Hallouis M, Martin JM. Colloidal antiwear additives – Part II: Tribological behaviour of colloidal additives in mild wear regime. Colloids and Surfaces A, Physicochemical and Engineering Aspects 1993;75:25-31.
[147] Chinas-Castillo F, Spikes HA. The behavior of colloidal solid particles in elastohydrodynamic contacts. Tribology Transactions 2000;43:357-394.
[148] Najman M, Kasrai M, Bancroft GM, Davidson R. Combination of ashless antiwear additives with metallic detergents: Interactions with neutral and overbased calcium sulfonates. Tribology International 2006;39:342–355.
[149] Morizur MJ, Teeysset O. Antiwear actions of additives in solid dispersion. Lubrication Science 1989;44:277-289.

[150] Liston TV. Engine lubricant additives. What they are and how they function. Lubrication Engineering 1992;48:389–97.
[151] Morizur MF, Teysset O. Engine oils and automotive lubrication: Anti-wear actions of additives in solid dispersion. Edited by Wilfried J Bartz. Marcel Dekker, 1993. ISBN 0-8247-8807-9.
[152] Costello MT, Urrego RA. Study of surface films of the ZDDP and the MoDTC with crystalline and amorphous overbased calcium sulfonates by XPS. Tribology Transactions 2007;50:217-226
[153] Costello MT, Urrego RA, Kasrai M. Study of surface films of crystalline and amorphous overbased sulfonates and sulfurized olefins by X-ray absorption near edge structure (XANES) spectroscopy. Tribology Letters 2007;26(2):173-180.
[154] Costello MT. Study of surface films of amorphous and crystalline overbased calcium sulfonate by XPS and AES. Tribology Transactions 2006;49:592-597.
[155] Kubo T, Fujiwara S, Nanao H, Minami I, Mori S. TOF-SIMS analysis of boundary films derived from calcium sulfonates. Tribology Letters 2006;23(2):171-176.
[156] Cizaire L, Martin JM, Gresser E, Truong Dinh N, Heau C. Tribochemistry of overbased calcium detergents studied by ToF-SIMS and other surface analyses. Tribology Letters 2004;17(4):715-721.
[157] Giasson S, Espinat D, Palermo T, Ober R, Pessah M, Morizur MF. Small angle x-ray scattering on calcium sulfonates dispersions-effects of friction on microstructure. Journal of Colloid and Interface Science 1992;153:355-367.
[158] Shirahama S, Hirata M. The effects of engine oil additives on valve train wear. Lubrication Science 1989;1(4):365-384.
[159] Sugimoto S. New researches in additives (1): Behavior of over-based sulfonates as extreme-pressure Aagents in metal working. Japanese Tribology Transactions 1995;40(4):269-275.
[160] Giasson S, Palermo T, Buffeteau T, Debsat B, Turlet JM. Study of boundary film formation with overbased calcium sulfonate by PM-IRRAS spectroscopy. Thin Solid Films 1994;252:111-119.
[161] Willermet PA, Carter RO, Schmitz PJ, Everson M, Scholl DJ, Weber WH. Formation, structure, and properties of lubricant-derived antiwear films. Lubrication Science 1997;9(4):325-348.
[162] Minami I, Ichihashi T, Kubo T, Nanao H, Mori S. Tribochemical approach toward mechanism for synergism of lubricant additive on antiwear and friction reducing properties. Proceedings of the 31st Leeds-Lyon Symposium on Tribology - Tribology and Interface Engineering Series 2005;48:259–268.
[163] Faure D, Hoornaert P, Roman JP, Gallo R, Martin JM. Study of the formation of colloidal overbased calcium sulfonate detergents. Proceeding of the Japan International Tribology Conference 1990:1043-1048.
[164] Delfort B, Born M, Daoudal B, Dixmier F, Lallement J. Functionalization of overbased calcium sulfonates-synthesis and evaluation of antiwear and extreme-pressure performances. Lubrication Engineering 1995;51(12):981-990.
[165] Kapsa P, Martin JM, Blanc C, Georges JM. Antiwear mechanism of ZDDP in the presence of calcium sulfonate detergent Trans. ASME, Journal of Lubrication Technology 1981;103:486-496.
[166] Costello MT, Kasrai M. Study of surface films of overbased sulfonates and sulfurized olefins by x-ray absorption near edge structure (XANES) spectroscopy. Tribology Letters 2006;24(2):163-169.
[167] Georges JM, Mazuyer D, Loubet JL, Tonck A. Friction with colloidal lubrication in E.I.Sa. Fundamentals of Friction. Edited by H. Pollock. Kluwer Academic Publishers, 1992. ISBN 1023-8883.
[168] Drauglis ACM. Boundary lubrication: Monolayer or multilayer. Wear 14:363-384;1969.
[169] Costello MT, Riff IL. Study of hydroforming lubricants with overbased sulfonates and friction modifiers. Tribology Letters 2005;20(3–4):201-208.
[170] Akhmatov AS. Molecular physics of boundary lubrication. Translation, Israel Program for Scientific Translations, 1963.
[171] Morina A, Neville A, Priest M, Green JH. ZDDP and MoDTC interactions and their effect on tribological performance: Tribofilm characteristics and its evolution. Tribology Letters 2006;24:243–56.

[172] Graham J, Spikes H, Korcek S. The friction reducing properties of molybdenum dialkyldithiocarbamate additives: I. Factors influencing friction reduction. Tribology Transactions 2001;44:626–36.
[173] Grossiord C, Varlot K, Martin JM, Mogne TL, Esnouf C, Inoue K. MoS_2 single sheet lubrication by molybdenum dithiocarbamate. Tribology International 1998;31:737–43.
[174] Davis FA, Eyre TS. The effect of a friction modifier on piston ring and cylinder bore friction and wear. Tribology International 1990;23:163–171.
[175] Martin JM, Mogne TL, Grossiord C, Palermo T. Tribochemistry of ZDDP and MoDDP chemisorbed films. Tribology Letters 1996;2(3)313–326.
[176] Spikes H. The history and mechanisms of ZDDP. Tribology Letters 2004;17(3):469-489.
[177] Barnes AM, Bartle KD, Thibon VRA. A review of zinc dialkyldithiophosphates (ZDDPS): Characterisation and role in the lubricating oil. Tribology International 2001;34(6)389-395.
[178] Gellman AJ, Spencer ND. Surface Chemistry in Tribology. Proceedings of the Institute of Mechanical Engineers, Part J: Journal of Engineering Tribology 2002;216(6):443-461.
[179] Fuller M, Yin Z, Kasrai M, Bancroft GM, Yamaguchi ES, Ryason PR, Willermet PA, Tan KH. Chemical characterization of Tribochemical and thermal films generated from neutral and basic ZDDPs using X-ray absorption spectroscopy. Tribology International 1997;30(4):305–315.
[180] Khorramain BA, Iyer GR, Kodali S, Natarajan P, Tupil R. Review of antiwear additives for crankcase oils. Wear 1993;169(1):87–95.
[181] Kennerly GW, Patterson Jr WL. Kinematic studies of petroleum antioxidants. Industrial & Engineering Chemistry 1956;48(10):1917-1924.
[182] Colclough T, Cunneen JI. Oxidation of organic sulphides, Part XV. The antioxidant action of phenothiazine, zinc isopropylxanthate, zinc di-isopropyldithiophosphate, and zinc dibutyldithiocarbamate, in squalene. Journal of the Chemical Society 1964:4790 – 4793.
[183] Howard JA, Ohkatsu Y, Chenier JHB, Ingold KU. Metal complexes as antioxidants. I. The reaction of zinc Dialkyldithiophosphates and related compounds with peroxy radicals. Canadian Journal of Chemistry 1973;51(10):1543-1553.
[184] Al-Malaika S, Coker M, Scott G. Mechanism of antioxidant action: Nature of transformation products of dithiophosphates Part 1. Their role as antioxidants in polyolefins. Polymer Degradation and Stability 1988;22(2):147-159.
[185] Willermet PA, Mahoney LR, Haas CM. The effects of antioxidant reactions on the wear behaviour of a zinc dialkyldithiophosphate. American Society of Lubrication Engineers Transactions 1978;22(4):301-306.
[186] So H, Lin YC. The theory of antiwear for ZDDP at elevated temperature in boundary lubrication condition. Wear 1994;177(2):105–115.
[187] Bec S, Tonck A, Georges JM, Coy RC, Bell JC, Roper GW. Relationship between mechanical properties and structures of zinc dithiophosphate antiwear films. Proceedings of The Royal Society: Mathematical, Physical and Engineering Sciences 1999;455:4181–203.
[188] Eglin M, Rossi A, Spencer ND. A combinatorial approach to elucidating tribochemical mechanisms. Tribology Letters 2003;15(3):193-198.
[189] Bell JC, Delargy KM, Seeney AM. The removal of substrate material through thick zinc dithiophosphate antiwear films. Procedings of the 18th Leeds-Lyon Symposium on Tribology, Tribology Series 1992;21:387–396.
[190] Varlot K, Kasrai M, Martin JM, Vacher B, Bancroft GM, Yamaguchi ES, Ryason PR. Antiwear film formation of neutral and basic ZDDP: Influence of the reaction temperature and of the concentration. Tribology Letters 2000;8(1):9-16.
[191] Martin JM, Grossiord C, Mogne TLe, Bec S, Tonck A. The two-layer structure of Zndtp tribofilms Part I: AES, XPS and XANES analyses. Tribology International 2001;34(8):523-530.
[192] Yin Z, Kasrai M, Fuller M, Bancroft GM, Fyfe K, Tan KH. Application of soft X-ray adsorption spectroscopy in chemical characterization of antiwear films generated by ZDDP Part I: The effects of physical parameters. Wear 1997;202(2):172-191.
[193] Kasrai M, Fuller M, Scaini M, Yin Z, Brunner RW, Bancroft GM, Fleet MK, Fyfe K, Tan KH. Study of tribochemical film formation using X-ray absorption and photoelectron spectroscopies. Procedings of the 21st Leeds-Lyon Symposium on Tribology, Tribology Series 1995:659-669.

[194] Palacios JM. Thickness and chemical composition of films formed by antimony dithiocarbamate and zinc dithiophosphate. Tribology International 1986;19(1):35-39.
[195] Fuller MLS, Fernandez LR, Massoumi GR, Lennard WN, Kasrai M, Bancroft GM. The use of X-ray absorption spectroscopy for monitoring the thickness of antiwear films from ZDDP. Tribology Letters 2000;8:187–92.
[196] Fujita H, Glovnea RP, Spikes HA. Study of zinc Dialkydithiophosphate antiwear film formation and removal processes, Part I: Experimental. Tribology Transactions 2005;48(4):558-566.
[197] Fujita H, Spikes HA. The formation of zinc dithiophosphate antiwear films. Proceedings of the Institution of Mechanical Engineers, Part J: Journal of Engineering Tribology 2004;218(4):265-277.
[198] Ji H, Nicholls MA, Norton PR, Kasrai M, Caperhart TW, Perry TA, Cheng Y. Zinc-dialkyl-dithiophosphate antiwear films: Dependence on contact pressure and sliding speed. Wear 2005;258(5-6):789–799.
[199] Yamaguchi ES, Ryason PR. Inelastic electron tunneling spectra of lubricant oil additives on native aluminum oxide surfaces. Tribology Transactions 1993;36(3):367-374.
[200] Dacre B, Bovington CH. Adsorption and desorption of dibenzyl disulfide and dibenzyl sulfide on steel. American Society of Lubrication Engineers Transactions 1982;25(2):272-278.
[201] Coy RC, Jones RB. The theramal degradation and EP performance of zinc Dialkydithiophosphate additives in white oil. American Society of Lubrication Engineers Transactions 1981;24(1):77-90.
[202] Ashford JS, Bretherick L, Gould P. The thermal decomposition of zinc di-(4-Methylpentyl-2) dithiophosphate. Journal of Applied Chemistry 1965;15:170.
[203] Dickert JJ, Rowe CN. Thermal decomposition of metal O, O-dialkyl phosphorodithioates. The Journal of Organic Chemistry 1967;32:647.
[204] Taylor L, Dratva A, Spikes HA. Friction and wear behavior of zinc Dialkyldithiophosphate additive. Tribology Transactions 2000;43(3):469-479.
[205] Fuller MLS, Kasrai M, Bancroft GM, Fyfe K, Tan KH. Solution decomposition of zinc dialkyl dithiophosphate and its effect on antiwear and thermal film formation studied by X-ray absorption spectroscopy. Tribology International 1998;31(10):627-644.
[206] Bancroft GM, Kasrai M, Fuller M, Yin Z, Fyfe K, Tan KH. Mechanisms of tribochemical film formation: Stability of tribo- and thermally-generated ZDDP films. Tribology Letters 1997;3(1):47-51.
[207] Piras FM, Rossi A, Spencer ND. Combined in situ (ATR FT-IR) and ex situ (XPS) study of the ZnDTP-iron surface interaction. Tribology Letters 2003;15(3):181-191.
[208] Neville A, Kollia V. Comparison of tribological properties of metal–metal and metal–cermet couples under lubricated and dry conditions. Surface Engineering 2000;16(2):131-136.
[209] Aktary M, McDermott MT, McAlpine GA. Morphology and nanomechanical properties of ZDDP antiwear films as a function of tribological contact time. Tribology Letters 2002;12(3):155-162.
[210] Willermet PA, Kandah SK. Some observations on the role of oxygen in lubricated wear. Lubrication Science 1993;5(5-2):129–47.
[211] Zhang Z, Yamaguchi ES, Kasrai M, Bancroft GM. Tribofilms generated from ZDDP and DDP on steel surfaces: Part 1, growth, wear and morphology. Tribology Letters 2005;19(3):211-220.
[212] Hutchings IM. Tribology: Friction and Wear of Engineering Materials. Edward Arnold, 1992. ISBN 0340 56184 X.
[213] Habeeb JJ, Stover WH. The role of hydroperoxides in engine wear and the effect of zinc dialkyldithio phosphates. American Society of Lubrication Engineers Transactions 1987;30(4):419-426.
[214] Rounds FG. Effects of hydroperoxides on wear as measured in four-ball wear tests. Tribology Transactions 1993;36(2):297-303.
[215] Belin M, Martin JM, Mansot JL. Role of iron in the amorphization process in friction-induced phosphate glasses. Tribology Transactions 1989;32(3):410-413.
[216] Martin JM. Antiwear mechanisms of zinc dithiophosphate: A chemical hardness approach. Tribology Letters 1999;6(1):1-8.
[217] Fujita H, Spikes HA. The influence of soot on lubricating films. Proceedings of the 30th Leeds-Lyon symposium on Tribiology, Tribology Series 2004;43:37-43.

[218] Morina A, Neville A, Green JH. Priest M. Additive/additive interactions in boundary lubrication: A study of film formation and tenacity. Proceedings of the 31st Leeds–Lyon Symposium on Tribology, Tribology Series 2005;48:757–766.
[219] Sheasby JS, Caughlin TA. Proceedings of the 27th Leeds-Lyon Symposium on Tribology, 1994.
[220] Minfray C, Martin JM, Lubrecht T, Belin M, Mogne TLe. A novel experimental analysis of the rheology of ZDDP tribofilms. Proceedings of the 29th Leeds-Lyon Symposium on Tribology, Tribological Research and Design for Engineering Series 2003;41:807-817.
[221] Bovington C, Spikes HA. Prediction of the influence of lubricant formulation on fuel economy, from laboratory bench tests. Proceedings of the International Tribology Conference Yokohama 1995:817-822.
[222] Sheasby JS, Caughlin TA, Blahey AG, Laycock KF. A reciprocating wear test for evaluating boundary lubrication. Tribolology International 1990;23(5):301-307.
[223] Wang FX, Cheng YQ, Guan DH. On the Tribological Behavior and Surface Analysis of a Sliding PSZ Ceramic-Steel Pair. Transactions of ASME, Journal of Tribology 1995;117(3):548-552.
[224] Cann P, Cameron A. Studies of thick boundary lubrication: Influence of zddp and oxidized hexadecane. Tribology International 1984;17(4):205-208.
[225] Cann P, Spikes HA, Cameron A. Thick film formation by zinc dialkyl dithiophosphates. American Society of Lubrication Engineers Transactions 1983;26(1):48-52.
[226] Spikes HA, Taylor L, Camenzind H. Film-forming properties of zinc-based and ashless antiwear additives. SAE Technical Paper 2000-01-2030.
[227] Taylor LJ, Spikes HA. Friction-enhancing properties of ZDDP antiwear additive: Part I - Friction and morphology of ZDDP reaction films. Tribology Transactions 2003;46(3):303-309.
[228] Taylor LJ, Spikes HA. Friction-enhancing properties of ZDDP antiwear additive: Part II - Influence of ZDDP reaction films on EHD lubrication. Tribology Transactions 2003;46(3):310-314.
[229] Topolovec-Miklozic K. Spikes HA. Application of atomic force microscopy to the study of lubricant additive films. ASME Transactions, Journal of Tribology 2005;127(2):405-415.
[230] Evans RD, Nixon HP, Darragh CV, Howe JY, Coffey DW. Effects of extreme pressure additive chemistry on rolling element bearing surface durability. Tribology International 2007;40(10-12):1649-1654.
[231] Bartz WJ, Kruger V. Influence of lubricants on the pitting fatigue of gears. Wear 1975;35(2):315–329.
[232] Stachowiak GW, Batchelor AW. Engineering Tribology, 2nd Ed. Butterworth-Heinemann, 2001.
[233] Forbes ES. The load-carrying action of organo-sulphur compounds-a review. Wear 1970;15(2):87–96.
[234] Lara J, Blunt T, Kotvis P, Riga A, Tysoe WT. Surface chemistry and extreme pressure lubrication properties of dimethyl disulfide. Journal of Physical Chemistry B 1998;102:1703–1709.
[235] Adams JH. Borate: A new generation EP gear lubricant. Lubrication Engeering 1977;34(5):241–246.
[236] Hu ZS, Dong JX, Chen GX, He JZ. Preparation and tribological properties of nanoparticle lanthanum borate. Wear 2000;243(1-2):43–47.
[237] Stanulov KG, Harhara HN, Cholakov GS. An opportunity for partial replacement of phosphates and dithiophosphates in EP packages with boron-containing additives. Tribology International 1998;31(5):257–263.
[238] Hu ZS, Lai R, Lou F, Wang LG, Chen ZL, Chen GX, Dong JX. Preparation and tribological properties of nanometer magnesium borate as lubricating oil additive. Wear 2002;252(5-6):370–374.
[239] Warren RE. New chemistry in gear lubricant-borate extreme pressure additive. Proceedings of the National Conference on Power Transmissions 6th Annual Meeting 1979;155-165.
[240] West WW, Cerrito E, Stokely JM, Rafael S. Oil dispersible inorganic borate in combination with EP agents as lubrication oil additives. US Patent 3,565,802, 1971.
[241] Sims MJ. Lubricant containing disperded borate and a polyol. US Patent 3,819,521, 1974.
[242] Peeler RL. Alkali Metal Borate E.P. Lubricants. US Patent 3,313,727, 1967.
[243] Adams JH. Lubricant containing potassium. US Patent 3997454, 1976.

[244] Adams JH. Synergistic combinations of hydrated potassium borate, antiwear agents, and organic sulfide sntioxidants. US Patent 4,089,790, May 1978.
[245] Adams JH. Synergistic combinations of hydrated potassium borate, antiwear agents, and organic sulfide antioxidants. US Patent 4,163,729, August 1979.
[246] Salentine CG. Synergistic combination of alkali metal borates, sulfur compounds, phosphites and neutralized phosphate. US Patent 4,717,490, January 1988.
[247] Dong JX, Hu ZS. A study of the anti-wear and friction-reducing properties of the lubricant additive, nanometer zinc borate. Tribology International 1998;31(5):219–223.
[248] Harrison JJ, Nelson KD. Dispersed hydrated potassium borate compositions having improved properties in lubricating oil compositions. US Patent 6,737,387, May 2004.
[249] Harrison JJ, Nelson KD. Lubricant composition comprising alkali metal borate dispersed in a polyalkylene succinic anhydride and a metal salt of a polyisobutenyl sulfonate. US Patent 6,632,781, October 2003.
[250] Harrison JJ, Nelson KD. Dispersed hydrated sodium borate compositions having improved properties in lubricating oil compositions. US Patent 6,534,450, March 2003.
[251] Tequi P, Iovine S, Conatans B, Ladaviere R, Martin JM, Le Mogne T. European Patent 1386956, 2004
[252] Hong HS, Huston ME, O'Connor BM, Stadnyk NM. Evaluation of surface fatigue performance of gear oils. Lubrication Science 1998;10(4):365–80.
[253] Toulhoat H. Potentielet limite d'utilisation, aux temperatures elevees, des lubrifiants liquids dans les moteurs. Revue de l'LFP V 1989;44(3):371-385.
[254] Shirahama S. Adsorption of additives on wet friction Pairs and their frictional characteristics. Japanese Journal of Tribology 1994;39(12):1479-1486.
[255] Ozbalik N, Tersigni SH. Power transmission fluids with enhanced anti-shudder characteristics. European Patent 1553158, July 2005.
[256] Matsuoka T, Ohashi A, Nakayama T. Effect of lubricating oils on flaking of a wet clutch. Japanese Society of Automotive Engine Review 1996;17:127-132.
[257] Matsuoka T, Muraki M. Study on the effect of oiliness agents on friction characteristics of paper based friction materials under low sliding velocity. Japanese Journal of Tribology 2001;46(4):239-252.
[258] Patterson DJ, Henein NA. Emissions from combustion engines and their control. Ann Arbor Science Publication, Michigan, 1972.
[259] Kornbrekke RE, Patrzyk-Semanik P, Kirchner-Jean T, Raguz MG, Bardasz EA. Understanding soot mediated oil thickening: Part 6 - Base oil effect. SAE Technical Paper 982665.
[260] Rausa R, Carati C, Vanelli M, Ponti G. Synthesis of diesel-like soots-influence of the operative parameters on the chemico-physical and morphological characteristics. SAE Technical Paper 982664 1998.
[261] Bérubé KA, Jones TP, Williamson BJ, Winters C, Morgan AJ, Richards RJ. Physicochemical charaterization of diesel exhaust particles: Factors for assessing biological activity. Atmospheric Environment 1999;33:1599–614.
[262] Rounds FG. Soots from used diesel engine oils-their effects on wear as measured in four-ball wear tests. SAE Technical Paper 810499.
[263] Kawamura M, Ishiguro T, Morimoto H. Electron microscopic observation of soots in used diesel engine oils. Lubrication Engineering 1987;43:572–5.
[264] Lowenthal D, Gautam M, Neuroth G. Characterization of heavyduty diesel vehicle emissions. Atmospheric Environment 1994;28(4):731–43.
[265] Fujiwara Y, Fukazawa S, Tosaka S, Murayama T. Formation of soot particulates in the combustion chamber of a precombustion chamber type diesel engine. SAE Technical Paper 8404171998.
[266] Mainwaring R. Soot and wear in heavy duty diesel engines. SAE Technical Paper 971631.
[267] Covitch MJ, Humphrey BK, Ripple DE. Oil thickening in the MAK T-7 engine test – fuel effects and the influence of lubricant additives on soot aggregation. SAE Technical Paper 852126.
[268] Rounds FG. The generation of synthetic diesel engine oil soots for wear studies. Lubrication Engineering, 1984;40:394–401.

[269] Darmstadt H, Roy C, Kaliaguine S. ESCA characterization of commercial carbon blacks and of carbon blacks from vacuum pyrolysis of used tires. Carbon 1994;32(8):1399–406.
[270] Smith DM, Chughtai AR. The surface structure and reactivity of black carbon. Colloids and Surfaces A 1995;105(1):47–77.
[271] McGeehan JA, Rynbrandt JD, Hansel TJ. Effect of oil formulations in minimizing viscosity increase and sludge due to diesel engine soot. SAE Technical Paper 841370.
[272] Ryason PR, Chan IY, Gilmore JT. Polishing wear by soot. Wear 1990;137:15–24.
[273] Ratoi M, Castle RC, Bovington CH, Spikes HA. The influence of soot and dispersant on ZDDP film thickness and friction. Lubrication Science 2004;17(1):25–43.
[274] Chinas-Castillo F, Spikes HA. The behavior of diluted sooted oils in lubricated contacts. Tribology Letters 2004;16(4):317–322.
[275] Gautam M, Chitoor K, Balla S. Contribution of soot contaminated oils to wear-part II. SAE Technical Paper 1999-01-1519.
[276] Soejima M, Ejima Y, Uemori K, Kawasaki M. Studies on friction and wear characteristics of cam and follower: Influences of soot contamination in engine oil. Japanese Society of Automotive Engine Review 2002;23:113–119.
[277] Nagai I, Endo H, Nakamura H, Yano H. Soot and valve train wear in passenger car diesel engines. SAE Technical Paper 831757.
[278] Berbeizer I, Martin J, Kapsa PH. The role of carbon in lubricated mild wear. Tribology Intrenational 1986;19:115-122.
[279] Bardasz EA, Cowling SV, Ebeling VL, George HF, Graf MM, Kornbrekke RE, Ripple DE. Understanding soot mediated oil thickening through designed experimentation — Part 1: Mack EM6–287, GM 6.2L. SAE Technical Paper 952527.
[280] Courtney S. Condition monitoring: Why it sometimes goes wrong. Proceedings of the International Conference on Condition Monitoring 2001:344-349.
[281] Kraus JD. Electromagnetics, 4th Ed. McGraw-Hill, 1991. ISBN: 0071126619.
[282] Unger BA. Electrostatic discharge failures of semiconducting devices. IEEE International Reliability Physics Symposium Proceedings 1981:193-199.
[283] Cartwright RA, Fisher C. Marine gas turbine condition monitoring by gas path electrostatic detection techniques. International Gas Turbine and Aero-engine Congress and Exposition, American Society of Mechanical Engineers Paper 91-GT-376.
[284] Powrie HEG, Tasbaz OD, Wood RJK, Fisher CE. Performance of an electrostatic oil monitoring system during FZG gear scuffing test. Proceedings of the International Conference on Condition Monitoring 1999:155-174.
[285] Morris S, Wood RJK, Harvey TJ, Powrie HEG. Use of electrostatic charge monitoring for early detection of adhesive wear in oil lubricated contacts. Journal of Tribology 2002;124:288-296.
[286] Gajewski JB, Glod BJ, Kala WS. Electrostatic method for measuring the 2-phase pipe-flow parameters. IEEE Transactions on Industry Applications 1993;29(3):650-655.
[287] Gajewski JB. Electrostatic, inductive ring probe bandwidth. Measurement Science & Technology 1996;7(12):1766-1775.
[288] Gajewski JB. Dynamic effect of charged particles on the measuring probe potential. Journal of Electrostatics 1997;40(1&2):437-442.
[289] Balmer RT. Electrostatic Generation in dielectric fluids: The viscoelectric effect. Proceedings of World Tribology Congress III, 2005.
[290] Parsons R. Electrical double layer: Recent experimental and theoretical developments. Chemical Reviews 1990;90(5):813-826.
[291] Harvey TJ, Wood RJK, Denault G, Powrie HEG. Effect of oil quality on electrostatic charge generation and transport. Journal of Electrostatics 2002;55:1-23.
[292] Nelson JK. Electrokinetic effects in pumped dielectric fluids. Whitehead Memorial Lecture, Annual Report IEEE CEIDP, 93CH3269-8, 1993:25–61.
[293] Harvey TJ, Wood RJK, Denuault G, Powrie HEG. Investigation of electrostatic charging mechanisms in oil lubricated tribo-contacts. Tribology International 2002;35:605-614.
[294] Tasbaz OD, Wood RJK, Powrie HEG, Harvey TJ, Denuault G. Electrostatic monitoring of oil lubricated contacts for early detection of wear. International Conference on Condition Monitoring, 1999.

[295] James AM, Lord MP. Chemical and physical data. MacMillan Press Ltd., 1992:174. ISBN 0333511670.
[296] Lowell J, Rose-Innes AC. Contact electrification. Advances in Physics 1980;29:947-1023.
[297] Blacker RS, Birley AW. Electrostatic charge occurrence, significance and measurements. Polymer testing 1991;10:241-262.
[298] Castle GSP. Contact charging between insulators. Journal of Electrostatics 1997;40-41:13-20.
[299] Diaz AF, Felix-Navarro RM. A semi-quantitive tribo-electric series for polymeric materials: The influence of chemical structure and properties. Journal of Electrostatics 2004;62(4):277-290.
[300] Coehn A. Ann. Phys. 1898;64:217.
[301] Henniker J. Triboelectricity in Polymers. Nature 1962;196:474.
[302] Adams CK. Nature's Electricity. Tab Books, Blue Ridge Summit 1987:63.
[303] Kasai T, Fu XY, Rigney DA, Zharin AL. Applications of a non-contacting Kelvin probe during sliding. Wear 1999;225-229(Part2):1186-1204.
[304] DeVecchio D, Bhushan B. Use of a nanoscale kelvin probe for detecting wear precursors. Review of Scientific Instruments 1998;69(10):3618-24.
[305] Zharin AL, Rigney DA. Application of the contact potential difference technique for on-line rubbing surface monitoring. Tribology Letters 1998;4:205-213.
[306] Sun J, Wood RJK, Wang L, Care I, Powrie HEG. Wear monitoring of bearing steel using electrostatic and acoustic emission techniques. Wear 2005;259:1482-1489.
[307] Tasbaz OD, Wood RJK, Browne M, Powrie HEG, Denuault G. Electrostatic monitoring of oil lubricated sliding point contacts for early detection of scuffing. Wear 1999;230:86-97.
[308] Powrie HEG, Wood RJK, Harvey TJ, Morris S. Re-analysis of electrostatic wear-site sensor data from ZFG gear scuffing test. International Conference on Condition Monitoring Proceedings, University of Oxford, Condition Monitor 2001:6-12.
[309] Wood RJK, Penchaliah R, Wang L, Harvey TJ, Nelson K, Yamaguchi ES, Harrison JJ, Powrie HEG, Otin N. Electrostatic Monitoring of the effects of carbon black on lubricated steel/steel sliding contacts. Proceedings of the 31st Leeds-Lyon symposium on Tribology, Tribology Series 2005;48:109-121.
[310] Wood RJK, Harvey TJ, Powrie HEG. Electrostatic wear monitoring of taper roller bearings. Wear 2007;263(7-12):1492-1501.
[311] Powrie HEG. Use of electrostatic technology for aero engine oil system monitoring. Proceedings of the IEEE Aerospace Conference 2000;6:57-72. ISBN: 0-7803-5846-5.
[312] Wang L, Wood RJK, Harvey TJ, Morris S, Powrie HEG, Care I. Wear performance of oil lubricated silicon nitride sliding against various bearing steels.Wear 2003;255:657-668.
[313] Wang L, Wood RJK, Care I, Powrie HEG. Electrostatic wear sensing of ceramic-steel lubricated contacts. Proceedings of the 30th Leeds-Lyon Symposium on Tribology, Tribological Series, 2003;711-720.
[314] Powrie HEG, Wood RJK, Harvey TJ, Wang L, Morris S. Electrostatic Charge Generation Associated with Machinery Component Deterioration. Proceedings of the IEEE Aerospace Conference, 2002;6:2927-2934. ISBN 0-7803-7232-8.
[315] Eyre TS, Baxter A. Formation of white layers at rubbing surfaces. Metals Materials 1972;6(10):435-439.
[316] Rogers MD. Metallographic characterisation of transformation phases on scuffed cast iron diesel engine components. Tribology 1969;2:123–127.
[317] Williams IM, Richardson AT, Poulter R. The origins of conduction in hydrocarbons. Proceedings of the 6th International Conference on Conduction and Breakdown in Dielectric liquids. Frontieres, 1978:49–55.
[318] Popl M, Stejskal M, Mostecky J. Determination of polycyclic aromatic hydrocarbons in white petroleum products. Annual Chemistry 1975;47(12):1947–1950.
[319] Harvey TJ, Wood RJK, Powrie HEG, Warrens C. Charging ability of pure hydrocarbons and lubricating oils. Tribology Transactions 2004;47:263-271.
[320] Bustin WM, Dukek WG. Electrostatic hazards in the petroleum industry. John Wiley and Sons, 1983. ISBN 9780471901631.
[321] Walmsley HL. Woodford G. The generation of electric currents by the laminar-flow of dielectric liquids. Journal of Physics D: Applied Physics 1981;14(10):1761-1782.

[322] Walmsley HL. Woodford G. The Polarity of the Current Generated by Laminar Flow of a Dielectric Liquid. Journal of Electrostatics 1981;10:283-288.
[323] Gladstone S. Textbook of physical chemistry, 2nd Ed. MacMillian, 1947:1227.
[324] Oommen TV, Petrie EM. Electrostatic charging tendency of transformer oils. IEEE Transactions on Power Apparatus and Systems 1984;103(7):1923-1931.
[325] Ramkumar P, Wang L, Harvey TJ, Wood RJK, Nelson K, Yamaguchi ES, Harrison JJ, Powrie HEG. The effect of diesel engine oil contamination on friction and wear. Proceedings of the World Tribology Congress III, 2005:63854.
[326] Penchaliah R. The influence of contaminants and their interactions on diesel engine oil tribology using electrostatic condition monitoring. PhD Thesis, University of Southampton, 2007.
[327] McCash EM. Surface chemistry. Oxford University Press, 2001:62. ISBN 0-19-850328-8.
[328] Beltzer M. Assessing adsorption of conventional friction modifying molecules by relative contact potential difference measurements. Transaction ASME, Journal of Tribology 1992;114:675-682
[329] Yamaguchi ES, Ryason PR, Yeh SW, Hansen TP. Boundary film formation by ZnDTPs and detergents using ECR. Tribology Transactions 1998;41(2):262-272.
[330] George S, Balla S, Gautam M. Effect of diesel soot contaminated oil on engine wear. Wear 2007;262:1113–1122.
[331] Ohkawa S, Kuse T, Kawasaki N, Shibata A, Yamashita M. Elasticity – an important factor of wet friction materials. SAE Technical Paper 911775.
[332] Harrison JJ, Ruhe W. Modified high molecular weight succinimides. US Patent 5,334,321, 1994.
[333] Bezot P, Hesse-Bezot C, Yamaguchi ES, Harrison JJ, Campbell CB. A light scattering study of the aggregation kinetics of carbon black suspensions in group I and group II base oils: Influence of dispersant additives. SAE Technical Paper 2003-01-1998.
[334] Harrison JJ, Ruhe W. Polyalkylene succinimides and post-treated derivatives thereof. US Patent 5,821,205, 1998.
[335] Vartanian PF. The chemistry of modern petroleum product additives. Journal of Chemical Education 1991;68:1015.
[336] Typical Properties of Performance Carbon Blacks, Columbian Chemicals Company. Product Specifications. www.columbianchemicals.com
[337] Hearn GL. Electrostatic ignition hazards arising from fuel flow in plastic pipes. Journal of Loss Prevention in the Process Industries 2002;15:105-109.
[338] http://www.soton.ac.uk/~wolfson/dev/
[339] Box GE, Hunter WG, Hunter JS. Statistics for experimenters: An introduction to design, data analysis, and model building. John Wiley and Sons, 1978. ISBN 0-471-09315-7.
[340] Kutner MH, Nachtsheim CJ, Neter J, Li W. Applied linear statistical models. 5th Ed. Irwin Professional Publishers, 2005. ISBN 9780073108742.
[341] Soejima M. Friction and wear characteristics of cam and tappet. Proceedings of the 6th International Congress on Tribology 1993;329-334.
[342] Poovamma PK, Jagadish R, Dwarakanath K. Investigation on static electrification characteristics of transformer oil. Journal of Electrostatics 1994:33;1–14.
[343] Peyraque L, Beroual A, Buret F. Static electrification of pressboard/oil interface and transient phenomena, oils. IEEE Transactions on Dielectrics and Electrical Insulation 1998;5(3):443–448.
[344] Huh CS, Jeong JI. Streaming electrification of thin insulating pipes under electric field. IEEE Transactions on Dielectrics and Electrical Insulation 1998;5(2):199–203.
[345] Romat H, Touchard G, Grimaud PO, Moreau O. Flow electrification in power transformers. Presented at 9th International Conference on Electrostatics, Institute of Physics Conference Series 1995;143:323–327.
[346] Brzostek E, Kedzia J. Examination of the static electrification of transformer oil. Journal of Electrostatics 1983;14:309–318.
[347] Brzostek E, Kedzia J. Static electrification in aged transformer oil. IEEE Transactions on Dielectrics and Electrical Insulation 1986;1(4):609–612.
[348] Shimizu S, Murata H, Honda M. Electrostatics in power transformers, IEEE Transactions on Power Apparatus and Systems 1979;98(4):1244–1250.
[349] Kedzia J. Investigation of transformer oil electrification in a spinning disc system, IEEE Transactions on Dielectrics and Electrical Insulation 1989;24(1):59–65.

[350 Rogachevskaya TA, Vipper AB, Malysheva TG, Lashkhi VL, Deryabin AA, Markov AA, Lisovskaya MA, Bauman VN. Properties of succinimides with modified chemical composition. Chemmotology of fuels and lubricants. 1976 UDC 665.521.5:547.461.4. Translated from Khimiya I Tekhnologiya Topliv I Masel 1975;9:47-50.

[351] Evans, HP, Snidle RW. A model for elastohydrodynamic film failure in contacts between rough surfaces having transverse finish. Journal of Tribology 1996;118(4):847-857.

[352] McGeehan JA, Ryason PR. Preventing catastrophic camshaft lobe failures in low emission diesel engines. SAE Technical Paper 2000-01-2949.

[353] Jacobson B. Regimes of elasto-hydrodynamic lubrication. Journal of Mechanical Engineering Science 1991:12(1):9-16.

[354] Chittenden RJ, Dowson D, Dunn JF, Taylor CM. EHL film thickness in concentrated contacts. Proceddings of the Royal Society 1985;A387:245-294.

[355] De Barros MI, Bouchet J, Raoult I, Le Mogne Th, Martin JM, Kasrai M, Yamada. Friction reduction by metal sulfides in boundary lubrication studied by XPS and XANES analyses. Wear 2003;254:863-870.

[356] Yin Z, Kasrai M, Bancroft GM, Fyfe K, Colaianni ML, Tan KH. Application of soft X-ray absorption spectroscopy in chemical characterization of antiwear films generated by ZDDP Part II: The effect of detergents and dispersants. Wear 1997;202:192-201.

[357] Ramakumar SSV, Rao AM, Srivastava SP. Studies on addition-additive interaction: formation of crankcase oil towards rationalization. Wear 1992;156:101-120.

[358] Wu YL, Dacre B. The effects of lubricant-additives on the kinetics and mechanisms of ZDDP adsorption on steel surfaces. Tribology International 1997;30(6):445–453.

[359] Peng P, Hong S-Z, Lu W-Z. The degradation of zinc dialkyldithiophosphate additives in fully formulated engine oil as studied by P-31 NMR spectroscopy. Lubricant Engineering 1994;50(3):230–5.

[360] Shiomi M, Tokashiki M, Tomizawa H , Kufibayashi T. Interaction between zinc dialkyldithiophosphate and amine. Lubrication Science 1986;1(2):131-147.

[361] Rounds FG. Some effects of amines on zinc dialkyldithiophosphate antiwear performance as measured in four-ball wear tests. ASLE Transactions 1981;24:431-440.

[362] Harrison PG, Brown P, McManus J. ^{31}P NMR study of the interaction of a commercial succinimide-type lubricating oil dispersant with zinc(II) bis(O,O'-di-iso-butyldithiophosphate). Wear 1992;156:345-349.

[363] Rounds FG. Some factors affecting the decomposition of three commercial zinc organodithiophosphates. ASLE Transactions 1975;18:79-89.

[364] Bartha L, Deak G, Kovacs M, Kocsis Z, Vuk T. Interaction of PIB-succinimides and other engine oil additives. Lubrication Science 1997;9(9-2):173–180.

[365] Rounds FG. Changes in friction and wear performance caused by interactions among lubricant additives. Proceedings of the 5th Intrenational Colloquium on Additives for Lubricants and Operational fluids 1986;1-21.

[366] Silver HB. The interaction between corrosion inhibitors and load carrying additives in mineral oil. Tribology International II 1978:185-188.

[367] Chevalier Y, Dubois-Clochard M-C, Durand J-P, Delfort B, Gateau P, Barré L, Frot D, Briolant Y, Blanchard I, Gallo R. Adsorption of poly(isobutenylsuccinimide) dispersants at a solid-hydrocarbon interface. Progress Colloid Polymer Science 2001;118:110-114.

[368] Yamada Y, Igarashi J, Inoue K. Lubrication Engineering 1992;48(6):511.

[369] Isoyama H, Sakurai T. The lubricating mechanism of di-u-thio-dithio-bis (diethyldithiocarbamate) dimolybdenum during extreme pressure lubrication Tribology International 1974;7:151–60.

[370] Mitchell PCH. Oil-soluble Mo–S compounds as lubricant additives. Wear 1984;100:281–300.

[371] Morina A, Neville A. Understanding the composition and low friction tribofilm formation/removal in boundary lubrication. Tribology International 2007;40(10-12):1696-1704.

[372] Eguchi M, Niikura T, Yamamoto T. Estimation of real contact area of paper-based friction materials for wet clutches by interference method using scanning laser microscope. Journal of Japanese Society of Tribologists 1997;42(10):813-9.

[373] Tasai M. Noise and vibration in wet type brakes and wet type clutches. Journal of the Japanese Society of tribologists

[374] Kitanaka, M. Friction Characteristics of Some Additives in ATFs. Tribology *2000*. 1992. Esslingen, Germany.
[375] Han S, Aihara S, Umesawa E, Matsumoto T. Study on mechanisms of running-in of wet-type paper-based friction materials. Journal of the Japanese Society of Tribologist 1997;42(3):233.
[376] Shimaya N, Ito H. ATF Additive adsorption characteristics of paper-based friction materials. Proceedings of the Conference on Tribology of the Japanese Society of Tribology 1991:517.
[377] Guan JJ, Willermet PA, Carter RO, Melotik DJ. Interactions between ATFs and friction material for modulated torque converter clutches. SAE Technical Paper 981098.
[378] Adams JH, Godfrey D. Borate gear lubricant—EP film analysis and performance. Lubrication Engineering 1981;37(1):16–21.
[379] Junbin Y, Dong J. Tribocatalysis reaction during antiwear synergism between borates and Sn(IV) compounds in boundary lubrication. Tribology International 1996;29(5):429-432.
[380] Kajdas CK. Importance of the triboemission process for Tribochemical reaction. Tribology International 2005;38:337-353.
[381] Zheng Z, Shen G, Wan Y, Cao L, Xu X, Yue Q, Sun T. Synthesis, hydrolytic stability and tribological properties of novel borate esters containing nitrogen as lubricant additives. Wear 1998;222:135–144.
[382] Allum KG, Ford JF. The influence of chemical structure on the load carrying properties of certain organo-sulfur compounds. Journal of the Institute of Petroleum Technology 1965;51:145-152.
[383] Sakurai T, Ikeda S, Okabe H. The mechanism of reaction of sulphur compounds with steel surface during boundary lubrication, using S^{35} as a tracer. American Society of Lubrication Engineers Transactions 1962;5:67-74.
[384] Hu ZS, Dong JX. Study on antiwear and reducing friction additive of nanometer titanium borate. Wear 1998;216:87-91.
[385] Baldwin BA. Relative antiwear efficiency of boron and sulfur surface species. Wear 1977;45:345.
[386] Taylor CM. Fluid film lubrication in automobile valve trains. Proceedings of the Institution of Mechanical Engineers Part J: Journal of Engineering Tribology 1994;208(NJ4):221-234.
[387] Perez JM, Kelley FA, Klaus EE, Bagrodia V. Development and use of the PSU Micro-oxidation test for diesel engine oils. SAE Technical Paper 872028.